Blackwell

No. ____

Booster Design Manual

Published — October 1986
Revision 1 — October 1988

AGS Booster Project*
Accelerator Development Department
Brookhaven National Laboratory
Upton, NY

*Supported by the U S. Department of Energy

TABLE OF CONTENTS

PREFACE

To meet the need of new physics research, there are three major objectives for the AGS Booster Project.

The first objective is to increase the proton intensity in the AGS by a factor of four (to 6×10^{13} ppp). This can be achieved by increasing the proton energy from 200 MeV to 1.5 GeV in the Booster and injecting the protons into the AGS four times per AGS pulse. Thus, a fast-cycling magnet guiding and focusing system (and its corresponding power supply system) has to be constructed, and a radio frequency acceleration and control system under heavy beam loading is required.

The second objective is to increase the AGS polarized proton intensity by a factor of twenty (to 10^{12} ppp). This objective can be achieved by accumulating 20 to 25 pulses of polarized protons from the linac while the AGS is in the acceleration and extraction portion of its cycle. Therefore, good field quality and minimal depolarization resonances have to be achieved in the Booster

The third objective is to accelerate heavy ions up to gold in the Booster for AGS and eventually for RHIC This objective requires the Booster to accept heavy ions at one-third of the proton injection field and to avoid electron stripping or capture for all species. Therefore, a high vacuum (three orders of magnitude better than required for normal proton operation) is needed. Furthermore, additional radio frequency systems to accelerate heavy ions at lower frequency are required. Extension of the sensitivity and linearity of all instrumentation to lower frequency and to three orders of magnitude lower intensity has to be accomplished.

The Booster is a circular accelerator with a circumference of about 200 meters, one-fourth that of the AGS, and is located at the north corner of the intersection between the AGS and the 200 MeV linac (see figure on following page). When completed, the Booster will receive proton beams from the 200 MeV linac and heavy ion beams from the existing Tandem Van de Graaf, and will provide higher energy beams for the AGS through a common extraction port and beam transfer line.

The design manual of the AGS Booster is a compilation of required specifications, characteristics and locations of the components necessary to build the machine. As such, its purpose is to bridge the transition from the conceptual design to the engineering and fabrication of the accelerator and to reflect design changes necessitated by future construction progress.

This manual reflects the contributions from Booster staff and many members of the AD and AGS Departments. Names of coordinators of each chapter or section are listed at the end of a particular chapter or section. The editorial staff is the Parameter

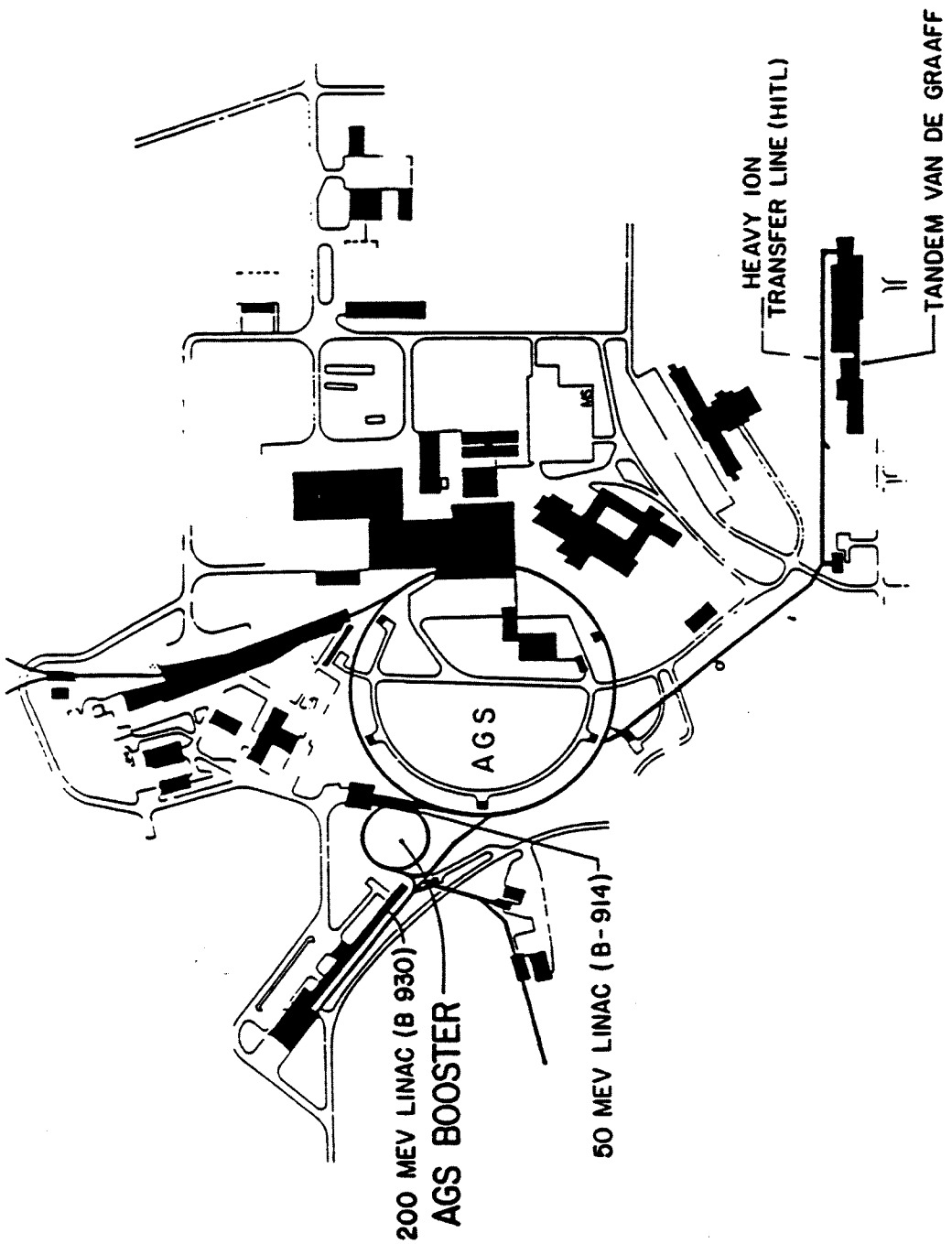
HEAVY ION
TRANSFER LINE (HITL)
TANDEM VAN DE GRAAFF
AGS
200 MEV LINAC (B 930)
AGS BOOSTER
50 MEV LINAC (B-914)

SITE MAP

Committee of the Booster Project; Y Y Lee, Chairman, G. Danby, F Dell, S. Y Lee, E. Raka, A. Ruggiero, A. Soukas, and R. Thomas, secretary

The revision of the design manual is the responsibility of the project manager All suggested changes, errors or omissions should be brought to his attention. After review, the actual changes will be made by authorized personnel and the new sheets will be issued to all holders of numbered manuals which will be assembled in ring binders.

The manual itself is structured for easy changes. Such changes will result from the on-going design process as mentioned above or may be simply due to the correction of errors. Missing entries mean that these values have not been calculated or verified at the date of printing. In order to avoid confusion caused by outdated information, each page of the manual is coded as follows:

1) Page Revision

This number will be changed sequentially each time a change is made to the contents of a page. If a change requires the number of pages to be increased, then all succeeding pages in that chapter are revised and/or renumbered.

2) Date

This shows the date on which the page was printed.

In conjunction with the Booster Design Manual, which specifies the design of the technical components, there are two related documents. The Booster Management Plan provides the baseline and controls which BNL and the Department of Energy will follow to meet the technical, cost, and schedule goals. The Preliminary Safety Analysis Report describes the conventional facilities and analyzes the safety issues in the radiation, fire, electrical, and personnel protection areas both during the construction period and in future operation.

W T Weng

CHAPTER 1. BOOSTER PARAMETER LIST

1.1. Introduction and Booster Parameter Summary

The goal of the AGS Booster Project is to enchance the capability of the AGS for basic research in high energy and nuclear physics. At present, the AGS is a proton synchrotron capable of accelerating protons to 30 GeV with intensities in excess of 1.5×10^{13} protons per pulse (ppp). In addition to proton acceleration the AGS has also accelerated polarized protons with intensities of approximately 5×10^{10} polarized protons per pulse. The newly completed heavy ion transfer line, interconnecting the AGS with the Tandem Van de Graff, provides the AGS with the capability of accelerating heavy ions up to mass number 32 (sulfur).

The Booster, by increasing the injection energy of the AGS, will:

- Increase proton intensity in the AGS by a factor of 4 (to 6×10^{13} ppp) to satisfy the demand for beam delivery for rare K decay, neutrino scattering, and other approved or planned experiments.
- Increase polarized proton intensity in the AGS by a factor of 20 (to 10^{12} ppp) for multi-target operation.
- Accelerate heavy ions in the AGS with mass numbers up to 200 (gold) and beyond for the AGS physics program and eventually for injection to the proposed Relativistic Heavy Ion Collider (RHIC).

The scope of this project consists of the construction of a rapid cycling synchrotron linking the Linac and the AGS capable of accelerating protons to 1.5 GeV at a 7.5 Hz frequency and heavy ions to a maximum field of 1.2743 T at a ~1 Hz frequency

The cost to complete the project is estimated to be 31.7 M$ including contingency (in actual year dollars). The project is to be completed in the second quarter of FY 1991.

As presently designed, the Booster will have: A circumference equal to one quarter that of AGS, with six identical superperiods. It will have a FODO lattice with bending magnets missing in some cells in order to accommodate the space needed for RF acceleration, injection, ejection and abort system without otherwise interrupting the periodicity The dipoles of the proposed lattice have an aperture of 152×70 mm and an injection field of about 1.6 kG (0.5 kG for heavy ions).

In total, the Booster will have 36 dipoles, each of 2.4 meter magnetic length, and 48 quadrupoles, each with a magnetic length of 0.50375 meters. A "separated function" structure with quadrupoles and zero-gradient dipoles has been chosen. Furthermore, for maximum tuning versatility the dipoles and the quadrupoles will be independently powered.

This chapter describes the parameter list of the AGS-Booster and the associated proton injection, heavy ion injection, and ejection lines. The revised design provides 48 chromaticity-correction sextupoles — one next to every quadrupole. The maximum eddy-current sextupoles strengths are taken to be 0.2 T/m^2 A schematic layout of the Booster lattice and its superperiods can be found in Chapter 2. (See Figure 2-2.) The present values of the Booster parameters are tabulated below (Note that the values listed are for use in design and in theoretical calculations.)

BOOSTER PARAMETER SUMMARY

type of machine: synchrotron for protons and heavy ions, polarized proton accumulator tor accelerator

beam energy, max

p	d	C	S	Cu	I	Au	
1.50	1.93	11.60	30.95	53.81	74.62	68.95	GeV
1.500	0.963	0.967	0.967	0.854	0.588	0.350	GeV/nucleon

circumference: 201.78 m (1/4 AGS)

magnetic bending radius: 13.75099 m

straight-sections (12 total)

- A3: RF (hvy ion, Band I)
- A6: RF (protons)
- B3: RF (hvy ion, Band II)
- B6: reserved
- C3: sector vac. valve
  - proton/hvy ion inj. kicker
  - elec. septum (hvy ion inj.)
- C6: vac. sector valve
  - current xfmr
  - damping kicker
  - proton/hvy ion inj. kicker
- D3: vac. sector valve
  - profile monitor
  - dump kicker
- D6: upstrm half reserv
  - absorber block (dwnstrm half)
- E3: vac. sector valve
  - tune kicker
- E6: RF (protons)
- F3: wall current monitor
  - vac. sector valve
  - ejection kicker
- F6: ejection septum
  - (bellows, PUE, sextupole require enlarged aperture here.)

special sections

- A1. vac. sector valve
  - (no pump)
- B1. vac. sector valve
  - (no pump)
- B8: hvy ion inj. kicker
- C5: stripper foil (protons)
  - graphite block
- C8: proton inj. kicker

bunch spacing, no. of bunches: 67.26 m center-to-center 3

no. of particles/pulse: protons, 1.5×10^{13}

polarized protons, $\sim 10^{12}$

C	S	Cu	I	Au	
54	~15	~10	~6.6	~3.2	x 10^9 ions*

transverse emittance, ϵ_N, (90% area/π): 50 mm-mrad, protons

*These values are based on the assumptions specified in BST/TN 55, "Expected Heavy Ion Intensity in the Booster, by Y Y Lee.

bunch size	protons bunched to <1.5 eV-s heavy ions bunched to 0.05 eV-s/nucleon
lattice, total no. of cells	FODO, 8.4075-m cells, 24
betatron tune, ν_x, ν_y	4.82, 4.83
natural chromaticity	ξ_x=−5.093, ξ_y=−5.447
β_x max, min	13.865/3.5754 m
β_y max, min	13.644/3.7033 m
horizontal dispersion, max, min	2.951/0.540 m
magnet type	iron-dominated, water-cooled Cu conductor
magnetic field, dipole, ejec.	protons, 0.546 T, heavy ions, 1.274 T, max
magnetic radius of curvature	13.75099 m
magnetic gradient, quad, ejec.	Gf: protons, 4.228 T/m Gd: protons −4.324 T/m
dipole length (magnetic/physical)	2.4/2.34 m, excl. coils
quad length (magnetic/physical)	0.50375/0.472 m, excl. coils
number of dipole and quadrupole magnets	36 dipoles, 48 quads
dipole excitation current, max	protons, 2220 A heavy ions, 5700 A
quad excitation current, max	protons, 2220 A heavy ions, 5500 A
vacuum chamber, dimen.	70 × 152 mm, dipoles 152 mm (circular), quads
RF harmonic number	3
RF frequency	

	p	d	C	S	Cu	I	Au	
inj.	2.523	0.788	0.562	0.446	0.349	0.265	0.213	MHz
ejec.	4.114	3.877	3.884	3.885	3.804	3.522	3.061	MHz

acceleration period	60 ms, protons; 620 ms (max), heavy ions
Injector system	200 MeV linac, protons 15 MV Tandem Van de Graaff, heavy ions

TABLE 1-1. Isotopes, Charge States, and Ionic Masses.

	Q	Z	A	Ionic Rest Mass (u)	Ionic Rest Mass Energy (GeV/nucleon)
p	+1	1	1	1.00728	0.93828
d	+1	1	2	2.01355	0.93781
C	+6	6	12	11.99671	0.93125
S	+14	16	32	31.96439	0.93047
Cu	+21	29	63	62.91808	0.93029
I	+29	53	127	126.88857	0.93068
Au	+33	79	197	196.94846	0.93126

TABLE 1-2. Injection Energies and Fields

	v/c	f	p	E_{inj}		B_{inj}
		(MHz)	(GeV/c)	(MeV)	(MeV/nucleon)	(kG)
p	0.5662	2.5235	0.6444	200.0	200.000	1.563
d	0.1767	0.7878	0.3368	30.0	15.000	0.817
C	0.1262	0.5623	1.4211	90.0	7.500	0.575
S	0.1000	0.4457	2.9925	150.0	4.688	0.519
Cu	0.0782	0.3485	4.5969	180.0	2.857	0.531
I	0.0595	0.2653	7.0489	210.0	1.654	0.590
Au	0.0478	0.2131	8.7805	210.0	1.066	0.645

TABLE 1-3. Ejection Energies and Fields — B_{max} = 12.74 kG

	v/c	f	p	E_{ejec}		B_{ejec}
		(MHz)	(GeV/c)	(GeV)	(GeV/nucleon)	(kG)
p	0.9230	4.114	2.251	1.500	1.5000	5.459
d	0.8699	3.877	3.308	1.927	0.9635	8.024
C	0.8714	3.884	19.847	11.602	0.9668	8.024
S	0.8716	3.885	52.926	30.952	0.9672	9.170
Cu	0.8534	3.804	95.932	53.810	0.8541	11.081
I	0.7901	3.522	152.345	74.623	0.5876	12.743
Au	0.6868	3.061	173.358	68.950	0.3500	12.743

1.2. Beam and Operational Parameters

injected particles — protons, polarized protons, heavy ions (through gold)

injection momenta

p	d	C	S	Cu	I	Au	
0.6444	0.3368	1.4211	2.9925	4.5969	7.0489	8.7805	GeV/c

$B\rho$, at injection

p	d	C	S	Cu	I	Au	
2.1496	1.1235	0.7901	0.7130	0.7302	0.8108	0.8875	T-m

output momenta

p	d	C	S	Cu	I	Au	
2.251	3.308	19.847	52.926	95.932	152.345	173.358	GeV/c

$B\rho$, at ejection

p	d	C	S	Cu	I	Au	
7.507	11.034	11.034	12.610	15.238	17.523	17.523	T-m

output kinetic energy

p	d	C	S	Cu	I	Au	
1.500	1.927	11.602	30.952	53.810	74.623	68.950	GeV
1.5000	0.9635	0.9668	0.9672	0.8541	0.5876	0.3500	GeV/nucleon

radio frequency

	p	d	C	S	Cu	I	Au	
inj.	2.523	0.788	0.562	0.446	0.349	0.265	0.213	MHz
ejec.	4.114	3.877	3.884	3.885	3.804	3.522	3.061	MHz

bunch spacing, center to center — 67.26 m

revolution time

	p	d	C	S	Cu	I	Au	
inj.	1.1888	3.8082	5.3353	6.7307	8.6076	11.3061	14.0791	μs
ejec.	0.7292	0.7737	0.7724	0.7723	0.7887	0.8519	0.9800	μs

no. of particles/pulse — protons, 1.5×10^{13}

polarized protons, $\sim 10^{12}$

C	S	Cu	I	Au	
54	~15	~10	~6.6	~3.2	x 10^9 ions

bunches per pulse — 3

acceleration time — 60 ms, protons & polarized protons
620 ms (max.) heavy ions

repetition rate	4 pulses/AGS pulse (7.5 Hz), protons 1 pulse/AGS pulse, polarized protons 1 pulse/AGS pulse, heavy ions
peak RF voltage	90 kV, protons & polarized protons 17 kV, heavy ions
circumference	201.78 m (1/4 AGS)
avg. radius	32.114 m
magnetic bending radius	13.75099 m

magnetic field, dipole

	p	d	C	S	Cu	I	Au	
inj.	0.1563	0.0817	0.0575	0.0519	0.0531	0.0590	0.0645	T
ejec.	0.5459	0.8024	0.8024	0.9170	1.1081	1.2743	1.2743	T

lattice type	separated function, FODO
superperiodicity	6
max β	13.9 m
max dispersion	2.95 m
horiz. tune	4.82
vert. tune	4.83
transition γ	4.88
natural chromaticity, horiz.	−5.093
natural chromaticity, vert.	−5.447
space-charge tune shift	−0.35 (proton, at injection)

1.3. Lattice Parameters

circumference	201.78 m (1/4 AGS)
ring	6 superperiods, 4 cells/superperiod

cell lattice

B CT SF QF | B CT SD QD | LS CT SF QF | B CT SD QD
B CT SF QF | LS CT SD QD | B CT SF QF | B CT SD QD

B	dipole bend magnets, horiz., 1.2743 T
CT	correction and trim coil assembly
SF, SD	sextupoles
QF, QD	quads
LS	long straight section
magnetic rigidity, ejec	7.507 T-m, protons & polarized protons
	17.523 T-m (max), heavy ions
magnetic bending radius	13.75099 m
lengths:	
superperiod	33.63 m
cell	8.4075 m
B	240 cm (magnetic)
CT	10 cm (magnetic)
SF, SD	10 cm (magnetic)
QF QD	50.375 cm (magnetic)

Component sequences are listed in the beam direction as seen from above.

Lattice Optics

phase shift per cell, x,y	72
betatron tune, ν_x, ν_y	4.82, 4.83
tuning range, $\Delta\nu_x$, $\Delta\nu_y$	$\pm$ 0.5
transition γ	4.8812
β_{max}, β_{min}	13.7 m, 3.6 m
dispersion; max, min	2.7 m, 0.5 m
natural chromaticity, ξ_x,ξ_y	−5.093, −5.447

Magnet Parameters

dipole field, protons	0.156 T (inj), 0.546 T (ejec)
dipole field, heavy ions	0.0519 T (inj, min), 1.2743 (ejec, max)
quadrupole fields, protons	0.126 T/m (inj), 4.23 T/m (ejec)
quadrupole fields, heavy ions\h β.25i'	
sextupole (zero chromaticity)	

1.4. Magnets and Power Supplies

1.4.1. Ring Dipole Magnets and Power Supplies

Parameter	Proton	Heavy Ion
type	curved H	
number of magnets	36 + 1	
bend angle	10	
radius of curvature	13.75099 m	
sagitta	5.23 cm	
core length	2.34 m	
magnetic length	2.40 m	
gap height	8.255 cm	
pole width	25.4 cm	
useful aperture	15.2 × 7.0 cm	
no. pancakes per magnet	4	
no. turns per pancake	4	
injection field (B_i)	1.56 kG	0.5 - 0.8 kG
extraction field (B_f)	5.46 kG	12.74 kG
inj. transfer function (B_i/I_i)	2.436 kG/kA	
extr transfer function (B_f/I_f)	2.320 kG/kA	
injection current (I_i)	640 A	~250 A
extraction current (I_f)	2250 A	5700 A
rms current	1700 A	3500 A
conductor dimensions (H × V)	24.5 × 50.8 mm	
current density (max)	525 A/cm^2	
resistance/magnet	1.5 mΩ	
resistance, total	65 mΩ	
inductance/magnet	3.2 mHy	
inductance, total	120 mHy	
coil insulation, dc volts	20 kV	
pulse repetition frequency	7.5 Hz	0.5 0.7 Hz
max. I	40 kA/s	10 kA/s
IR max	150 V	360 V
LI max	4800 V	1200 V
total voltage	4950 V	1560 V
peak power	11 MW	8.6 MW
dissipated power	200 kW	800 kW
stored energy	300 kJ	1800 kJ
correction windings	PBLW 2 T total	
	Other 6 T total	

1.4.2. Ring Quadrupole Magnets

Parameter	Proton	Heavy Ion
type	iron core quads	
number of magnets (H, V, H_{ref}, V_{ref})	24, 24, 1, 1	
core length	0.47 m	
magnetic length	0.50 m	
pole tip radius	8.255 cm	
pole width	12.7 cm	
useful aperture (radius)	6.6 cm	
no. pancakes per pole	1	
no. turns per pancake	5	
pole-tip gradient (max.)	12 kG/m	
injection field (B_i)	1.0 kG	0.4 kG
extraction field (B_f)	3.5 kG	8.3 kG
inj. transfer function (B_i/I_i)	1.5625 kG/kA	
extr transfer function (B_f/I_f)	1.512 kG/kA	
injection current (I_i)	640 A	~250 A
extraction current (I_f)	2240 A	5500 A
rms current	1700 A	3500 A
conductor dimensions (H × V)	31.7 × 31.7 mm	
current density (max)	600 A/cm^2	
resistance/magnet	0.90 mΩ	
resistance, total	32.5 mΩ	
inductance/magnet	0.35 mHy	
inductance, total	9.0 mHy	
coil insulation, dc volts	20 kV	
pulse repetition frequency	7.5 Hz	0.5 0.7 Hz
max. I	40 kA/s	10 kA/s
IR max	75 V	180 V
LI max	360 V	90 V
total voltage	435 V	270 V
peak power	0.975 MW	1.48 MW
dissipated power	100 kW	400 kW
stored energy	23 kJ	135 kJ

1.4.3. Ring Sextupole Magnets

number of sextupoles	48
number of families	2
B'	+8.8 T/m^2, focusing
	−8.8 T/m^2, defocusing
iron length	10.0 cm
length, coil end to coil end	~ 20 cm
aperture	165 mm (circular)
coil package	250 Amp × 20 Turns

1.4.4. Correction and Trim Magnets

Device and Strength	*No. of Units*	*No. of Power Supplies*
1. orbit bump 2500 × 2 Amp-Turns	36	3
2. dipole chamber eddy current correction 10 × 6 A-turns	36	0
3. orbit correctors 20 × 50 A-turns	48	48
4. QF trim (tune) 500 × 1 A-turns	24	1
5. QD trim (tune) 500 × 1 A-turns	24	1
6. QF resonance correction 50 × 2 A-turns	24	4 — 8
7 QD resonance correction 50 × 2 A-turns	24	4 — 8
8. skew quads 20× 50 A-turns	24	8
9. SF resonance correction 50 × 1 A-turns	24	4 — 8
10. SD resonance correction 50 × 1 A-turns	24	4 — 8

1.4.5. Injection Magnets

H^- Injection Line

External

Injection Dipoles (Horizontal-Bend)	
number	4 main bending dipoles
magnetic field	0.974 T
length, magnetic	1.20 m
Injection Steering Magnets	
number	3 horiz. steering dipoles 4 conventional vert. steering dipoles 1 fast vert. steering dipole (for painting)
magnetic field	200 G-m
length, magnetic	
length, physical	
Injection Quads	
number	13
magnetic field	4 T/m, max
length, magnetic	0.30 m

In ring

Injection kicker (fast-bump) magnets	
number	3; located at C3, C6, and C8
type	ferrite
field strength	0.0170, 0.0056, and 0.0175 T-m
displacement required, max.	0.0508 m
bend angle, max.	8.153 mrad
rise and fall time	50 μs
pulse length	up to 500 μs
pulse shape	programmable
Injection slow orbit-bump magnets	
number	3; located at dipoles C4, C8 and D1
type	back-leg windings on dipoles

Heavy Ion Injection Line (from 69 point to Booster)

External

Injection Dipoles (Horizontal-Bend)	
number	main bending dipoles
magnetic field	
length, magnetic	
Injection Pitching and Steering Magnets	
number	pitching dipoles steering dipoles
magnetic field	
length, magnetic	
Injection Quads	
number	
magnetic field	
length, magnetic	

In ring

Injection kicker (fast-bump) magnets	
number	3; located at B8, C3, and C6
type	
field strength	0.009220, 0.000632, and 0.00590 T-m
rise and fall time	$< 100\ \mu s$
pulse length	up to 500 μs
pulse shape	programmable
Injection slow orbit-bump magnets	
number	3; at dipoles B6, C1, and C5
type	back-leg windings on dipoles

1.4.6. Ejection Magnets

External

Ejection Dipoles (Horizontal-Bend)	
number	5 dipoles
Ejection Trim Magnets	
number	2 vert., 2 horiz.
magnetic field	1 kG-m
Ejection Quads	
number	16
magnetic strength	-9 T/m (1), -10 T/m (10), 16 T/m (1), -18 T/m (3)
length, magnetic	0.50 m (16), 1.0 m (1)

In ring

Ejection kicker magnets	
number	1, located at F3
type	
field strength	
magnet gap	
eff. length of module	
total length of module	
bend angle	3.77 mrad, hvy ion; 5.03 mrad, protons
rise time	110 ns ±3%
pulse length	
fall time	
voltage	
current	
flat top uniformity	
Ejection septum magnet	
number	1, located at F6
type	
field strength	
magnet gap	
eff. length of module	
total length of module	
bend angle, direction	142.80 mrad, horiz.
rise time	
pulse length	
fall time	

voltage	
current	
flat top uniformity	
Ejection slow orbit-bump magnets	
number	4; at dipoles F2, F4, F7, and A1
type	back-leg windings on dipoles
AGS injection magnets	
fast kicker	strength, 2.85 mrad
injection septum	strength, 109.73 mrad
slow orbit bump 1	strength, -4.48%
slow orbit bump 2	strength, -5.82%

1.4.7 Magnet Tolerances

Magnet Alignment and Uniformity Tolerances (rms)

Dipole	
Δx-rms	0.10 mm
pitch	0.1 mrad
roll	0.1 mrad
Δy-rms	0.10 mm
$\Delta\phi$-rms	0.1 mrad
$\Delta(BL)/BL$, rms	2×10^{-4}
Quad	
Δx-rms	0.10 mm
pitch	0.1 mrad
roll	0.1 mrad
Δy-rms	0.10 mm
$\Delta\phi$-rms	0.2 mrad
$\Delta(B'L)/B'L$, rms	2×10^{-4}
Correction and Trim Assembly	
Δx-rms	0.10 mm
Δy-rms	0.10 mm
$\Delta\phi$-rms	0.1 mrad
Beam-position monitor relative to quad	
Δx-rms	0.1 mm
Δy-rms	0.1 mm

1.5. Ring Vacuum System

average pressure	3×10^{-11} torr (N_2 equivalent)
vacuum chamber	
half-cell length	4.2 m
number	48
dipole length	curved, 2.4 m
	total, 2.8 m
number	36
cross section	horiz., 165 mm
	vert., 70 mm
	wall, 2.0 mm
material	Inconel 625
quadrupole length	550 mm
number	48
cross section	o.d., 152 mm
	wall, 1.6 mm
material	Inconel 625
conductance	1.5×10^5 cm-l/s
sextupole length	150 mm
number	42
cross section	same as quad
PUE length	240 mm
number	48
cross section	o.d., 200 mm
	i.d., 152 mm
material	316L stainless steel
bellows cross section	o.d., 178 mm
	i.d., 152 mm
	wall, 0.3 mm
number	48
material	Inconel 625
flange conflat type	316 LN
vacuum pumps	
UHV	titanium pump, 1000 l/s active gases
	ion pump, $<$ 20 l/s inert gases
number	48 titanium, 48 ion
roughing	portable turbo-pump
number	6

1.6. Radio Frequency Acceleration System

harmonic	3
acceleration time	60 ms, protons ~620 ms, heavy ions
repetition rate	4 pulses/AGS pulse (7.5 Hz), protons 1 pulse/AGS pulse, polarized protons 1 pulse/AGS pulse, heavy ions
no. of stations	4 total Band I, 0.1785-0.675 MHz Band II, 0.600-2.5 MHz Band III, 2.4-4.2 MHz (2 stations)

	p	p↑	S^{+14}	Au^{+33}
RF Amplitude				
injection	45 kV	7.35 kV	0.67 kV	1.77 kV
ejection	53 kV	40 kV ?	< 17 kV	< 17 kV
at max. accel.	90 kV	40 kV	≤ 17 kV	≤ 17 kV
Harmonic Number	3	3	3	3
RF Frequency				
injection	2.5 MHz	2.5 MHz	0.446 MHz	0.213 MHz
ejection	4.11 MHz	4.11 MHz	3.89 MHz	3.06 MHz
Phase Space Area/A	1.5 eV-s	0.3 eV-s	0.071 eV-s	0.071 eV-s
Intensity (per bunch)	0.5×10^{13}	3×10^{11}	5×10^{9}	1.1×10^{9}
Total Gap Impedance ($f_{rf} = 4.1$ MHz)	< 24 kΩ	—	—	—
Acceleration Time	62 ms	≥ 66.5 ms	≤ 0.7 s	≤ 0.7 s
Max. Beam Power Delivered to Beam	140 kW	—	< 0.5 kW	< 0.5 kW
Maximum B	9.ɔ T/s	9.ɔ T/s	$< 3.ɔ$ T/s	$< 3.ɔ$ T/s
B_{inj}	1.5 T/s	0.0 T/s	0.0 T/s	0.0 T/s

radio frequency

	p	d	C	S	Cu	I	Au	
inj.	2.523	0.788	0.562	0.446	0.349	0.265	0.213	MHz
ejec.	4.114	3.877	3.884	3.885	3.804	3.522	3.061	MHz

valves	
sector	all metal, 150 mm w/ RF contact
number	6
roughing	all metal, 38 mm right angle
number	12
gauges	
Bayard-Alpert	10^{-11} — 10^{-4} torr
number	48
Convectron	10^{-3} to atm
number	6
RGA	w/ electron multiplier
number	6
in situ bake	200 C for 40 hrs.

revolution time

	p	d	C	S	Cu	I	Au	
inj.	1.1888	3.8082	5.3353	6.7307	8.6076	11.3061	14.0791	μs
ejec.	0.7292	0.7737	0.7724	0.7723	0.7887	0.8519	0.9800	μs

synchrotron frequency

	p	d	C	S	Cu	I	Au	
inj.	5.143	0.537	0.562	0.559	0.349	0.265	0.213	kHz
max.	7.268	1.724	1.788	1.814	1.784	1.661	1.529	kHz
ejec.	1.442	0.428	0.430	0.433	0.479	0.616	0.789	kHz

bucket lengths and time between buckets (at ejection)

	p	d	C	S	Cu	I	Au	
length	126.4	83.1	82.3	82.0	87.3	110.0	147.7	ns
separation	116.7	174.8	175.2	175.4	175.6	174.0	179.0	ns

1.7 Booster Injection System

Transfer line from linac (from HEBT MD60 magnet in linac to Booster dipole magnet C5)

length	
magnet sequence	See Table 3-1 of Chapter 3.
120-cm dipole parameters	
number	4
field	0.974 T
bend angle	31.54
length, effective	1.20 m
magnet gap	2.5
current	1000 A
quadrupole parameters	
number	13
gradients	0.6 — 1.6 T/m
length, effective	0.30 m
current	< 450 A
stripper	carbon, 100 200 $\mu g/cm^2$
vacuum required	10^{-9} Torr

Transfer line from Tandem (from 69 -bend point to A3 Booster straight section)

length	
magnet sequence	See Table 4-5 of Chapter 4.
main bending dipole parameters	
number	
field	
bend angles	
length, effective	
magnet gap	
current	
resistance	

current regulation	
quadrupole parameters	
number	
gradients	See Table 4-7 of Chapter 4.
pole-tip diameter	
current	
resistance	
vacuum required	10^{-9} Torr
Heavy-ion injection electrostatic septum	
number	1 at C3
electric field strength	32 kV/cm, max
electrostatic gap	
effective length	2.55 m
aperture (good field region)	2 × 2 cm
radius of curvature	9.65 m
deflection angle	15.04
septum thickness	< 0.25 mm — as thin as practical
motion adjustment	2 in. at both up and downstream ends
total physical length of module	
rise time	
pulse length	
fall time	
voltage	
flat top uniformity	

1.8. Booster Ejection System

Transfer line to AGS (from Booster F6 straight section to AGS section L20)

length	
magnet sequence	See Tables 5-2 and 5-3 of Chapter 5.
dipole parameters	
number	5
bend angles	0.03636, 0.2757, 0.2757 rad 0.01194, 0.12187 rad
length, effective	0.5, 2.4, 2.4 m 0.10258, 1.04740 m
quadrupole parameters	
number	15
strengths	See Table 5-4 of Chapter 5.
length, effective	0.50 m (16), 1.0 m (1)
pole-tip diameter	4 (6), 6.5 (10)
current	
resistance	
stripper	copper, 70 mg/cm^2
vacuum required	10^{-9} Torr

CHAPTER 2. THE BOOSTER LATTICE AND BEAM DYNAMICS

2.1. Introduction

The booster is designed to have a circumference equal to one quarter of that of the AGS with 24 quadrupole and sextupole periods. There are 24 FODO cells with separate function magnets organized into six superperiods due to two missing dipoles in each superperiod in order to accommodate spaces needed for RF acceleration, injection, ejection, and abort systems. The overall layout of the booster ring is shown in Fig. 2-1, where the superperiods are designated as A through F The angle α is defined to the angle between East and the center of quadrupole F8.

There are 48 quadrupoles, 48 sextupoles, and 36 dipoles in the booster ring. Each dipole has a magnetic length of 2.4 m and an aperture of $3.25'' \times 10''$ The injection field is about 1.6 kG for protons and 0.7 kG for gold ions. The field at ejection is 12.7 kG for heavy ion operation. The magnetic length of the quadrupole is 0.50375 m, and the pole tip aperture is $6.5'' \times 6.5''$ These choices are based on the matching of beam size for booster and AGS operation. The dipoles and quadrupoles will be separately powered. (See Chapter 3 for details.)

The lattice design issues are discussed in the next section, and chromatic, closed-orbit, and stop-band corrections in sections 2.3-2.5. The performance limitations, such as the space-charge limit and the impedances are discussed in sections 2.6-2.9. Magnet alignment and the magnet coordinates are covered in section 2.10.

2.2. The Booster Lattice

The booster lattice is a six superperiod machine with four FODO cells in each superperiod. Within the superperiod, there are two missing dipoles at the third and sixth half-cell locations.

From the betatron motion point of view, the booster has 24 periods. The systematic half-integer stop band is located at a tune of 12. The chromatic correction sex tupoles are also organized in 24 periods. The third-order systematic resonance is at a tune of 8. The machine therefore has a wide range of tunability Since there are no dipoles in the third and sixth half-cell locations of each superperiod, the eddy current and saturation sextupoles due to the acceleration process have a periodicity of only six. Systematic third-order resonances are located at tunes of 4 and 6, and a fourth-order resonance is located at 4.5. The fourth-order resonance will be relatively unimportant to the performance of the machine. Thus the operating tunes are chosen to be ν_x=4.82 and ν_y=4.83 with a tuning range of $\pm$ 1 unit.

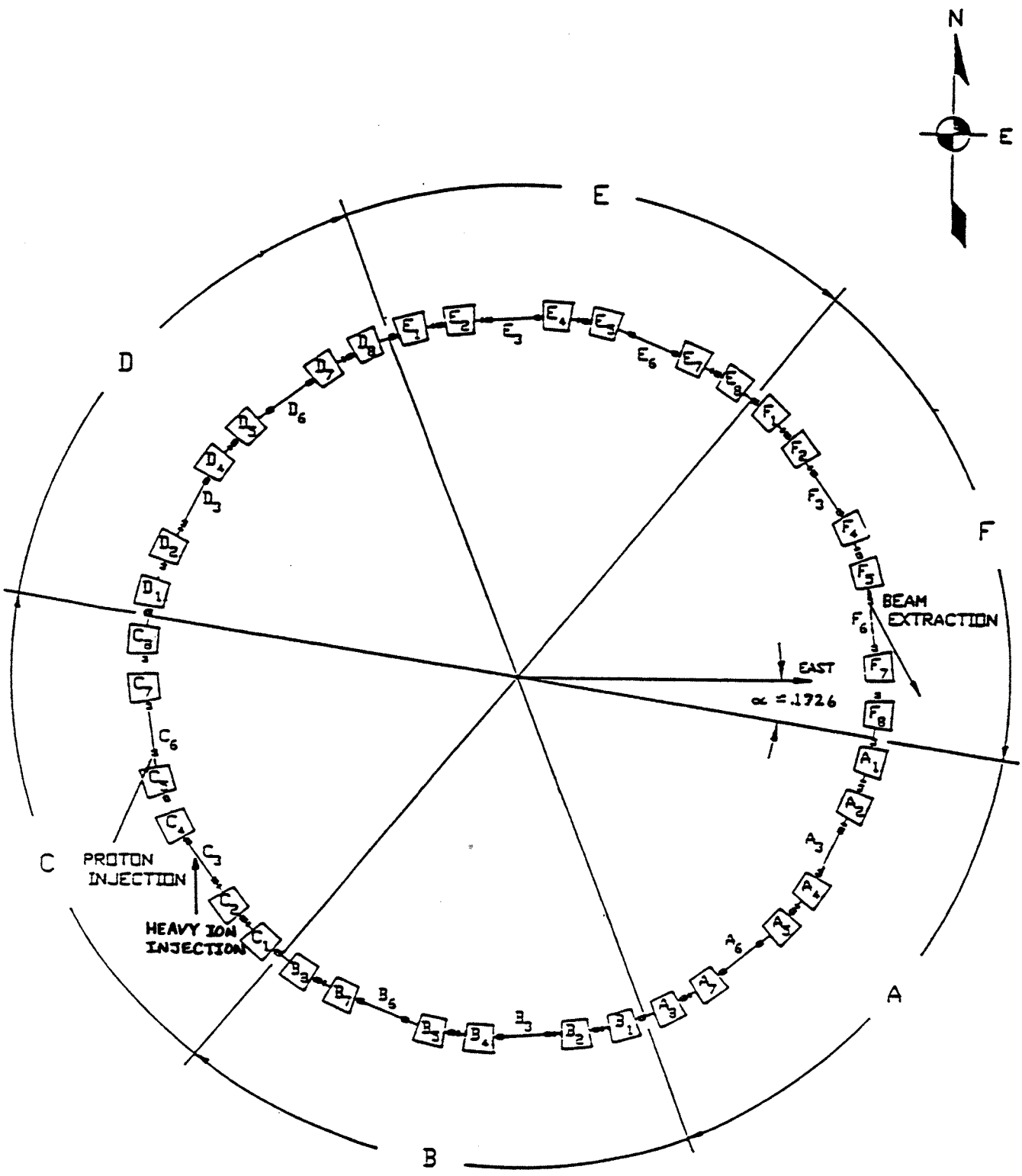

Figure 2-1. The layout of the Booster

The half-cells of the six superperiods are labelled A1-A8, B1-B8, C1-C8, D1-D8, E1-E8, and F1-F8. Figure 2-2 shows the schematic layout of a superperiod. There are four FODO cells in each superperiod. The label however is associated with the dipole which lies fully within the half-cell while the name of the quadrupole is derived from that of the dipole which precedes it. There are 48 sextupoles in the ring, shown in Fig. 2-2, each 10 cm long. Sextupoles, the correction package, and the beam position monitors are located in the 1 meter free space available between the dipole and the quadrupole which follows it.

TABLE 2-1 Lattice parameters.

Lattice Parameters			
circumference		201.78 m	
ν_x		4.82	
ν_y		4.83	
Quadrupoles	QF	0.281199 m^{-1}	0.50375 m
	QD	0.289866 m^{-1}	0.50375 m
Dipoles		$2\pi/36$ rad	2.4 m
bending radius	ρ	13.75099 m	
transition energy	γ_t	4.88	
tuning range		± 1	
phase advance/cell		72	
max. betatron func.	β_x	13.87 m	
	β_y	13.64 m	
	X_p	2.95 m	
natural chromaticity	ξ_x	−5.093	
	ξ_y	−5.447	

Figure 2-3 shows the betatron amplitude and dispersion function for the booster lattice. The available vacuum chamber size is $2.60'' \times 6.33''$ Thus the vertical admittance is 82π mm-mrad. The horizontal admittance is considerably larger

Because the half-integer stop band is far away from the operational tune, the betatron function variation is very small. We obtain $\Delta\beta/\beta = 0.014$ at $\Delta p/p = 0.5\%$. Because of the low energy injection of the 200 MeV proton, considerable space-charge tune shift is expected. The half-integer stop band correction at ν=4.5 due to the random quadrupole error, and the random third-order correction are discussed in later sections.

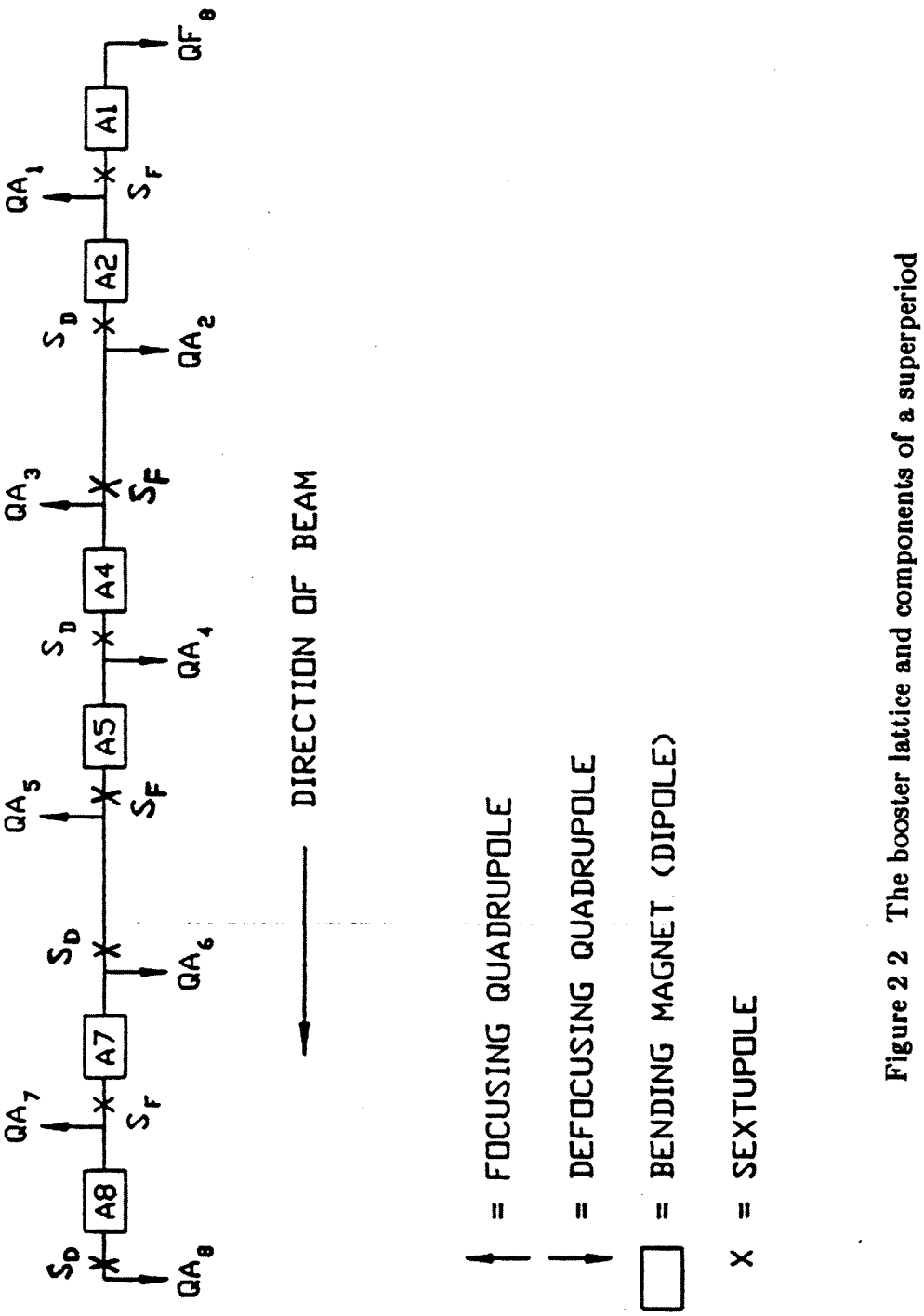

Figure 2 2 The booster lattice and components of a superperiod

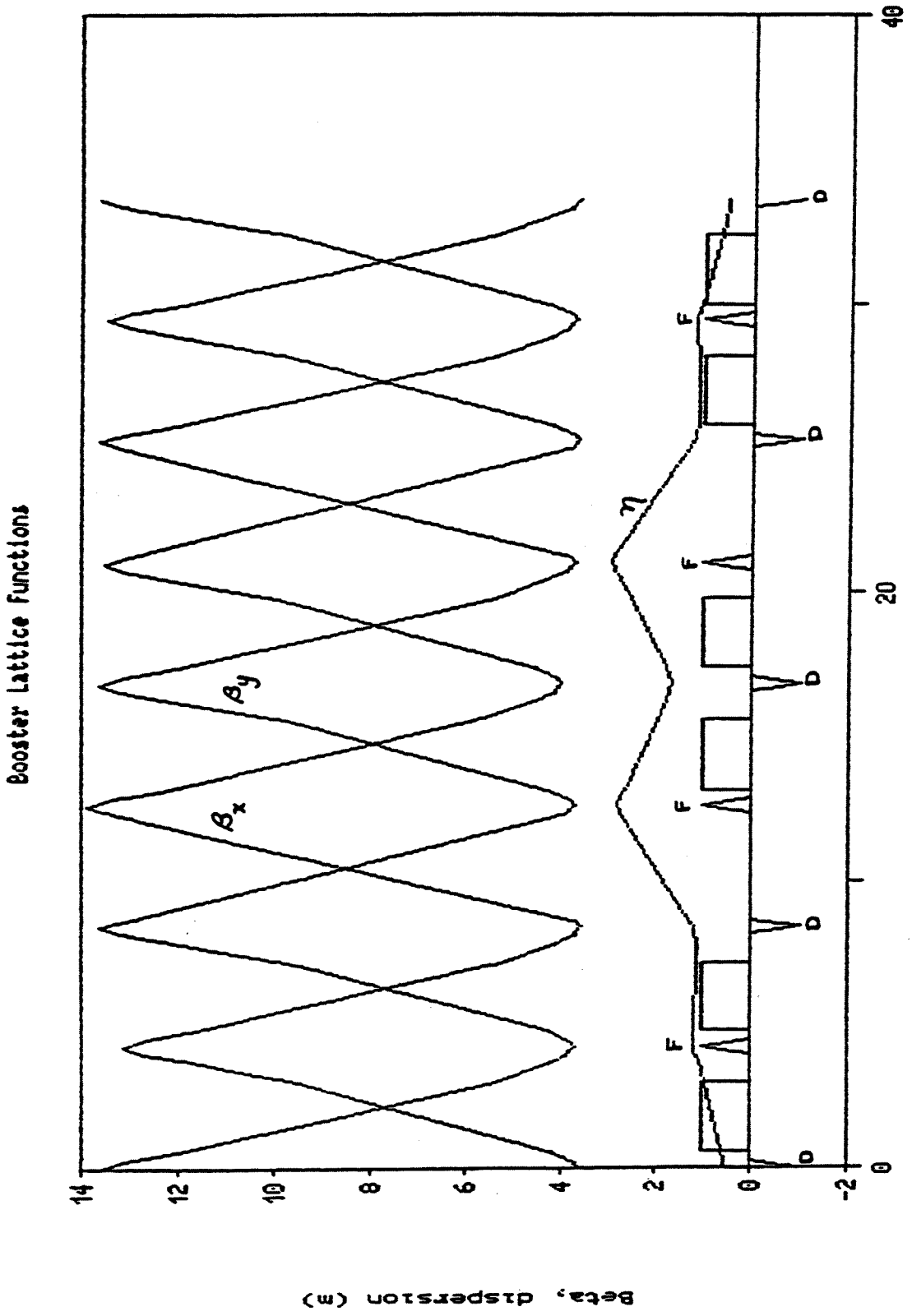

Figure 2 3 Amplitude and dispersion functions for the Booster lattice

The sensitivity of the particle motion to the error of the magnetic alignment can be expressed in the closed-orbit error and the half-integer stop band. The booster is a small accelerator in comparison with the AGS and RHIC and is less sensitive to errors. The expectation values of the closed orbit distortion can be expressed as,

$$\sigma_{x,y} = 7.5\ \sigma_{\Delta x,\Delta y}$$
$$\sigma_x\ (\mathrm{m}) = 3.7\ \sigma_{\Delta B/B}$$
$$\sigma_y\ (\mathrm{m}) = 2.7\ \sigma_{\Delta\theta}\ (\mathrm{rad})$$

where $\sigma_{\Delta x,\Delta y}$, $\sigma_{\Delta B/B}$, and $\sigma_{\Delta\theta}$ are the quadrupole misalignment, the dipole field, and the dipole rotation errors (rms), respectively The half-integer stop-band width is

$$\delta\nu = 3.7\ \sigma_{\Delta G/G}$$

where $\sigma_{\Delta G/G}$ is the quadrupole gradient rms error.

2.2.1. Natural Chromaticity

The natural chromaticities of the booster at the selected operating point of ν_x=4.820, ν_y=4.830, are ξ_x=−5.093 and ξ_y=−5.447 in the horizontal and vertical planes, respectively

2.2.2. Eddy Current and Saturation Effects

2.2.2.1. Eddy Current Multipoles

Vacuum chambers having Inconel walls will be used in both the dipoles and quadrupoles; the wall thickness for the dipoles chambers is 2 mm, and that for the quadrupoles is 0.065″ The maximum B (8 T/s) is reached when B_o=2.4 kG. The conductivity of Inconel is 57% that of 316L stainless steel.

Studies of eddy current effects from the dipole vacuum chambers have been based on B_o=1.56 kG, B=5 T/s, and a chamber of 316L stainless steel having a wall thickness of 1.5 mm. Eddy current multipoles generated for a stainless steel chamber are listed in Table 2-2. Eddy currents in the Inconel chamber are expected to scale linearly from the stainless values with conductivity, wall thickness, B, and inversely with B_o Hence, the ratio of eddy current effects for the Inconel and stainless chambers is expected to be:

$$(\mathrm{Inconel/stainless}) = 0.57 \times (2.0/1.5) \times (8/5) \times (1.56/2.4) = 0.79.$$

The ratio is close enough to unity to justify using the results of eddy current studies made for the stainless steel vacuum chamber Inclusion of sextupoles from eddy currents introduces an extra chromaticity of approximately 8 units in each plane, hence the net chromaticity is $\chi = +3.162$ and $\chi = -13.164$ in the x and y planes, respectively However the eddy current effects are time dependent — they vary with $B/B\rho$ and change throughout the acceleration period. With the exception of a short interval, early in the period, when B first becomes maximum, the eddy current effect is not as important as would be inferred from the multipoles of Table 2-2.

TABLE 2-2 Eddy current multipoles in the vacuum dipole chambers at maximum B/B

Multipole	Strength (m^{-n})
b_2	0.78
b_4	-2.4×10^1
b_6	-1.6×10^3

2.2.2.2. Multipoles from Dipole Saturation

The dipole field reaches 1.275 T during heavy ion acceleration. At this field strength, sextupole effects from magnet saturation are more important than the sextupoles due to eddy currents. The multipoles from saturation are listed in Table 2-3. The values are for a two-dimensional calculation; end effects will cause these multipoles to be larger

TABLE 2-3 Dipole saturation multipoles expressed as b_n (m^{-n})

Mult	B_o (T)					
	0.16	1.00	1.10	1.20	1.25	1.30
b_o	2.6×10^{-3}	-5.0×10^{-2}	-8.7×10^{-2}	-0.17	-0.24	-0.33
b_4	0.51	-9.73	-2.0×10^1	-4.1×10^1	-5.9×10^1	7.9×10^1
b_6	4.1×10^2	-1.2×10^3	-3.3×10^3	-6.1×10^3	$-7\ 4 \times 10^3$	7.8×10^3
b_8	6.6×10^5	-6.6×10^5	0.0	0.0	0.0	0.0
b_{10}	0.0	0.0	0.0	0.0	0.0	0.0

2.2.3. Correction Sextupoles

Correction sextupoles consist of three types: 1) two families of sextupoles, SF and SD to adjust the overall chromaticity of the lattice to the desired value, 2) correction coils to compensate effects of dipole rotation and variation of eddy current effects from chamber to chamber, and 3) coils on the vacuum chamber to compensate for eddy current effects. The sextupoles used to adjust the chromaticity are discussed in the next section. These sextupoles have a nominal effective length of 10 cm and are located with their centers 30 cm upstream of the quadrupoles.

2.2.4. Chromaticity Correction

Several schemes for chromaticity correction have been considered; however extensive studies show that placement of sextupoles in all half cells results in low sextuple strengths and in improved performance over a large range of final chromaticities; this scheme has been selected for use in the Booster The results presented in the following sections have been obtained with this sextupole configuration.

The sextupole strengths needed to correct the natural chromaticity as well as the extra chromaticity due to eddy currents are listed in Table 2-4.

TABLE 2-4 Sextupole strengths for correcting the chromaticity to zero.

Chromaticity	Integrated Strength	
Natural (-5.093,-5.447)	SF -0.1822	SD 0.2950
Nat. + Eddy (+3.162,-13.164)	SF -0.03982	SD 0.4905

Units of SF and SD are m^2

Tracking studies for $\epsilon_x = \epsilon_y = 50\pi$ mm-mrad indicate a broad valley, centered around the natural chromaticity, in which there is little transfer of emittance between the horizontal and vertical motion (See Figure 2-4). There is a large chromaticity interval over which motion in the horizontal and vertical planes is loosely coupled.

Saturation effects become important for heavy ion acceleration; the contributions to chromaticity from eddy currents and saturation are shown in Figure 2-5.

The sextupole strengths, SF and SD, listed in Table 2-4 are related to the integrated sextupole field by the relation:

$$\Delta B_2 l = 0.5\ S\ B\rho \quad (\mathrm{T/m}).$$

The maximum values of $\Delta B_2 l$ during acceleration are listed in Table 2-5.

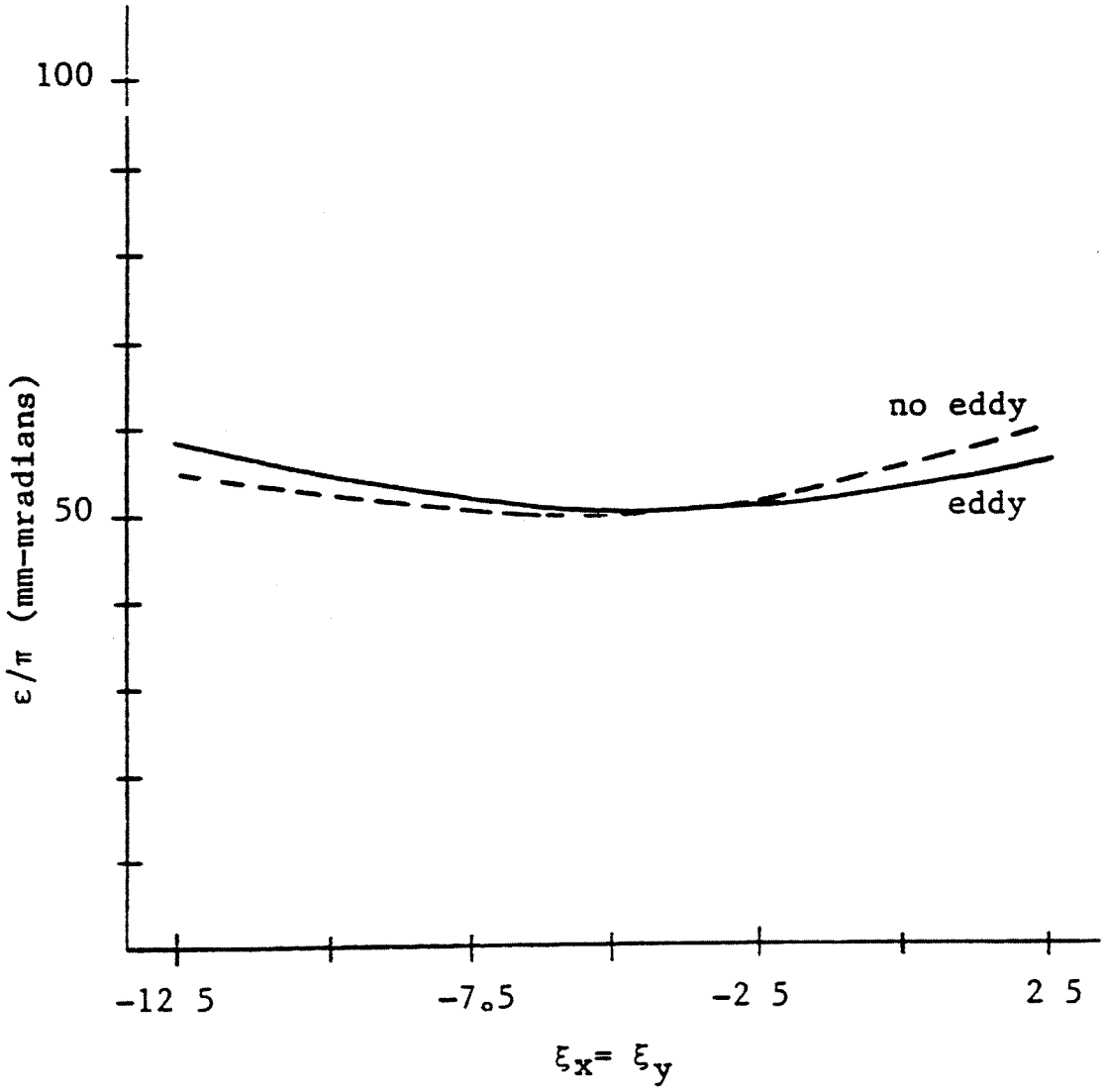

Figure 2-4. Chromaticity scan showing maximum emittance of a particle during a 600 turn tracking run.

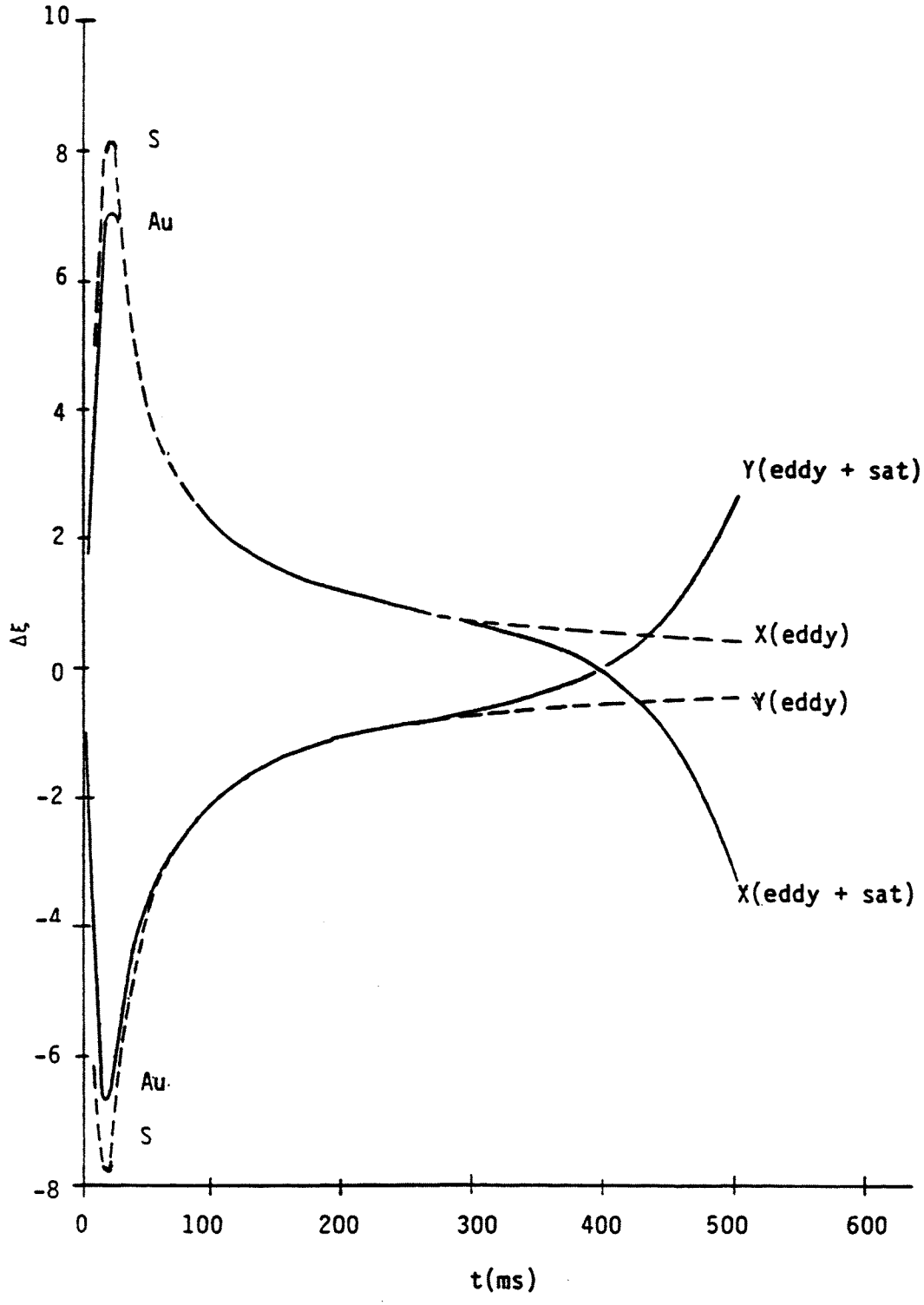

Figure 2-5. Time dependence of the chromaticity change.

TABLE 2-5 Maximum $\Delta B_2 l$ (T/m) required for correcting the chromaticity of the AGS-Booster to 0.0 or −5.0.

	Final Chromaticity			
	Protons		Heavy Ions†	
	0.0	-5.0	0.0	-5.0
SF	-0.4	0.28	2.2	-0.55
SD	1.5	0.48	1.9	-0.50

†indicates the inclusion of saturation multipoles

The maximum pole tip fields corresponding to the largest values of $\Delta B_2 l$ of Table 2-5 have been determined for sextupoles with 10 cm length and bore radius of 8.26 cm. These values are listed in Table 2-6.

TABLE 2-6 Maximum sextupole pole tip fields for realistic proton and heavy ion acceleration cycles. A sextupole bore of 16.52 cm is assumed.

Maximum Pole Tip Fields (kG)			
Protons		Heavy Ions	
Chromaticity		*Chromaticity*	
0.0	-5.0	0.0	-5.0
1.02	0.33	1.50	0.04

2.2.5. Dynamic Aperture

The term "dynamic aperture" is used to indicate the maximum initial amplitude for which betatron motion is stable. Tracking studies at zero chromaticity, $\xi_x = \xi_y = 0$, and equal initial emittances, $\epsilon_x = \epsilon_y$, indicate stable motion for initial amplitudes at the QF quadrupoles of x=85 mm and y=45 mm. The dynamic aperture over the momentum interval, $-0.5\% \leq \Delta p/p \leq +0.5\%$, required for the Booster is much larger than the aperture of the vacuum chamber The values of x and ϵ_x/π obtained for the dynamic aperture are listed in Table 2-7

TABLE 2-7 Dynamic aperture of the AGS Booster with the eddy current multipoles of Table 2-2 included.

Initial conditions: $\epsilon_x = \epsilon_y$ and $x' = y' = 0$.

	$\Delta p/p$ (%)				
	-0.50	-0.25	0.0	0.25	0.50
x_i (mm)	67	75	85	80	82
ϵ_x/π (mm-mrad)	330	420	530	480	490

Complete coupling between the x and y motion would limit the total emittance, $\epsilon_t = \epsilon_x + \epsilon_y$, that could be contained in the vertical aperture to 60π mm-mrad, or to y_{max} = 29 mm. Consequently most tracking has been performed using emittances that correspond to those required for Booster operation and not those that correspond to the dynamic aperture. Typically, initial emittances of $\epsilon_x = \epsilon_y = 50\pi$ have been used for aperture studies, even though this corresponds to a total emittance that is larger than the vertical acceptance of the vacuum chamber Results are shown in Figure 2-4 for the maximum emittance of a test particle in either the x or y plane during a 600-turn run when the initial emittances are $\epsilon_x = \epsilon_y = 50\pi$ mm-mrad. There is a broad valley in which the emittance increases little from its initial value. The small coupling should permit operation with beam profiles having $\epsilon_x > \epsilon_y$.

2.2.6. Correction Coil on Vacuum Chamber

The results of Figure 2-4 were obtained when all eddy current multipoles were included; their effects were compensated by the lumped sextupoles, SF and SD Local correction of the eddy current effects with a three-turn loop on the top and bottom of each dipole vacuum chamber is being considered. This strategy would allow the SF and SD sextupoles to be set to the "natural chromaticity" values listed in Table 2-4. These loops could be connected to a special secondary winding included in each dipole to assure that the sextupole compensation tracks the B responsible for generating the eddy current sextupoles. However, if desired, they could be powered externally and programmed to compensate for sextupoles from eddy currents plus magnet saturation. Using the b_2 from Table 2-2, a field of 8.6 gauss would compensate the sextupole field from saturation at a distance of 10 cm from the chamber axis when the magnetic field is B=1.275 T

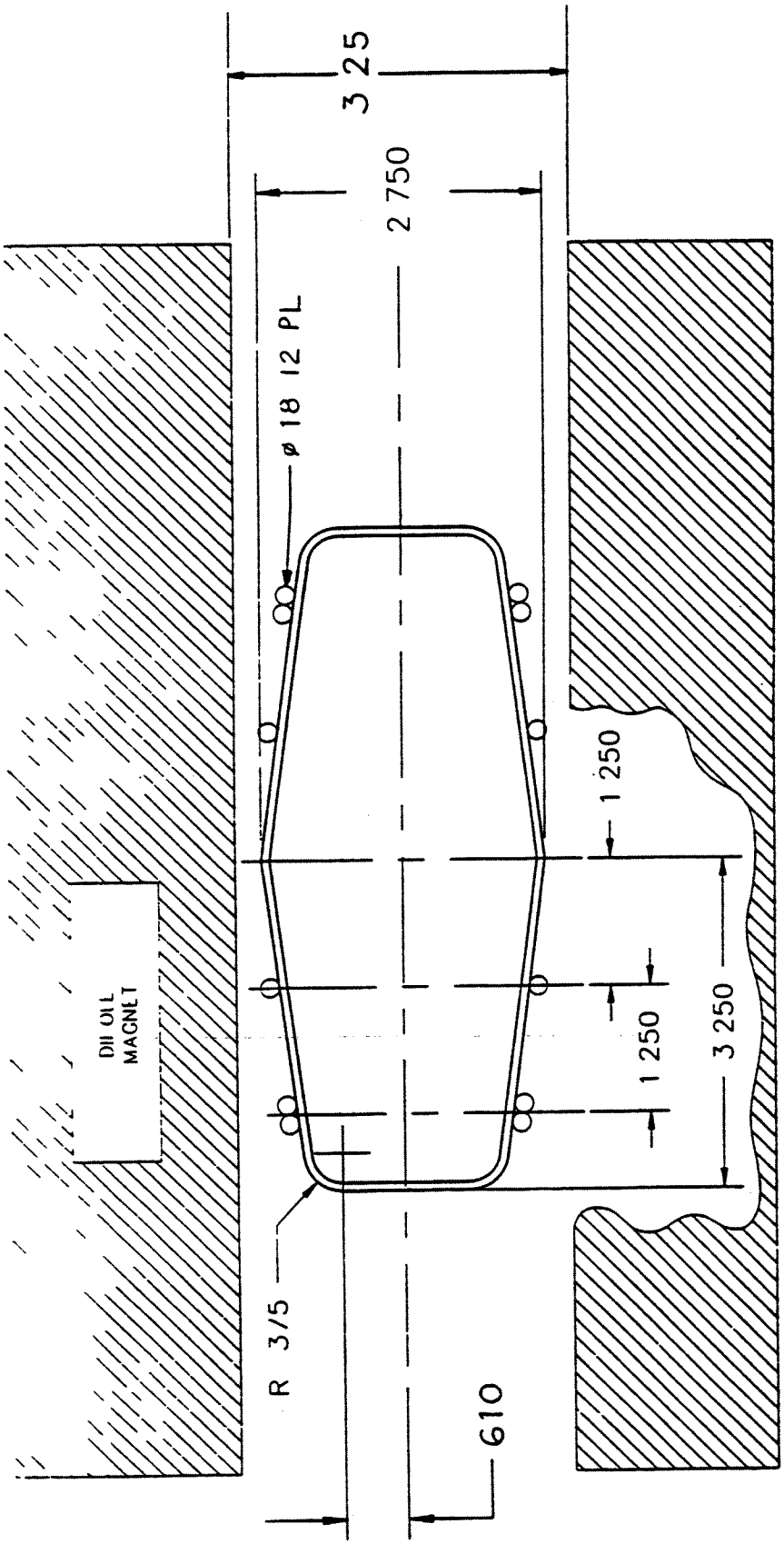

Figure 2 6 Three turn loop on top and bottom of dipole vacuum chamber for local correction of eddy current effects

2.3. Closed Orbit in the AGS Booster

To estimate the expectation value of the closed orbit distortion in the AGS Booster we have assumed the following misalignment and field errors[1].

(1) Dipole field error Random variation from magnet to magnet with gaussian distribution and rms error

$$<\frac{\Delta(Bl)}{B\rho}> = 3 \times 10^{-4}$$

(2) Dipole axial rotation — Random variation from magnet to magnet with gaussian distribution and rms error for the rotation angle

$$<\theta> = 3 \times 10^{-4} \text{ rad}$$

(3) Random variation of quadrupole lateral displacement, horizontal and vertical, with gaussian distribution and rms error for the displacement

$$<d> = 3 \times 10^{-4} \text{ m}$$

Fig. 2-7 shows the expectation value of the closed orbit distortion with the errors above and uncorrected. The contribution from the several sources of errors are summarized in Fig. 2-8 for the case of the uncorrected machine.

To correct the closed orbit , the Fermilab method[2] has been examined. Pairs of beam position monitors and steering elements, located next to each other, are placed next to each quadrupole and divided into two families. Those pairs located next to QF act on the horizontal plane, and those next to QD on the vertical plane. The method applies a cascade of local three-bump corrections. Only linear lattice behavior is assumed in the algorithm.

Fig. 2-9 shows realistic closed orbit deviations before and after correction. The residual errors (< 1 mm) are caused by the presence of the sextupoles in the lattice which are not taken into account in the correction algorithm.

The required strength for the steering elements is

$$\int B\ dl = 60 \text{ Gauss—meters}$$

adequate for a maximum rigidity of 20 T-m.

2.4. Stopband Correction

2.4.1. Half-Integer Stopband Correction

The nominal values of the betatron tunes in the Booster are ν_H=4.82 and ν_V=4.83. There are four half-integer stopbands in the proximity of these values corresponding to the resonances: $2\nu_H$=10, $2\nu_V$=10 and, a little further away, $2\nu_H$=9, $2\nu_V$=9. These

---

[1] J. Milutinovic and A.G. Ruggiero. Booster Tech. Note No. **107** BNL, January 1988.

[2] R. Raja, et. al., "The Tevatron Orbit Program," *Nuclear Instrum. and Methods in Physics Research*, **A242** (1985), p. 15-22.

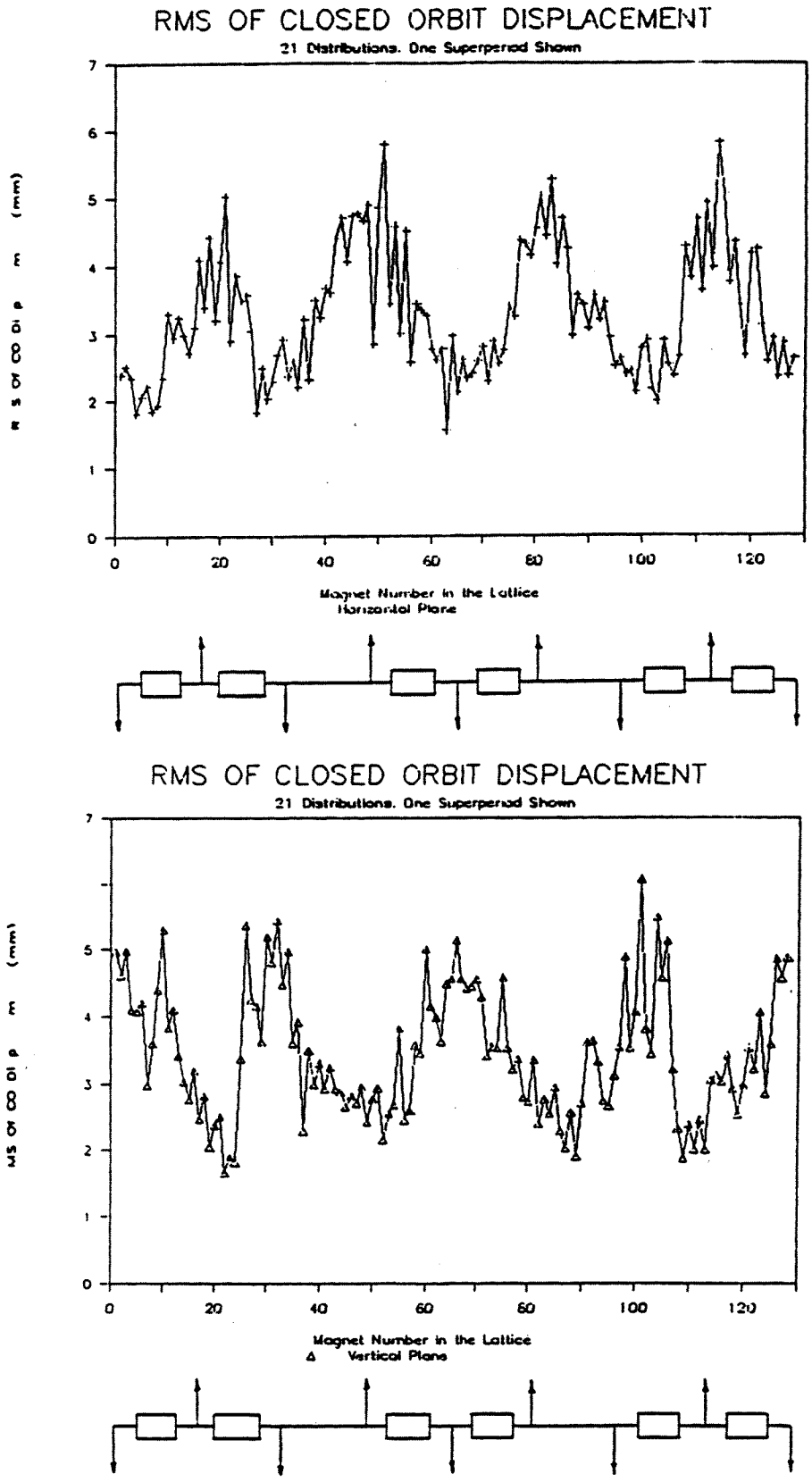

Figure 2-7 The expectation value of the closed orbit distortion with errors uncorrected.

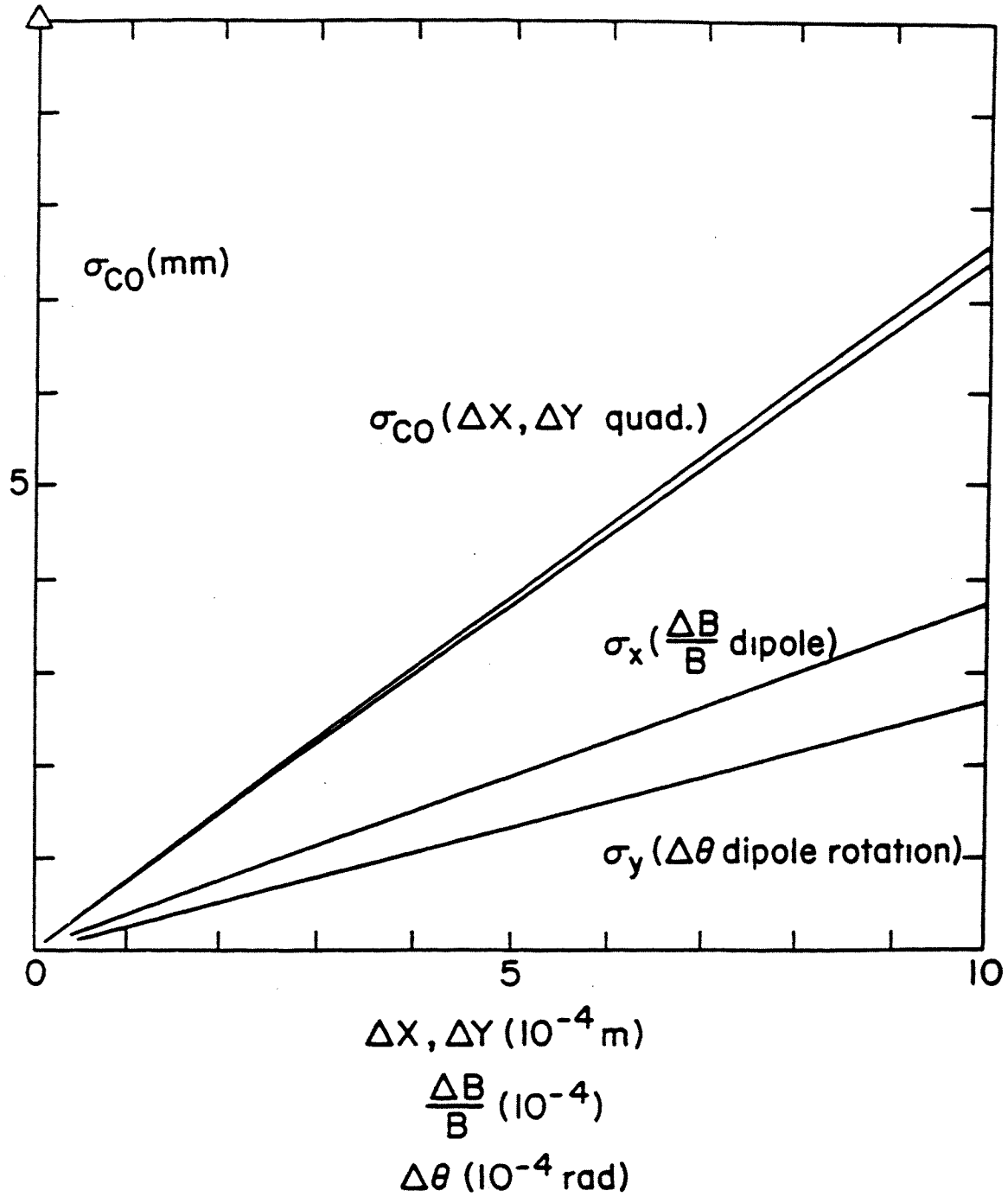

Figure 2-8. The contribution from several sources of errors for the case of the uncorrected machine.

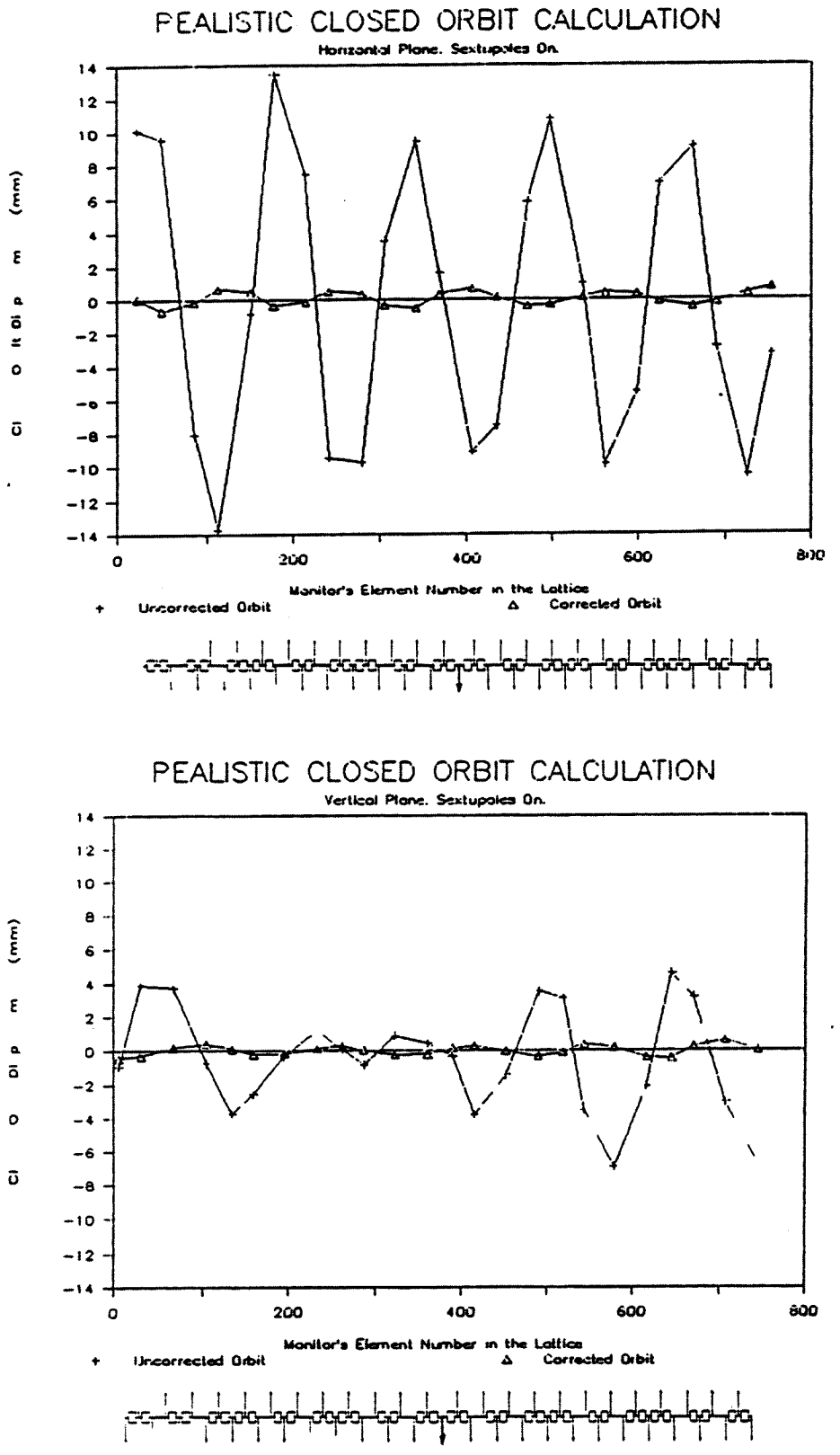

Figure 2-9. Realistic closed orbit deviations before and after correction.

resonances can be excited only by random quadrupole errors. Assuming an rms value of 10^{-3} for the relative integrated gradient error per quadrupole, the rms expectation values of the stopband widths are

$$\delta\nu_H = 0.0035 \quad \text{and} \quad \delta\nu_V = 0.0038$$

sufficiently small so that during most of the accelerating cycle in the booster they are expected to be of no consequence. The exception is during injection, when the tune spread within the beam, about 0.3 (created by space charge), is so large that part of the beam might have to cross one of the neighboring stopbands during the bunching process and the early stages of acceleration.

Half-integer stopband correctors are located in each of the 48 quadrupoles. The corrector is made of a special coil winding along the length of the quadrupole. The maximum strength corresponds to about 1% of the full magnet excitation, which corresponds to the case of beams of ions of gold at top energy The correctors[3] are arranged in eight families as shown in Figure 2-10. All the correctors in one booster period are independently adjusted, but they are all connected by the same power supply bus to the corresponding one in the other periods. Thus, in principle, the width and phase of the nearest four stopbands can be corrected, since each stopband correction requires two sets of correctors. The linear tune-shift introduced can be compensated with the main QF and QD quadrupole windings.

At the maximum strength of the correctors, it is possible to compensate for a stopband width as large as 0.01 at injection with any phase angle and all four near half-integer resonances simultaneously The resulting, uncorrected, tune-shift is small and does not exceed 0.02.

2.4.2. Third-Order Resonance Correction

The Booster has a large tune spread and strong eddy-current sextupoles at injection. As a result, particles in the beam may cross four major third-order resonances during the injection process, rf capture, and early stages of acceleration. These resonances can be excited only by random sextupole field errors around the machine and are

$$3\nu_H = 14$$
$$2\nu_H + 2\nu_V = 14$$
$$3\nu_H = 13$$
$$\nu_H + 2\nu_V = 13$$

We have examined two sources of random errors: 1) from eddy currents in the dipoles at injection, and 2) from errors in the chromaticity sextupoles[4] Each of these errors introduces a resonance width (and a phase) around each of the resonances listed above. These

---

[3] A. G. Ruggiero, to be published as a Booster Technical Note, December 1988.

[4] S. Tepikian, BSTN No. **125**, August 5, 1988.

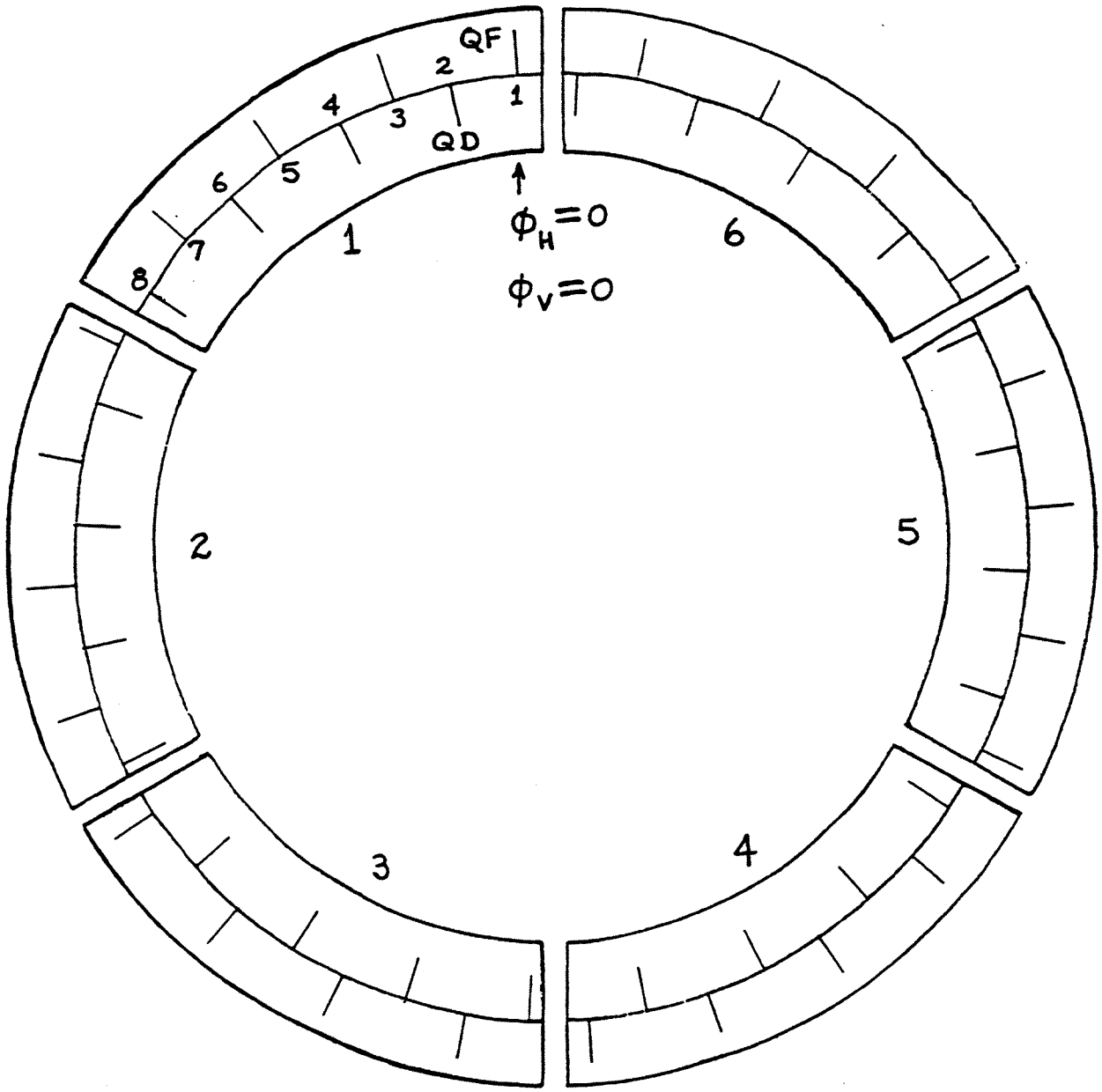

Figure 2-10. Corrector arrangement for half-integer stopband correction.

imperfection resonances can be cancelled by including sextupole correctors in the chromaticity sextupole magnets. Each resonance requires two sets of correctors for cancellation: amplitude and phase. Thus a total of eight independent sets of correctors are required if the four resonances ar to be controlled simultaneously Moreover, the correction scheme should leave unchanged the chromaticity in both planes to the desired values.

The sextuple correctors are made of extra coil windings available in each chromaticity sextupole magnet. The excitation of the corrector is independent from the main one and the maximum value corresponds to about 1% of the maximum excitation of the corresponding magnet. Since there are two families each of 24 main sextupoles, there are then 48 independent correctors. They are connected to each other as shown in Fig. 2-11 which shows also the connections among the stopband correctors. There are eight families of correctors, all independent from each other Each period of the booster has all the correctors in sequence. Correctors of the same family are connected to each other with a predetermined phase relation from one period to the next. The phase value depends on the correction requirement and will be an input to the software available during control and operation of the machine.

The maximum pole tip field of 35 gauss is required to correct for all four third-order resonances caused by random sextupole fields from 10% of the systematic eddy current effect. The effect of 0.1% error in the chromaticity sextupole is found to be negligible.

2.4.3. Skew Quadrupole Correctors

There are two sources of skew quadrupole errors: 1) rotation of the quadrupole magnets, and 2) vertical displacements of the sextuples. These misalignments can generate the following resonances:

$$\nu_x - \nu_y = 0$$
$$\nu_x + \nu_y = 9$$

The first resonance is the induced coupling which would contribute to the smear The second resonance can be crossed due to the large space-charge tune shift at injection.

To correct these two resonances, we must correct both the amplitude and phase of each resonance. This leads to four conditions that must be satisfied. Thus, a total of four independent sets of correctors are required.

The skew quadrupole correctors will be placed in the trim coil assembly as shown in Fig. 2-12. In each superperiod, there will be two correctors in the first cell and two correctors in the third cell. This leads to a total of 24 skew quadrupole correctors in the entire ring. Four families of correctors correspond to the four correctors in each superperiod. However, the strength of the skew quadrupoles from one superperiod may differ from the next superperiod. These differences are due to phase differences between the superperiods and the harmonic number of the resonance.

For 0.3 mm vertical displacements of the sextupoles (and dipoles which includes the eddy current sextupoles at injection) whose center may vary by $\pm$0.3 mm from the center of the dipoles and 0.3 mrad rotational errors in the quadrupoles (note, three standard

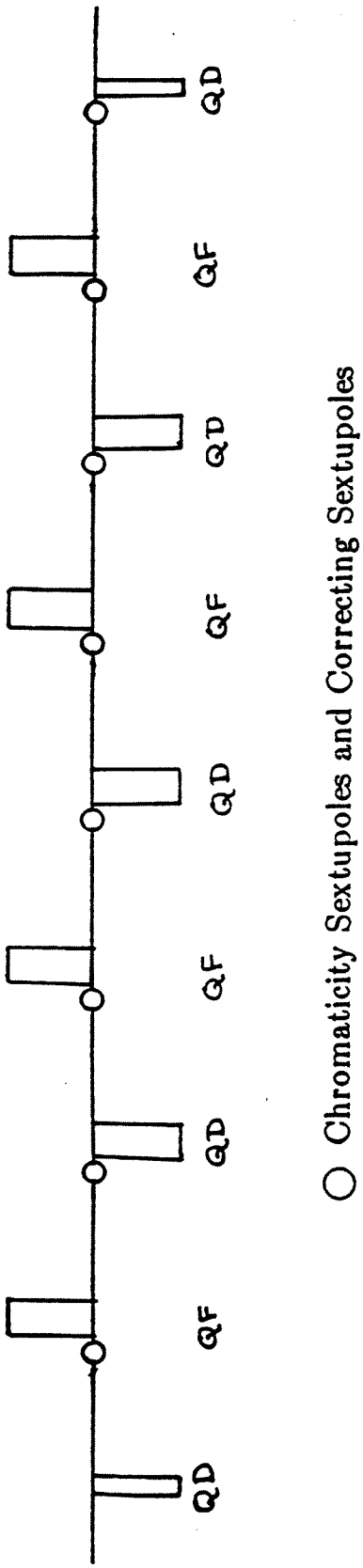

Figure 2 11 Sextupole corrector arrangement for correction of third order resonances

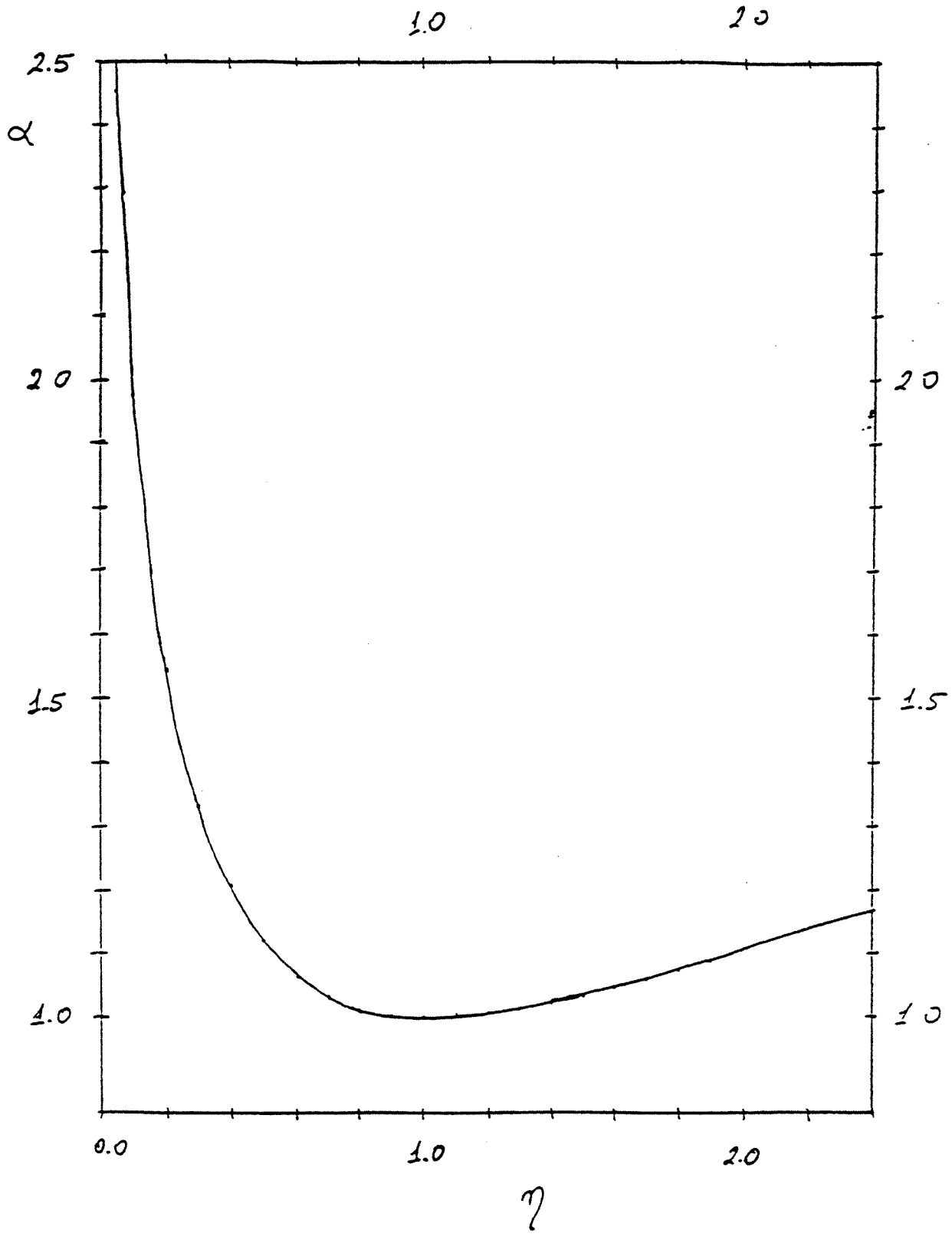

Figure 2-13. α vs. η.

where ϵ is in π mm-mrad. For a uniform distribution ϵ is the full emittance of the beam. For a gaussian distribution ϵ is the emittance of the contour at $\sqrt{2}$ times the standard deviation σ

The tune depression $\Delta\nu_V$ is plotted in Fig. 2-14 versus the beam emittance for different bunching factors.

2.6. Longitudinal Motion

2.6.1. RF Capture

RF capture will be different for each of the three modes of operation of the Booster In each case the rf frequency will be three times the particle revolution frequency, hence there will be three rf buckets. For protons and heavy ions the capture process will result in a considerable increase in the longitudinal phase-space area of the injected beam. On the other hand, for polarized protons the increase can be less than 50%, if necessary, but for all species the final bunch area will be determined by the capture parameters, i.e. RF voltage, B and the frequency program at injection.

A computer simulation was run for Au^{+33} using an initial voltage of 1.6 kV which for ϕ_s=0 results in buckets of height $(\Delta p/p) = \pm 5.4 \times 10^{-3}$ This is an order of magnitude greater than the $\pm 0.5 \times 10^{-3}$ momentum spread (due primarily to the stripping process) expected in the injected beam. When the cycle is continued as described in Section 2-2.6.1.2, more than 93% of the beam should be captured in an area of 0.06 eV-s/nucleon.

Proton injection from the 200 MeV linac results in a momentum spread of $\pm 1.1 \times 10^{-3}$ corresponding to a total phase-space area of 1 eV-s for three bunches. For polarized protons, B=0 during the multicycle filling process from the linac. Thus, adiabatic capture into three buckets each of 0.4 eV-s at ϕ_s=0 can be used without significantly adding to the overall cycle time for this mode of operation. This type of capture process results in high capture efficiency (>95%) while minimizing the aperture required for synchrotron oscillation. (The bucket height will be $\leq 2.5 \times 10^{-3}$ in $\Delta p/p$)

In the high-intensity proton case the requirements are minimum acceleration time, high capture efficiency, and large bunch area. These goals will be accomplished by using a large voltage during capture and acceleration along with large initial and final B's or magnetic field rise rates. The rf voltage will be 45 kV during the injection process and then it will be rapidly increased to 90 kV in order to capture additional particles. Initially B = 1.5 T/s so that the bucket area at 90 kV and a ϕ_s = 2.6 will be 1.5 eV-s with a height of $\Delta p/p = \pm 8.7 \times 10^{-3}$ The bunch length will be 320 resulting in a bunching factor of 1.7 for a uniform distribution in longitudinal phase space.

Booster $N = 5 \times 10^{12}$ in 3 bunches

AGS $N = 1.25 \times 10^{12}$ in 12 bunches

($\varepsilon_N = 20\pi$ mm mrad $\rightarrow$ $\varepsilon = 30\pi$ mm mrad)

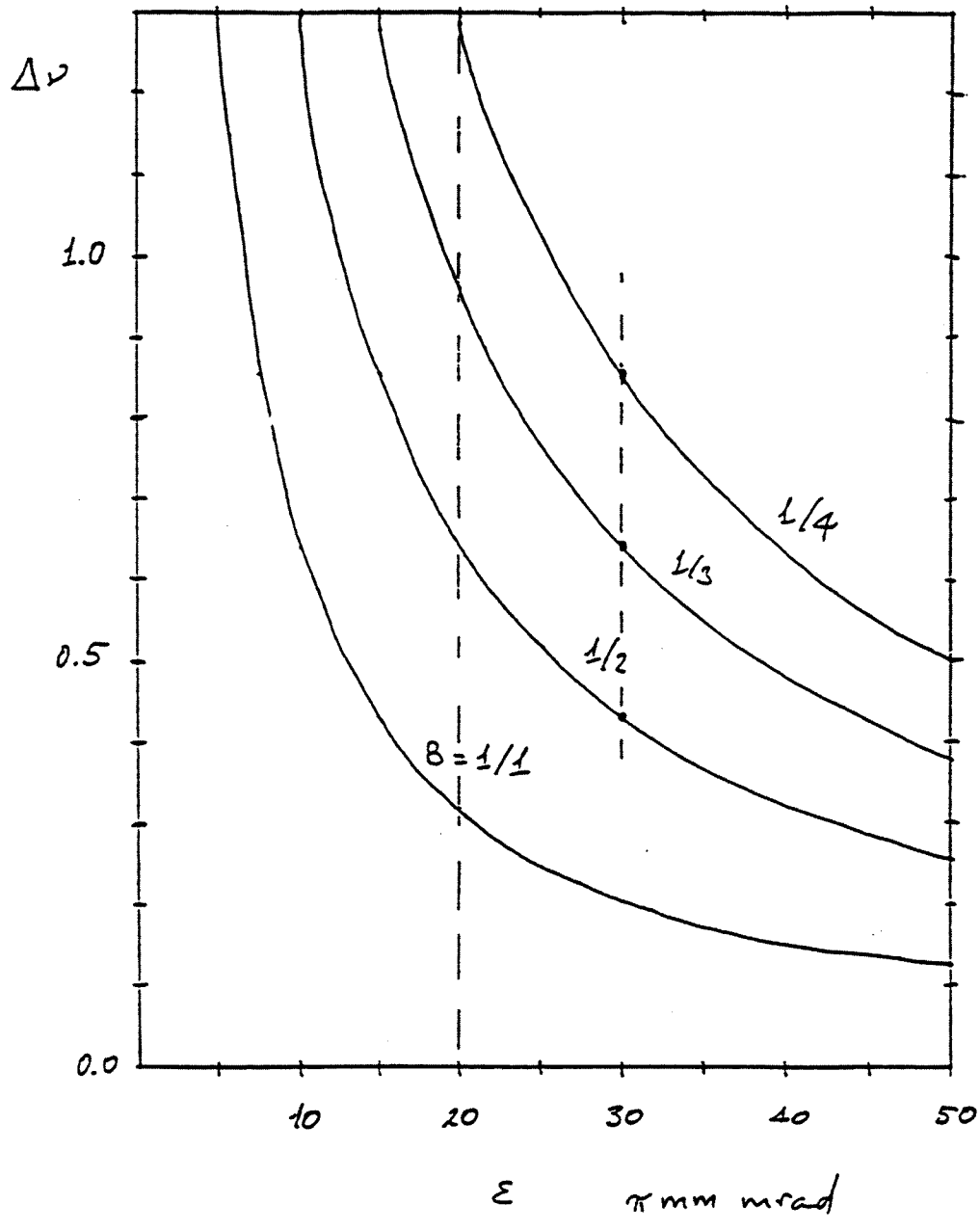

Figure 2-14. Tune depression $\Delta\nu$ vs. beam emittance.

2.6.1.1. RF Capture — Protons

Protons are injected into the booster from the 200 MeV linac, with an energy spread of 0.2 MeV The macropulse from the linac is approximately 100 μs long, hence the process of injection is multiturn. The revolution period of the booster at 200 MeV is 1.19 μs: the injection takes 84 turns to be completed.

The proton intensity goal is $N = 1.5 \times 10^{13}$ in three bunches, or 5×10^{12} protons per bunch. The longitudinal capture efficiency of the protons in the rf buckets is affected by several factors, among which we consider space charge and beam-to-wall longitudinal coupling impedance. These effects have been studied by computer simulation, with a modified version of the simulation code ESME of Fermilab.[6]

Space charge and wall impedance effects can be described by means of an additional voltage acting on the protons in the bucket, superimposed on the rf accelerating voltage, expressed by

$$\delta V = \mathrm{Re}\left[\sum_n Z_n I_n\right]$$

where I_n is the nth harmonic component of the beam current

$$I_n = eN\omega_{rf}\, a_n\, e^{j(n\theta + \theta)}$$

with a_n and θ_n the amplitude and phase of the component. Z_n contains two components: a contribution due to space charge Z_n^{sc} and a contribution Z_n^W expressing the beam-to-wall impedance.

The longitudinal space-charge impedance is an imaginary quantity given by

$$\frac{Z_n^{sc}}{n} = -j\frac{Z_o\, g}{2\beta\gamma^2}$$

where $n = \omega/\omega_{rf}$ is the beam harmonic number, $Z_o = 377\ \Omega$, the impedance of free space, β and γ the usual relativistic parameters, and g is a form factor[7]

$$g = 1 + 2\ln\frac{b}{a}$$

Here, we have assumed a cylindrical geometry of a proton beam of radius a in a round beam pipe of radius b

The longitudinal beam-to-wall coupling impedance is a complex quantity

$$Z_n^W = |Z_n^W|\, e^{j\chi_n}$$

of amplitude $|Z_n^W|$ and phase χ_n

With $a = 2.5$ cm and $b = 7.5$ cm, it is obtained $Z_n^{SC} = -j\ 700\ \Omega$ at injection energy, and $Z_n^{SC} = -j\ 100\ \Omega$ at extraction (1.5 GeV proton kinetic energy). The

---

[6] J. A. MacLachlan, *Proc. of IEEE Particle Accel. Conf.*, 1087 (1987).

[7] C. E. Nielsen and A. M. Sessler, *Rev. Sci. Inst.* **30**, 80 (1959).

absolute value of the additional acceleration due to space charge, averaged over the proton bunch, at completion of the multiturn injection, is 6.5 KeV This effect, due to the distribution of the space charge voltage inside the proton bunch, tends to increase the size of the phase space area occupied by the beam in the bucket.

To optimize the longitudinal capture efficiency, defined as the fractional number of particles contained in the rf buckets at a given time, several rf voltage and dipole magnetic field vs. time curves have been investigated. For multiturn injection in the presence of substantial space charge and continuous linac beam during its macropulse, it is found that a good strategy is to maintain the rf voltage constant to 45 kV during injection and to increase it to 90 kV afterwards, as shown in Fig. 2-15 The booster magnetic field will be kept constant in this case, for injection at constant proton energy, and then it will be raised to its final value, corresponding to the proton kinetic energy of 1.5 GeV at 60 ms.

In these conditions, the area of the rf buckets start at a value of 1.2 eV-s, and reach a value of 1.7 eV-s at the end of the injection process. Capture efficiency by the end of injection is approximately 90% in this case, but it tends to drop steadily due to a gradual spill of the protons captured at phase angles close to $\pm \pi/3$.[8]

To counteract this effect, a possibility is to modulate or chop the linac beam in order to fill the buckets more efficiently At the same time, the dipole magnetic field in the booster ca be raised during injection, thus producing a larger bucket. It was indicated by computer simulation that an efficiency of capture of 98% can be obtained by (i) raising the field vs. time during injection according to a 3/2 power curve, (ii) at the same time chopping the linac beam by 5 on each side of every bunch (reducing by about 8% the total beam delivered by the source), and (iii) start injection at a slightly higher energy than the center of mass of the bucket at time t=0. Under these conditions, the initial bucket area is 1.5 eV-s and the rate of increase of the magnetic field at 1 ms is 1.23 T/s.

Beam-to-wall coupling impedances are not yet well known for the booster Available data seem to indicate that the space-charge effect is dominant, and also that an effect of wall impedance is to produce coherent oscillations of the beam in the bucket and then of the capture rate around values well in excess of 90%.[9]

2.6.1.2. RF Capture — Heavy Ions

The beam of heavy ions comes from the Tandem Van de Graaf accelerator Due primarily to the stripping process, the beam has a r.m.s kinetic energy spread of $\pm 0.5 \times 10^{-3}$ Each single pulse of the 300 μs $^{197}Au^{+33}$ ions is able to provide about 20 booster revolutions of "ribbon" beam. The RF frequency is three times the particle revolution frequency For the $^{197}Au^{+33}$ ions, the goal is a beam intensity of 2.2×10^9 particles per RF bucket.

---

[8] F Z. Khiari, A. U Luccio and W T. Weng, BSTN No. **118**, April 25, 1988.

[9] F Z. Khiari and A. U. Luccio, BSTN No. **128**, August 22, 1988.

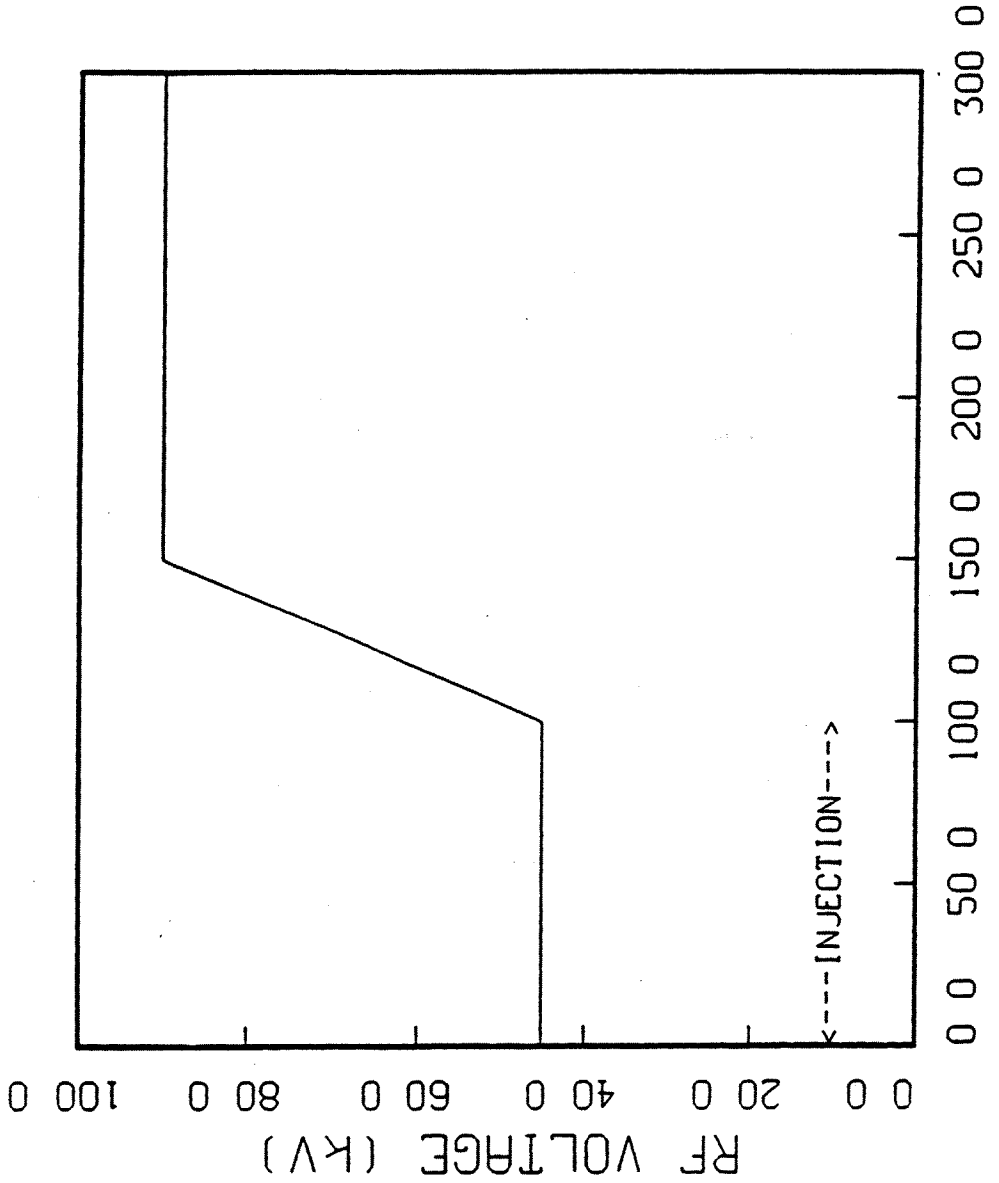

Figure 2 15 RF voltage program for maximizing capture efficiency

In a computer simulation[10] of the multi-turn injection of $^{197}Au^{+33}$ ions, a 1.6 kV RF peak injection voltage was chosen. The initial synchronous phase was as small as possible to optimize the capture efficiency At injection this gave a bucket area of 0.07 eV-s/nucleon, and a bucket height of $\Delta p/p = \pm 5.4 \times 10^{-3}$ (Note that the voltage program used in this simulation differs from the one proposed in Chapter 10, section 10.2, which has not been simulated.)

The capture efficiency and the final bunch area are essentially determined by the programming of the RF parameters. At injection, the synchrotron oscillation period is 2 ms. During the capture process, the peak RF voltage and the synchronous phase angle were smoothly and adiabatically raised in about 10 ms, from 1.6 kV and 0 radians to 17 kV and 0.6 radians. This type of programming resulted in a high capture efficiency During this time, the bunch area was preserved and was less than 0.07 eV-s/nucleon.

The space-charge voltage induced by the circulating beam provides a defocusing force and thus increases the bunch area. The computer simulation results are summarized in Table 2-8. Ninety-four percent of the $^{197}Au^{+37}$ beam is finally captured. The beam-populated longitudinal phase-space area is 0.06 eV-s/nucleon.

TABLE 2-8 RF capture efficiency for a multi-turn injected beam of $^{197}Au^{+33}$ ions.

RF Programming	Space Charge	Bunch Area	Capture Efficiency
V 1.6 — 17 kV	w/o	0.05 eV-s/nucleon	94.1%
ϕ_s 0 — 0.6 rad 10 ms	w/† 2.2×10^9 per bunch	0.06 eV-s/nucleon	93.8%

†Calculation performed using three-point formula, 200 bins, 2000 representative particles.

2.6.2. Beam Loading Compensation

Significant transient beam loading will occur in the Booster only during the rf capture process in the high intensity proton case. The component of circulating beam current at the rf frequency of 2.5 MHz will go from zero to 5 amperes in about 0.5 ms. In order to eliminate the effect of the voltage induced by this current in the accelerating cavities on the capture process, a feed-forward compensation scheme will be employed. The rf component of the bunch signal induced on a pickup electrode will be phase shifted, amplified and added to the drive voltage applied to the power amplifier that

[10]J. Wei and S. Y Lee, BSTN No. **102**, December 8, 1987

excites the cavity so as to cancel the beam current signal. Once the capture process is completed this_compensating signal can be removed since the normal phase, amplitude and tuning loops can provide adequate control thereafter

2.6.3. Robinson Instability

In addition to the transient beam loading mentioned previously there is a static beam loading condition that must be considered when accelerating the high intensity proton beam. In the absence of control loops, phase stability of the bunches (due to that part of the total cavity voltage arising from the power amplifier current) will be lost when the power supplied to the beam is equal to the power dissipated in the cavities and the internal impedance of the amplifier With control loops closed it is possible to operate at or exceed this so called Robinson limit. In the Booster the maximum power delivered to the beam will occur at the end of the proton acceleration cycle. For 7.5×10^{12} proton/bunch it will be 131.7 kW so that at 70 kV total voltage one finds that the impedance looking into the power amplifier and cavity in parallel should be <4.65 kΩ per gap. The present design calls for an impedance of <2 kΩ/gap so that there is considerable margin for stable operation.

2.7 Coherent Instabilities and Damping

2.7.1. Transverse Single Bunch

In the worst case of no Landau damping, the growth rate of an instability within an individual bunch in the transverse plane is given by

$$\tau^{-1} = \frac{I_p r_o}{e \nu \gamma Z_o} \mathrm{Re}\left(Z_\perp\right)$$

This formula is valid in the case that the growth rate is larger than a synchrotron oscillation period (fast head-tail instability). For a slower rate, one would recover the conventional head-tail instability that can be controlled by letting the chromaticity take a slightly negative value. (We are below the transition energy at all times!) Only the real part of the transverse coupling impedance $Z_\perp$ gives a contribution to the instability growth rate. The other parameters are: I_p, the bunch peak current, $r_o = 1.535 \times 10^{-18}$ m, the classical proton radius, ν the betatron tune, and $Z_o = 377\ \Omega$.

We could identify only the resistivity of the wall as the major contributor to the real part of $Z_\perp$, especially in the low frequency range. Inserting the values, we obtain for $\gamma \sim 1$, at injection,

$$\tau \approx 1 \text{ ms}$$

The imaginary part enters in the stability criterion that can be written as

$$\left|Z_\perp\right| < \left(\frac{E_o}{e}\right) \frac{\pi \nu \beta \gamma}{I_p R} \left|(n-\nu)\eta + \xi\right| \frac{\Delta p}{p}$$

where $\Delta p/p$ is the bunch momentum spread, ξ the chromaticity, $\eta = \gamma_T^{-2} - \gamma^{-2}$ and R the average radius. Because of the large contribution of space charge to the transverse coupling impedance, the stability criterion cannot be easily satisfied. There is thus the need of a transverse active damper capable of acting on the bunches individually and able to provide a damping rate of at least 1000 s ^{1}

2.7.2. Longitudinal Single Bunch

To estimate the longitudinal stability of individual bunches in the AGS Booster one calculates the following complex quantity

$$U' - iV' = -i \frac{2eI_p \beta^2 (Z/n)}{\pi |\eta| E (\Delta E/E)_{FWHM}} \frac{Q}{A}$$

where

e	=	charge on the electron
Q	=	particle charge state
A	=	particle atomic mass number
β	=	ratio of particle velocity to speed of light = v/c
Z	=	the complex beam-environment coupling impedance
n	=	the harmonic number of the instability
E	=	the total energy *per nucleon* of the particle
$(\Delta E/E)_{FWHM}$	=	the full-width half-maximum relative bunch energy spread

Also

$$\eta = \gamma_T^{-2} - \gamma^{2}$$

where

$$\gamma = E/E_o$$

E_o = the particle rest energy *per nucleon*
and γ_T is evaluated at the Booster transition energy

Finally I_p is the bunch peak current

$$I_p = \frac{NQe\beta c}{\sqrt{2\pi}\sigma}$$

N = number of particles in a bunch
σ = rms bunch length

The bunches are assumed to have a bi-gaussian distribution.

If we define

$$I_\infty = \frac{NQec}{2\pi R} \text{ average current per bunch for } \beta \rightarrow 1$$

$$B = \frac{\sqrt{2\pi}\sigma}{2\pi R} \text{ bunching factor}$$

$$S = \pi\sigma_\tau\delta \text{ rms bunch area}$$

with $\sigma_\tau = \sigma/\beta c$
and $\delta = \Delta E/2.355$, rms energy spread
and $f_\infty = c/2\pi R$, revolution frequency for $\beta \longrightarrow 1$, then we can also write

$$U' - iV' = -0.18i \frac{eI_\infty E_0 \beta\gamma B(Z/n)}{f_\infty^2 |\eta| S^2} \frac{Q}{A}$$

In our notation $Z = X + iY$ with $X>0$ a resistance and Y is positive for a capacitive reactance and negative for an inductive reactance.

In the AGS Booster there are three modes of operation to consider:

(1) Acceleration of protons from 200 MeV to 1.5 GeV with 3 bunches. Each bunch has 5×10^{12} protons and an rms bunch area of 0.10 eV-s.

(2) Acceleration of heavy ions for RHIC in one single bunch. The beam parameters are those appearing in Table 2-9. In practice, each heavy-ion beam will be accelerated to a different β. (The Booster can accelerate heavy ions up to a magnetic rigidity of 17.52 T-m. The transfer line from the Booster to the AGS is designed to transport particles that have a magnetic rigidity equal to or less than 11.0336 T-m after further stripping in the extraction line. For the heavier ions the first limit is more restrictive, while for the fully-stripped or nearly fully-stripped ions, the second limit sets the maximum final energy.) The individual bunch rms area is 0.05 eV-s/nucleon.

(3) Acceleration of heavy ions for fixed target experiments following acceleration in the AGS. In this mode there are three bunches, each with an intensity three times smaller than in the previous mode for RHIC, and each with an rms bunch area of 0.015 eV-s/nucleon. The acceleration in the Booster is up to $\beta = 0.872$, but depends on the species being accelerated.

For all these modes of operation, the final energy is always below the Booster transition energy ($\gamma_T = 4.88$).

The largest contribution to the coupling impedance for the Booster is the "space charge"

$$\frac{Z}{n} = i \frac{Z_0 g}{2\beta\gamma^2} \qquad Z_0 = 377\,\Omega$$

where $g = 1 + 2\log(b/a)$ is 1 at injection and 4.5 at extraction for all modes of operation (for a long round beam of radius a moving in a circular pipe of radius b). The value of this impedance for the heavy-ion cases is given in Table 2-9. For the proton beam case

$$Z/n = i\,226\ \Omega \text{ at injection}$$
$$= i\,136\ \Omega \text{ at extraction}$$

TABLE 2-9 Space Charge Z/n for Heavy Ion Beams.

	Carbon	Sulfur	Copper	Iodine	Gold
A	12	32	63	127	197
Q	6	14	21	29	33
$N \times 10^9$	22	6.7	4.7	3.2	2.2
$\beta_{\text{injection}}$	0.1262	0.1002	0.0782	0.0595	0.0478
$\beta_{\text{extraction}}$	0.8714	0.8716	0.8534	0.7900	0.6868
S (eV-s/nucleon)	0.05	0.05	0.05	0.05	0.05
Z/n (kΩ) from space charge					
at injection	1.47	1.86	2.40	3.16	3.93
at extraction	0.23	0.23	0.27	0.40	0.65

This impedance is so large that it is hard to imagine an inductive wall impedance of the same magnitude.

Provisional Conclusion: If there is no resistance, the reactance being positive (capacitive) and the accelerating cycle always below the Booster transition energy, the individual bunches are always stable.

Only the presence of a resistance in the coupling impedance can cause the bunches to be unstable. We can calculate the tolerances on X/n.

Observe that the energy dependence of U' is given by the quantity

$$\frac{\beta\gamma B\,(Y/n)}{|\eta|} \approx \gamma B$$

for the space charge impedance and since one is so well below the transition energy for all cases. Since B decreases with increasing energy, it is seen that U' has indeed only a very weak dependence with energy We will take $B = 0.3$ at injection and $B = 0.03$ at top energy for all cases. The results are given in Table 2-10. We show the values of U' with space charge at injection and extraction for each case. Based on the stability diagram shown in Figure 2-16 we can then infer the maximum allowed values for V' Since we are below the transition energy, $\text{sign}\,(K_o) > 0$.

The choice of V' depends critically on the shape of the energy distribution.

The range of U' for the proton beam during the acceleration cycle is shown in Figure 2-16. With the exception of a truncated cosine distribution (8) and a first-order parabolic distribution (9), the beam bunch is always stable provided $V' < 0.4$, the limit being set by a second-order parabolic distribution (7) at top energy This corresponds to the resistive impedance limit $X/n < 60\ \Omega$.

TABLE 2-10 Bunch stability requirement in the Booster

	U'		V'	X/n
	Injection	Extraction†		
Proton	0.67	0.90	0.4	60 Ω
Fixed Target:				
Carbon	0.11	0.066	0.5	5.3 kΩ
Sulfur	0.066	0.041	0.5	8.5
Copper	0.052	0.033	0.5	10.6
Iodine	0.034	0.021	0.5	16.7
Gold	0.019	0.012	0.5	29.2
RHIC:				
Carbon	0.029	0.018	0.5	19 kΩ
Sulfur	0.018	0.011	0.5	32
Copper	0.014	0.009	0.5	39
Iodine	0.009	0.006	0.5	58
Gold	0.005	0.003	0.5	117

†Assuming $\beta_{\text{extraction}} = 0.669$.

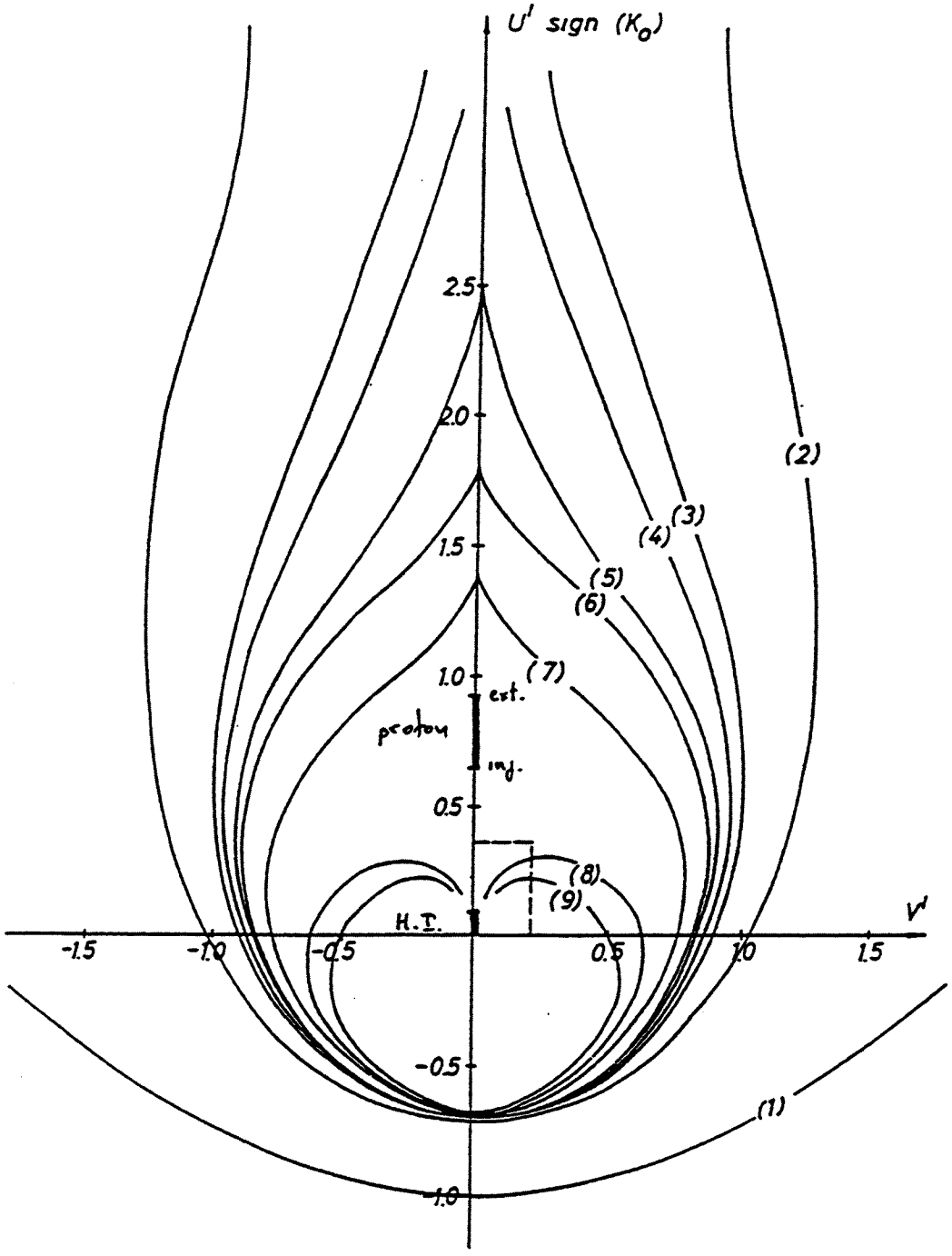

Figure 2-16. Stability diagram. Distributions: (1) Lorentzian, (2) Gaussian, (3) 5th-order parabolic, (4) 4th-order parabolic, (5) 3rd-order parabolic, (6) squared cosine, (7) 2nd-order parabolic, (8) truncated cosine, (9) 1st-order parabolic.

Heavy-ion bunches are even more stable than proton bunches. The range of U' for all heavy-ion cases is also shown in Figure 2-16. At the very most $U' = 0.11$ for carbon at injection in fixed-target mode. All the distributions considered in Figure 2-16 are stable provided $V' < 0.5$. The tolerance on the resistive impedance is very high: tens of kilo-ohms! It is possible to double the number of heavy ions per bunch and reduce considerably the initial bunch area.

2.7.3. Coupled Bunch Instabilities

Using codes like ZAP and with analytical calculations, we found that the beam in the booster is easily *stable* against longitudinal bunch-to-bunch coherent motion.

This is true for both the smooth wall components and the parasitic resonating modes.

The beam in the booster is *unstable* against transverse bunch-to-bunch motion. The instability is induced by the wall resistivity, with $n - \nu = 0.2$ being the predominant mode. There is not enough Landau damping to make the beam stable, especially at low energy, because of the very large space-charge forces. The estimated growth time is 3 ms. There is a need of a transverse damper acting on any bunch-to-bunch mode providing a damping rate of at least 300 s^{-1}

Higher order parasitic modes do not seem again to cause any harm to the beam transverse stability

2.7.4. Damping

As pointed out above for high-intensity proton operation, the three booster bunches will be unstable against coherent, transverse-coupled bunch, dipolar motion. In order to suppress these instabilities, wideband feedback damping will be employed in both the vertical and horizontal planes. A system similar to that used in the CERN Booster will be used. Existing pickup electrodes (at C7 and C8) will provide the necessary signals. The sum and difference signals from a pair will produce an analog output that is proportional to any coherent displacement of a bunch about the closed orbit. This output will be delayed, amplified, and applied to traveling-wave deflectors (50 Ω strip lines) after approximately one turn and an odd number of quarter betatron wavelengths later

In addition to the pickup electrodes and deflectors, the system will include a closed-orbit suppressor (since only that part of the difference signal due to coherent motion needs to be amplified); switched cable delays to maintain the one-turn delay as the rotation frequency increases; a band-limiting filter to insure loop stability; and four wideband power amplifiers (100 Watt, 100 kHz — 100 MHz).

2.8. Impedance of Beam Components

The particles circulating in the booster induce currents and fields in the vacuum chamber, bellows, pick-up electrodes, rf cavities, and other beam components such as kickers, dampers, and septum magnets. These induced currents and fields react back on the beam and can give rise to unstable beam motion. To calculate these effects, a coupling impedance Z is defined. For the longitudinal case, Z is the longitudinal voltage produced per unit of current.

The impedances of the beam components were estimated using the program *ZOVERN* developed by A. Ruggiero. The dominating impedance is that of the vacuum chamber Since γ never exceeds 2.6 and because of the low cut-off frequency, the beam is well-shielded from free space by the vacuum chamber The total contribution is displayed in Fig. 2-17 where both real and imaginary parts of Z/n are given versus n.

2.8.1. Space Charge

The space charge contribution to the longitudinal coupling impedance is:

$$\frac{Z}{n} = i\frac{Z_0\, g}{2\beta\gamma^2}$$

with $Z_0 = 377$ ohm and $g = 1 + 2\log(b/a)$, $n = f/f_0$, where f_0 is the revolution frequency

At injection $g = 1$.

At extraction $g = 4.5$.

	proton	carbon	sulfur	copper	iodine	gold
$\beta_{\text{injection}}$	0.5662	0.1262	0.1002	0.0782	0.0595	0.0478
$\beta_{\text{extraction}}$	0.923	0.8714	0.8716	0.8534	0.7900	0.6868
$\lvert Z/n\rvert$ inject.	0.226 kΩ	1.47	1.86	2.40	3.16	3.93
extract.	0.136	0.23	0.23	0.27	0.40	0.65

The space-charge impedance has a cut-off in the proximity of:

$$n_c \approx \frac{\gamma R}{b}$$

For b=5 cm, the cut-off harmonics range between 640 and 865 for the heavy-ion beam case and between 780 and 1670 for protons.

2.8.2. Vacuum Chamber Resistivity

Model:

Smooth vacuum chamber of cylindrical geometry Vacuum chamber radius b=6 cm. Wall material; stainless steel, room temperature. Wall thickness 1.9 mm.

Skin Depth of the wall material

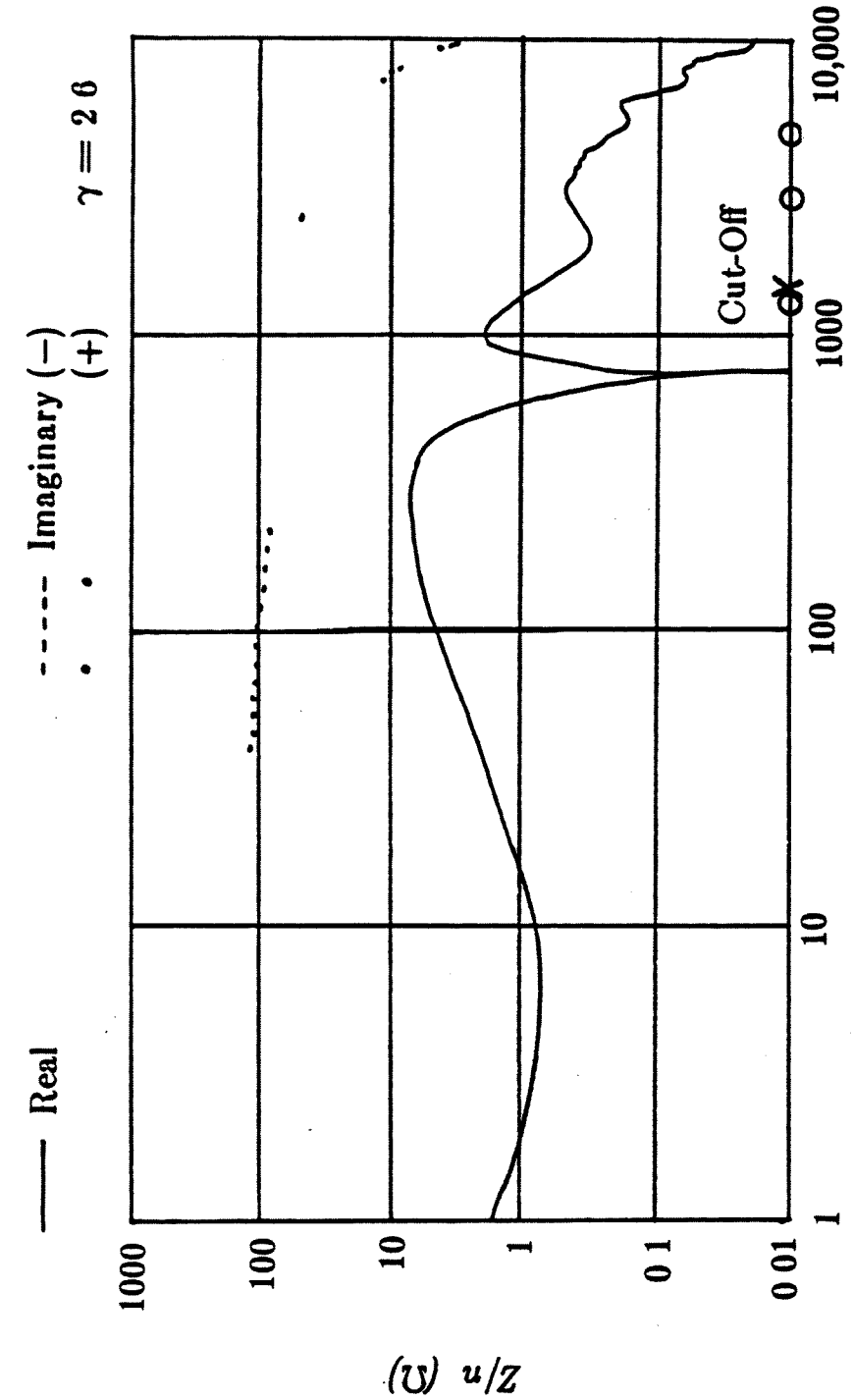

Figure 2 17 Z/n versus n, $\gamma = 2\,6$

$$\delta = \frac{0.36 \text{ mm}}{\sqrt{n}}$$

Contribution of the resistive vacuum chamber to the longitudinal coupling impedance

$$\frac{Z}{n} = \frac{1.3\,(1-i)\text{ ohm}}{\sqrt{n}}$$

All the quantities above are independent of the beam energy and of the ion species being accelerated.

There is a cut-off harmonic number n_c for this contribution which is 1400.

2.8.3. Pick-Up Electrodes

There are 48 beam monitors, each made of two plates capacitively coupled to each other The size and shape of these two plates are equivalent to what would be obtained by diagonally splitting a cylinder that is about 15.3 cm in diameter and 20 cm long. (At one end the angular aperture of a plate is 360 and at the other it is 0)

The program *ZOVERN* was specifically written for the case where the pick-up electrodes are strip lines. In this case, each half of the monitor has a capacitance of about 40 pF (plate capacitance plus stray capacitance). There is a single connection to each plate through the beam pipe wall, first to a matching network, then to about ten feet of RG114A/U coaxial cable (characteristic impedance 185 Ω), and then to a terminating network. The electrode matching network consists of a five-turn transformer winding in series with a 300 Ω resistor The secondary of the 5:1 transformer is connected to a 3.6 Ω resistor as shown in Figure 2-18.

For protons, where $\beta > 0.56$, Z/n for 48 units is calculated to be

$$\frac{Z}{n} < -i\ 2.2\ \Omega$$

2.8.4. Bellows

There are 48 bellows. Each one has 15 ribs or convolutions. The convolutions are 12 mm high and the distance from the peak of one convolution to the next is 20 mm. Each convolution acts as a small resonating cavity with several dominant modes. The capacitance, inductance, and characteristic impedance of each convolution are calculated to be 4.564 pF, 0.244 nH, and 7:308 Ω respectively The resonant frequencies are

$$f_r = 6.246\,(2k-1)\ \text{GHz},$$

the Q is

$$Q = 3477\,\sqrt{2k-1},$$

and the shunt impedance is

3.1.2.1. Quadrupole Magnet Construction

The quadrupole magnet, Fig. 3-3, consists of four identical quadrants, Fig. 3-4, fastened to and supported by two precision end plates. Each quadrant contains: a main coil, a trim coil, coil clamps, two extension plates, four tie-rods, insulating bushings, and a nominal 710 laminations.

The laminations, Fig. 3-5, will be made from one heat of 0.025 -thick M36 silicon steel. They will be stamped so that the steel rolling direction is radial at the pole. Both faces of the lamination will have an AISI Type C-5 coating for electrical surface insulation.

Each core quadrant will be made of a stack of laminations pre-weighed to within ± 0.03 lbs of the design value prior to loading into the stacking fixture. Shouldered tie-rods, inserted into the four holes through the laminations, load and compress the stack to 17.750″ The two tie-rods nearest to the quadrant parting surfaces will fit within 0.002 of the lamination holes to act as pilots and prevent any shifting of the laminations. These two, and the pole-tip tie-rod, will be made of aluminum alloy with a hard anodized finish to electrically insulate them from the laminations. Bushings made of hard anodized aluminum will insulate the tie-rod ends from the extension plates. The large-diameter center tie-rod, made of 304 stainless steel, will provide most of the clamping to maintain the integrity of the bolted core. The stainless extension plates at each end of the core will serve to distribute the tie-rod clamping loads uniformly over the lamination stack and will also provide a mounting surface for the main coil clamps. Kapton spacers 0.005 thick will provide a controlled, insulated gap at the horizontal and vertical mid-planes between quadrants. The two tie-rods adjacent to the insulated gaps of each quadrant will pass through the precision holes of the magnet end plates, and insulated, close-fitting bushings will maintain the alignment of the quadrants to the end plates.

3.1.3. Correction Package

A correction package will be installed in the one meter drift space following the main dipole magnets. However, because of space limitations, six locations of the possible 48 will not have packages. Each of the 42 correction packages will contain the following magnets: a vertical orbit correction dipole, a horizontal orbit correction dipole, a correction quadrupole, and a correction sextupole. Each magnet winding of each correction package requires its own regulated power supply The six locations where correction packages will *not* be installed are: A5, C5, C8, F3, F6, and F8.

3.1.3.1. Correction Dipoles

The correction dipoles are needed to correct 5θ harmonics at the injection energy, and to correct 3θ harmonic polarization resonances at $B\rho = 4.2$. The major sources of error which will require vertical dipole correction are quadrupole survey error of 0.1 mm rms and dipole roll of 0.2 mrad rms. These give field errors of 119 G-cm and 147 G-cm for the quadrupole and dipole sources, respectively The probable in-phase component is

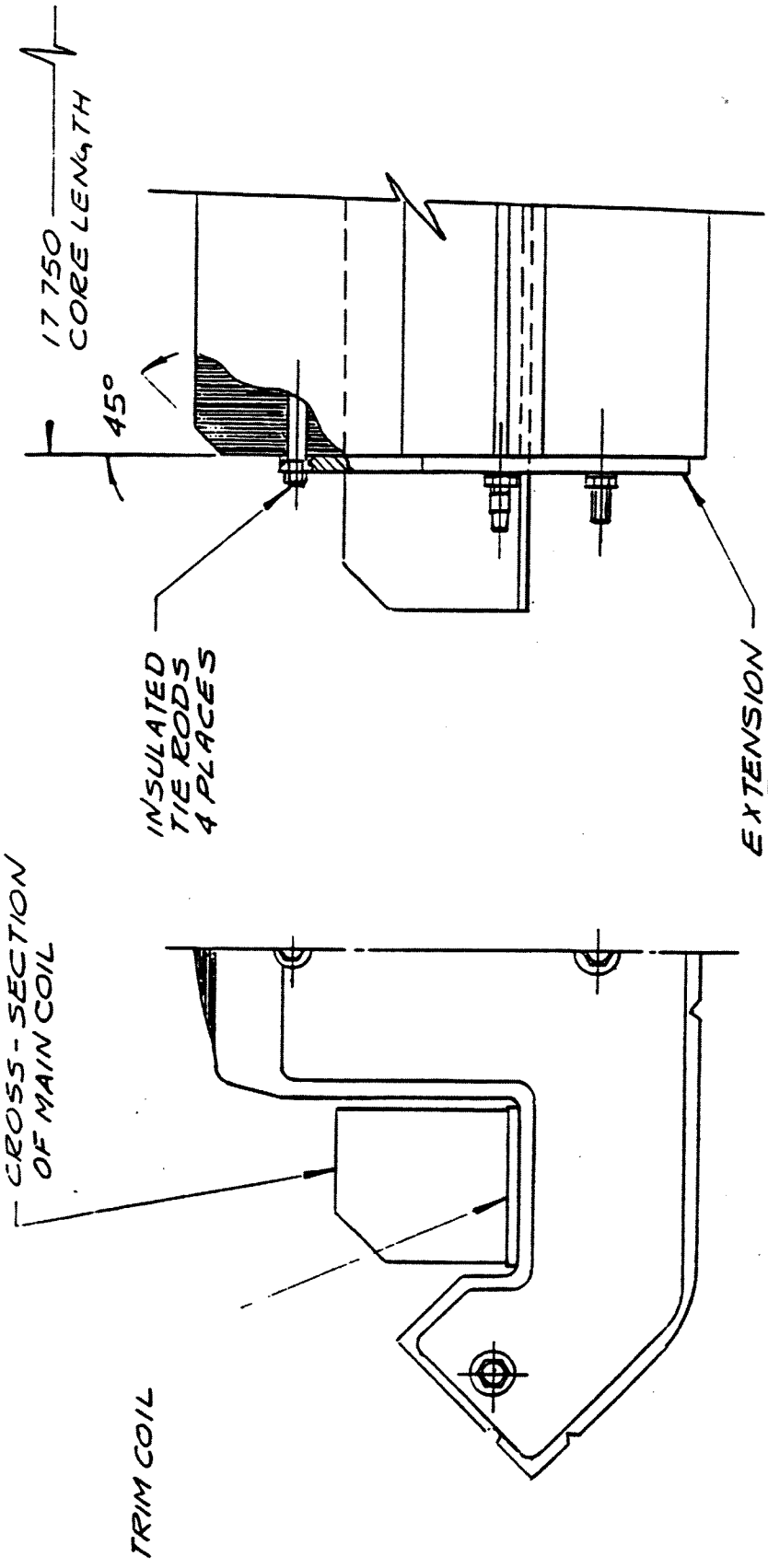

Figure 3 4 Quadrant of a quadrupole magnet

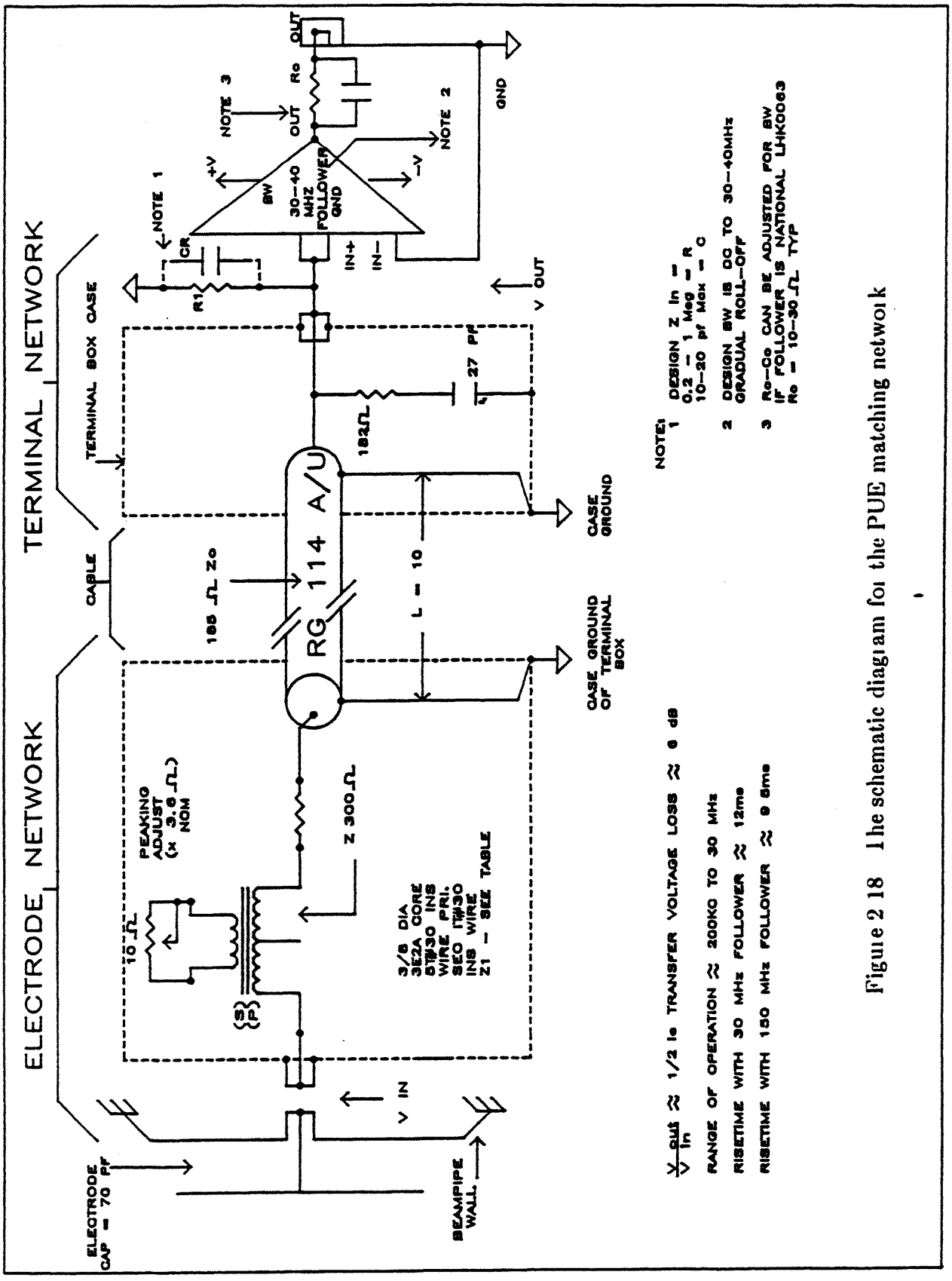

Figure 2.18 The schematic diagram for the PUE matching network

$$Z_s = \frac{32.35}{\sqrt{2k-1}}\ \mathrm{k}\Omega,$$

where $k = 1$ or 2, since $k = 2$ roughly corresponds to the convolution cavity high frequency cut-off.

If all the convolutions were identical in shape, their total contribution to the longitudinal coupling impedance would be, at resonance,

$$\frac{Z}{n} = \frac{5.115}{(2k-1)^{3/2}}\ \mathrm{k}\Omega.$$

However, the convolutions will not be identical (and if they would naturally be too much alike they can be intentionally altered so as to be dissimilar). Since they are not all the same, there will not be single sharp resonance lines for each mode but instead a distribution of resonanting frequencies. If it is assumed that the resonanting frequencies are randomly distributed over a range equal to 10% of the central frequency, then, for $k = 1$, at resonance,

$$\frac{Z}{n} = 11.54\ \Omega.$$

Below the first resonanting frequency, the coupling impedance is inductive and small,

$$\frac{Z}{n} = -i\ 2.0\ \Omega.$$

2.8.5. Vacuum Chamber Steps

There are 72 locations where the vacuum chamber changes shape. *ZOVERN* treats steps as going from one circular geometry to another In the Booster, the portion of the beam tube in the dipoles is somewhat elliptical in cross section with truncated ends along the semi-major axis. But if the chamber is treated as a circular pipe of 3.5 cm radius going to one with a 7.6 cm radius, for the total coupling impedance contribution,

$$\frac{Z}{n} = (1 - i\,\pi)\ 0.06\ \Omega$$

with a cutoff at $n \sim 4 \times 10^6$

2.8.6. RF Cavities

The beam sees four rf cavities, each with two gaps. For the protons, two of these cavities will be active simultaneously, but for the heavy ions only one cavity is active at any one time. For all the cavities, $h = 3$. In order to determine Z/n, it is necessary to know the shunt impedance of each gap and the Q of each cavity for the beam loading of interest. This information is not yet available.

2.8.7 Other Beam Components

In order to calculate the longitudinal coupling impedance of the other beam components — kicker magnets, magnets for the damping system, septum magnets, electrostatic septum, etc. — it is necessary to know the length of each component, the resistivity of the ferrite, the relative permeability of the ferrite, and the mean distance of the ferrite from the beam. For the transverse coupling it is necessary to know the distance from one side of coil to the other for each coil. This information is not yet all available.

2.8.8. Transverse Coupling Impedance

There are four major contributions to the transverse coupling impedance in the AGS Booster

- The space charge. The expression for the contribution is

$$Z_\perp = \frac{iRZ_o}{\beta^2\gamma^2}\left(\frac{1}{a^2} - \frac{1}{b^2}\right)$$

where as usual $Z_o = 377\,\Omega$, a is the average beam radius and b is the vacuum chamber radius. There is a variation of the value of $Z_\perp$ during the acceleration cycle. For protons

$$Z_\perp \approx 1.53 \text{ M}\Omega/\text{m} \quad \text{at injection}$$

$$\approx 1.14 \text{ M}\Omega/\text{m} \quad \text{at extraction}$$

- The resistivity of the vacuum chamber

$$Z_\perp = \frac{(1-i)R}{b^3}\left(\frac{2RZ_o\rho}{\beta(n-\nu)}\right)^{1/2}$$

where R is the average radius of the closed orbit, ρ the wall resistivity, and ν the betatron tune number The contribution is small compared to the space-charge effect. For protons again, for $(n-\nu) = (5 - 4.8)$,

$$Z_\perp = (1-i)\,0.058 \text{ M}\Omega/\text{m} \quad \text{at injection}$$

$$0.045 \text{ M}\Omega/\text{m} \quad \text{at extraction}$$

- In the circular approximation, by virtue of the deflection theorem, the longitudinal coupling impedance estimate can be translated into an equivalent transverse coupling impedance

$$Z_\perp = \frac{2R}{\beta b^2}\frac{Z_\parallel}{n-\nu}$$

If we take $|Z_\parallel/n| \approx 10\,\Omega$ as previously estimated, then

$$\left|Z_{\perp}\right| \approx 0.2\ \mathrm{M\Omega/m}$$

- Finally there are transverse modes proper due to several resonanting structures, like rf cavities, but they are difficult to estimate and can usually be observed with the beam itself.

2.9. Magnet Alignment

2.9.1. Main Ring Magnet Coordinates

2.9.1.1. Introduction

In this section a Booster-centered reference frame is defined, the orientation of the Booster frame is specified, and the coordinates of the Booster magnets are discussed.

2.9.1.2. Booster-Centered Coordinate System

A reference frame has been defined with origin at the center of the Booster and with x and y axes coinciding with East and North, respectively The symmetry of the Booster in this frame and the use of the meter as the unit of length are convenient for design work. The Booster is oriented to optimize transfer of its beam to the AGS. This orientation is specified by an angle α between East and a line from the Booster center to the center of quadrupole MQF8; $\alpha = 0.1725872$ radians and is measured in a clockwise direction from the x (East) direction.

2.9.1.3. Transfer of Coordinates to the AGS and BNL Grids

For survey and installation purposes, it is necessary to relate the Booster centered reference frame to the other reference frames (BNL grid and AGS grid) used at BNL. For the convenience of surveyors, the coordinates of magnetic elements are tabulated in the BNL grid; however, transformations from the Booster frame to both the AGS and BNL grids are listed below

The AGS and BNL grids have x and y axes oriented in the East and North directions, respectively The origins do not coincide; the unit of length in the AGS grid is the inch, and the unit of length in the BNL grid is the foot. Standard conversions are used:

$$1\ \text{inch} = 0.0254\ \text{m, and}$$
$$1\ \text{foot} = 0.3048\ \text{m.}$$

1. AGS Grid

$$\mathrm{N\ (inch)} = \mathrm{N_{o,AGS}\ (inch)} + y_{\mathrm{bst}}\ \mathrm{(inch)}$$

$$\mathrm{E\ (inch)} = \mathrm{E_{o,AGS}\ (inch)} + x_{\mathrm{bst}}\ \mathrm{(inch)}$$

$$\mathrm{N_{o,AGS}} = 15{,}459.36\ \text{inches.}$$

$$E_{o,AGS} = 1{,}148.88 \text{ inches}$$

2. BNL Grid

$$N \text{ (feet)} = N_{o,BNL} \text{ (feet)} + y_{bst} \text{ (feet)}$$

$$E \text{ (feet)} = E_{o,BNL} \text{ (feet)} + x_{bst} \text{ (feet)}$$

$$N_{o,BNL} = 102{,}438.28 \text{ feet},$$

$$E_{o,BNL} = 98{,}517.19 \text{ feet}.$$

2.9.2. Coordinates of Beam Components

The coordinates reported in this section correspond to the physical lengths of the magnets (previous tabulations used magnetic length). Reference markers to be used for survey and alignment purposes will be located on the dipoles and quadrupoles and probably on the sextupoles. These markers will consist of precision bushings in a groove in the magnet laminations above the centerline of the magnets. There is considerable freedom in choosing the position of the bushings along the length of the magnets, however at present they are centered over the junction of the magnet laminations and the magnet end plates. This location is convenient in that the fixtures holding the bushings can be pinned to the end plates of the magnets. If this location interferes with electrical or water connections, the bushing locations can be moved with little or no impact to the survey system. As the yoke of sextupoles is only three inches long, placing more than one survey bushing on a sextupole serves little purpose. Hence one bushing placed at the center of the laminations is suggested. The magnetic and physical lengths of the various elements are listed in Table 2-11.

TABLE 2-11 Effective and actual lengths of magnetic elements for the Booster

	Magnetic Length (m)		Lamination Length (m)	
	arc	chord	arc	chord
Dipole	2.40	2.39696	2.31744	2.31470
Quad	0.50375		0.45085†	
Sextupole	0.10		0.075	

†Lamination length is 17 3/4"

Coordinates of the survey bushings have been generated with the standard geometry program modified to use the lamination length rather than the magnetic length of the elements. The coordinates of the survey bushings in the BNL grid are listed in Table 2-12.

TABLE 2-12 Coordinates of magnet survey points in the BNL grid.

Index	Name	Survey Pt #1		Survey Pt #2	
		N (ft)	E (ft)	N (ft)	E (ft)
1	MDA1	102418.1377	98621.4064	102410.7775	98619.5347
2	MSFA1	102408.4819	98618.7319		
3	MQA1	102407.4709	98618.3785	102406.0746	98617.8904
4	MDA2	102404.9357	98617 4925	102398.0124	98614.3711
5	MSDA2	102395.8911	98613.1819		
6	MQA2	102394.9568	98612.6583	102393.6664	98611.9351
7	MSFA3	102383.8599	98606.4391		
8	MQA3	102382.9256	98605.9154	102381.6353	98605.1923
9	MDA4	102380.5828	98604.6027	102374.3067	98600.3265
10	MSDA4	102372.4241	98598.7870		
11	MQA4	102371.5949	98598.1091	102370.4497	98597.1729
12	MDA5	102369.5157	98596.4095	102364.0774	98591.1084
13	MSFA5	102362.4908	98589.2654		
14	MQA5	102361.7919	98588.4538	102360.8267	98587.3329
15	MSDA6	102353.4914	98578.8143		
16	MQA6	102352.7925	98578.0027	102351.8273	98576.8818
17	MDA7	102351.0400	98575.9678	102346.6049	98569.8029
18	MSFA7	102345.3624	98567.7124		
19	MQA7	102344.8150	98566.7918	102344.0592	98565.5203
20	MDA8	102343.4425	98564.4835	102340.1453	98557.6421
21	MSDA8	102339.2847	98555.3676		
22	MQA8	102338.9055	98554.3659	102338.3819	98552.9825
23	MDB1	102337.9547	98551.8544	102335.8956	98544.5444
24	MSFB1	102335.4430	98542.1550		
25	MQB1	102335.2435	98541.1027	102334.9681	98539.6494
26	MDB2	102334.7432	98538.4642	102333.9848	98530.9077
27	MSDB2	102333.9540	98528.4760		
28	MQB2	102333.9403	98527 4050	102333.9214	98525.9260
29	MSFB3	102333.7779	98514.6853		
30	MQB3	102333.7642	98513.6143	102333.7453	98512.1353
31	MDB4	102333.7297	98510.9291	102334.2949	98503.3556
32	MSDB4	102334.6869	98500.9555		
33	MQB4	102334.8594	98499.8985	102335.0976	98498.4386
34	MDB5	102335.2917	98497.2480	102337.1634	98489.8878
35	MSFB5	102337.9662	98487.5922		
36	MQB5	102338.3196	98486.5812	102338.8077	98485.1849
37	MSDB6	102342.5174	98474.5730		
38	MQB6	102342.8708	98473.5619	102343.3589	98472.1656
39	MDB7	102343.7568	98471.0268	102346.8782	98464.1034
40	MSFB7	102348.0674	98461.9821		
41	MQB7	102348.5910	98461.0478	102349.3142	98459.7575
42	MDB8	102349.9038	98458.7050	102354.1800	98452.4289
43	MSDB8	102355.7195	98450.5463		
44	MQB8	102356.3974	98449.7171	102357.3336	98448.5719

TABLE 2-12 Coordinates of magnet survey points in the BNL grid. (cont.)

Index	Name	Survey Pt #1		Survey Pt #2	
		N (ft)	E (ft)	N (ft)	E (ft)
45	MDC1	102358.0970	98447.6379	102363.3981	98442.1996
46	MSFC1	102365.2411	98440.6129		
47	MQC1	102366.0527	98439.9141	102367.1736	98438.9489
48	MDC2	102368.0875	98438.1616	102374.2524	98433.7265
49	MSDC2	102376.3429	98432.4839		
50	MQC2	102377.2636	98431.9366	102378.5350	98431.1807
51	MSFC3	102388.1980	98425.4361		
52	MQC3	102389.1186	98424.8888	102390.3901	98424.1329
53	MDC4	102391.4269	98423.5162	102398.2683	98420.2190
54	MSDC4	102400.5428	98419.3584		
55	MQC4	102401.5445	98418.9793	102402.9279	98418.4557
56	MDC5	102404.0560	98418.0284	102411.3660	98415.9693
57	MSFC5	102413.7554	98415.5167		
58	MQC5	102414.8077	98415.3173	102416.2610	98415.0418
59	MSDC6	102427.3060	98412.9485		
60	MQC6	102428.3583	98412.7491	102429.8116	98412.4737
61	MDC7	102430.9968	98412.2488	102438.5534	98411.4904
62	MSFC7	102440.9851	98411.4596		
63	MQC7	102442.0560	98411.4459	102443.5350	98411.4270
64	MDC8	102444.7413	98411.4114	102452.3147	98411.9766
65	MSDC8	102454.7148	98412.3685		
66	MQC8	102455.7718	98412.5410	102457.2317	98412.7793
67	MDD1	102458.4223	98412.9733	102465.7825	98414.8451
68	MSFD1	102468.0781	98415.6478		
69	MQD1	102469.0892	98416.0013	102470.4855	98416.4894
70	MDD2	102471.6243	98416.8872	102478.5477	98420.0087
71	MSDD2	102480.6690	98421.1978		
72	MQD2	102481.6033	98421.7215	102482.8936	98422.4446
73	MSFD3	102492.7001	98427.9407		
74	MQD3	102493.6344	98428.4643	102494.9248	98429.1875
75	MDD4	102495.9772	98429.7771	102502.2534	98434.0533
76	MSDD4	102504.1360	98435.5927		
77	MQD4	102504.9651	98436.2707	102506.1103	98437.2069
78	MDD5	102507.0444	98437.9703	102512.4826	98443.2714
79	MSFD5	102514.0693	98445.1144		
80	MQD5	102514.7682	98445.9260	102515.7333	98447.0468
81	MSDD6	102523.0687	98455.5655		
82	MQD6	102523.7675	98456.3771	102524.7327	98457 4980
83	MDD7	102525.5201	98458.4119	102529.9551	98464.5768
84	MSFD7	102531.1977	98466.6673		
85	MQD7	102531.7450	98467.5880	102532.5009	98468.8594
86	MDD8	102533.1175	98469.8962	102536.4147	98476.7376
87	MSDD8	102537.2754	98479.0121		
88	MQD8	102537.6545	98480.0138	102538.1781	98481.3972

TABLE 2-12 Coordinates of magnet survey points in the BNL grid. (cont.)

Index	Name	Survey Pt #1		Survey Pt #2	
		N (ft)	E (ft)	N (ft)	E (ft)
89	MDE1	102538.6054	98482.5254	102540.6645	98489.8354
90	MSFE1	102541.1171	98492.2248		
91	MQE1	102541.3165	98493.2771	102541.5919	98494.7304
92	MDE2	102541.8168	98495.9156	102542.5752	98503.4721
93	MSDE2	102542.6061	98505.9038		
94	MQE2	102542.6197	98506.9747	102542.6386	98508.4538
95	MSFE3	102542.7821	98519.6945		
96	MQE3	102542.7958	98520.7654	102542.8147	98522.2445
97	MDE4	102542.8303	98523.4507	102542.2651	98531.0241
98	MSDE4	102541.8732	98533.4242		
99	MQE4	102541.7007	98534.4813	102541.4624	98535.9411
100	MDE5	102541.2684	98537.1318	102539.3966	98544.4920
101	MSFE5	102538.5939	98546.7876		
102	MQE5	102538.2404	98547.7986	102537.7523	98549.1949
103	MSDE6	102534.0426	98559.8068		
104	MQE6	102533.6892	98560.8178	102533.2011	98562.2142
105	MDE7	102532.8032	98563.3530	102529.6818	98570.2764
106	MSFE7	102528.4926	98572.3977		
107	MQE7	102527.9690	98573.3320	102527.2459	98574.6223
108	MDE8	102526.6563	98575.6748	102522.3800	98581.9509
109	MSDE8	102520.8406	98583.8335		
110	MQE8	102520.1627	98584.6627	102519.2264	98585.8078
111	MDF1	102518.4631	98586.7419	102513.1619	98592.1802
112	MSFF1	102511.3190	98593.7668		
113	MQF1	102510.5074	98594.4657	102509.3865	98595.4309
114	MDF2	102508.4725	98596.2182	102502.3076	98600.6533
115	MSDF2	102500.2171	98601.8958		
116	MQF2	102499.2965	98602.4431	102498.0250	98603.1990
117	MSFF3	102488.3620	98608.9437		
118	MQF3	102487.4414	98609.4910	102486.1700	98610.2469
119	MDF4	102485.1331	98610.8635	102478.2917	98614.1607
120	MSDF4	102476.0172	98615.0214		
121	MQF4	102475.0156	98615.4005	102473.6322	98615.9241
122	MDF5	102472.5040	98616.3514	102465.1940	98618.4105
123	MSFF5	102462.8046	98618.8631		
124	MQF5	102461.7523	98619.0625	102460.2990	98619.3379
125	MSDF6	102449.2540	98621.4312		
126	MQF6	102448.2017	98621.6307	102446.7484	98621.9061
127	MDF7	102445.5632	98622.1309	102438.0067	98622.8894
128	MSFF7	102435.5750	98622.9202		
129	MQF7	102434.5040	98622.9339	102433.0250	98622.9528
130	MDF8	102431.8188	98622.9684	102424.2453	98622.4031
131	MSDF8	102421.8452	98622.0112		
132	MQF8	102420.7882	98621.8387	102419.3283	98621.6005

2.9.2.1. Survey Monuments

Survey monuments have been arbitrarily placed a distance of 1.1 m radially outwards from the upstream survey marker of each horizontally focusing quadrupole; there are 24 monuments. These monuments consist of bushings located in the tunnel floor at positions where they will not interfere with the magnet installation. The use of 24 regularly spaced monuments gives uniformity in location and also provides more than the minimum required number so that redundant measurements needed to sort out errors and inconsistencies are possible. The choice of monument location is arbitrary and can be changed if there are disadvantages to this location or if there are extra advantages to other locations. There is some indication that placement near defocusing quadrupoles could reduce interference from beam lines for injection and extraction. In some areas, such as those with penetrations to the linac and AGS, more monuments and/or irregularly spaced monuments may be required. The coordinates of the survey monuments located in the tunnel floor are listed in Table 2-12.

TABLE 2-13 Survey monuments 1.1 m outward from upstream end of the QF's.

No.	Quad	Booster Frame		BNL Grid	
		X (m)	Y (m)	N (ft)	E (ft)
1	MQA1	31.31983	-10.38154	102404.220	98619.945
2	MQA3	27.34176	-17.93082	102379.452	98606.894
3	MQA5	21.63933	-24.41053	102358.193	98588.185
4	MQA7	14.84751	-29.55419	102341.317	98565.902
5	MQB1	6.66921	-32.31456	102332.261	98539.071
6	MQB3	-1.85769	-32.64410	102331.180	98511.095
7	MQB5	-10.32049	-30.94550	102336.753	98483.330
8	MQB7	-18.17094	-27.63545	102347.613	98457.574
9	MQC1	-24.65065	-21.93302	102366.321	98436.315
10	MQC3	-29.19948	-14.71327	102390.008	98421.391
11	MQC5	-31.95986	-6.53497	102416.840	98412.335
12	MQC7	-33.01849	1.91875	102444.575	98408.862
13	MQD1	-31.31990	10.38155	102472.340	98414.434
14	MQD3	-27.34183	17.93083	102497.108	98427 486
15	MQD5	-21.63940	24.41054	102518.367	98446.195
16	MQD7	-14.84759	29.55420	102535.243	98468.477
17	MQE1	-6.66928	32.31458	102544.299	98495.309
18	MQE3	1.85761	32.64411	102545.380	98523.285
19	MQE5	10.32042	30.94551	102539.807	98551.050
20	MQE7	18.17087	27.63546	102528.948	98576.806
21	MQF1	24.65058	21.93303	102510.239	98598.065
22	MQF3	29.19941	14.71329	102486.552	98612.989
23	MQF5	31.95979	6.53498	102459.720	98622.045
24	MQF7	33.01842	-1.91873	102431.985	98625.518

2.9.2.2. Monuments for Vertical Surveys

The availability of monuments near the level of the survey plane would ease vertical surveys. Such secondary monuments will be affixed to the outer wall of the Booster tunnel. The locations will be chosen to avoid interference with conduits and with water mains for the sprinkler system. Their mounting will require ease of use without interference with other operations such as magnet transport. These monuments can be installed after most installation work is complete when their optimum location will become more evident.

2.9.3. Alignment Algorithm

The alignment algorithm used to smooth the location of the magnets will be selected on the basis of simulation results. "Realistic" survey files can be generated from the suggested magnet survey points and tunnel survey monuments. Errors, both systematic and random, will be assigned to computer generated measurements of position plus magnet offsets, and the data with and without errors will be analyzed to smooth the magnet positions and establish how well the smoothing algorithms work. From this simulation, an acceptable smoothing algorithm will be selected.

2.9.4. Alignment Tolerances

Listed below is a table of tolerances for dipoles and quadrupoles.

TABLE 2-14 Principal alignment tolerances.

	Quantity	Note
Dipoles		
Integrated field	$\Delta(Bl)/Bl \simeq 10^{-4}$	(1)
Roll	$\sigma = 0.2$ mrad	(2)
Quadrupoles		
Position	$\sigma = 0.1$ mm	(3)
Roll	As much as 0.1 mrad	(4)

Notes.

(1) Variations of packing factor of the laminations, length of the dipole, and of field differences produce an estimated $\Delta l/l \simeq 10^{-4}$ that requires horizontal orbit correction. For a sector magnet $\Delta l/l = \Delta\rho/\rho$. Hence, placement errors of $\Delta\rho = 10^{-4}\ \rho_0 = 1.375$ mm result in $\Delta(Bl)/Bl = 10^{-4}$ Placement of dipoles to $\pm 1/16''$ produces a $\Delta(Bl)/Bl = \pm 1.15 \times 10^{-4}$ This uncertainty requires further horizontal orbit correction; however, the dipoles can also be purposely displaced to help provide horizontal closed orbit correction.

(2) Dipole roll with $\sigma = 0.2$ mrad. This rotation produces a horizontal component of the bending field. Vertical correctors are provided to to compensate a 2σ effect at injection energy

(3) Quad position with $\sigma = 0.1$ mm in the horizontal and vertical planes; correctors for 2σ at injection are provided. There is an amplification of the closed orbit displacement resulting from an rms quadrupole displacement of δ.

$$x_{rms} = (N\beta_{max}(\beta_{max} + \beta_{min}))^{0.5} \frac{\delta_{rms}}{2\sqrt{2}f \sin(\pi\nu)}$$

with
$N = 24$ cells,
$\beta_{max} = 13.14$ m,
$\beta_{min} = 3.64$ m,
$\nu_x = 4.82$,
$\nu_y = 4.83$,
$f = 3.563$ m.

$x_{rms} = 13.5\ \delta_{rms}(x)$ $\quad x_{rms}(\delta = 0.1\text{ mm}) = 1.35$ mm
$y_{rms} = 14.2\ \delta_{rms}(y)$ $\quad y_{rms}(\delta = 0.1\text{ mm}) = 1.42$ mm.

(4) Quadrupole roll — as much as 0.1 mrad. This produces a skew quadrupole field that will be corrected by skew correctors in the correction elements.

CHAPTER 3. MAGNETS AND MAGNET POWER SUPPLIES

3.1. Main Ring Magnets

A flexible, multipurpose lattice design has been adopted. This permits space for fully distributed magnet correction elements, tune control, free space for other necessary components, and unused space for future developments.

Either independent or series excitation of the dipoles and the quadrupoles is possible. Equal currents give the nominal design tunes $\nu_{x,y} = 4.83$. The dipole and quadrupole $I_{max} = 5700$ amperes.

The rapid cycling capability (7.5 pulses/s) required for high intensity proton injection into the AGS requires $B = 9.5$ T/s in the dipoles. For the nominal tune, this requires 6.3 T/s in the quadrupoles at the pole tips.

The lattice consists of 24 cells with 48 quadrupoles and 36 dipoles. The 12 "missing" dipoles in the lattice provide free space and produce a six-fold periodicity

The principal choice affecting magnet and power supply costs is the magnet gap. This was chosen to be 3.25″ (8.255 cm), which is consistent with the aperture requirement.

Table 3-1 lists the magnet parameters.

TABLE 3-1 Dipole, Quadrupole, and Sextupole Magnet Parameters.

	Dipole	Quadrupole	Sextupole
Number	36	48	48
Gap/Bore	3.25	6.5	6.5
Useful Aperture	2.75 × 6	5.8	5.8
B/I (high B)	2.320 kG/kA	1.547 kG/kA	—
B_{max} (heavy ions)	12.74 kG	8.4 kG	3 kG
Length (magnetic), L	2.40 m	0.504 m	0.12 m

The 2.4 m long dipole magnets are curved (10) with a total sagitta of 2.060 (5.23 cm). For the same useful aperture, straight magnets would have considerably greater cost and stored energy. For 7.5 Hz operation this would require a much more expensive power supply

3.1.1. Dipole Design — H Magnet with One Piece Lamination

The ring dipole H magnet design provides the smallest cross section and therefore the least expensive design for the beam pipe size required. The one piece lamination, shuffled and rotated as stacked, insures the complete averaging of most errors including those from material inhomogeneities and punch and die errors. Figures 3-1 and 3-2 show

the dipole magnet.

Excellent stacking control is maintained during the core block construction. The four-fold rotation during stacking results in very accurate magnets with minimal horizontal field errors. The magnet poles are 10 wide, ~ 3 gap widths, and they have edge ridges to provide the required large good field region and dynamic range with minimum stored energy

The magnet coils, eight turns per pole. are low inductance and thus low voltage at the 7.5 Hz rep rate. Two pancakes of four turns each are used around each pole. The conductor, 1 × 2 (nominal), was selected based on bend radius and power considerations.

A small "pancake" coil is located at the base of each pole. This "pancake" coil package contains a main ring bump coil for orbit deformation, a series of four turns to power the beam tube correction windings, and an instrumentation or diagnostic winding.

The coil forces are very low, because the dipole coils are located in the low field region. Computer calculations show for each of the eight-turn coils:

(i) For 12 kG, (1 Hz), $F_{radial} = 18$ lbs/linear inch.

$F_{vertical} = 46$ lbs/linear inch *away* from the horizontal mid-plane.

(ii) For 4 kG (10 Hz) total $F_{radial} = 2$ lbs/inch

total $F_{vertical} = 5$ lbs/inch

(Note, 1 lb/inch = 17.9 kg/m)

The very small value computed for the forces at 4 kG and 10 Hz implies that it will not be difficult to control vibrations at the operating field of 5.46 kG at 7.5 Hz.

The simple racetrack coils require only intermittent support with their low forces. The open horizontal mid-plane provides optical freedom in the lattice to use the "space" beyond the normal horizontal aperture for special purposes, such as injection and ejection. It is noted that the field is relatively uniform to about four inches (10 cm) in radius.

Radial or geometrical wedge focusing was chosen, rather then vertical focusing as would be produced by parallel ends of the 10 curved magnet. The coil conductors on the entrance and exit faces of the magnet are perpendicular to the central closed orbit trajectory, minimizing integrated orbital field errors caused by conductor placement errors, considering the necessary transposition of turns in the ends.

3.1.1.1. Dipole Magnet Construction

The Booster is a small machine with less than 100 m of total dipole length. It is practical to have complete shuffling of laminations. The iron is stamped with a fiducial notch and assembled into pallets with a known sequence so that heat numbers are identified. Four-fold rotational stacking with complete shuffling averages heats, rolling direction, die geometry and die wear (if significant).

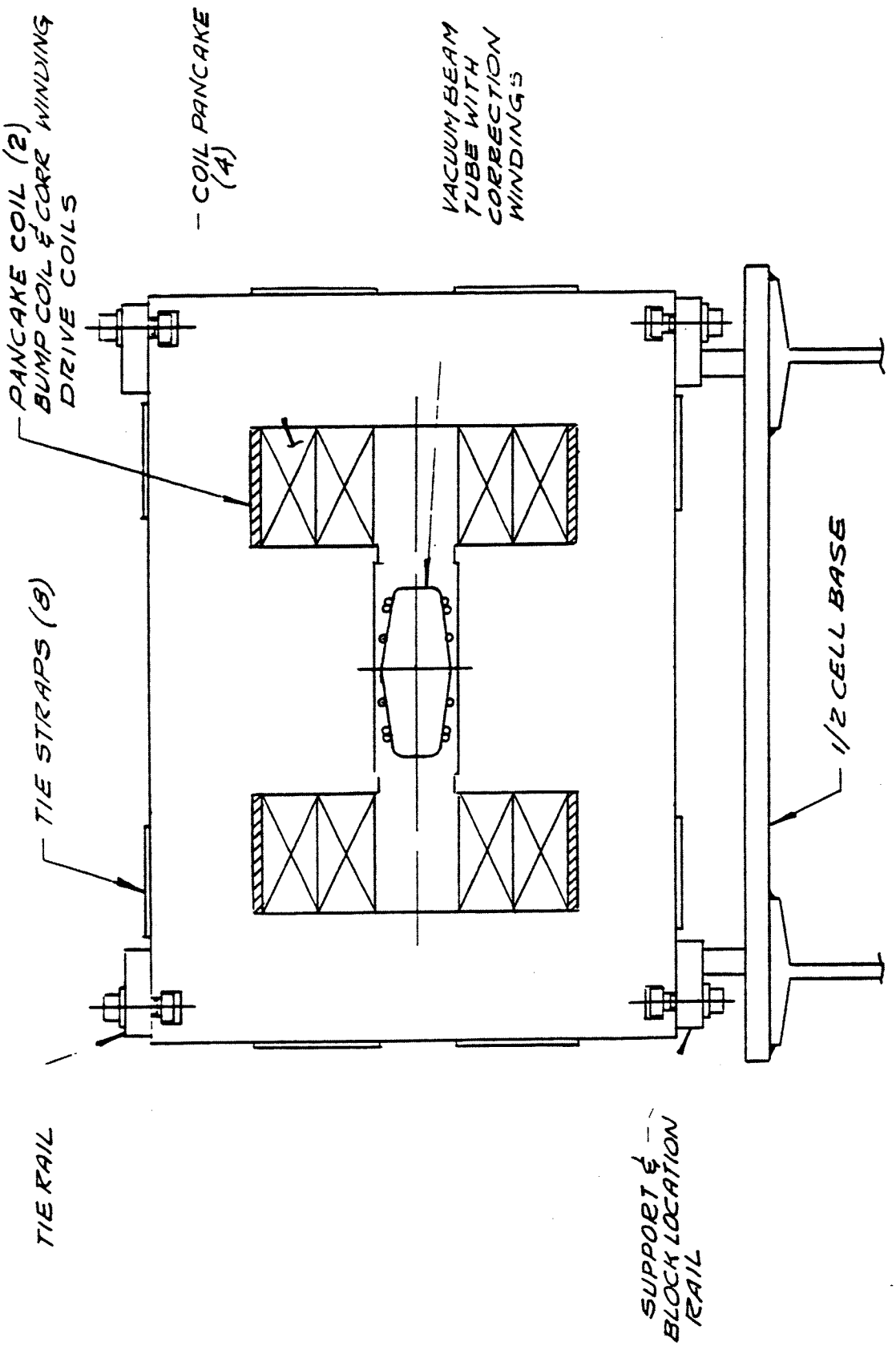

Figure 3 1 Dipole magnet, cross section

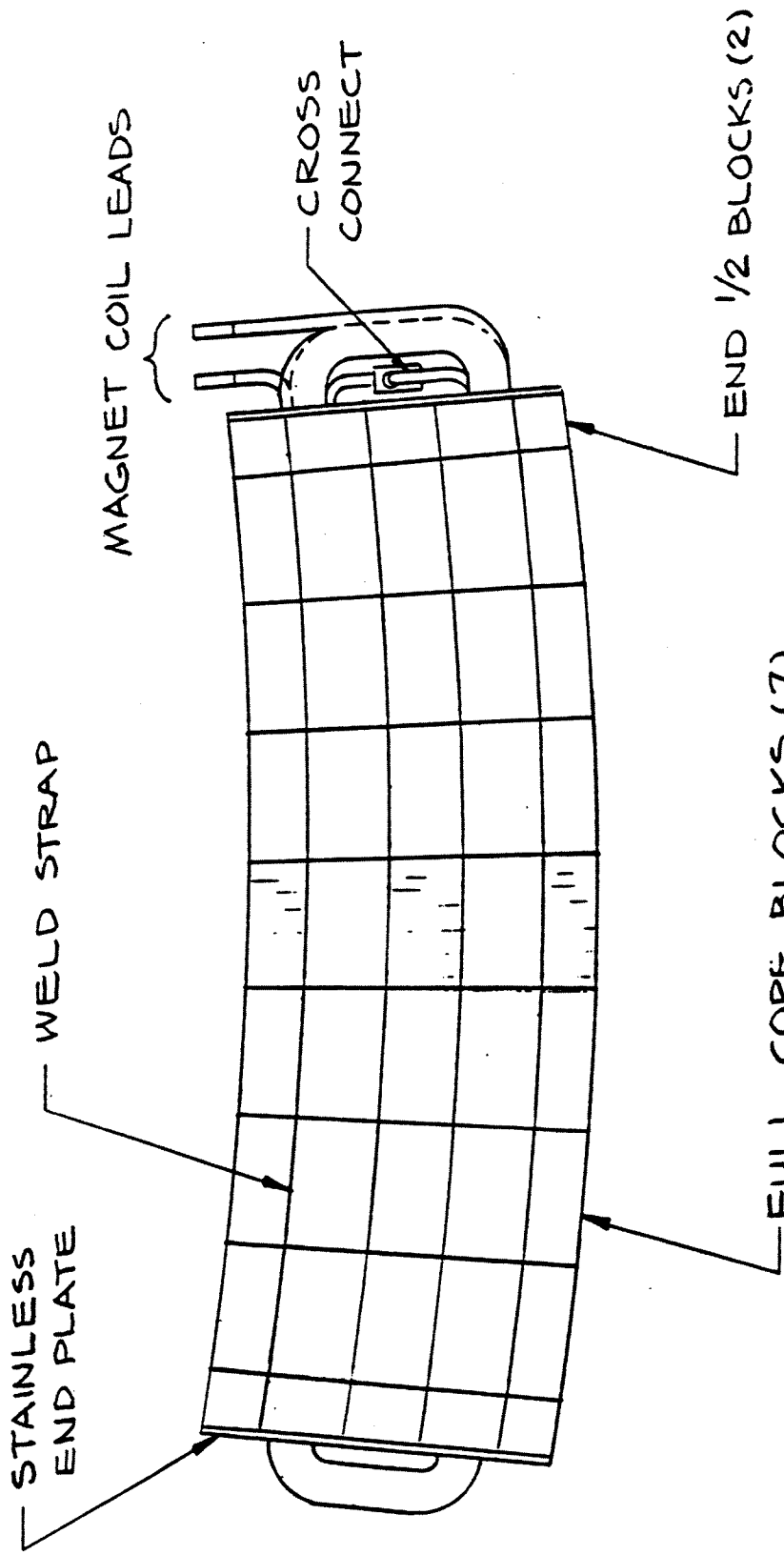

Figure 3-2. Dipole magnet, top view.

The laminations in each block are weighed and compressed to a predetermined length on the stacking fixture. The overall magnet iron packing factor is controlled to $\sim 1 \times 10^{-3}$ The effect of this packing factor tolerance on field quality will be discussed in the following section.

The stacking fixture contacts each side of the precision pole-face surface of each lamination to establish the alignment. To the extent that this is accomplished with very small errors, the four-fold symmetric stacking permits no significant odd multipole field in the blocks; i.e., no normal or skew quadrupoles or octupoles.

After the lamination stack is compressed to size, steel straps are welded along each outer surface of the block. Sections of end laminations are then removed producing the desired taper on the blocks.

Completed blocks are positioned and lightly clamped on the magnet base. The blocks are then pulled together, bringing the overall core to size. Stainless steel end plates are inserted, and the core is locked in place on its base. Coil pancakes are then inserted into the core, shimmed, positioned, and clamped in place using "midplane" jacks between the upper and lower coil package. The magnet assembly and its base are then ready for magnetic measurements.

3.1.2. Quadrupole Magnet Design

The parameters are given in Table 3-1.

The quadrupole field is iron-dominated, and therefore very insensitive to coil location.

The ratio of quadrupole length to bore is small ~3:1), as can be seen in Figure 3-3. To control end-effect error aberrations due to the coil, it is important to have the conductors at considerably larger radius than the pole tip. This resulting free space between coil ends and the beam vacuum chamber can be put to use for other purposes; e.g., PUE's and correction magnets. Simple racetrack coils with large area conductors can be used, with small coil forces, even at 7.5 Hz.

The aperture field is insensitive to eddy currents in the coils at 7.5 Hz.

The wide open horizontal mid-plane between the coils gives open "space" for lattice design purposes such as injection and extraction.

The disadvantage of the iron-dominated design is that it is hard to reach high pole-tip fields with straight poles. However the maximum $B_{tip} \simeq 8$ kG for heavy ions was achieved without difficulty by shaping the pole. The computed pole shape evolved from a NSLS design. A high current, compact quadrupole design with a small coil cross-section of only five turns per pole was chosen. This gives low inductance and voltage in 7.5 Hz operation.

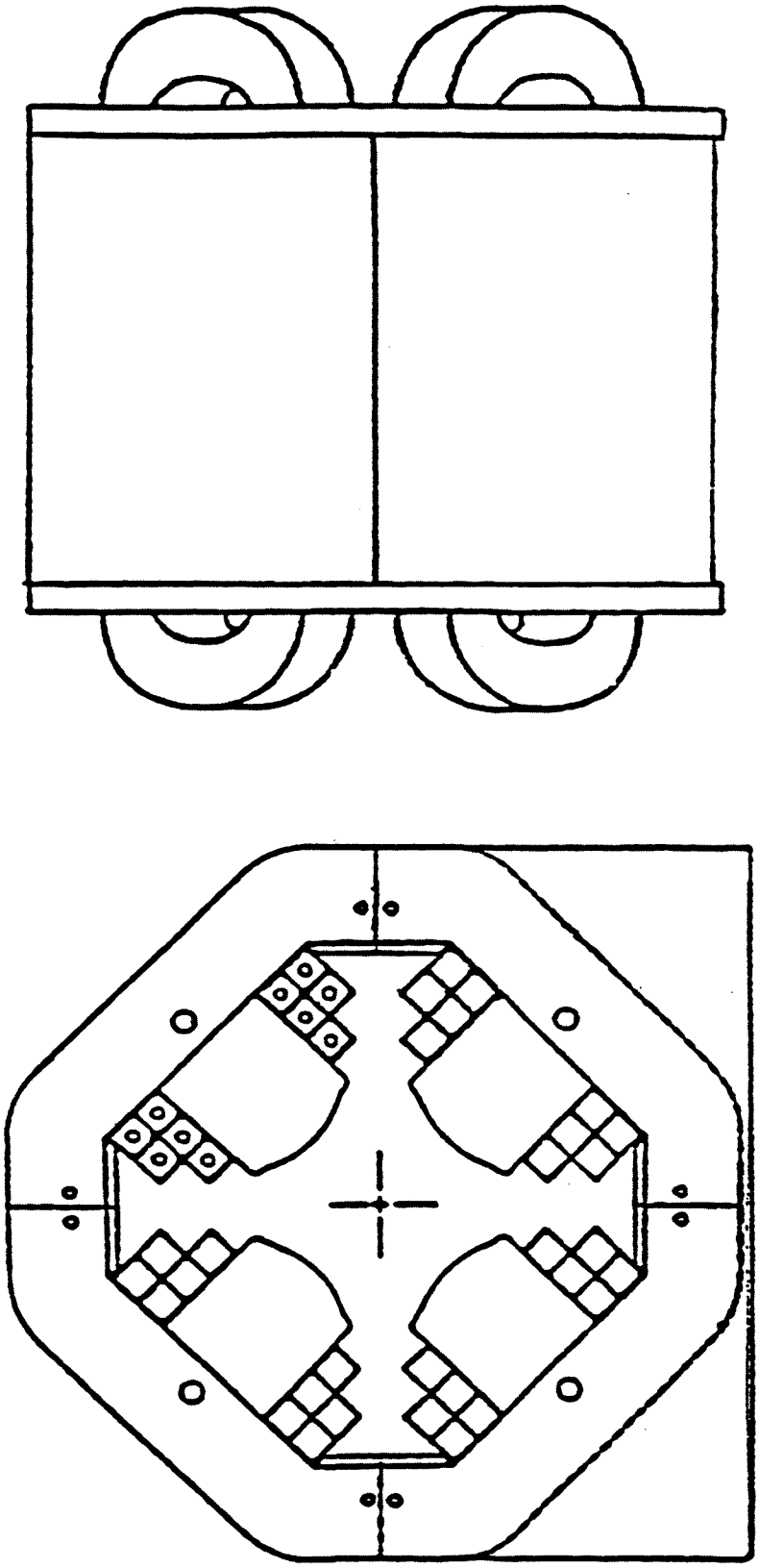

Figure 3 3 Quadrupole magnet

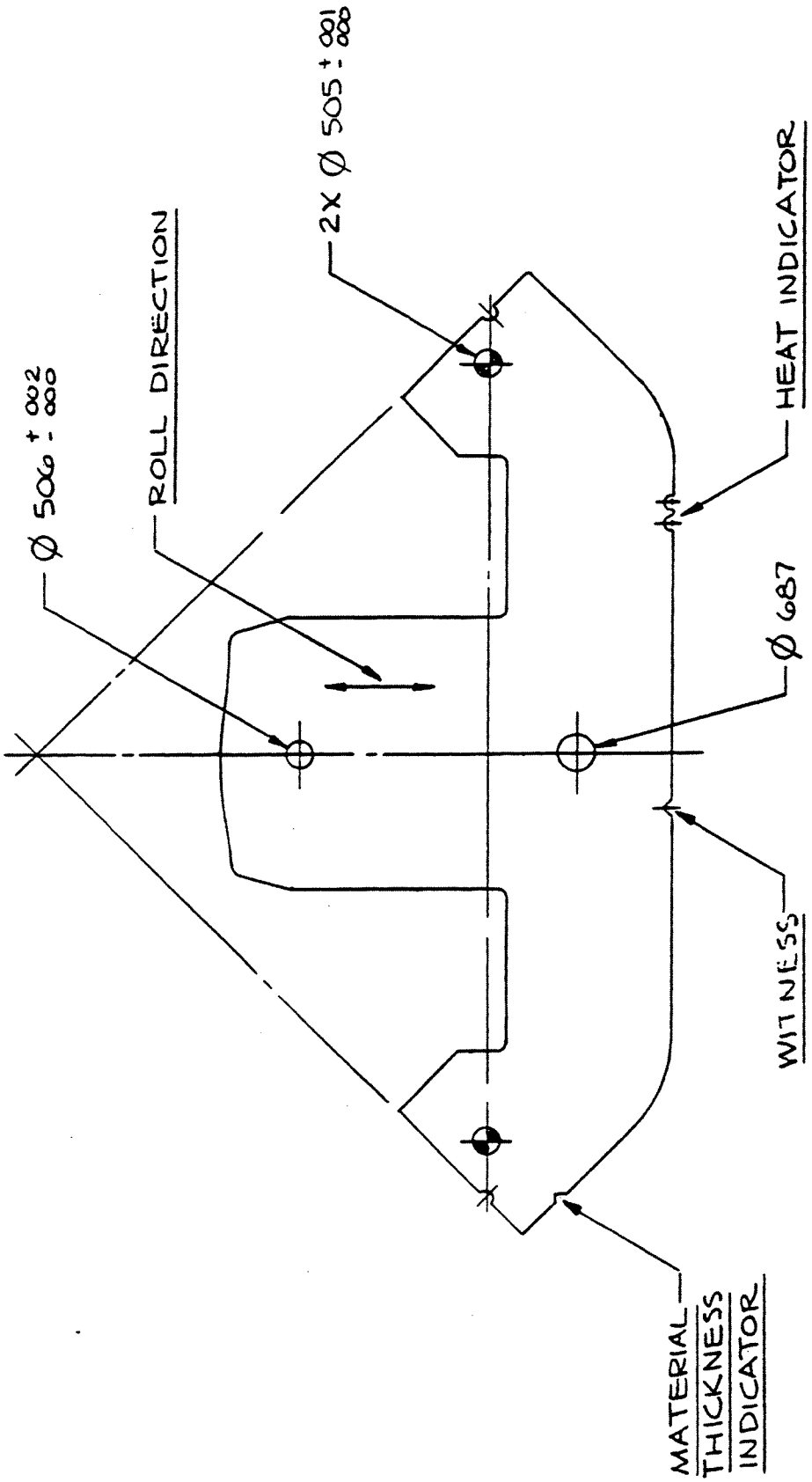

Figure 3 5 Quadrupole magnet lamination

then

$$[119^2 \times 48 + 147^2 \times 36]^{1/2} \simeq 1210 \text{ G-cm}$$

Thus the required strength of the 42 vertical-orbit correction dipoles, half of which would be in-phase, is about 60 G-cm.

The main dipole random error that will require horizontal-orbit correction is expected to be about 4×10^{-4} rms. The total horizontal correction requirement is then about 1000 G-cm. Thus each horizontal-orbit correction dipole requires a strength of approximately 50 G-cm.

3.1.3.2. Correction Quadrupoles

Corrections are needed for the ninth and possibly 10th harmonic random quadrupole error. The total in-phase error is estimated to be 30 G at injection and 41 G at 1 GeV Trim windings on the main ring quadrupole magnets will provide these corrections.

Skew quadrupole correction magnets are needed to correct the 0 θ coupling resonance. The field roll of the quadrupoles may be as big as 0.5 mrad, which gives an effective in-phase component of about 21 G. The required strength of the skew quadrupole correction magnets is then about one half that for the random quadrupole correction magnets.

3.1.3.3. Correction Sextupoles

The fourteenth and possibly the thirteenth and fifteenth harmonic produced by random sextupoles should be corrected. The major random sextupole errors are from the eddy current (10^{-2}) and the chromaticity sextupole error (10^{-3}), which amounts to a total in-phase component of 190 G/m^2-m. The correction fields will be provided by trim windings on the main sextupole magnets.

The major source of skew sextupole errors are from the roll of the dipoles and its vacuum chambers, and from the roll of the chromaticity sextupoles. Both errors can be as large as 5×10^{-4} and the total in-phase error is about 85 G/m^2-m — about half the random sextupole correction requirement.

3.2. Booster Power Supplies

3.2.1. Main Ring Power Supplies

3.2.1.1. Introduction

The requirements for the AGS Booster main ring power supplies (BMRPS) are quite varied. They must act as accurate, low-voltage supplies for beam injection; they must ramp rapidly up and down, in two (2) distinctly different modes, for beam acceleration and cycle recovery; and also be capable of flattop operation for a period greater than two (2) seconds for accumulation of polarized proton beams. The difference in the acceleration part of the cycles referred to above, arise due to the fact that protons are to be accelerated to an energy of 1.5 GeV ($B\rho$ =7.5 T-m) in a machine cycle requiring a pulse repetition frequency of 7.5 Hertz (133.3 millisecond period), while heavy ions will be accelerated to an energy corresponding to a $B\rho$ = 17.6 T-m, requiring a pulse repetition frequency of between 0.5 and 0.7 Hertz (1.4 to 2.0 second period). The cycles are described in section 3.2.1.2.1.

Not only must the BMRPS accommodate the cycles described above, but they must also perform to several other exacting performance specifications. These are reproducibility of cycles, and high accuracy at certain parts of the cycles such as injection and extraction. By accuracy we refer to deviations in the main guiding and focusing fields from ideal. This is usually caused by ripple in the dc power supply output or by regulation problems both within a given pulse or from one pulse to another The term reserved for these variations by industry is PARD (periodic and random deviations). The design details and parameters are described in section 3.2.1.2.2.

In sections 3.2.1.2.3 and 3.2.1.2.4, the actual design details are described. Sections 3.2.1.2.5 and 3.2.1.2.6 cover the installation, hook-up, monitoring and protection schemes. Section 3.2.1.3 describes the main ring quadrupole systems, and 3.2.1.4 describes the main ring corrector power supplies (including sextupoles). Table 3-7 lists the total number and types of power supplies required for the Booster

3.2.1.2. Dipole Power Supply

3.2.1.2.1. General Requirements

Since the Booster's primary function is to be an injector for the AGS, its acceleration cycles are very closely tied to those of the AGS. For the proton case, the AGS accelerates in two (2) distinctly different modes, the Fast Extracted Beam (FEB) mode and the Slow Extracted Beam (SEB) mode. For each of these, the primary objective of the Booster is to deliver a series of four (4) high intensity pulses to the AGS which is sitting at an injection flattop energy of 1.5 GeV This will result in an increase in the AGS intensity by a factor of four The AGS then accelerates the entire beam to an energy approaching 30 GeV and spills the beam in one revolution ($\sim$ 2.4 μs) for FEB or over a time of 1.5 seconds for SEB. These operations are shown in Figures 3-6(a) and 3-6(b). In these figures the waveforms are shown in an idealized form. As can be seen, the major requirement for the Booster is rapid cycling (period of 133.3 milliseconds, pulse repetition

frequency 7.5 Hertz) from an injection energy of 200 MeV to a final energy of 1.5 GeV

For polarized proton operation, the Booster is basically an accumulator ring where 200 MeV H^- polarized pulses from the Linac are stacked for a period greater than 2.0 seconds. Approximately once every 2.4 seconds, the stacked beam is accelerated rapidly to 1.5 GeV and transferred to the AGS where it is used in the SEB mode, at the present time. The waveforms for this scheme are shown in Figure 3-7(a). The Booster acceleration cycle requirements are the same as described above except a single pulse is delivered rather than four

In Figure 3-7(b) is shown a very different cycle requirement for the Booster This shows the heavy ion or slow acceleration cycle. The Booster is required to pulse to higher fields and to extract heavy ion beams up to a rigidity of 17.6 Tesla-meters. Since only one beam transfer is required per AGS cycle, the Booster cycle has only to match that of the AGS. Thus, its maximum pulse repetition frequency is approximately 0.7 Hertz.

Cycle flexibility for the Booster is also maintained as a requirement. This would enable a form of pulse-to-pulse modulation to occur The major reason for this is to enhance the switch-over of the AGS complex between various experimental physics runs as well as to enable the use of the Booster as a machine physics accelerator This type of flexibility is already built into the Booster ring magnets in that they are laminated, excellent high field quality components. For example, cycle flexibility in the BMRPS will enable a mix of cycles, in a supercycle mode, which could intersperse a heavy-ion commissioning pulse while the Booster/AGS are operating in a proton mode. Also, machine physics study cycles can be placed in the unused spaces of the Booster cycle. This will facilitate machine understanding in a shorter time, as well as enable the complex to switch over between the various beam modes or ion species in as rapid a time as possible. Also, dedicated mode or scheduled running can be minimized.

The Booster main ring power supplies described in this design report will support the cycle requirements described above and will enable switch-over to other modes on a pulse-by-pulse basis.

3.2.1.2.2. Options

In assessing the type of powering system to use for the Booster main ring magnets, several types were considered, with each having certain advantages and disadvantages. The following describes some of the different choices and the rationale behind our final decision. For the proton rapid-cycling mode (i.e. 7.5 Hertz), a resonant supply system would have served the application well. For the accumulation or storing of polarized proton beams, a well-regulated dc supply would be required. For the higher energy equivalent heavy ion acceleration, a lower voltage but higher current is required. Using two (2) systems or some combination of units would have been prohibitively expensive and overly complicated to operate. Therefore, we chose a programmable, multiphase, dc power supply, using silicon controlled rectifiers (SCR'S) as the controlling elements. If the system is broken up into a series of modules, it enables some optimization at the various points in the cycle, namely, injection and flattops, extraction, and switching

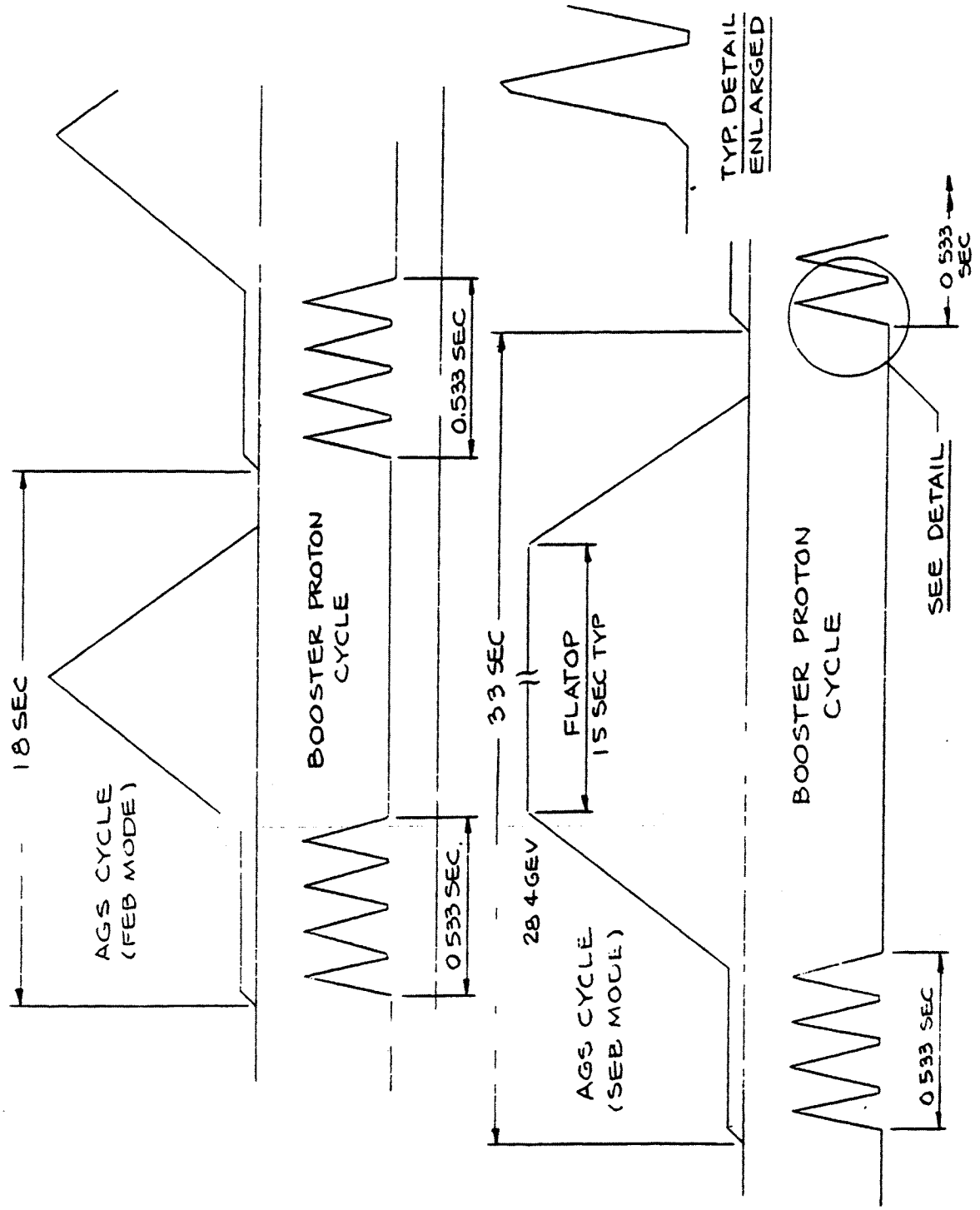

Figure 3 6(a) & (b) Proton cycles, (a) FEB, (b) SEB

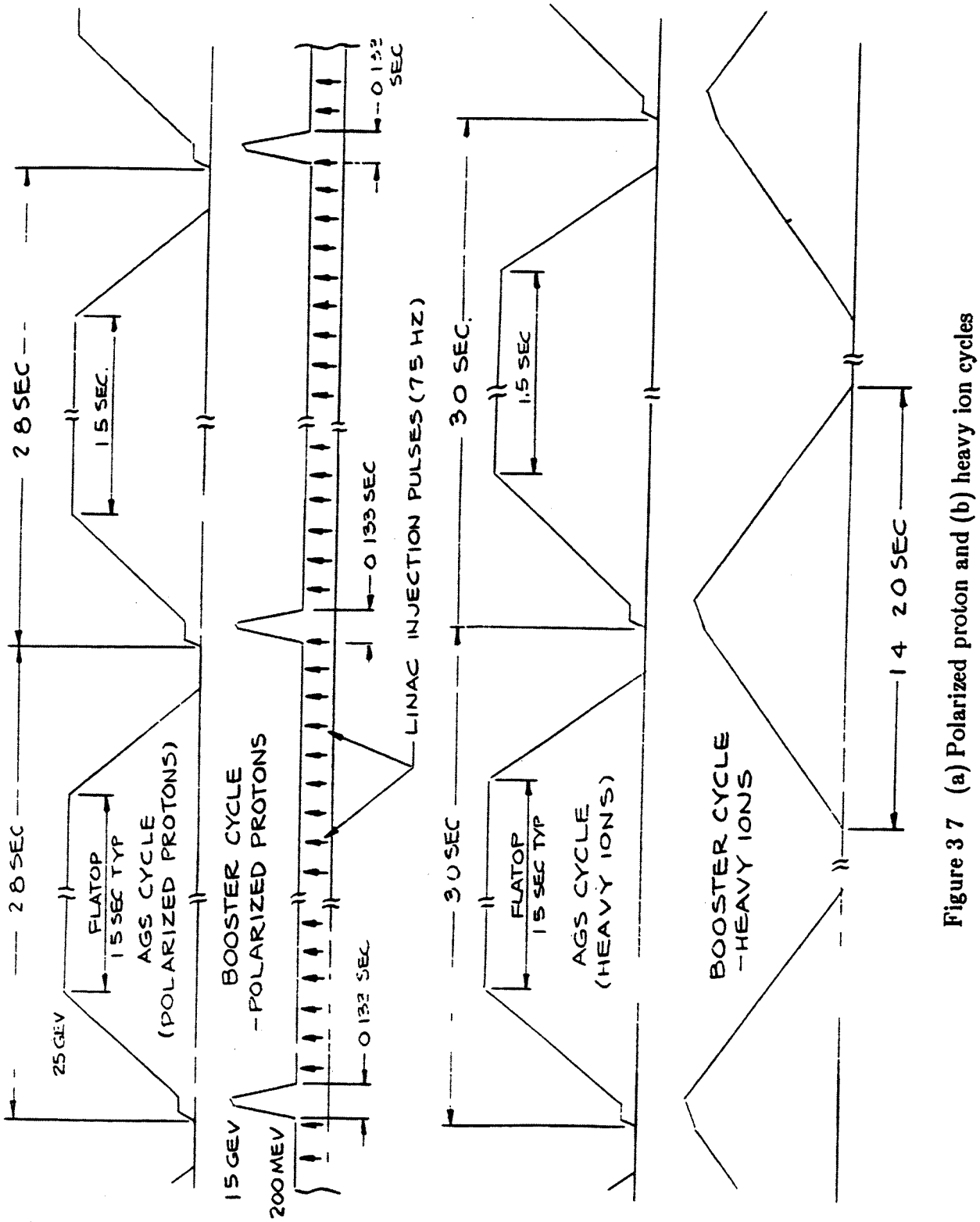

Figure 3.7 (a) Polarized proton and (b) heavy ion cycles

between 7.5 and 0.5 Hertz operation. The latter requirements represent electrically opposite extremes in that protons require a high voltage, low current power supply, and heavy ions require a lower voltage but much higher current unit. (See Table 3-2). These requirements can be met by constructing the p.s. in many identical modules, thus permitting switching of some form between series/parallel arrangements, switching at the load, or by-pass operation of units.

TABLE 3-2 Main dipole and quad power supply system requirements.

Cycle	Voltage (Volts)	Current (Amperes)		Power (MW)	
		peak	rms	peak	rms
Dipoles:					
Protons	4950	2400	1700	11.9	8.4
Heavy Ions	1550	5600	3400	8.7	5.3
Quadrupoles:					
Protons	435	2400	1700	1.0	0.74
Heavy Ions	270	5600	3400	1.5	0.92

Therefore, our final choice of adjustable SCR multiphase supplies presents the Booster with a scheme that meets the requirements of the machine as specified and also offers a large amount of design and operational flexibility Modularization of the system also results in further enhancement of the operation as well as optimization of cost.

3.2.1.2.3. Design Considerations

The previous sections described the macroscopic requirements of the Booster Main Ring Power Supply (BMRPS). This section will give more specific requirements as well as describe the overall design of the dipole PS. Table 3-3 lists the major parameters of the Booster dipole magnet and PS. As can be seen from the table, the Booster magnet requires different injection and extraction fields for the proton and heavy-ion modes. The other major parameters affecting the power supply design are the p.r.f. and the accuracy and reproducibility of the cycles. The power supply load time constant is 2.0 seconds.

TABLE 3-3 List of parameters for the Booster dipole system.

Parameter	Unit	Proton	Heavy Ion
Type		Curved H	
Number of Magnets	each	36 + 1	
Bend Angle	degrees	10	
Core Length	m	2.34	
Magnetic Length	m	2.40	
Gap Height	cm	8.255	
Pole Width	cm	25.4	
Useful Aperture	cm	15.2 × 7.0	
No. Pancakes per Magnet		4	
No. Turns per Pancake		4	
Injection Field (B_i)	kG	1.56	0.5 - 0.8
Extraction Field (B_f)	kG	5.46	12.74
Inj. Transfer Function (B_i/I_i)	G/A	2.436	
Extr Transfer Function (B_f/I_f)	G/A	2.320	
Injection Current (I_i)	A	640	~300
Extraction Current (I_f)	A	2250	5700
rms Current	A	1700	3500
Conductor Dimensions (H × V)	mm	24.5 × 50.8	
Current Density (max)	A/cm^2	525	
Resistance/Magnet	mΩ	1.5	
Resistance, total	mΩ	65	
Inductance/Magnet	mHy	3.2	
Inductance, total	mHy	120	
Coil Insulation, dc volts	kV	20	
Pulse Repetition Frequency	Hz	7.5	0.5 - 0.7
Max. I	kA/s	40	10
IR max	V	150	360
LI max	V	4800	1200
Total Voltage	V	4950	1560
Peak Power	MW	11	8.6
Dissipated Power	kW	200	800
Stored Energy	kJ	300	1800
Correction Windings		PBLW 2 T total Other 6 T total	

The actual shape of the Booster cycle is determined by the low B injection period, the constant rf bucket (1.5 eV-s) area acceleration,[1,2] and the invert or recovery part of the cycle.[3] Calculated waveshapes of voltage and current resulting from the above considerations are shown in Figure 3-8(a) for protons. The maximum current (I) for operation at 1.5 GeV is 2254 amperes. The maximum I is 40 kA/s. For heavy ions, a calculated cycle (voltage, current) of approximately 1.4 seconds is shown in Figure 3-8(b). The maximum dipole field (current) depends on the heavy ion species, with a value of 12.74 kG. (5700 amps) for gold. The maximum I is 10 kA/s. Table 3-2 summarizes the final dipole BMRPS requirements.

Several other criteria were considered in determining the power supply configuration. These primarily concern reliability issues, economics issues, and the ultimate performance. Keeping the voltage stress on semiconductor devices and on the magnets at a low value increases both the lifetime and the reliability of the system. Feeding the magnet string at two (2) locations reduces the magnet voltage to ground to a more reliable level and results in fewer magnet coil failures. This would reduce the number of bleedups and bakeouts of the vacuum system. For performance improvements in the ripple and response time, a larger number of SCR phases would be preferable. A larger number of phases also gives a smoother control and output function. Provided the phases can be kept balanced, the improvements in performance as well as the reduction in size of the ripple filter would be appreciable. Also, if we standardize on more readily available commercial power supply units, a cost savings should result upon the procurement of these units.

Based on the above, and together with the fact that a larger number of modules would accommodate a more exact match to the cycle variations and requirements, (without exceeding the accuracy specifications), we decided to construct a dipole power supply system that consists of two (2) stations composed of three (3) groups each. One group (consisting of two modules) will be on continuously and be capable of handling proton and heavy ion injection, and polarized proton accumulation. All other modules will have bypass switches and would normally be in bypass mode. As more voltage is required for any acceleration mode, additional groups would be turned on (unbypassed). A block diagram of this system is shown in Figure 3-9. Groups I and II (total of four modules) are rated 867 volts, 3500 amperes (rms) each. All the other groups, III through VI (eight modules) have ratings of 867 volts, 1750 amperes (rms) each. A detailed schematic of a group (two modules) is given in Figure 3-10. Table 3-4 summarizes the voltages, currents, and power values that can be obtained from the combinations of modules for the various anticipated modes of operation. The additional 30% rating available from groups I and II, result in complete cycle flexibility for the Booster without having to shut down or reduce the power to zero to mechanically switch cycles. It also eliminates the need for very complex, unreliable dynamic-mode changing switches (i.e.

---

[1] J. G. Cottingham, "Proton Cycle for the Booster" BSTN No. 49, September 1986.

[2] M. Meth, "Calculation of Booster Power Requirements Based on Constant RF Bucket Area" BSTN No. 45, June 1986.

[4] J. G. Cottingham, "Considerations Affecting the Booster Magnet Cycle" April 1986.

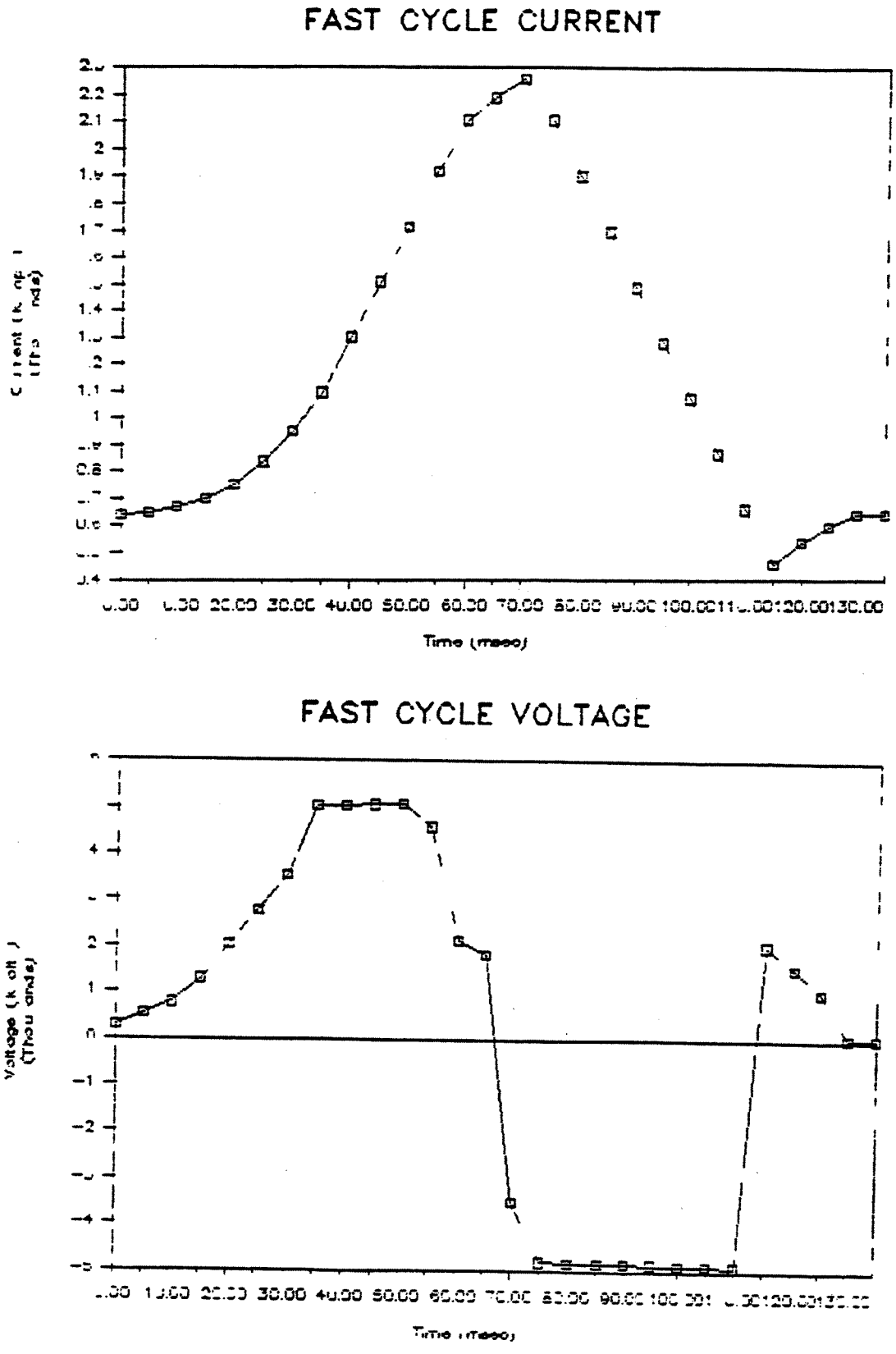

Figure 3-8(a). Voltage and current for fast cycle.

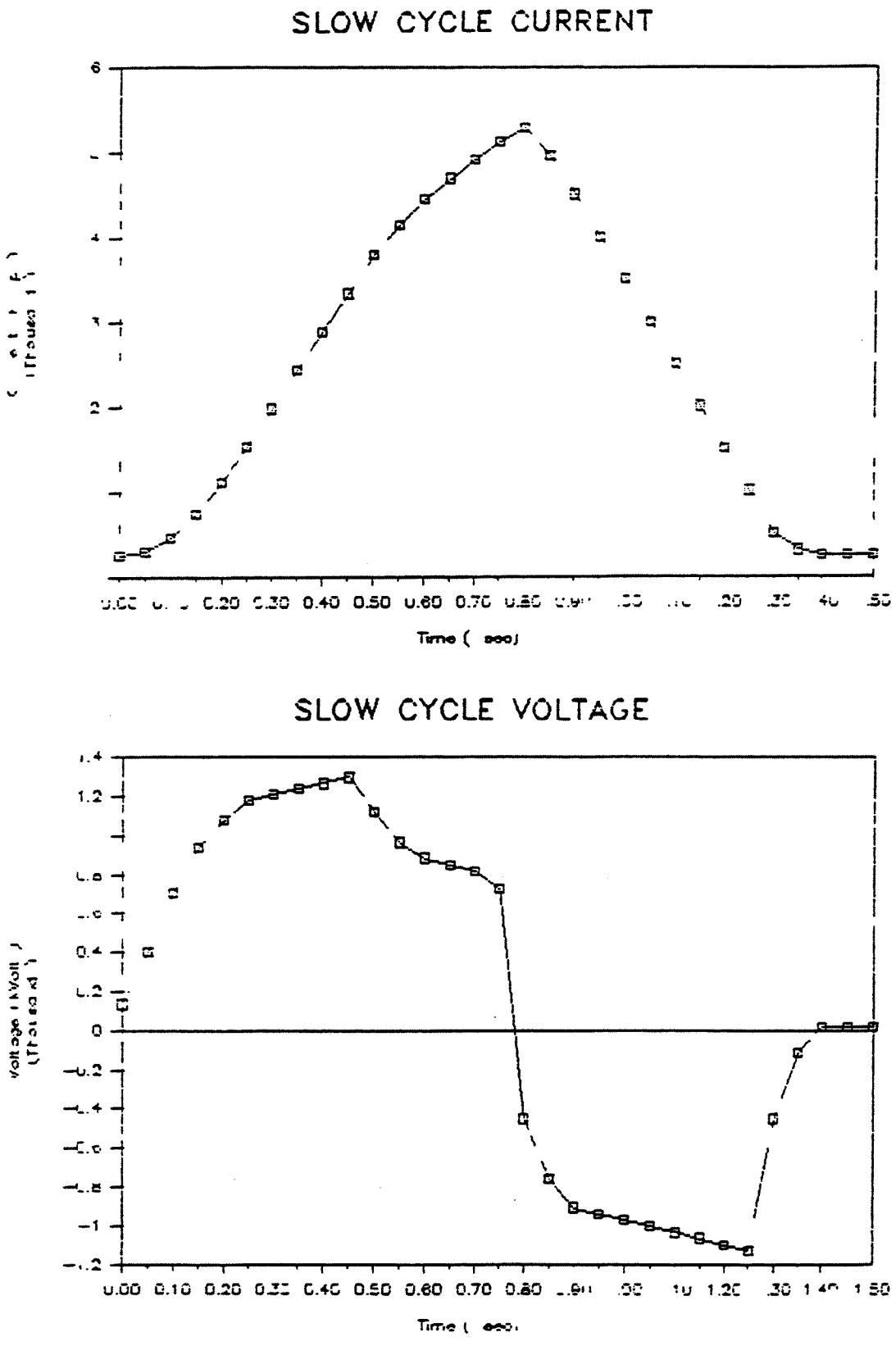

Figure 3-8(b). Voltage and current for slow cycle.

solid-state units). This will cut down specifically scheduled single-mode operation and results in faster change-over between modes. It will also enhance machine understanding.

TABLE 3-4 Design values for the modules of the magnet power supplies.

a) Dipole System Modules:

Modules	Voltage/Mod. (Volts)	Current/Mod. peak	Current/Mod. rms	Power/Mod peak	Power/Mod rms	Use	V_{Net}	I_{pk}
$V_1 - V_4$	433.3 V	6000 A	3500 A	2.6 MW	1.5 MW	1 — H. I. 2 — Proton	1733 V 1733 V	6000 A 3000 A
$V_5 - V_{12}$	433.3 V	3000 A	1750 A	1.3 MW	0.76 MW	1 — H. I. 2 — Proton	by-passed 3466 V	by-passed 3000 A

b) Quadrupole System Modules:

Modules	Voltage/Mod. (Volts)	Current/Mod. peak	Current/Mod. rms	Power/Mod peak	Power/Mod rms	Use	V_{Net}	I_{pk}
V_{Q_H} V_{Q_V}	433.3 V	6000 A	3500 A	2.6 MW	1.5 MW	1 — H. I. 2 — Proton	433.3 V 433.3 V	6000 A 3000 A

To reduce the amplitude of the power supply output fundamental ripple component, damped passive low-pass filters will be used. These filters will have optimized transient response so they do not cause any large unnecessary loop delays.[4]

3.2.1.2.4. Control

The control of the various cycles required by the Booster will be by computer-controlled function generators. Dedicated cycle modes or supercycle modes will be set up and stored in the local device control computer The host computers can download different functions as desired. The local station computer, acting through the local device controller, will convert the host commands to local parameters (14-16 bit) stored in tables and they will in turn generate the output vectors that comprise the detailed cycle.

The timing will be derived from the Booster master timing generator, which is ultimately driven by the AGS complex supercycle generator (SCG). This device is line synchronized. (See Chapter 9.)

The power supply will have real-time feedback loops to assure cycle reproducibility and to assure that the outputs have followed the desired commands. The performance will be verified via computer monitoring of the output voltages and current, the loop error signal, and the output ripple. Appropriate A to D converters (12-16 bit) will be

[4] *ibid.*

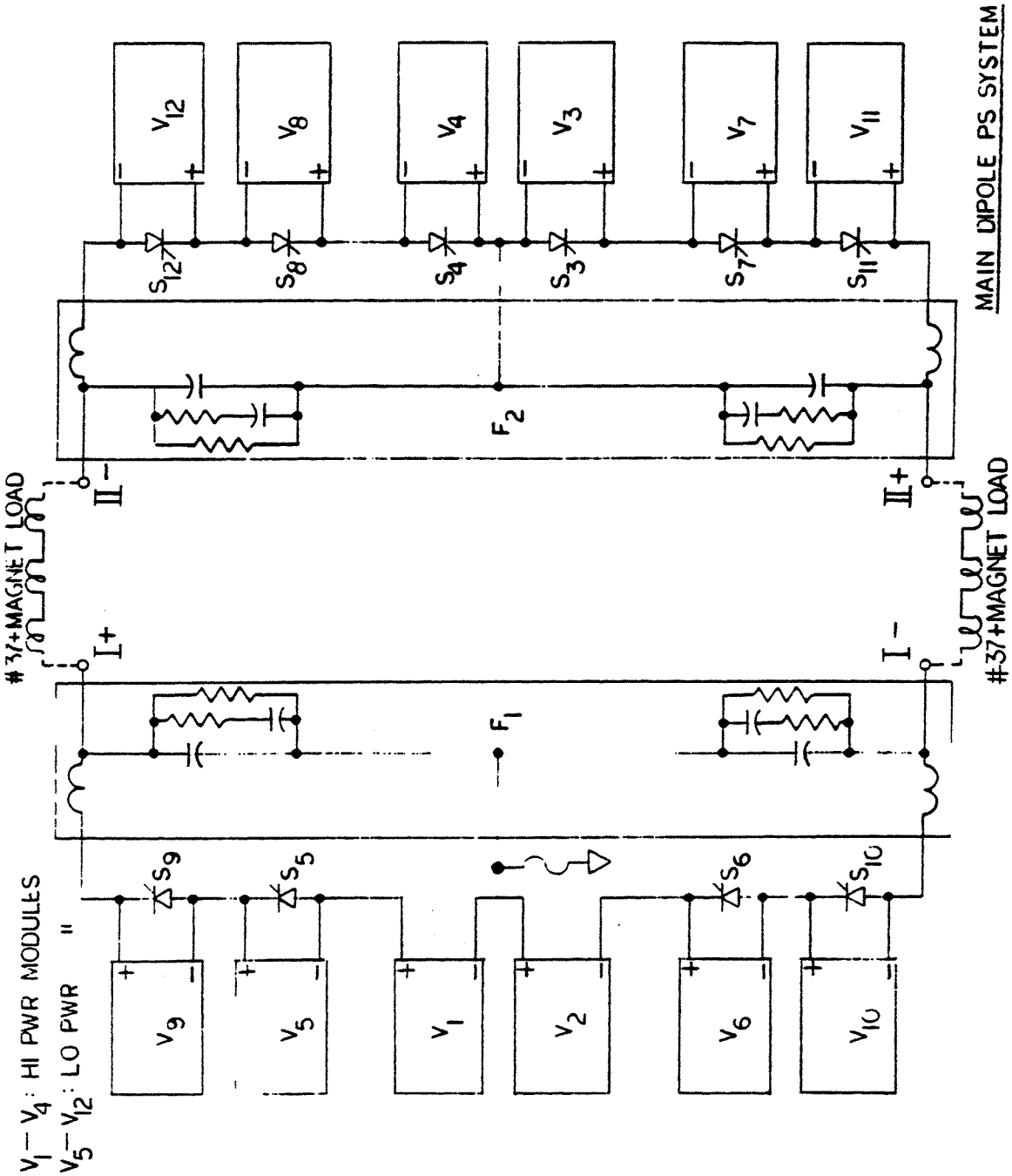

Figure 3 9 Block diagram main dipole power supply system

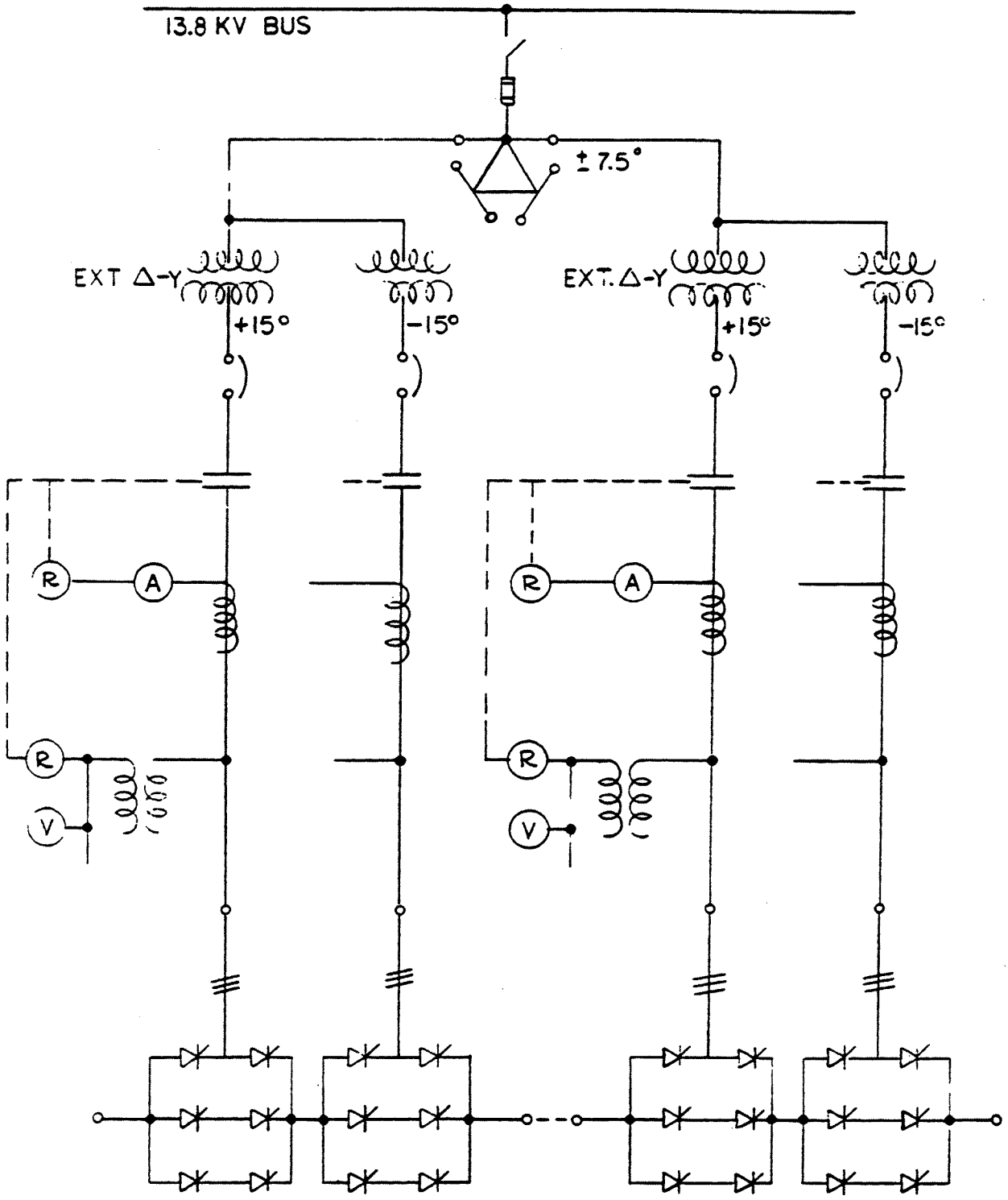

Figure 3-10. Typical dipole group schematic diagram.

used for the analog signal monitoring. A Fast Fourier Transform will be used to analyze and present the various ripple components on the output voltage waveforms. The computer will also have the capability (since it has prior knowledge of the cycle) to give feed-forward information to assist in setting up the proper cycle and its control. Items such as which groups of modules to energize and which by-pass switches should be activated will be available. Cycle information will also be acquired from previous pulses and this will subsequently be used to alter the present or future cycles.

3.2.1.2.5. Magnet Bus, Monitoring, Protection

The dipole magnet load parameters are 120 mHy and 65 mΩ for the 37 magnets connected in series. The magnet upper and lower coils will be hooked up in a folded or doubled-back series configuration which has a loop break 180 opposite to the first feed point. Power will be fed to the magnets at two (2) points to decrease the voltage stress to ground. A simplified schematic is shown in Figure 3-11.

A ground monitoring system will be used to check the integrity of the system and to alarm and interlock the power supply if ground faults have developed. The magnets and power supply will also have over-voltage limiting devices and detection systems. Thermal protection in the form of water-flow switches and over-temperature devices on all parallel water cooling paths will be provided.

Extra dipole windings will be incorporated in each dipole magnet and used for various purposes. The low power, single-turn windings will be wired to a monitoring point and used as a diagnostic for any abnormal magnetic field behavior in individual magnets. Other windings will be used for beam orbit deformations and as possible trim or correction windings.

The magnet current will be measured by a very accurate ($<0.001\%$) direct current transformer or DCCT The magnet voltages will be measured via isolated voltage sensing devices or compensated dividers that have good frequency response and good temperature and voltage stability

An additional dipole magnet (No. 37) will be placed in series with the rest of the ring dipole magnets and used as a reference or measuring magnet. This unit will have the field measuring devices both for absolute and relative measurements. A fast, bipolar gauss clock will generate the pulsed field signals for the timing of other accelerator functions, rf, extraction, etc. Magnet No. 37 will also contain Hall probe(s) as well as a nuclear magnetic resonance (NMR) probe. These will be used for remnant field corrections and for absolute calibration and checking of the running gauss clock.

3.2.1.2.6. AC Line Effects

Powering a synchrotron or any cyclical, high peak power device directly off the commercial power line has several potentially harmful drawbacks. The pulsed real and reactive power variations cause phase and voltage flicker This problem has been studied for

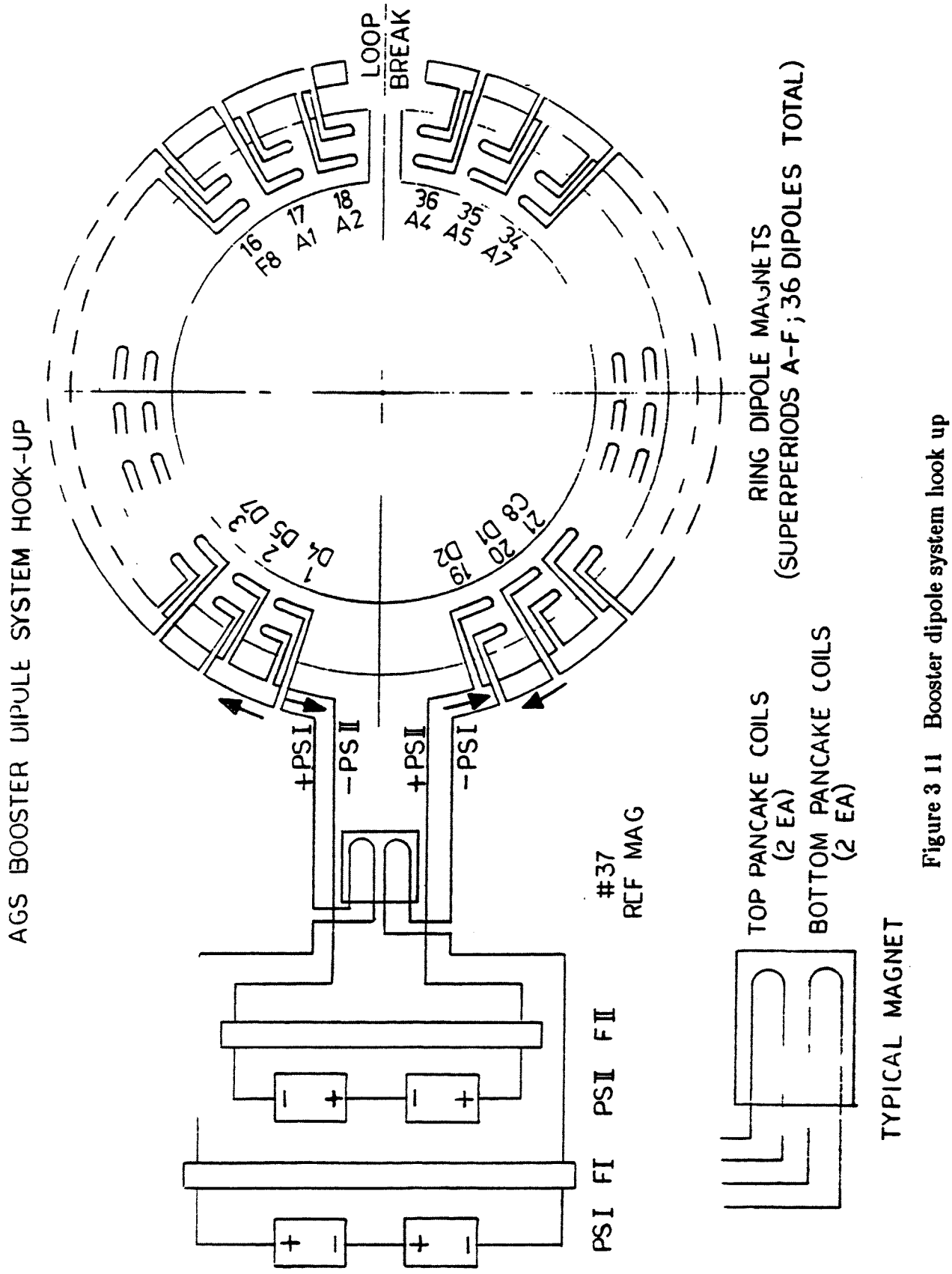

Figure 3 11 Booster dipole system hook up

previous large accelerator installations[5,6,7,8] and for arc furnace installations. In our case for the Booster, the short-circuit capacity of our feeders and the use of an alternate 69 kV line results in acceptable values of <0.5% voltage variation and <0.5 phase variation. Complete details and studies of this problem are given in the references.[9,10,11]

From the above studies, the scheme chosen is depicted in Figure 3-12. The figure shows a dedicated 20/27 MVA transformer which steps down the incoming 69 kV to 13.8 kV This voltage is then fed via selectable switchgear to a local switchgear cubicle. This is then transformed via a series of phase-shifting transformers and a series of rectifier transformers to the low voltages required by the Booster SCR modules (see section 3.2.1.2.3).

Future enhancements for the dedicated Booster main powering system, would be to include dynamic reactive power compensation and harmonic filtering techniques.

3.2.1.3. Quadrupole Power Supplies

3.2.1.3.1. Requirements

The AGS Booster is a separated-function machine, and the lattice incorporates 24 horizontal and 24 vertical focusing quadrupoles. In order to accurately hold the tunes of the machine during acceleration, the quadrupoles must track the dipoles to within ±0.1%. This will assure tune accuracies of $\pm$ 0.01 ν In addition, it is required to have a range in tunes of $\pm$ 0.5 ν so that the optimum range of values in tune space can be exploited.

The parameters for the ring quadrupoles and power supplies are given in Table 3-5. As can be seen from the table, similar cycle variations in parameters exist for the quadrupoles as for the dipoles. Many of the dipole comments apply equally well to the quadrupoles.

---

[5]J. A. Fox, "Static Power Supplies for Pulsed Loads," *IEEE Transactions on Nuclear Science*, **NS-16**, June 1969.

[6]R. Cassel, J. E. Van Ness, "Direct Powering of the 200 GeV Synchrotron Magnets from the Utility System" *op. cit.*, **NS-16**, June 1969.

[7]R. Cassel, "Power Supply for NAL Main Ring," *op. cit.*, **NS-20**, 1973.

[8]A. Rohrmayer, "Operation of Accelerators Directly Off the Utility System," *op. cit.*, **NS-14**, June 1967

[9]M. Meth, "Preliminary Study of AC Power Feeders for the AGS Booster," AD Tech. Note #220, October 1985.

[10]M. Meth, "Line Flicker for 1.5 GeV Proton Operation," BSTN No. 54, July 1986.

[11]M. Meth, A. Ratti, "Frequency Spectrum Generated by AGS Booster Power Swings, Heavy Ion Cycle," BSTN No. 106, January 1988.

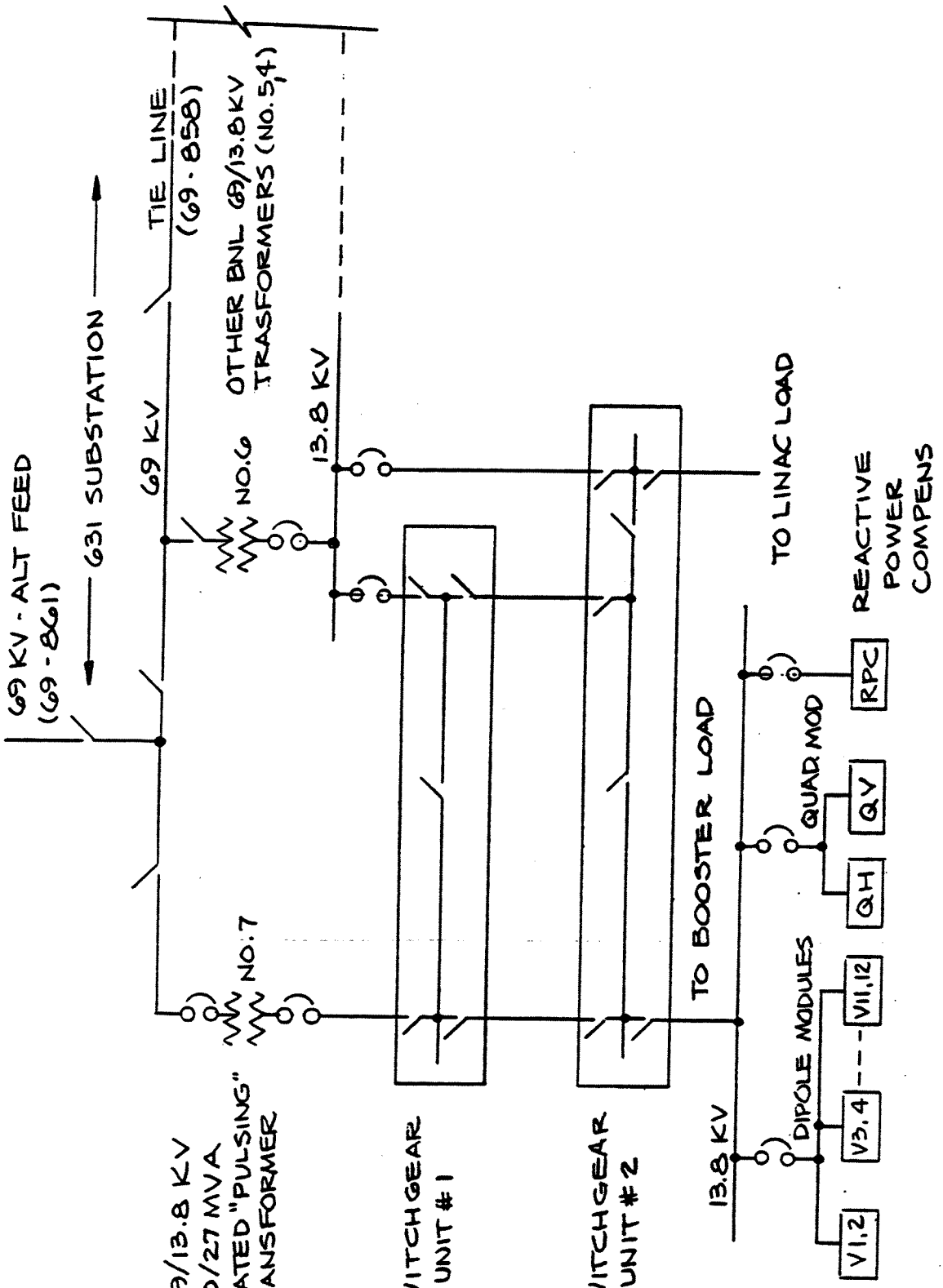

Figure 3-12. Booster main AC power distribution.

TABLE 3-5 List of parameters for the Booster quadrupole system.

Parameter	Unit	Proton	Heavy Ion
Type		Iron Core Quads	
Number of Magnets (H, V, H_{ref}, V_{ref})	each	24, 24, 1, 1	
Core Length	m	0.47	
Magnetic Length	m	0.50	
Pole Tip Radius	cm	8.255	
Pole Width	cm	12.7	
Useful Aperture (radius)	cm	6.6	
No. Pancakes per Pole		1	
No. Turns per Pancake		5	
Poletip Gradient (max.)	kG/m	12	
Injection Field (B_i)	kG	1.0	0.4
Extraction Field (B_f)	kG	3.5	8.3
Inj. Transfer Function (B_i/I_i)	G/A	1.5625	
Extr Transfer Function (B_f/I_f)	G/A	1.512	
Injection Current (I_i)	A	640	250
Extraction Current (I_f)	A	2240	5700
rms Current	A	1700	3500
Conductor Dimensions (H × V)	mm	31.7 × 31.7	
Current Density (max)	A/cm^2	600	
Resistance/Magnet	mΩ	0.90	
Resistance, total	mΩ	32.5	
Inductance/Magnet	mHy	0.35	
Inductance, total	mHy	9.0	
Coil Insulation, dc volts	kV	20	
Pulse Repetition Frequency	Hz	7.5	0.5 - 0.7
Max. I	kA/s	40	10
IR max	V	75	180
LI max	V	360	90
Total Voltage	V	435	270
Peak Power	MW	0.975	1.48
Dissipated Power	kW	100	400
Stored Energy	kJ	23	135

The time constant (L/R) for the quadrupoles is much shorter than that of the dipoles. If one takes into account vacuum chamber and magnet eddy current effects, this

makes tracking adjustments in the quadrupole currents much more critical. Therefore, it was decided to power the horizontal and vertical quadrupole strings separately with their own individual power supply The major requirements for these units are that they be accurate, low ripple, fast response, full power units.

3.2.1.3.2. Design

Since the quadrupole power supplies have to be very accurate power function generators, we have decided to design the units as modified series regulators with slaved silicon controlled rectifier (SCR) feedback loops. The scheme will consist of multiphase transformers, SCR'S, passive low pass (*RLC*) filters and series regulators. The scheme is shown in Figure 3-13, in block diagram form.

An alternative approach to the above scheme is to power separate, isolated, high-power windings which are included in the quadrupole magnet design. These windings will be connected in series in all 25 quadrupole magnets and would be used to superimpose a trimming current ($\pm 10\%$) on the quadrupoles in addition to the main current which is obtained from the large SCR power supplies. A limitation of this scheme is the net amount of I that can be coupled through the trim windings.

The 25 (24 ring quads + 1 reference quad) horizontal and 25 vertical quadrupoles will be connected in series as two completely independent strings. The time constant (L/R) of each string is approximately 0.25 seconds. The power feeds are folded back at the loop continuity break point which is at the same place as the dipole break. For details, see Figure 3-14.

The quadrupole currents will be measured by a very accurate DCCT Isolated, stable, compensated voltage dividers will be used for voltage monitoring and for feedback.

Reference magnets hooked up in series with the ring quadrupole strings will be used to monitor the pole tip fields and to check the match or tracking to the dipoles. The measuring probes will be coils inside vacuum chambers, whose outputs are integrated to obtain the field at any point in the cycle. Hall effect plates that are temperature compensated will be used to calibrate the field coil gauss clocks. The schemes will be similar to those used for the dipole.

The quadrupole power supplies will be interfaced to the Booster computer control system. The control system will supply the analog function (D/A) generators for voltage or current references. This will be as described in the section on dipole control. (3.2.1.2.4) The D/A hardware will be located in the power supply unit where isolated, digital information will be transmitted to it. In addition, the computer will monitor the following power supply analog signals: the output currents, the output voltages, the regulator error signals, and the reference magnet quantities.

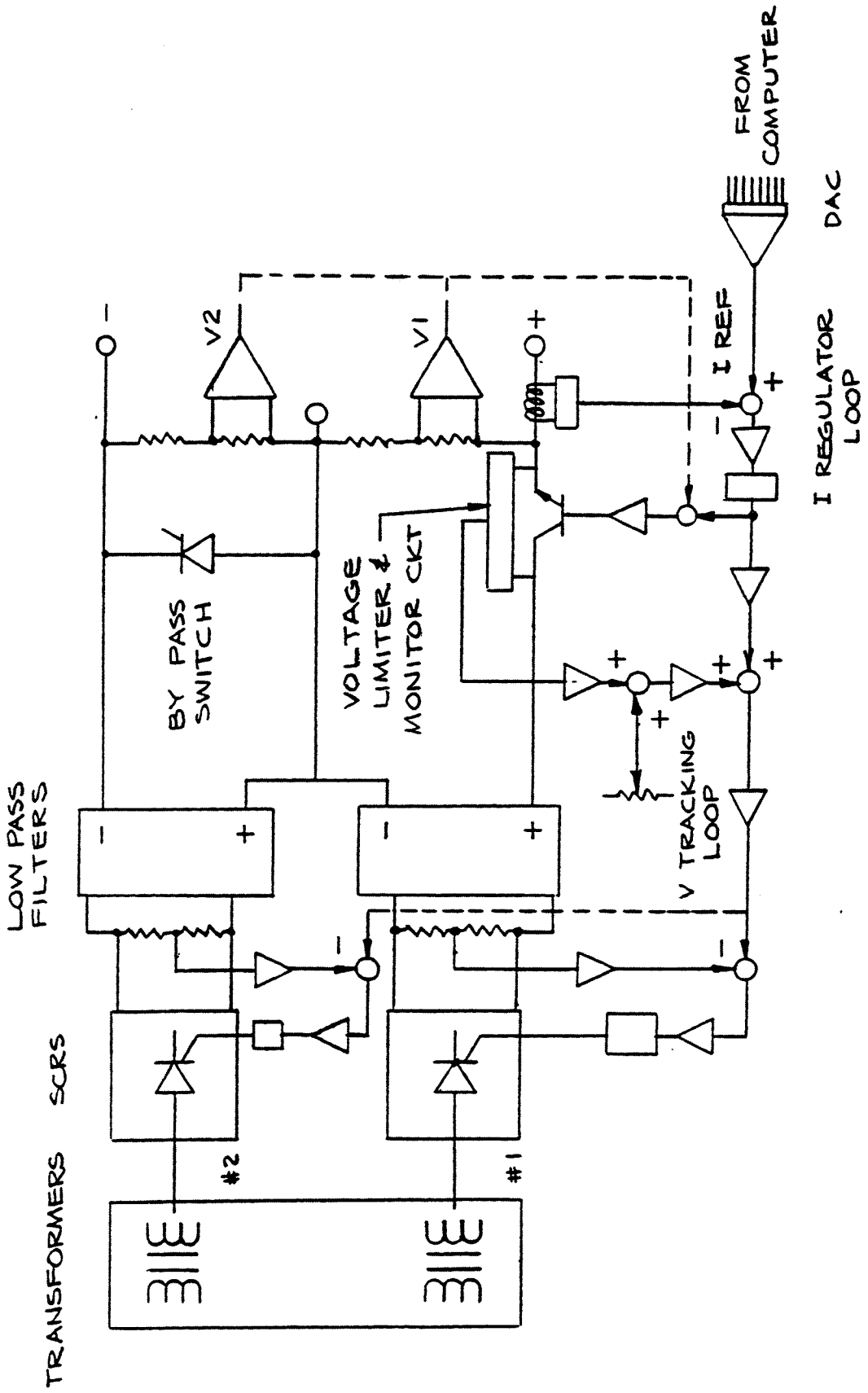

Figure 3 13 Booster quadrupole schematic

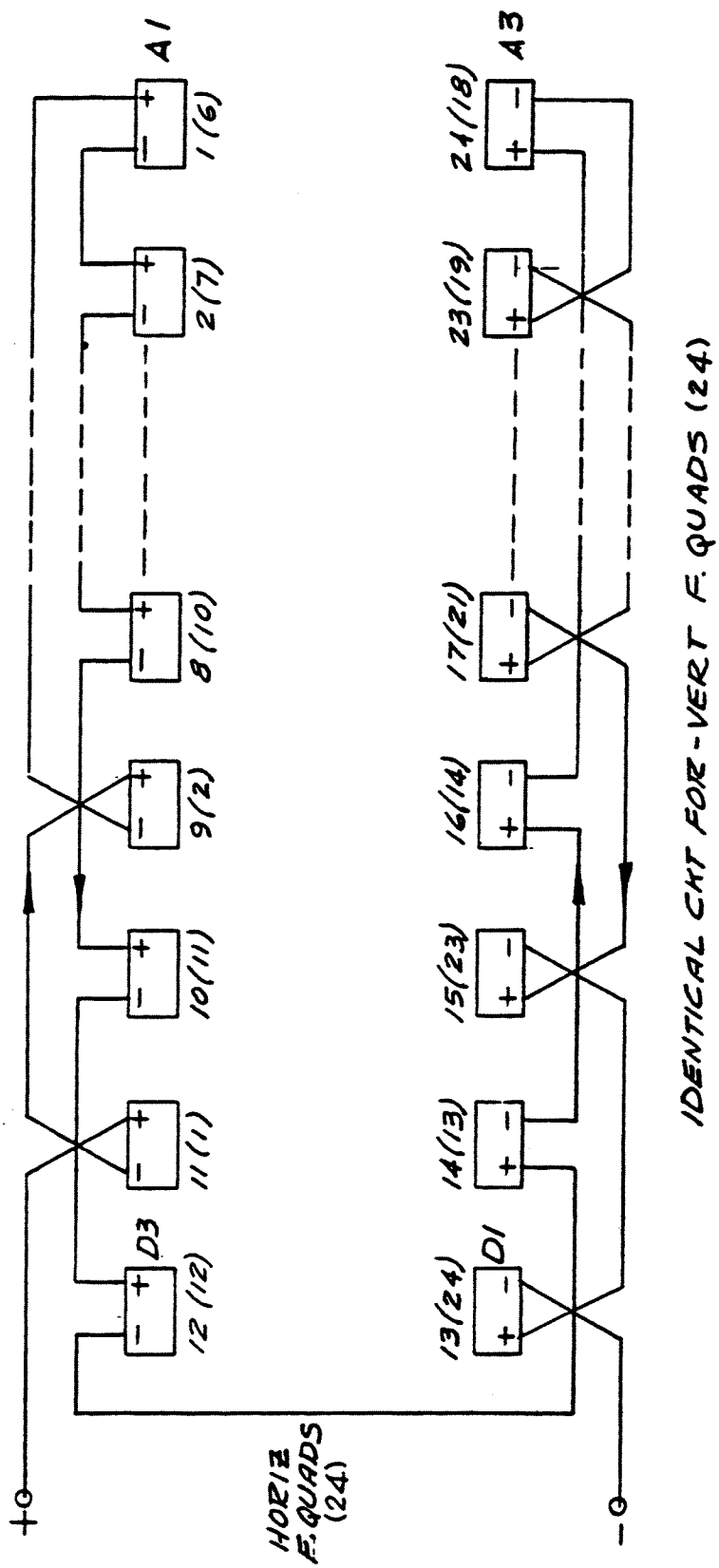

Figure 3 14 Booster quadrupole hook up

3.2.1.4. Corrector Power Supplies

3.2.1.4.1. Sextupole

The parameters for the main chromaticity sextupoles are shown in Table 3-6. Since the power requirements are quite low, two (2) regulated, pulsed supplies will be constructed, one for the horizontal sextupoles and one for the vertical. The units will consist of commercially available dc supplies, and either commercial or BNL constructed transistor banks. They will be controlled by function generators available from the Booster Control System. Readbacks of magnet current, magnet voltage, DAC output and regulator error voltage will be provided to check the operation of the supplies.

TABLE 3-6 List of parameters for the Booster sextupole system.

Parameter	Unit	Proton	Heavy Ion
Type		Iron Core Sextupoles	
Number of Magnets (H, V)	each	24, 24	
Core Length	cm	10	
Magnetic Length	m	0.1	
Pole Tip Radius	cm	7.62	
Pole Width	cm	—	
Useful Aperture (radius)	cm	—	
No. Pancakes per Pole		1	
No. Turns per Pancake		20	
Poletip Strength (max.)	kG/m^2	500	
Injection Field (B_i)	kG	0	
Extraction Field (B_f)	kG	3.0	
Inj. Transfer Function (B_i/I_i)	kG/A	0	
Extr. Transfer Function (B_f/I_f)	kG/A	0.01	
Injection Current (I_i)	A	0	
Extraction Current (I_f)	A	250	
rms Current	A	150	
Conductor Dimensions (H × V)	mm	13 × 13	
Current Density (max)	A/cm^2	150	
Resistance/Magnet	mΩ	3.6	
Resistance, total	mΩ	86.4	
Inductance/Magnet	mHy	0.06	
Inductance, total	mHy	1.5	
Coil Insulation, dc volts	kV	5	
Pulse Repetition Frequency	Hz	7.5	0.5 - 0.7
Max. I	kA/s	5	
IR max	V	26.5	
LI max	V	7.2	
Total Voltage	V	40	
Peak Power	kW	10	
Dissipated Power	kW	7	
Stored Energy	J	2	

3.2.1.4.2. Dipole and Quadrupole

The other correction power supplies required for proper Booster operation will be constructed as bipolar units of various ratings. Several schemes will be investigated that provide full four-quadrant operation. Two simplified versions are shown in Figure 3-15(a) & (b). The main control elements as shown are transistors. For higher power correctors, SCR's (dual or back-to-back) may be substituted. The transistors may be either bipolar units or V-MOSFETS in module or block form. Some low current, bipolar units are also available commercially The applicability of these units will be investigated. The power supplies will provide versatile correction controls for the various beam correction schemes required for Booster operation. The programs will be stored locally in device controllers and be called up by control programs required to run in supercycle mode. It will then be possible to run different corrections for each cycle. Standardization of the various corrector units is most important from the controls, operations, and economics points of view A preliminary list of correction magnets and Power Supplies are shown in Table 3-7

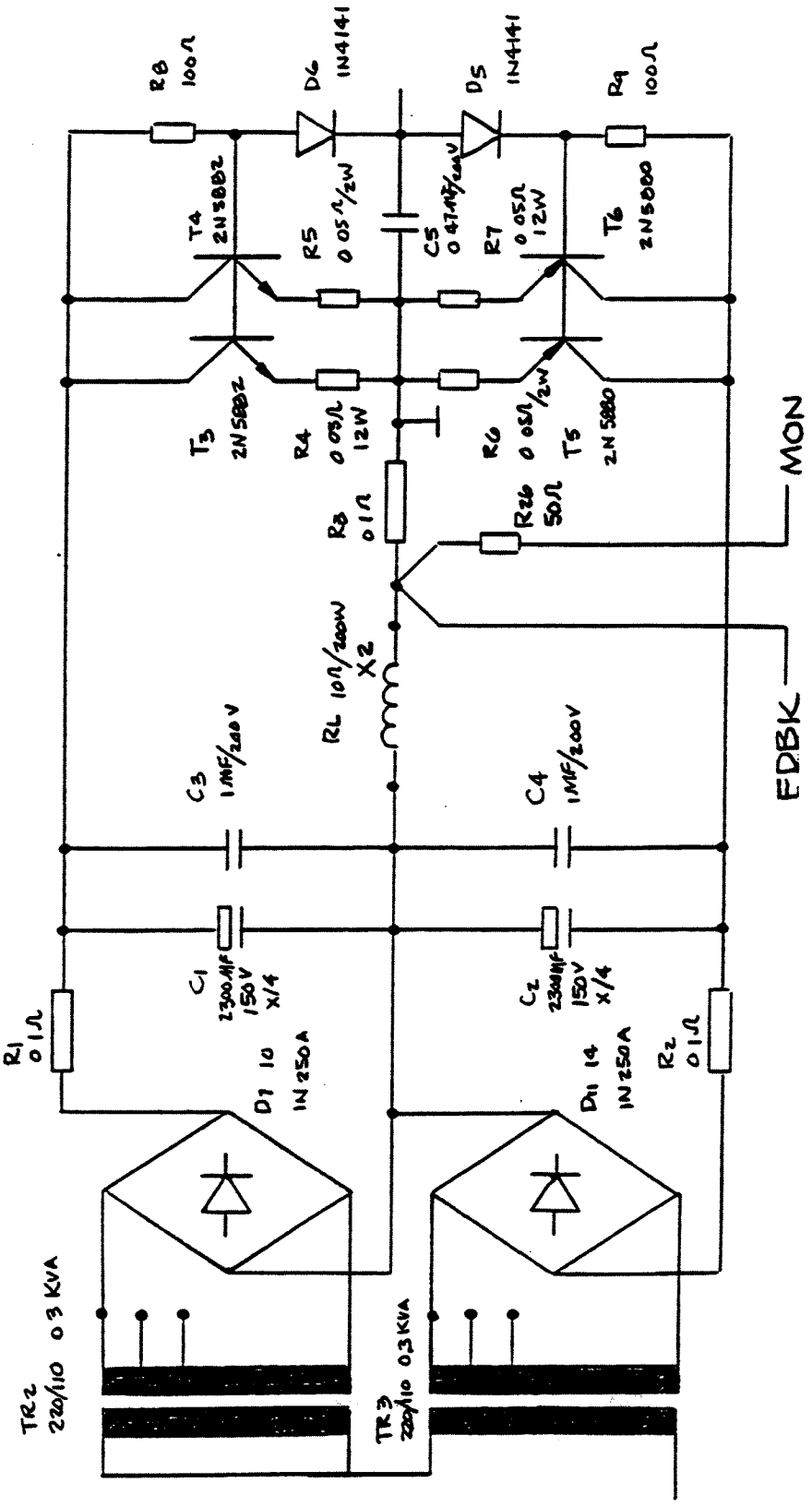

Figure 3 15(a) Bipolar power supply, model A

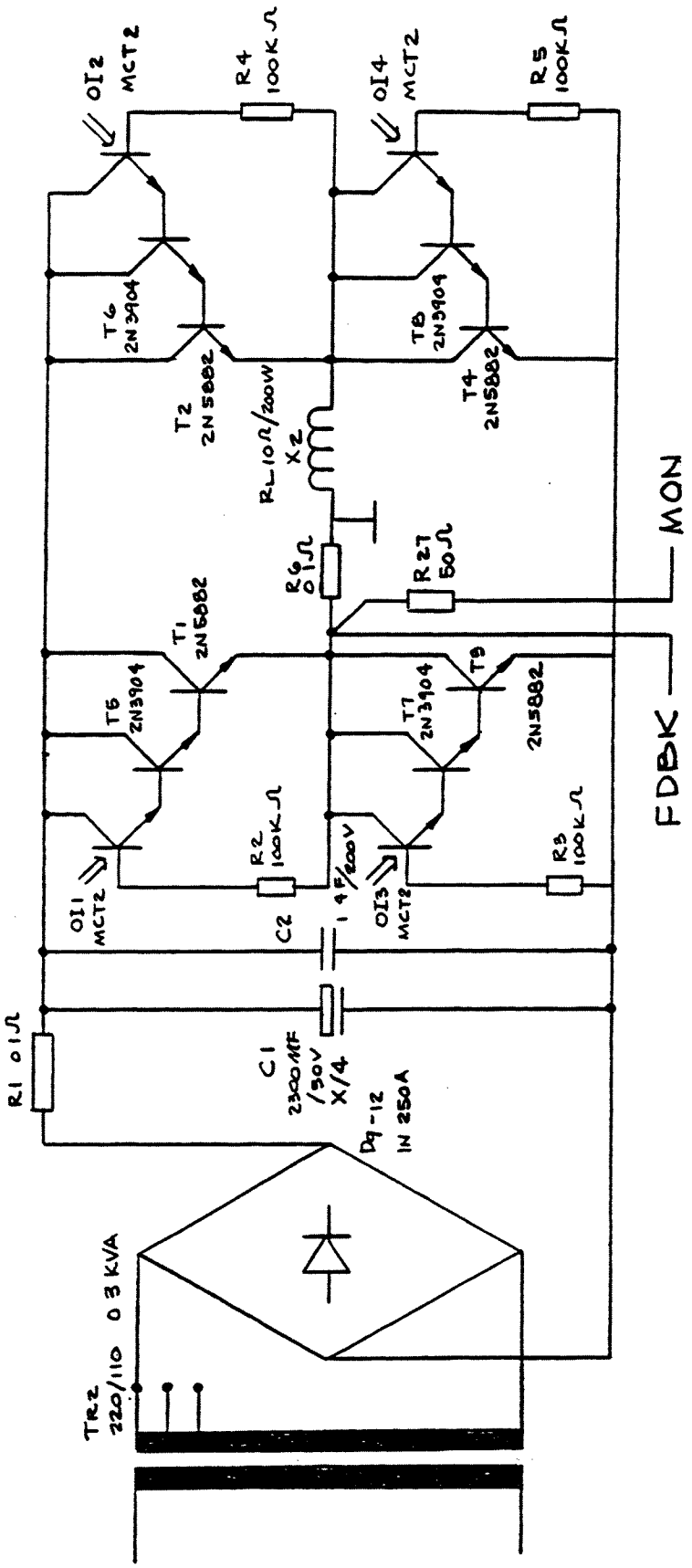

Figure 3 15(b) Bipolar power supply, model B

TABLE 3-7 Number and types of AGS Booster power supplies.

a) Transport Lines

	DC P S.		
	D	Q	ST.
I. hvy ion inj.	6	16	6
II. proton inj.	1	13	6
III. extraction	5	16	3
Total	12	45	15
Sum Total	62		

b) Main Ring

	Pulsed DC P S.													Special, Pulsed			
	Main		Multipole Correctors											Orbit Bumps		Fast	Sept.
	D	Q	S		D		Q			S			Eddy	BLW	Slow		
			H	V	H	V	H	V	S	H	V	S	I		Krs	Kr.	
I. hvy ion inj														3	1		1
II. p inj														3	1		
III. inj (both)															2		
IV extraction														4		1	1
V Main Ring	1	2	1	1													
VI. M.R. corr.								96								1	
VII. AGS inj														2		1	1
Total	1	2	2		96									12	4	3	3
Sum Total	101													22			

Grand Total: 195

CHAPTER 4. BOOSTER INJECTION LINES

4.1. Proton Injection Line

The AGS Booster will use H^- injection, as is presently done on most of the world's accelerators, for both polarized and unpolarized proton operation. H^- charge exchange injection has the well known advantage of permitting brighter beams because it allows injection to continue into already occupied phase space in apparent violation of Liouville's Theorem. The use of a charge stripping foil converts H^- into protons, thus changing the direction of curvature in a magnetic field. This is an irreversible process and thus Liouville's Theorem is not applicable.

For H^- charge exchange injection, the closed orbit of the synchrotron is moved to the injection orbit where a stripping foil is located. For 200 MeV H^-, the foil is made of 100 – 200 $\mu g/cm^2$ of carbon or aluminum oxide. The foil should be located downstream of the dipole field which separates the circulating proton orbit from the injected H^- from the linac. Because of the difference in sign of the charges, the circulating beam and the injected beam merge tangentially at the foil location. The injected beam should be on an orbit which merges with the circulating beam at the edge of the dipole field. (Figure 4-1)

There are several factors that dictate the particular injection geometry used on the booster The chief of these is that it is very desirable to be able to inject polarized protons where β_v is a minimum and β_h is a maximum. Since the booster's function in the polarized proton mode is that of an accumulator one wants to accumulate the maximum possible intensity, maximize the ratio of the admittance and foil area (β_h = max.), while at the same time minimizing vertical emittance growth due to multiple scattering because depolarization is proportional to the vertical amplitude (β_v = min.). This leads to positioning a foil near a magnet end and injecting through the magnet.

4.1.1. Proton Injection Line Components

After the kicker in the HEBT line, the H^- proton injection line has five quadrupoles and four bending dipoles. Each dipole bends the beam 31.54 and has a field of 9.1 kG. The magnetic length of each of the dipoles is 1.3 m. There are 13 quadrupoles in the line. These have field gradients in the range of 0.6 to 1.6 T/m and their magnetic length is 0.3 m. In addition, there are three horizontal steering magnets, four conventional vertical steering magnets, and a fast vertical steering magnet (for painting). The line has been designed to be operated with two different sets of quadrupole field gradients in order to allow injection of both polarized and unpolarized H^- beams into the Booster A kicker in the linac line (MD60)imparts an initial deflection of 7.5° to the beam of protons. The protons enter the main Booster ring through one corner of dipole magnet C5. The path followed by the protons in going from the linac to the Booster is shown in Figure 4-3. Details of the entry of the beam through the Booster ring magnet are displayed in Figure 4-4. The magnets and their locations in the polarized proton injection line are

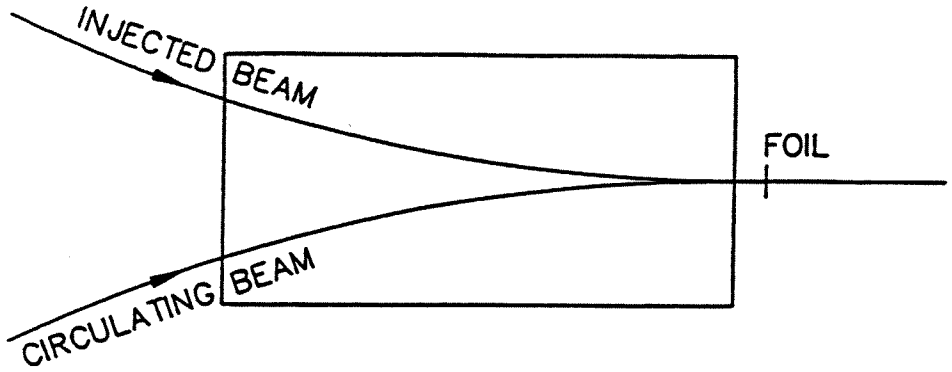

Figure 4-1. Foil location downstream of dipole.

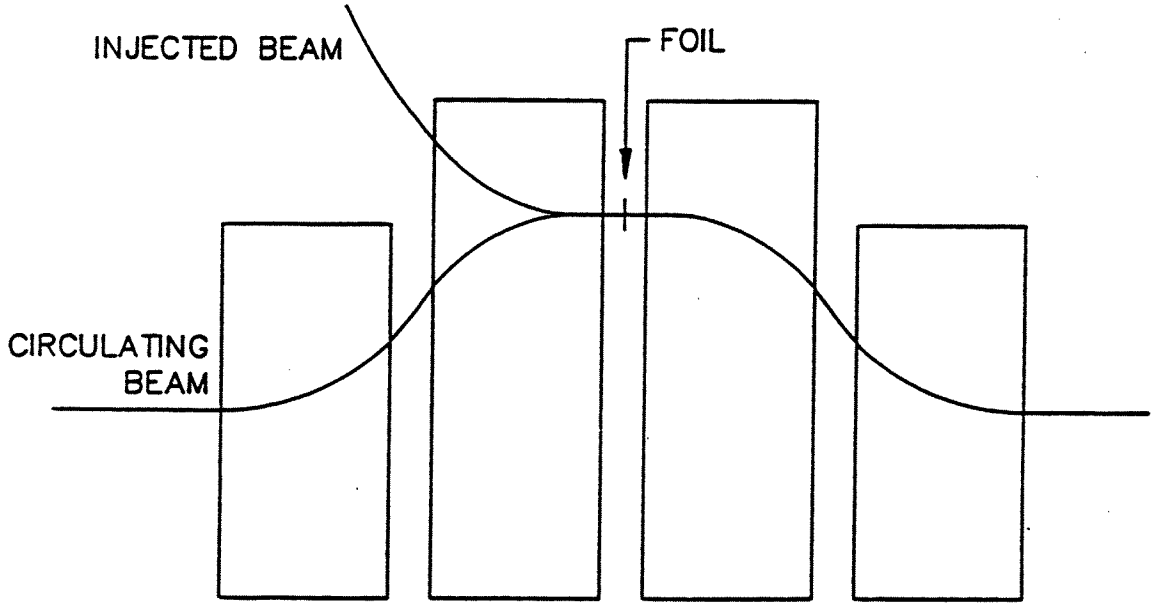

Figure 4-2. Bump in the circulating beam at injection.

given in Table 4-1 below The field gradients for the quadrupoles are shown in Table 4-2.

TABLE 4-1 Location of the proton injection line elements.

Location of Proton Injection Line Elements							
No.	Name	Booster Coord.		AGS Coord.		BNL Coord.	
		x (m)	y (m)	E (in.)	N (in.)	E (ft.)	N (ft.)
1	PIK1	-46.0014	23.8598	-662.200	14520.000	98366.267	102360.000
2	PIQF1	-41.9376	26.4383	-502.207	14418.480	98379.602	102351.539
3	PIQD1	-40.8400	27.1349	-458.994	14391.056	98383.203	102349.258
4	PIQF2	-39.7424	27.8315	-415.781	14363.63	98386.805	102346.969
5	PIQD2	-38.6448	28.5281	-372.568	14336.205	98390.406	102344.688
6	PIQF3	-37.5472	29.2247	-329.355	14308.780	98394.008	102342.398
7	PID1	-35.8441	-30.3055	262.307	14266.230	98399.591	102338.853
8	PID2	-34.2106	-30.3300	197.994	14265.265	98404.951	102338.772
9	PIQF4	-33.2500	29.7601	160.174	14287.702	98408.702	102340.641
10	PID3	-32.2894	29.1902	122.358	14310.139	98411.254	102342.512
11	PIQF5	-31.7689	28.2020	-101.863	14349.047	98412.961	102345.758
12	PID4	29.6531	24.1853	18.566	14507.183	98419.903	102358.932
13	PIQF6	29.8577	21.0750	26.619	14629.636	98419.234	102369.133
14	PIQD3	29.9430	19.7778	29.979	14680.707	98418.953	102373.391
15	PIQF7	-30.0940	17 4828	-35.923	14770.063	98418.461	102380.922
16	PIQD4	-30.1793	16.1856	-39.283	14822.134	98418.180	102385.180
17	PIQF8	-30.3303	13.8905	-45.227	14912.489	98417.688	102392.711
18	PIQD5	-30.4682	11.7951	-50.654	14994.988	98417.234	102399.586

The coordinates given in the table are the coordinates at the *apex* of each magnet (not the center).

In order to inject the transported beam into the Booster ring, it must pass through a hole in the yoke of the C5 dipole magnet (Fig. 4-4). It is then deflected by the field of this magnet to a position that is tangent to the inwardly displaced circulating beam orbit at the location of the stripping foil.

The horizontal aperture of the Booster is six inches. In order to utilize the maximum aperture effectively, the stripping foil is located at 2″ from the center line of the closed orbit. The optimum location of the foil will be determined experimentally A fixed DC orbit bump is used to move the closed orbit outward, and a fast-rising ferrite kicker deflects the closed orbit to the inside where the stripping foil is located. Three injection kickers are used, they are located at C3, C6 and C8. The slow orbit deformation is accomplished by additional deflection at the dipoles C4, C8 and D1 from fields produced by extra or trim windings. The properties of these elements are given in Table 4-3.

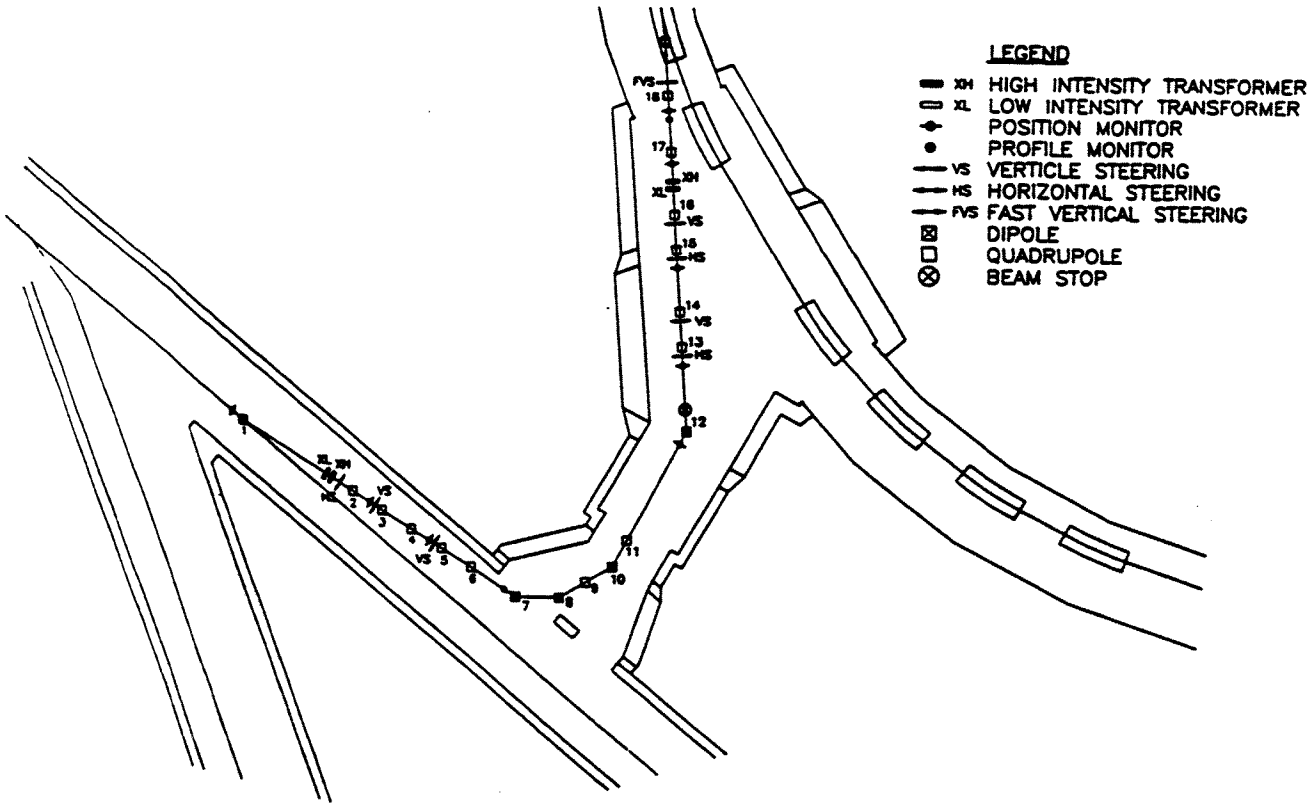

Figure 4-3. Linac to Booster Injection Line.

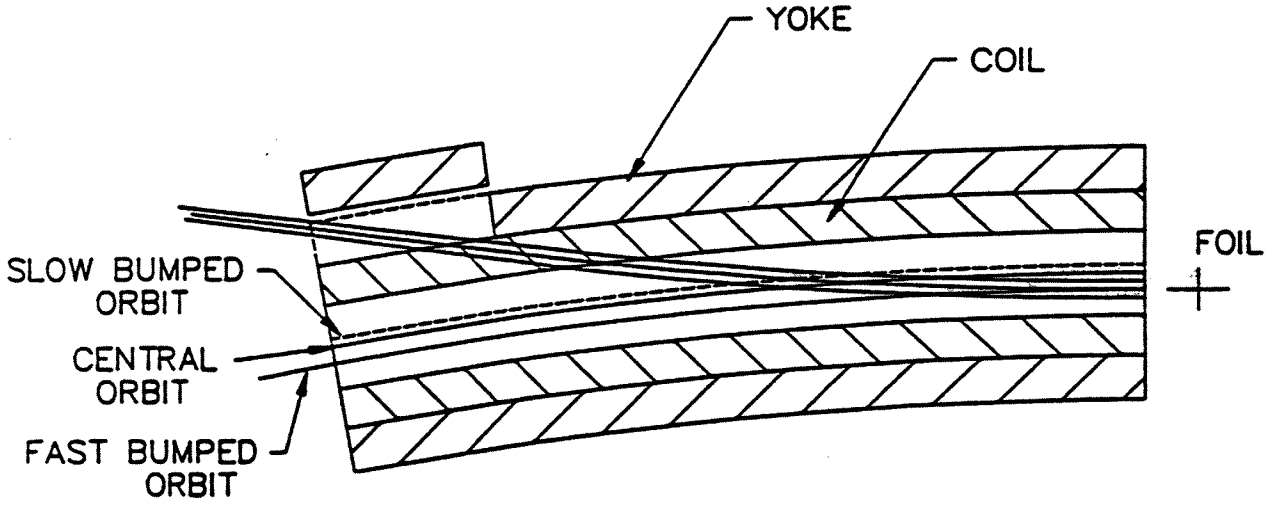

Figure 4-4. Injection trajectory in dipole magnet MDC5.

TABLE 4-2 Field gradients for the proton injection line quadrupoles.

Field Gradients for Proton Injection Line Quads			
No.	Name	Non-Polarized (T/m)	Polarized (T/m)
1	PIQF1	1.4288	1.2455
2	PIQD1	1.6000	1.5000
3	PIQF2	0.6000	0.6000
4	PIQD2	1.1630	1.0938
5	PIQF3	1.6000	1.5000
6	PIQF4	1.3245	1.2221
7	PIQF5	1.0132	1.5000
8	PIQF6	1.0450	1.0019
9	PIQD3	1.2039	1.0938
10	PIQF7	0.9462	1.0407
11	PIQD4	-0.6651	1.0029
12	PIQF8	1.4150	1.0022
13	PIQD5	1.6000	1.0009

TABLE 4-3 Proton injection elements located in the Booster ring.

Name	Device	Location	Strength	
			rad	Amp-Turns
PIB1C4	Slow Orbit Bump 1	C4	0.00136	80.0
PIB2C8	Slow Orbit Bump 2	C8	0.00039	23.0
PIB3D1	Slow Orbit Bump 3	D1	0.00094	55.4
PIFC5	Injection Foil	C5	-	T-m
PIK1C3	Injection Kicker 1	C3 (upstream end)	0.007889	0.0170
PIK2C6	Injection Kicker 2	C6 (downstream end)	0.002609	0.0056
PIK3C8	Injection Kicker 3	C8 (center)	0.008153	0.0175

The carbon stripping foil has a mass of 100 to 200 μg per square centimeter and a stripping efficiency of close to 100 percent. Alternatively, the aluminum oxide stripping foil recently developed at Rutherford Laboratory may be used. With ~25 mA of H^- current available from the linac, one can inject up to the space-charge limit of the Booster

4.1.2. High-Intensity Unpolarized Proton Beam Injection

As in the case of the AGS, the stripping foil position must be experimentally determined to utilize the maximum available aperture and to achieve the maximum possible intensity The closed orbit bump is to be minimized and yet the available aperture is to be maximized. The good field region of the main dipole magnet is 3 inches and the foil will be located somewhere between 1″ and 3″ from the central orbit as determined by maximizing the accelerator intensity This is shown schematically in Figure 4-4.

The final foil position determines the useful aperture, and when this is set, a d.c. orbit bump, produced by using extra windings at three lattice dipole locations, will move the closed orbit to the center of this aperture. If the optional foil position is 2″, then this d.c. bump is 0.5″ As the magnet field ramps, the effect of this d.c. bump becomes smaller and smaller and is essentially zero at full energy

Next a fast orbit bump is used to move the circulating orbit onto the foil. The foil is located downstream of the C5 dipole and upstream of the C5 quadrupole. The trajectories of the H^- beam injected through the displaced yoke of the C5 dipole are shown in Figure 4-4 for the 1″, 2″ and 3″ foil positions.

With the dc and fast bumps on, injection starts at the center of the booster acceptance and moves toward the outside of the phase space as the size of the fast bump is decreased. The bump amplitude should decrease parabolically with a slope that matches the phase-space area located at the orbit bump position. This will uniformly populate the available phase space. The fast bump is turned off at the end of injection and the size of the orbit bump at this time is the size of the injected beam plus the momentum space required after capture. Figure 4-5 shows the time sequence of this process.

Figure 4-6 shows the bump location in the ring lattice.

The bump magnet has a rise time of 50 μs and the length of injection is 300-400 μs. One can also introduce a vertical fast dipole to spread the beam uniformly in the vertical phase space if this proves advantageous.

4.1.3. Polarized Proton Injection

The Booster is acting as an accumulator in this mode, and therefore injection must occur over some 20 - 30 linac pulses (2 to 3 seconds). One cannot keep the beam on the foil for this long without losing it due to multiple coulomb scattering. The solution for this is to bump the injected beam onto the foil during the 300 - 400 μs injection pulses. Since pulses occur only every 133 ms, this leads to a good beam survival efficiency Because of this bump, the available aperture must be equally divided between the injected and circulating beams. This dictates that the foil position be at −1″ and the d.c. bump at +1″ This allows 4″ of aperture for both the injected and circulating beam. See Figure 4-7

Every time the linac is ready to inject into the Booster, the circulating beam is bumped over to the stripping foil position. To minimize the multiple scattering losses, the bump rise time should be made as fast as possible, say 50 μs.

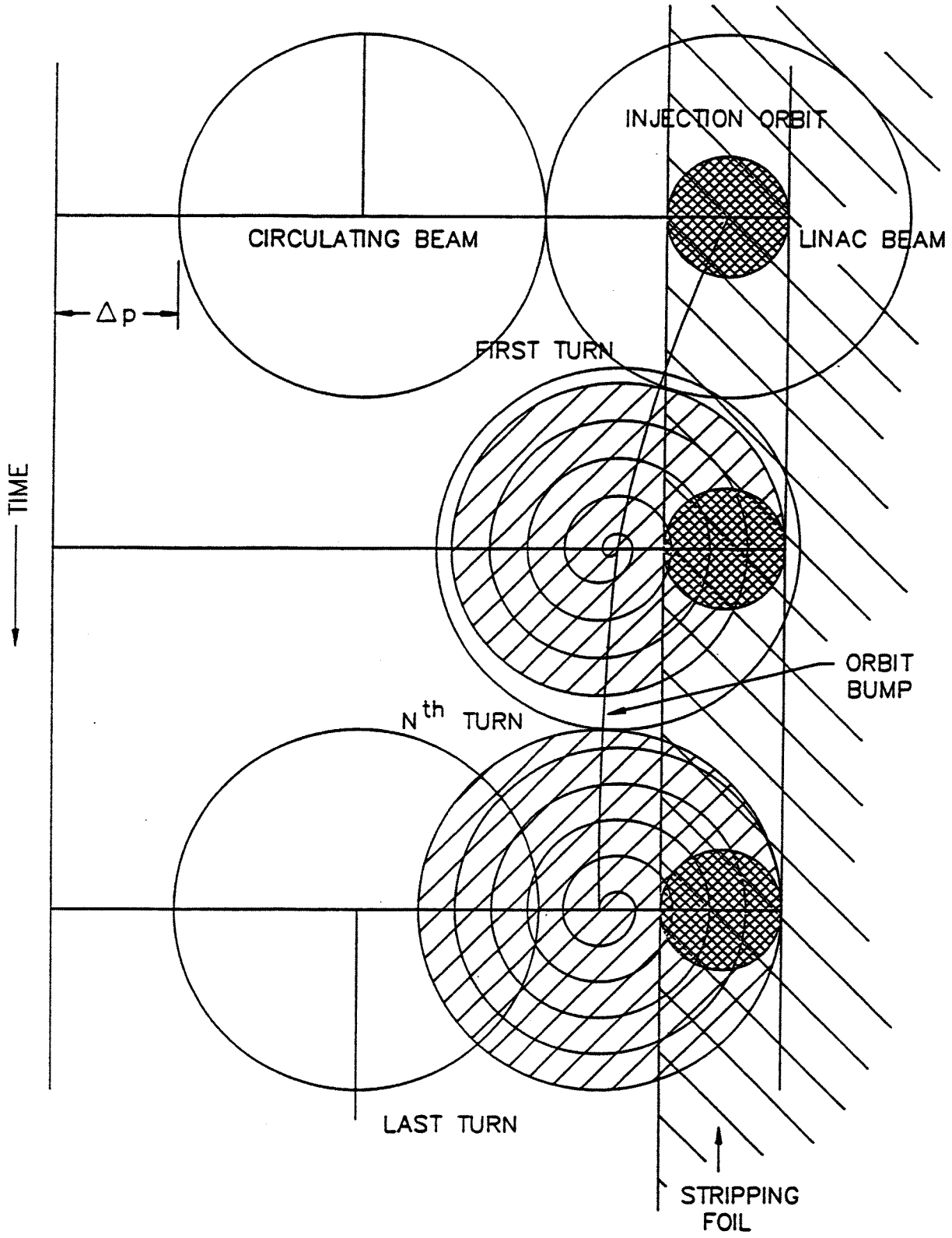

Figure 4-5. Populating the phase space with the injected beam.

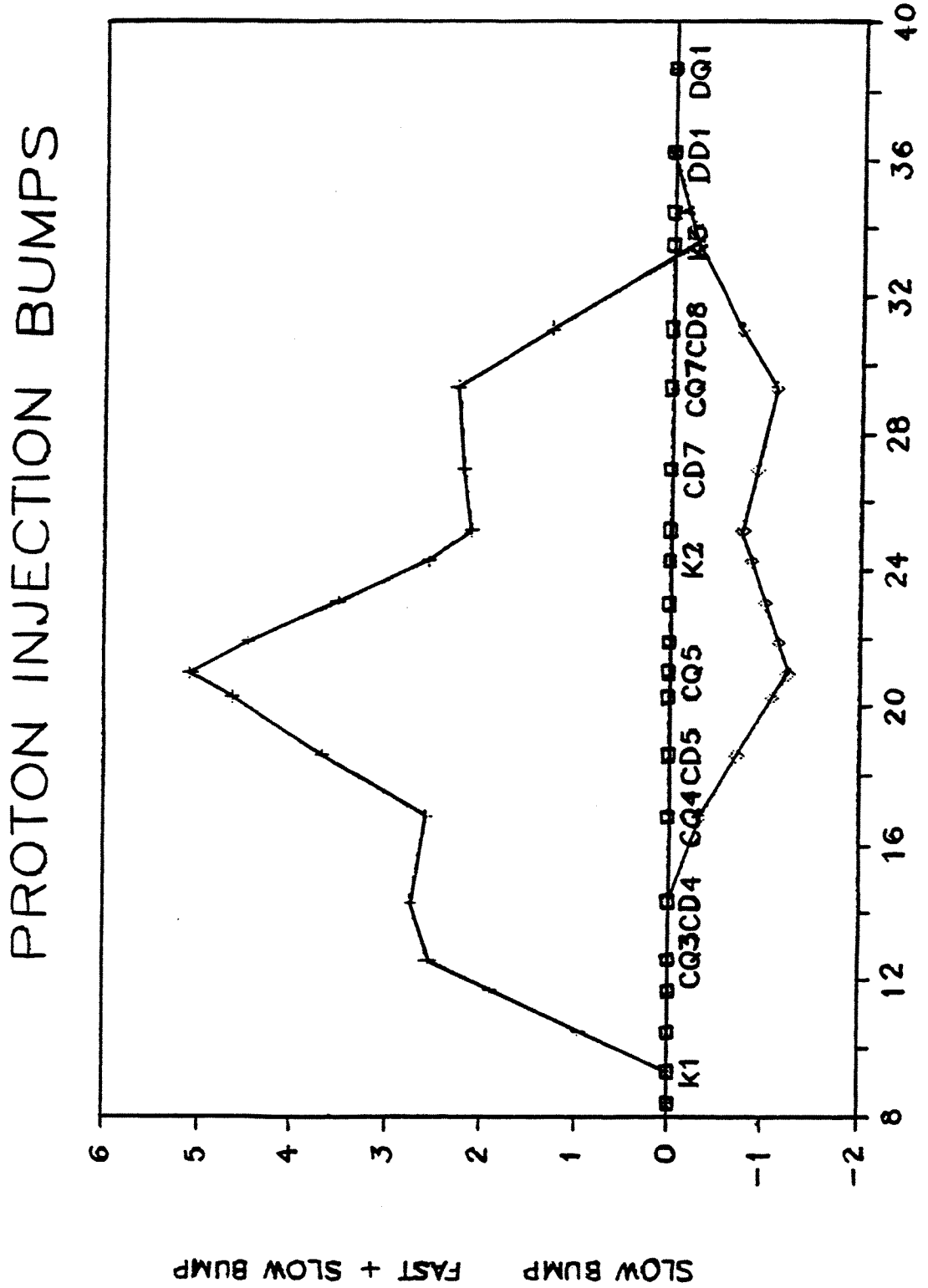

Figure 4 6 Location of the bump in the ring lattice

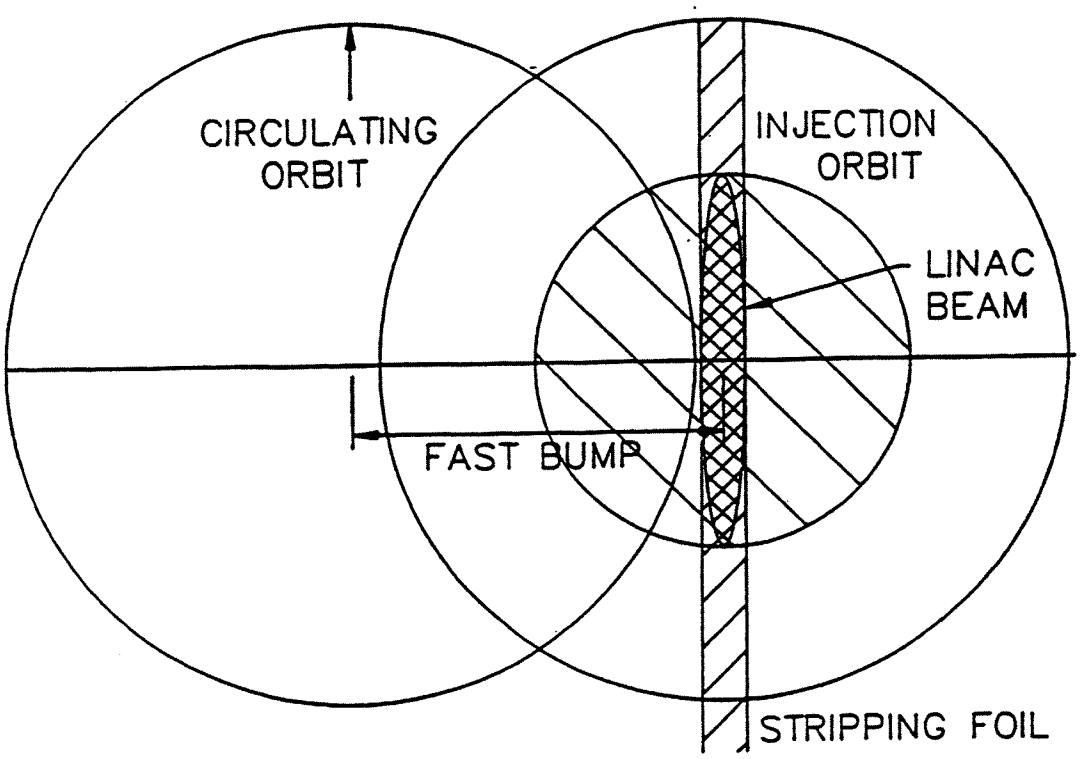

Figure 4-7 Injected and circulating polarized proton beams.

Another difference in this mode from the high intensity mode is the geometry of the stripper foil. As shown in AGS Tech. Note 186, it is important to focus the linac beam at the foil and to make the foil as small as the horizontal dimension of the linac beam. This is necessary to make the maximum number of circulating particles miss the foil. Also the foil is at a horizontal β_{max} which also helps the accumulation efficiency

4.1.4. Booster Aperture

Table 4-4 compares the Booster acceptance with the AGS acceptance.

In addition to the elements listed in Table 4-1, proton injection requires certain hardware that is located in the ring itself. These items are listed in Table 4-2.

The injection kicker requirements for polarized proton injection are:

Maximum displacement required	0.0762 m
Aperture	2.65 × 6 in.
Rise and fall time	50 μs
Pulse length	up to 500 μs
Pulse shape	Programmable

TABLE 4-4 Comparison of Booster and AGS Acceptances

Acceptance Comparison				
	AGS		BOOSTER	
Horizontal				
Physical size	127	mm	127	mm*
Momentum space (0.5%)	11	mm	14.7	mm
Betatron space available	116	mm	112.3	
Maximum beta function	22.75	m	13.8	m
Betatron admittance	127.9 π	x 10^{-6}	228.5 π	x 10^{-6}
Vertical				
Physical size	75	mm	66	mm
Closed orbit error	5		5	
Betatron space available	70		61	
Maximum beta function	22.75		13.8	m
Admittance	54 π	x 10^{-6}	67 4 π	x 10^{-6}

*Nominal position of injection stripping foil at 2 inches from center

4.1.5. Injection Power Supplies

4.1.5.1. Introduction

Since the AGS Booster has to accelerate protons, polarized protons and heavy ions, it must accommodate various different injection schemes. The proposed schemes fall into two (2) major categories, namely H^- stripping injection (protons) and multiturn injection (heavy ions). The required devices for injection into the Booster are dc beam transport elements, orbit deformation bumps, slow programmable injection beam kickers, and an electrostatic septum. The number and types of devices are listed in Table 4-7

The power supplies for these various systems are described in the following sections.

4.1.5.2. DC Beam Transport

The beam transport power supplies used in the proton 200 MeV injection line will be medium curent dc types. The four dipole magnets will be connected in series and driven by one 1000 ampere supply All the quadrupoles will use the same type of power supply (13 each) that will be rated 350 amperes. (The gradients are given in Table 4-2.). Regulation will be 1 part in 10^3 or better This is readily available in commercial units.

The regular horizontal and vertical steering magnets will have bipolar series-regulator type power supplies. These will be constructed identically to the corrector power supplies used in the main booster ring (see 3.2.1.4.2).

4.1.5.3. Pulsed Injection Power Supplies

4.1.5.3.1. Orbit Bumps

The orbit bumps are created by "backleg" windings (BLW's) on the main ring dipole magnets. These are flat pancake coils sandwiched beteen the main coils and the core on the top and bottom magnet coil surfaces. The power supplies will be either dc or pulsed type. The dc units create a permanent orbit shift which decreases as the energy of the Booster increases. The pulsed units will be capacitor-discarge types that use a solid state thyistor switch. The pulse times, currents, and hence the voltages are quite low, thus enabling an SCR or GTO switch. A simplified schematic is shown in Figure 4-8. These units will be the same for proton and heavy ion injection. BLW's on three booster dipole magnets will be required to create the orbit deformation in each injection scheme.

4.1.5.3.2. Injection Kickers

Each injection scheme (H^- charge exchange or HI multiturn) requires three injection kicker magnets and power supplies. For protons (H^- beam) the magnets are located at C3, C6, and C8. For heavy ion injection they are located at B8, C3, and C6. (See Tables 4-2 and 4-6.) Since magnets are required at C3 and C6 in both schemes, only one magnet will be installed at each of these locations, and each will serve a double function,

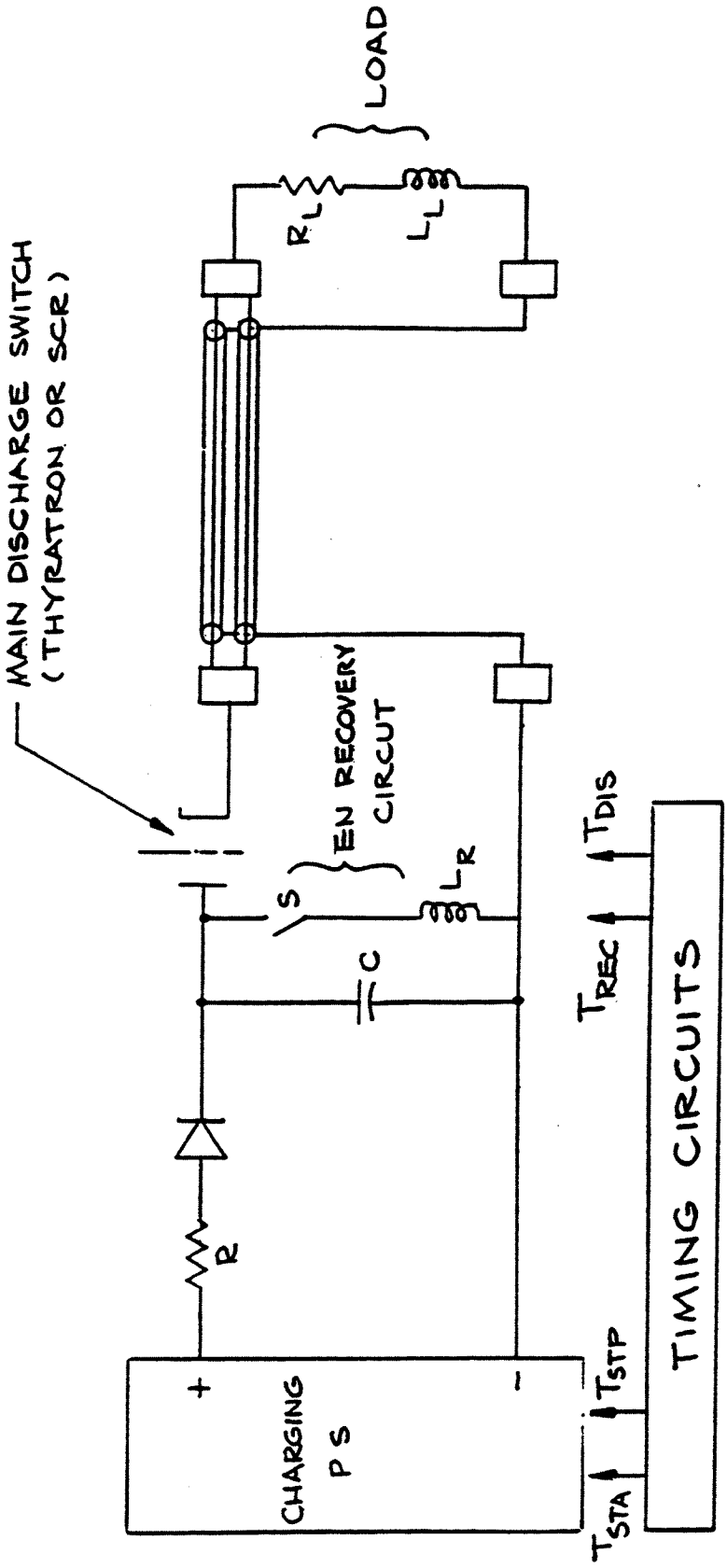

Figure 4 8 Simplified schematic for capacitor discharge type power supply

operating during both proton and heavy ion injection.

The beam kickers are fast-pulsed (50 μs risetime), programmable power supplies that are used to deflect the circulating beam so that it merges at the foil with the injected beam (flattop times of 300 μs). Units of this type are presently in operation in the AGS and units of similar design will be constructed for the Booster The programmability is required to accommodate the different injection schemes. The basic scheme uses energy stored in a large capacitor bank and controls its flow to the magnet via a transistor reulator

4.1.5.3.3. HI Injection Septum

The injection septum is used for heavy ion injection and is an electrostatic type operating in the vicinity of 50=60 kilovolts. The septum will be a thin foil of titanium. A similar septum and dc power source are in use in the AGS for the directly injected Tandem Van de Graaf beam, and will be duplicated for Booster operation. At present, the electrostatic septum unit is not pulsed, although capability for pulsing can be implemented.

4.2. Heavy Ion Transfer and Injection Line

For the Booster the heavy ion transfer and injection line is assumed to start at what is now called the 69° point. This is the point near the Southwest Experimental Area where the Tandem Van de Graff heavy ion beam now make a sharp bend for direct transfer and injection into the AGS.

The optical matching of the beam starts from the quadrupole doublet upstream of the 69° bend (AGS coordinates N6025.28, E4543.8).

DESCRIPTION OF NEW HEAVY ION LINE GOES HERE.

The elements of the heavy ion injection line are given in Table 4-5. There are xx dipoles and yy quadrupoles. The dipoles are of three types: xx main bending dipoles, xx pitching dipoles, and xx steering dipoles. The pitching dipoles and steering dipoles have not been included in the table because their positions have not yet been specified. Figure 4-8 shows the path of the heavy ion transfer and injection line from the 69° bend point to the Booster ring.

TABLE 4-5 Location of the heavy ion injection line elements.

Heavy Ion Injection Line Elements					
No.	Name	Booster Coord.		AGS Coord.	
		x (m)	y (m)	E (in.)	N (in.)
1	HID1	00.000	00.000	0000.0000	0000.0000

In addition to the elements listed, the elements given in Table 4-6 are required in the main Booster ring itself for heavy ion injection:

Figure 4-8. Heavy ion transfer and injection line to the Booster

TABLE 4-6 Heavy ion injection elements located in the Booster ring.

Name	Function	Location	Strength	
			Sulfur	Gold
HIB1B8	Slow Orbit Bump 1	B8	49.1 A-t	59.2 A-t
HIB2C1	Slow Orbit Bump 2	C1	13.8	16.7
HIB3C5	Slow Orbit Bump 3	C5	63.7	76.7
HISC3	Electro-static Septum	C3	22.3 kV/cm	12.4 kV/cm
HIK1B8	Injection Kicker 1	B8 (center)	0.007650 T-m	0.009220 T-m
HIK2C3	Injection Kicker 2	C3* (upstream end)	0.000524	0.000632
HIK3C6	Injection Kicker 3	C6* (downstream)	0.004890	0.00590

*Note: C3 and C6 injection kickers are the same identical units as the ones in the same locations in Table 4-2.

A thin electrostatic septum, HISC3, will be used to deflect the beam about 15° for injection into the horizontal phase space of the Booster

The electrostatic septum must meet the following specifications:

Deflection angle	15.04°
Length	2.55 m
Aperture (good field region)	2×2 cm
Radius of curvature	9.65 m
Electro-static field	Carbon 31.1 kV/cm
	Sulfur 22.3 kV/cm
	Gold 12.4 kV/cm
Septum thickness	< 0.25 mm – as thin as practical

In the table, the location given for a injection kicker magnet refers to the straight section immediately following the indicated main dipole magnet. The injection kickers located at the center of the B8 straight section, the upstream end of the C3 straight section, and at the downstream end of C6 are used to deform the closed orbits just inside the septum, further displacing successive turns. Since the beam of heavy ions from the Tandem Van de Graaf accelerator has a small emittance ($\sim$ 1 mm-mrad), it is expected that more than 20 turns can be efficiently injected into the Booster betatron phase space of 50π mm-mrad.

The injection kicker requirements for heavy ion injection are:

Maximum displacement	0.0762 m (for $p_{max} = 8.78$ GeV/c)
Maximum displacement	0.0762 m
Aperture	2.65 × 6 in.
Rise and fall time	< 100 μs
Pulse duration	up to 500 μs
Pulse shape	Programmable

The strength of the quadrupoles has been determined, and the bending to be produced by each dipole magnet in the injection line has been calculated. These results are shown in Table 4-7

TABLE 4-7 Lengths and strengths of the heavy ion injection line elements.

Size of Heavy Ion Injection Line Elements				
No.	Name	Length (m)	Strength	
			K1 (T/m)	Angle (deg)
1	HID1	0.0000	-	00.000

The strength of the xx pitching dipoles, HIDnn, nn, nn, and nn, is 0.15 T-m, and the strength of the steering dipoles, HIDnn and HIDnn, is 0.05 T-m.

4.2.1. Heavy Ion Intensity in the Booster

As shown in Figure 4-9 and also in the overview of Figure 4-8, a Tandem Van de Graaf accelerator is used for injecting heavy ions into the Booster. Recent work has demonstrated, that in a pulsed mode of operation, the source can be made to yield over 500 particle-μA of beam for light ions such as carbon. As the nuclear mass increases, the available source current decreases. For the heaviest nucleus, ^{197}Au, approximately 240 particle-μA is currently available.

Assuming particle loss in the beam transfer line can be neglected, the number of heavy ions *available for injection* into the Booster is given by:

$$N_{Booster} = (N_T S_i T_T) \times S_F$$
$$\text{TANDEM}$$

where N_T is the number of particles at the source

S_i stripping foil efficiency (internal foil) for the most probable charge state

T_T transmission probability through the Tandem

S_F stripping foil efficiency for foil following the Tandem

Both T_T and S_i have been determined. $T_T \equiv 0.75$ and S_i is heavy ion species dependent. In Table 4-8, the valves of S_i are shown for various species together with the most probable charge state after traversing the two foils in Figure 4-8. The velocity for each species, on leaving the Tandem, is also shown.

Although $N_{Booster}$ represents the number of heavy ions available for storage in the Booster, the actual number per bunch depends on the multi-turn stacking efficiency (section 4.2). This efficiency is a function of the pulse length from the Tandem. In Table 4-9, the number of particles at the source, N_T, is shown as a function of the pulse length, P_L, and source current, I_S.

TABLE 4-8 Stripping Foil Efficiencies and Tandem Velocity of Heavy Ions

Species	^{12}C	^{32}S	^{63}Cu	^{127}I	^{197}Au
Atomic Number	6	16	29	53	79
Q_T	5	9	11	13	13
Q_F	6	14	21	29	33
S_T	0.39	0.36	0.27	0.20	0.19
S_F	0.9	0.40	0.27	0.20	0.17
γ	1.0075	1.0047	1.0029	1.0017	1.0011
β	0.1219	0.0966	0.0756	0.0575	0.0462

TABLE 4-9 Number of Particles Emitted by Tandem.

Label	I^S	P^L	N^T
1.	80 μA	80 μs	4.0×10^{10}
2.	80 μA	110 μs	5.5×10^{10}
3.	80 μA	200 μs	10.0×10^{10}
4.	80 μA	500 μs	25.0×10^{10}
5.	110 μA	80 μs	5.5×10^{10}
6.	110 μA	110 μs	7.55×10^{10}
7	110 μA	200 μs	13.73×10^{10}
8.	110 μA	500 μs	34.32×10^{10}
9.	200 μA	80 μs	10.0×10^{10}
10.	200 μA	110 μs	13.73×10^{10}
11.	200 μA	200 μs	25.0×10^{10}
12.	200 μA	500 μs	62.4×10^{10}
13.	300 μA	110 μs	20.59×10^{10}

In order to calculate the number of heavy ions per bunch for the h=3 mode in the Booster, we need the number of possible revolutions N_R for a given pulse length P^L from the Tandem. N_R is given by $\beta c P^L / C$ where C is the circumference of the Booster

In Tables 4-10 - 4-14 the expected particle numbers/bunch are shown[1] for both an eight-turn injection with 100% stacking efficiency and a 32-turn injection with 50% stacking efficiency At present, eight turns can be accommodated easily in betatron phase space. To go beyond this will require experimental work with the on-line machine. We note that a 32-turn injection with 50% efficiency is consistent with the more theoretical work of Wei and Lee[2]

The label (1-13) in Tables 4-10 - 4-14 corresponds to the Tandem currents and pulse lengths in Table 4-9.

---

[1]M. J. Rhoades-Brown and A. G. Ruggiero, "Source Current into the AGS, An Analysis of the RHIC Front-End Injection System." RHIC Technical Note No. **32**.

[3]J. Wei and S. Y Lee, "Simulation of the Multi-Turn Heavy-Ion Injection into the Booster." Booster Technical Note No. **102**.

TABLE 4-10 Number of Ions/Bunch Injected into Booster ^{12}C

	$N^T T^T S^T$	$N^T T^T S^T S^F$	No. of Revolutions	No. Injected in 8 Turns	No. Injected in 32 Turns†
1.	1.17×10^{10}	1.058×10^{10}	15	0.187×10^{10}	—
2.	1.606×10^{10}	1.446×10^{10}	21	0.183×10^{10}	—
3.	2.92×10^{10}	2.63×10^{10}	37	0.189×10^{10}	0.379×10^{10}
4.	7.301×10^{10}	6.572×10^{10}	93	0.188×10^{10}	0.378×10^{10}
5.	1.606×10^{10}	1.446×10^{10}	15	0.257×10^{10}	—
6.	2.209×10^{10}	1.989×10^{10}	21	0.252×10^{10}	—
7	4.02×10^{10}	3.618×10^{10}	37	0.260×10^{10}	0.521×10^{10}
8.	10.00×10^{10}	8.99×10^{10}	93	0.257×10^{10}	0.515×10^{10}
9.	2.92×10^{10}	2.63×10^{10}	15	0.467×10^{10}	—
10.	4.02×10^{10}	3.618×10^{10}	21	0.459×10^{10}	—
11.	7.30×10^{10}	6.57×10^{10}	37	0.473×10^{10}	0.946×10^{10}
12.	18.26×10^{10}	16.43×10^{10}	93	0.471×10^{10}	0.942×10^{10}
13.	6.02×10^{10}	5.42×10^{10}	21	0.688×10^{10}	—

†50% Stacking Efficiency

TABLE 4-11 Number of Ions/Bunch Injected into Booster ^{32}S.

	$N^T T^T S^T$	$N^T T^T S^T S^F$	No. of Revolutions	No. Injected in 8 Turns	No. Injected in 32 Turns†
1.	1.08×10^{10}	0.432×10^{10}	11	0.104×10^{10}	—
2.	1.49×10^{10}	0.596×10^{10}	15	0.106×10^{10}	—
3.	2.70×10^{10}	1.08×10^{10}	28	0.103×10^{10}	—
4.	6.75×10^{10}	2.70×10^{10}	71	0.102×10^{10}	0.203×10^{10}
5.	1.49×10^{10}	0.596×10^{10}	11	0.144×10^{10}	—
6.	2.04×10^{10}	0.816×10^{10}	15	0.145×10^{10}	—
7	3.71×10^{10}	1.48×10^{10}	28	0.141×10^{10}	—
8.	9.27×10^{10}	3.70×10^{10}	71	0.139×10^{10}	0.278×10^{10}
9.	2.70×10^{10}	1.08×10^{10}	11	0.262×10^{10}	—
10.	3.71×10^{10}	1.48×10^{10}	15	0.263×10^{10}	—
11.	6.75×10^{10}	2.70×10^{10}	28	0.257×10^{10}	—
12.	16.84×10^{10}	6.73×10^{10}	71	0.253×10^{10}	0.506×10^{10}
13.	5.56×10^{10}	2.22×10^{10}	15	0.395×10^{10}	—

†50% Stacking Efficiency

TABLE 4-12 Number of Ions/Bunch Injected into Booster ^{63}Cu

	$N^T T^T S^T$	$N^T T^T S^T S^F$	No. of Revolutions	No. Injected in 8 Turns	No. Injected in 32 Turns†
1.	0.810×10^{10}	0.219×10^{10}	9	0.064×10^{10}	—
2.	1.11×10^{10}	0.3×10^{10}	12	0.066×10^{10}	—
3.	2.02×10^{10}	0.545×10^{10}	22	0.066×10^{10}	—
4.	5.06×10^{10}	1.366×10^{10}	56	0.065×10^{10}	0.129×10^{10}
5.	1.11×10^{10}	0.3×10^{10}	9	0.088×10^{10}	—
6.	1.53×10^{10}	0.413×10^{10}	12	0.091×10^{10}	—
7	2.78×10^{10}	0.750×10^{10}	22	0.090×10^{10}	—
8.	6.95×10^{10}	1.876×10^{10}	56	0.089×10^{10}	0.178×10^{10}
9.	2.03×10^{10}	0.548×10^{10}	9	0.162×10^{10}	—
10.	2.78×10^{10}	0.751×10^{10}	12	0.166×10^{10}	—
11.	5.06×10^{10}	1.37×10^{10}	22	0.166×10^{10}	—
12.	12.64×10^{10}	3.41×10^{10}	56	0.162×10^{10}	0.324×10^{10}
13.	4.17×10^{10}	1.126×10^{10}	12	0.250×10^{10}	—

†50% Stacking Efficiency

TABLE 4-13 Number of Ions/Bunch Injected into Booster ^{127}I

	$N^T T^T S^T$	$N^T T^T S^T S^F$	No. of Revolutions	No. Injected in 8 Turns	No. Injected in 32 Turns†
1.	$.6 \times 10^{10}$	0.120×10^{10}	6	0.040×1016	—
2.	$.825 \times 10^{10}$	0.165×10^{10}	9	0.049×10^{10}	—
3.	1.5×10^{10}	0.3×10^{10}	17	0.047×10^{10}	—
4.	3.75×10^{10}	0.750×10^{10}	42	0.047×10^{10}	0.0952×10^{10}
5.	$.825 \times 10^{10}$	0.165×10^{10}	6	0.055×10^{10}	—
6.	1.13×10^{10}	0.226×10^{10}	9	0.067×10^{10}	—
7	2.06×10^{10}	0.412×10^{10}	17	0.065×10^{10}	—
8.	5.15×10^{10}	1.03×10^{10}	42	0.065×10^{10}	0.131×10^{10}
9.	1.5×10^{10}	0.3×10^{10}	6	0.1×10^{10}	—
10.	2.06×10^{10}	0.412×10^{10}	9	0.122×10^{10}	—
11.	3.75×10^{10}	0.750×10^{10}	17	0.117×10^{10}	—
12.	9.36×10^{10}	1.87×10^{10}	42	0.118×10^{10}	0.237×10^{10}
13.	3.09×10^{10}	0.618×10^{10}	9	0.183×10^{10}	—

†50% Stacking Efficiency

TABLE 4-14 Number of Ions/Bunch Injected into Booster ^{197}Au

	$N^T T^T S^T$	$N^T T^T S^T S^F$	No. of Revolutions	No. Injected in 8 Turns	No. Injected in 32 Turns†
1.	0.569×10^{10}	0.096×10^{10}	5	0.032×10^{10}	—
2.	0.780×10^{10}	0.132×10^{10}	7	0.044×10^{10}	—
3.	1.423×10^{10}	0.243×10^{10}	14	0.046×10^{10}	—
4.	3.56×10^{10}	0.605×10^{10}	35	0.046×10^{10}	0.092×10^{10}
5.	0.780×10^{10}	0.132×10^{10}	5	0.044×10^{10}	—
6.	1.074×10^{10}	0.182×10^{10}	7	0.0607×10^{10}	—
7	1.96×10^{10}	0.333×10^{10}	14	0.0633×10^{10}	—
8.	4.893×10^{10}	0.830×10^{10}	35	0.0633×10^{10}	0.126×10^{10}
9.	1.423×10^{10}	0.243×10^{10}	5	0.0810×10^{10}	—
10.	1.960×10^{10}	0.333×10^{10}	7	0.111×10^{10}	—
11.	3.558×10^{10}	0.586×10^{10}	14	0.111×10^{10}	—
12.	8.89×10^{10}	1.51×10^{10}	35	0.112×10^{10}	0.23×10^{10}
13.	2.933×10^{10}	0.499×10^{10}	7	0.166×10^{10}	—

†50% Stacking Efficiency

CHAPTER 5. EJECTION LINE AND TRANSFER LINE TO AGS

5.1. Beam Transfer to AGS

To minimize the beam dilution, bunch to bunch transfer from the Booster to the AGS has been considered. This scheme is straight-forward and highly efficient. Its operation would be as follows: After the acceleration period, a slow orbit deformation of the beam is executed which brings the beam close to the septum of the ejector magnet located at straight section F6. Then, the fast kicker located at straight section F3 is energized and deflects the particles past the septum of the ejector magnet which ultimately kicks the beam out to the extraction channel (located 75 mm away from the booster central orbit) for transport to the AGS. Stripping of the heavier heavy ions will be accomplished outside of the Booster, before the first bending magnet of the extraction channel. After the 32 bend section, a set of matching quadrupoles are used to transport the beam onto a septum located at the L20 straight section of AGS. A kicker at A5 is used to kick the beam onto the bumped AGS orbit. The transported beam is matched onto the betatron phase space of the AGS. Figure 5-1 shows the geometric constraints of the transfer line.

5.2. Beam Bumps

The beam size at the extraction energy is shown in Table 5-1, where the initial beam size is assumed to fill up the horizontal aperture of 50 mm, which corresponds to an emittance of 228π mm-mrad. If the beam size at the injection is smaller, the corresponding beam size at the extraction energy will be smaller

TABLE 5-1 Beam size at extraction energy

Species	Z_i	Z_f	$(B\rho)_{inj}$ (T-m)	$(B\rho)_{max}$ (T-m)	Expected maximum beam size at extraction (mm)	Effective $(B\rho)$ after stripping (T-m)
p	1	1	2.150	7.507	27	7.507
C	6	6	0.790	11.034	13	11.034
S	14	16	0.713	12.61	12	11.034
Cu	21	29	0.730	15.24	11	11.034
I	29	53	0.811	17.52	11	9.63
Au	33	79	0.8875	17.52	11	7.35

A set of slow beam bumps is used to excite the closed orbit locally so as to produce a maximum distortion at the septum location. Because of the smaller beam size at the extraction energy, the maximum closed orbit distortion required is $x_{co} = 25$ mm for protons and $x_{co} = 37.5$ mm for heavy ions. The septum is located at 50.8 mm from the central orbit. The kicker located at F3 is excited with a rise time of <140 ns and

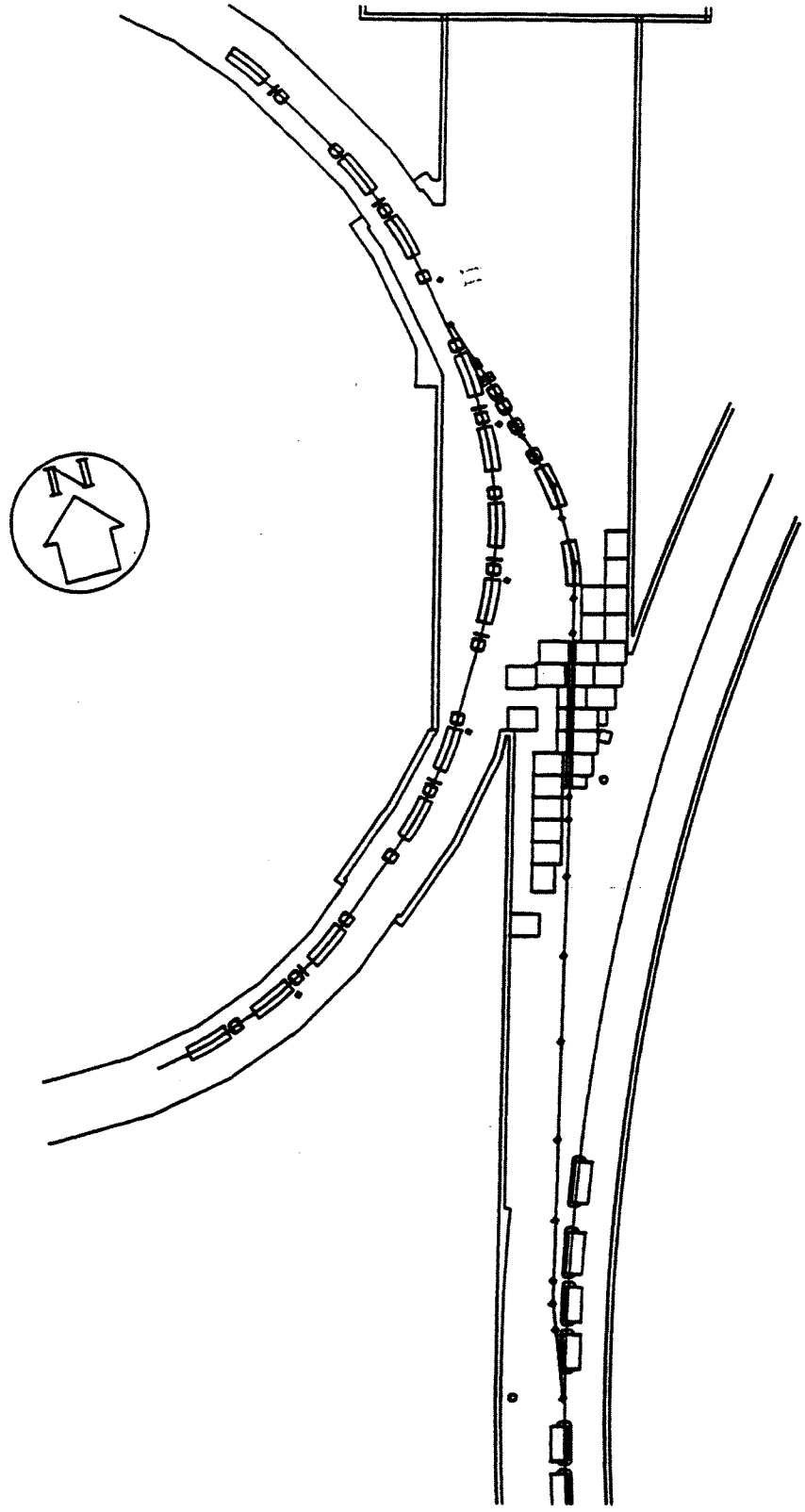

Figure 5-1. The Booster ejection and transfer line to the AGS.

deflects the beam 50 mm for protons and 37.5 mm for heavy ions. The total kick angles are about 5.0 and 3.8 mrad for the protons and heavy ions, respectively

The septum, located at F6, with a width smaller than or equal to 10 mm (including the vacuum chamber), kicks the beam 142.8 mrad away from the booster central orbit to reach 35 mm outside the main quadrupole MQF6. These elements, which are located in the main booster ring, are listed in Table 5-2.

TABLE 5-2 Ejection elements located in the Booster ring.

Name	Device	Location	Strength†	
			Heavy Ion Operation	Proton Operation
EB1F2	Slow Orbit Bump 1	F2	- 1.53%	- 1.02%
EB2F4	Slow Orbit Bump 2	F4	- 0.92%	- 0.61%
EB3F7	Slow Orbit Bump 3	F7	- 1.84%	- 1.23%
EB4A1	Slow Orbit Bump 4	A1	- 0.74%	- 0.49%
EK1F3	Fast Kicker 1	F3	3.77 mrad	5.03 mrad
	Bl (kG-m)		0.66	0.38
ES1F6	Ejection Septum	F6	142.80 mrad	142.80 mrad
	Bl (kG-m)		25.02	10.72

†The strength given corresponds to heavy ion operation with $B\rho$ as given in Table 5-1.

Note that the heavy ion and proton beams have different magnetic rigidities at extraction. The kicker is more constrained by the heavy ion operation than by proton operation (assuming that the proton extraction energy is 1.5 GeV). However, the kicker rise-time requirement for heavy ions is 200 ns instead of the 140 ns needed for the proton beam. The ejection septum requirement is also more stringent for heavy ion operation.

The major problem in the design of the ejection septum is to find a compromise between the choice of pulse width, iron lamination thickness, energy storage capacitor size, and the pulse voltage. The capacitor size considerations favor short pulses, but short pulses lead to thin iron laminations. A three section design for this septum is given in "Ejection Septum Concept Design," BST/TN 14, by J. G. Cottingham. At present the septum with appropriate vacuum plating is designed for a width of 10 mm. A smaller septum width would help to give better performance. A two section septum with a thickness of 8.6 mm has been designed by Erwin Rodger which meets the transfer line specifications.

5.3. Focusing at the Stripper

The extracted beam of heavy ions will then be transported to a copper stripper of sufficient thickness to give 70 mg/cm^2 Three quadrupoles are used to tune the betatron amplitudes. A dipole (ED1) of 0.5 m is used to pitch the beam line to a location where the radiation shielding can be easily accommodated. After the stripper, the emittance of the beam is expected to increase by 1 π mm-mrad. In summary,

stripper foil	70	mg/cm^2
β at foil	3	m (x and y)
x_p	0	
E loss	5	MeV/nucleon
σ_E	0.5	MeV/nucleon

On the other hand, the proton beam does not pass through the stripper, so the 95% emittance is expected to be about 15 $\pi\mu$m with $\Delta p/p = 0.3\%$ for a phase space area of 1.3 eV-s.

5.4. Beam Transport

Based on the above estimation of the extracted beam property, the following beam transport line will be designed to meet two requirements:

(1) It will match the lattice functions at the AGS injection point.

(2) The total beam size in the transfer line will be less than the good field aperture (50 mm) of the regular main quadrupoles, i.e. $\beta_{max} \leq 50$ m.

The momentum width ($\Delta p/p$) of the beam would increase 0.3% for the Au ions due to the stripper Depending on the r.f. scenarios for the beam extraction from the booster, we expect to have a total beam momentum window of about $\pm$ 0.5%. The betatron beam size increment is about 20% for heavy ion beams. We expect therefore a 95% emittance of about 5 $\pi\mu$m after the stripper This estimation depends on the actual emittance injected into the booster (the nominal number is 50 $\pi\mu$m with betatron admittance of 175 $\pi\mu$m). The aperture requirement in the transfer line for the following transport system will be based on the assumption of $B\rho = 11$ T-m for the fully charged ions with emittance of 5 $\pi\mu$m and $\Delta p/p = 0.5\%$.

The beam is transported with five dipoles (ED1—5) onto the AGS L20 straight section. The location and parameters of the dipoles are given in Table 5-3.

TABLE 5-3 Location and size of the ejection line dipoles.

Location and Size of the Ejection Line Dipoles					
Name	AGS Coord.		Length	Strength	Aperture
	North (inch)	East (inch)	(m)	(m^{-1}) quad (rad) dipole	(h × v)
$B\rho$ = 17.6 T-m					
ED1	2448.5336	15483.1451	0.5000	0.0364	2″ + sagitta × 2″
$B\rho$ = 11 T-m					
ED2	2523.0049	15225.8703	2.4000	0.2757	main dipole
ED3	2524.0535	15052.9457	2.4000	0.2757	main dipole
ED4	2376.0916	14517.5578	0.1562	0.0182	2.5″ + sagitta × 2.5″
ED5	2093.1100	13561.6156	1.2345	0.1436	2.5″ + sagitta × 2.5″

The dipoles ED2 and ED3 will each bend the beam 0.27570 rad. Thus the bending radius is 8.7052 m. The regular dipole has a radius of curvature of 13.7510 m. The sagitta resulting from the use of the regular main ring dipole will be 64 mm. The maximum half beam size at this section is about 25 mm. Thus the good field aperture requirement would be 89 mm at 1.29 T for $B\rho$ = 11 T-m.

The magnet alignment for the matching section is designed with the consideration of the radiation shielding required for separate operation of the Booster and the AGS rings. Table 5-4 lists the strengths and coordinates of the major components of the transfer line. Beam position monitors located in four of the quadrupoles will provide diagnositic information. The information obtained can then be used to realign the beam line.

The last dipole, ED5, is needed to horizontally deflect the beam into the AGS septum located at the L20 straight section of the AGS. The betatron functions are then matched at the entrance of the AGS A1 magnet.

TABLE 5-4 Strengths of the ejection line magnets.

Strengths of Ejection Line Magnets						
No.	Name	AGS Coord. North (inch)	AGS Coord. East (inch)	Length (m)	Strength (m^{-1}) quad (rad) dipole	Aperture (h × v)
	$B\rho$ = 17.6 T-m					
	Septum	2379.9487	15711.5102	1.0	0.07386	2″ + sagitta × 1.0″
	Septum	2404.7712	15616.0374	1.4	0.06894	2″ + sagitta × 1.5″
1	EQ_d1	2436.2189	15520.5407	0.5000	0.4916	4″ quad
2	ED1	2448.5336	15483.1451	0.5000	0.0364	2″ + sagitta × 2″
3	EQ_f2a	2458.3860	15449.1082	0.5000	0.4972	4″ quad
	EQ_f2b	2466.0487	15422.6358	0.5000	0.4972	4″ quad
4	EQ_d3	2480.7655	15371.7940	0.5000	0.4972	4″ quad
5	stripper	2487.8809	15347.2126			
	$B\rho$ = 11 T-m					
6	EQ_f4	2501.5644	15299.9406	0.5000	0.7198	4″ quad
7	ED2	2523.0049	15225.8703	2.4000	0.2757	main dipole
8	EQ_d5	2523.4486	15152.6977	0.5000	0.4934	6.5″ quad
9	ED3	2524.0535	15052.9457	2.4000	0.2757	main dipole
10	EQ_f6	2503.5128	14978.6209	0.5000	0.4242	6.5″ quad
11	EQ_d7	2483.5868	14906.5205	0.5000	0.4490	6.5″ quad
12	EQ_f8	2389.2008	14564.9922	0.5000	0.1617	6.5″ quad
13	ED4	2376.0916	14517.5578	0.1562	0.0182	2.5″ + sagitta × 2.5″
14	EQ_d9	2348.3331	14423.7866	0.5000	0.2268	6.5″ quad
15	EQ_f10	2319.8443	14327.5482	0.5000	0.2352	6.5″ quad
16	EQ_d11	2250.7088	14094.0012	0.5000	0.0949	6.5″ quad
17	EQ_f12	2201.4317	13927.5379	0.5000	0.2337	6.5″ quad
18	EQ_d13	2142.8553	13729.6605	0.5000	0.3699	6.5″ quad
19	EQ_f14	2108.4010	13613.2705	0.5000	0.3395	6.5″ quad
20	ED5	2093.1100	13561.6156	1.2345	0.1436	2.5″ + sagitta × 2.5″
21	EQ_d15	2078.2117	13458.9906	0.5000	0.3854	4″ quad
	SeptAGSB1	2063.4153	13357.0668	4	0.06107	2.5″ + sagitta × 1.8″
	SeptAGSE1	2055.1242	13310.0027			
	SeptAGSB1	2054.9638	13309.2305	4	0.06107	2.5″ + sagitta × 1.8″
	SeptAGSE1	2043.8984	13262.9069			

5.5. AGS Injection Components

The septum, located at two inches away from the AGS central orbit, is placed one foot from the A1 magnet. The total kick angle is 109.73 mrad. The injected beam will

be at least 11.7 inches away from the AGS central orbit at the end of the L20 magnet. This is necessary to eliminate the fringe field effect of the AGS magnets. The half beam size to be injected into the AGS is less than one inch. A set of orbit bumps located near L13 and A7 will locally distort the closed orbit a maximum of one inch at the septum location. The fast kicker at A5 is then excited to kick the beam onto the closed orbit. After the injection process is completed, the orbit bump is reduced adiabatically, and the acceleration cycle of the AGS begins.

5.6. Booster Extraction Power Supplies

The following sections describe the details of the power supplies required to extract the beams from the booster, transport it to the vicinity of the AGS and finally to deflect it into its proper AGS orbit. The power supplies have to operate at rates up to 7.5 Hz for proton operation and at approximately 0.7 Hz for heavy ion operation.

5.6.1. Extraction

Extraction from the Booster to the AGS is accomplished by the same scheme for both protons and heavy ions. The extraction is a fast extracted beam process using a fast ferrite kicker and thick septum in the two-step process. The harmonic number in the Booster being three (h=3) and the maximum rf frequency being 4.114 MHz, presents the major requirement for the fast kicker Its rise time shall be 140 nanoseconds. Its flattop time shall be $\sim$ 800 nanoseconds. The parameters for the extraction kicker system are given in Table 5-5. In order to keep the voltages low ($\sim$40 kilovolt range) the kicker magnet will be broken up into three (3) sections. This will keep the inductance around 2.2 μHy per section. The pulsed power will be supplied by a matched pulse-forming network (pfn) that is switched by hydrogen thyratrons. At present the design calls for placing the pfn and switch tube modules in the ring close to the kicker magnet. The charging and trigger electronics will be outside the ring.

TABLE 5-5 List of parameters for the Booster extraction kicker.

Parameter	Unit	Proton ($B\rho$ = 7.51 T-m)	Heavy Ion ($B\rho$ = 17.6 T-m)
Type		Full Aperture Ferrite	
Number of Magnets/Sections	each	1/3	
Bend Angle	mrad	5.0	3.8
Core Length	m	2.25	
Core Material		Ferrite	
Aperture (H × V)	cm	17.8 × 7.6	
Conductor (Septum) Thickness	cm	< 1	
No. of Turns		1	
Peak Field	kG		0.311
Current — peak	amps		2000
— rms	amps		
Pulse Repetition Rate	Hz	7.5	0.5 - 0.75
Current Waveform		Sq. Wave	
Base Width	μs	~1000	
Rise/Fall/Flattop Time	μs	0.14/—/0.8	
Stability/Reproducibility		10^{-2}	
Resistance — dc/ac	ohm		
Inductance	μHy	2.21/section	
Stored Energy	J	4.5	
Voltage (max)	Volts	30,000	
Power — peak	W		
— dissipated	W		
No. of Power Supplies		3	
Type		PFN	
Cable			

The next step in the extraction process is the creation of a closed-orbit deformation in the vicinity of the ejector septum magnet (F6). The orbit bump will be created by pulsing the "backleg" windings (BLW's) via capacitor discharge power supplies. The basic scheme is shown in Figure 4-8. The switches in this case will be solid state thyristors (SCR's). Four units will be required at F2, F4, F7 and A1. The BLW pulse will be a half sine wave, with approximately 5 ms at its base. The units will be similar in design to those described in section 4.1.5.2.1 for injection, except that they will be higher current.

The final step in extraction from the booster is accomplished by the thick-septum ejector magnet. This unit occupies the F6, 2.4-meter straight section. Its main parameters are shown in Table 5-6. The power supply will be a large capacitor discharge type

capable of producing a 1 - 2 ms, ~20 kA pulse. A unit of this type is now used to extract the FEB beam from the AGS, and a unit similar to this will be constructed for the Booster

TABLE 5-6 List of parameters for the Booster extraction septum.

Parameter	Unit	Proton ($B\rho$ = 7.51 T-m)	Heavy Ion ($B\rho$ = 17.6 T-m)
Type		Copper Septum	
Number of Magnets/Sections	each	1/2	
Bend Angle	mrad	142.8	
Core Length	m	#1. 1.0, #2: 1.69	
Core Material		Iron	
Aperture (H × V)	cm	#1 (7.6 × 2.54), #2 (7.6 × 3.81)	
Conductor (Septum) Thickness	cm	1. < 1.0, #2: 2.54	
No. of Turns		#1. 1, #2: 2	
Peak Field	kG	#1. 8.0, #2: 10.67	
Current — peak	amps		16,200
— rms	amps		
Pulse Repetition Rate	Hz	7.5	0.5 - 0.75
Current Waveform		Half Sine	
Base Width	μs	1000	
Rise/Fall/Flattop Time	μs		
Stability/Reproducibility		10^{-3}	
Resistance — dc/ac	ohm		
Inductance	μHy	#1. 3.8, #2: 17.0	
Stored Energy	J		
Voltage	volts		#1. 200 #2: 860
Power — peak	W		
— dissipated	W		
No. of Power Supplies		1	
Type		Cap. Disch.	
Cable		Multiple 4/0 Quadruplexed	

5.6.2. Beam Transport

The beam transport elements are shown in Table 5-4. Two criteria will be used in the design of the power supplies for the beam transport elements. In order to accommodate pulse-to-pulse modulation capability, the power supplies must be pulsed to different levels for protons, up to 1.5 GeV, or for various heavy ion species. Also, power should be conserved whenever possible. For example, the dipoles are high power devices, thus

pulsing will reduce the dipole power consumption and hence lower the operational costs.

Therefore, the power supplies that will be used will be of the pulsed dc variety The pulsing has to be accomplished in 50 ms or less to permit settling of the fields in the gaps. These units are available commercially and will be purchased to our specifications. For maximum cost effectiveness, standardization of types and sizes will be necessary The large dipole units will have a regulation of $\pm 0.01\%$ while the quadrupoles will be $\pm 0.1\%$. These requirements can be met by standard three-phase or single-phase SCR controllable units. All units will include dc filtering, regulation circuitry and computer interface modules.

The horizontal and vertical steerer power supplies will be bipolar, programmable dc types as in section 4.1.5.1.

5.6.3. AGS Injection

In order to deflect the beams from the booster into the AGS, three pulsed systems are required in the AGS. These are, a local orbit deformation or orbit bump, an injection septum, and a kicker (See Table 5-7)

TABLE 5-7 Injection elements in the AGS ring.

Name	Device	Location	Strength
IL13	slow orbit bump 1	AGS L13	- 4.48%
IA7	slow orbit bump 2	AGS A7	- 5.82%
IKA5	fast kicker	AGS A5	2.85 mrad
ISL20	injection septum	AGS L20	109.73 mrad

The orbit bump will be created by pulsing backleg windings in two AGS main ring magnets (L13 and A7). The power supplies will be capacitor discharge type units as in the booster extraction bumps (section 5.6.1).

The other two systems, namely the injection septum and the fast kicker are the complementary systems to the booster ejection septum and extraction fast-kicker respectively These two systems are electrically very similar to those described in section 5.6.1. The parameters are given in Tables 5-8 and 5-9. One additional problem arises in the AGS injection fast kicker which is not present in the Booster unit. During the final (or fourth) transfer from the booster to the AGS, the fall time of the AGS kicker has to be very fast (<140 ns), so that it does not appreciably deflect the first injected pulse. This means that the AGS kicker modules must incorporate some form of tail-biting circuit to reduce the kicker-current fall time to an acceptable value.

TABLE 5-8 List of parameters for the AGS injection septum. (L20)

Parameter	Unit	Proton ($B\rho$ = 7.51 T-m)	Heavy Ion ($B\rho$ = 11 T-m)
Type		Copper Septum	
Number of Magnets/Sections	each	1/1	
Bend Angle	mrad	109	
Core Length	m	2.3	
Core Material		Iron	
Aperture (H × V)	cm	7.6 × 5.1	
Conductor (Septum) Thickness	cm	< 1.0	
No. of Turns		1	
Peak Field	kG		5.2
Current — peak	amps		21,300
— rms	amps		
Pulse Repetition Rate	Hz	7.5	0.5 - 0.75
Current Waveform		Half Sine	
Base Width	μs	1000	
Rise/Fall/Flattop Time	μs		
Stability/Reproducibility		10^{-3}	
Resistance — dc/ac	ohm		
Inductance	μHy	4.3	
Stored Energy	J		
Voltage	volts		290
Power — peak	W		
— dissipated	W		
No. of Power Supplies		1	
Type		Cap. Disch.	
Cable		Multiple 4/0 Quadruplexed	

TABLE 5-9 List of parameters for the AGS injection kicker (A5)

Parameter	Unit	Proton ($B\rho$ = 7.51 T-m)	Heavy Ion ($B\rho$ = 11 T-m)
Type		Full Aperture Ferrite	
Number of Magnets/Sections	each	1/2	
Bend Angle	mrad	~3.0	
Core Length	m	1.0 (0.5 + 0.5)	
Core Material		Ferrite	
Aperture (H × V)	cm	17.8 × 7.6	
Conductor (Septum) Thickness	cm	0.5	
No. of Turns		1	
Peak Field	kG		0.330
Current — peak	amps		2000
— rms	amps		
Pulse Repetition Rate	Hz	7.5	0.5 - 0.75
Current Waveform		Sq. Wave	
Base Width	μs	~1000	
Rise/Fall/Flattop Time	μs	0.14/0.14/0.700	
Stability/Reproducibility		10^{-2}	
Resistance — dc/ac	ohm		
Inductance	μHy	1.5/section	
Stored Energy	J		
Voltage	Volts	21,000/section	
Power — peak	W		
— dissipated	W		
No. of Power Supplies		2	
Type		PFN	
Cable			

CHAPTER 6. VACUUM SYSTEM

6.1. Introduction

The Booster vacuum system can be conveniently divided into four interconnecting areas:

The Booster ring: with a circumference of 200 m
and a designed vacuum of 3×10^{-11} Torr (N_2 equivalent).
The proton injection line: with a length of ~ 35 m
and a vacuum of 10^{-10} to 10^{-8} Torr
The heavy ion injection line: with a length of ~ 280 m
and a vacuum of 10^{-10} to 10^{-9} Torr; this is the extension
of the existing HITL.
The booster extraction line: with a length of ~ 62 m
and a vacuum of 10^{-10} to 10^{-8} Torr

The design parameters of the ring vacuum system are given in detail in Sections 6.2 to 6.4; and those of the three beam transport lines in Section 6.5. Instrumentation and control is covered in Section 6.6 for both ring and transfer lines.

6.2. Vacuum Requirement

Pressure in the low 10^{-8} Torr range is sufficient to avoid beam blowup or beam loss caused by nuclear scattering and Coulomb scattering for both protons and heavy ions. However, the highly stripped, yet still electron rich, heavy ions will also exchange electrons with the residual gas molecules with much higher cross-sections, which causes immediate beam loss.

The charge-exchange cross-sections (both capture σ_c and loss σ_l) are functions of velocity $\beta = v/c$, the charge states q, and the atomic number Z_t of the residual gas molecules. At known q and Z_t, the σ_c decreases rapidly with increasing energy ($\propto \beta^{6-7}$). The σ_l falls off more slowly with increasing energy ($\propto \beta^{1-2}$) and becomes the predominant factor of the total cross-section at higher energy

For the least favorable species injected from the Tandem, such as Au^{+33} at 1 MeV/nucleon, the capture cross-sections[1,2] are $\sim 5 \times 10^{-16}$ cm^2 (in N_2) and drop below 1×10^{-17} cm^2 at 10 MeV/nucleon. The loss cross-sections[3,4] decrease slowly from $\sim 10^{-17}$ cm^2 at 1 MeV/nucleon to high 10^{-18} cm^2 at 10 MeV/nucleon. Using the RF capture and

[1]A.S. Schlachter, et. al. *Phys. Rev* **A27** 3372(1983).

[2]W B. Graham, et. al. *Phys. Rev.* **A30**, 722(1984).

[3]B. Franzke, *IEEE Trans. on Nucl. Sci.* **NS-28**, 2116(1981).

[4]I. S. Dmitriev et. al. *Nucl. Instr. Methods*, **164**, 329(1979).

ramping scheme in the design manual, the beam loss due to charge exchange can be estimated by integrating $\sigma(\beta)$ over t

$$I(t) = I(0)\, e^{-\int_0^t \sigma(\beta) P\, \beta(t)\, c\, dt}$$

here P is the residual gas pressure (density).

A residual gas pressure of low 10^{-11} Torr is necessary if the beam losses due to charge exchange are to be limited to a few percent.

6.3. Vacuum Specification

6.3.1. Vacuum Chamber and Half-Cell

The ring will be divided by all metal valves into six vacuum sectors; and each vacuum sector into 8 half-cells of 4.2 m each in length. One UHV pump station will be provided for each half-cell. The standard half-cell chamber is shown in Fig. 6-1. Each standard half-cell vacuum chamber consists of a curved dipole chamber (Fig. 6-2), connecting to a straight, circular chamber for the quadrupole and sextupole sections. The vacuum chamber will be fabricated out of Inconel 625. One set of pickup electrodes will be located between the quadrupole and the sextupole chambers (see Fig. 6-3). An Inconel formed bellows will be mounted at the end of sextupole chamber to take up motion due to thermal expansion. The last component is a transition piece with a pump-out connection (see Fig. 6-4 for detail), which reduces the circular chamber to the cross-section of the dipole chamber

The insulation and bakeout of the tightly-enclosed dipole chamber will be accomplished by the use of a custom-made insulating blanket having integral resistive-heating elements. For the remainder of the half-cell where access is easier, industrial-type heating tape with conventional glass or ceramic wool insulation is planned.

To reduce the eddy current effect during 7.5 Hz operation, correction windings will be mounted on the face of the dipole chamber For faster pulsed magnets, such as kickers, metallized ceramic chambers are also envisioned.

6.3.2. Pressure Distribution

The achievable vacuum inside the Booster ring can be expressed by the following formula:

$$P_{avg} = P_o + uq\left(\frac{L}{S} + \frac{L^2}{12C}\right)$$

Here P_o blankoff pressure of pump, $<1 \times 10^{-11}$ Torr

- u perimeter of the vacuum chamber
  ~ 47 cm for quad, ~ 42 cm for dipole
- q unit outgassing rate
- L distance between pumps, 420 cm

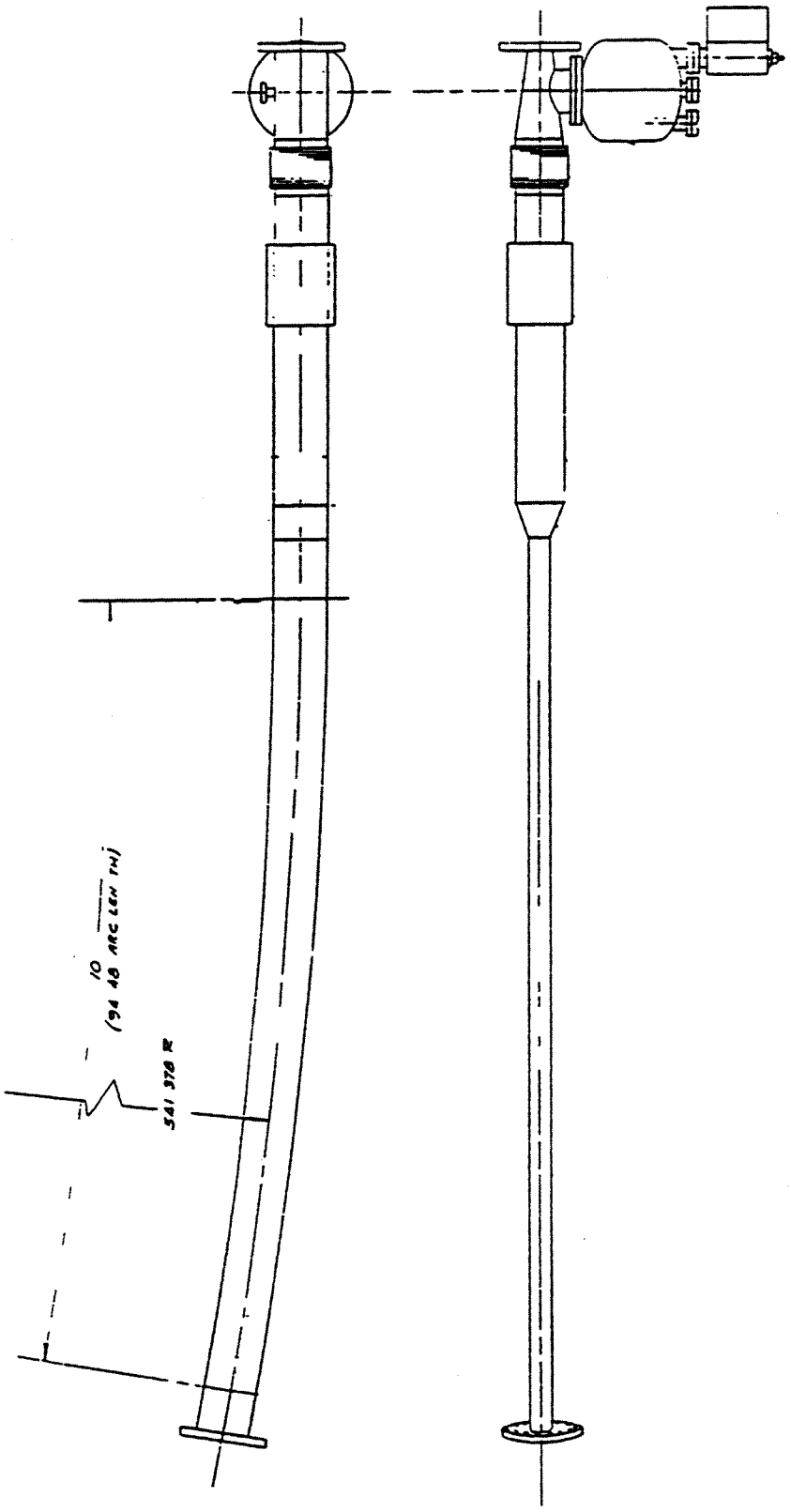

Figure 6 1 Standard half cell vacuum chamber and UHV pump station

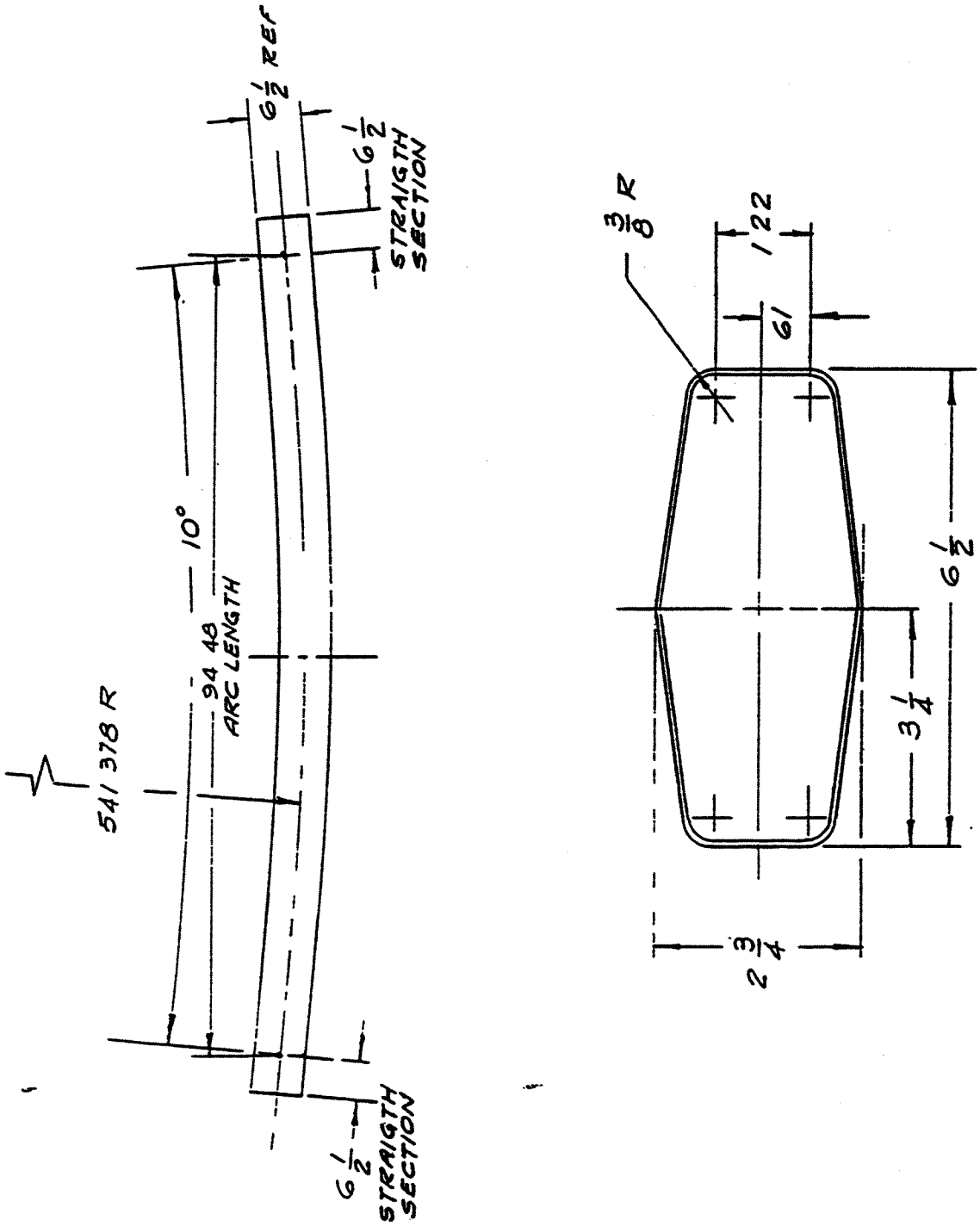

Figure 6 2 Curved dipole vacuum chamber

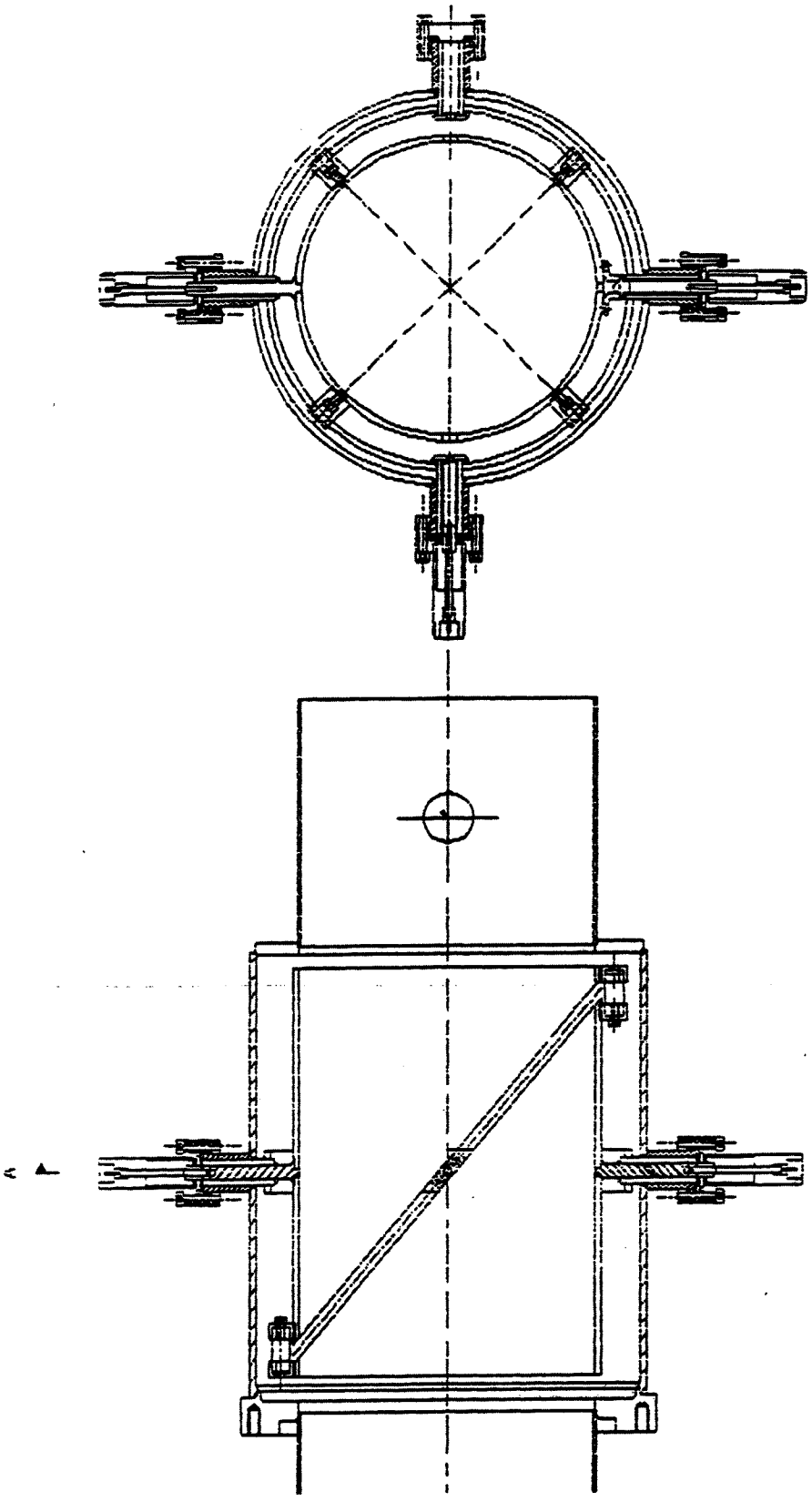

Figure 6 3 One of the prototype PUE detector/vacuum housing designs

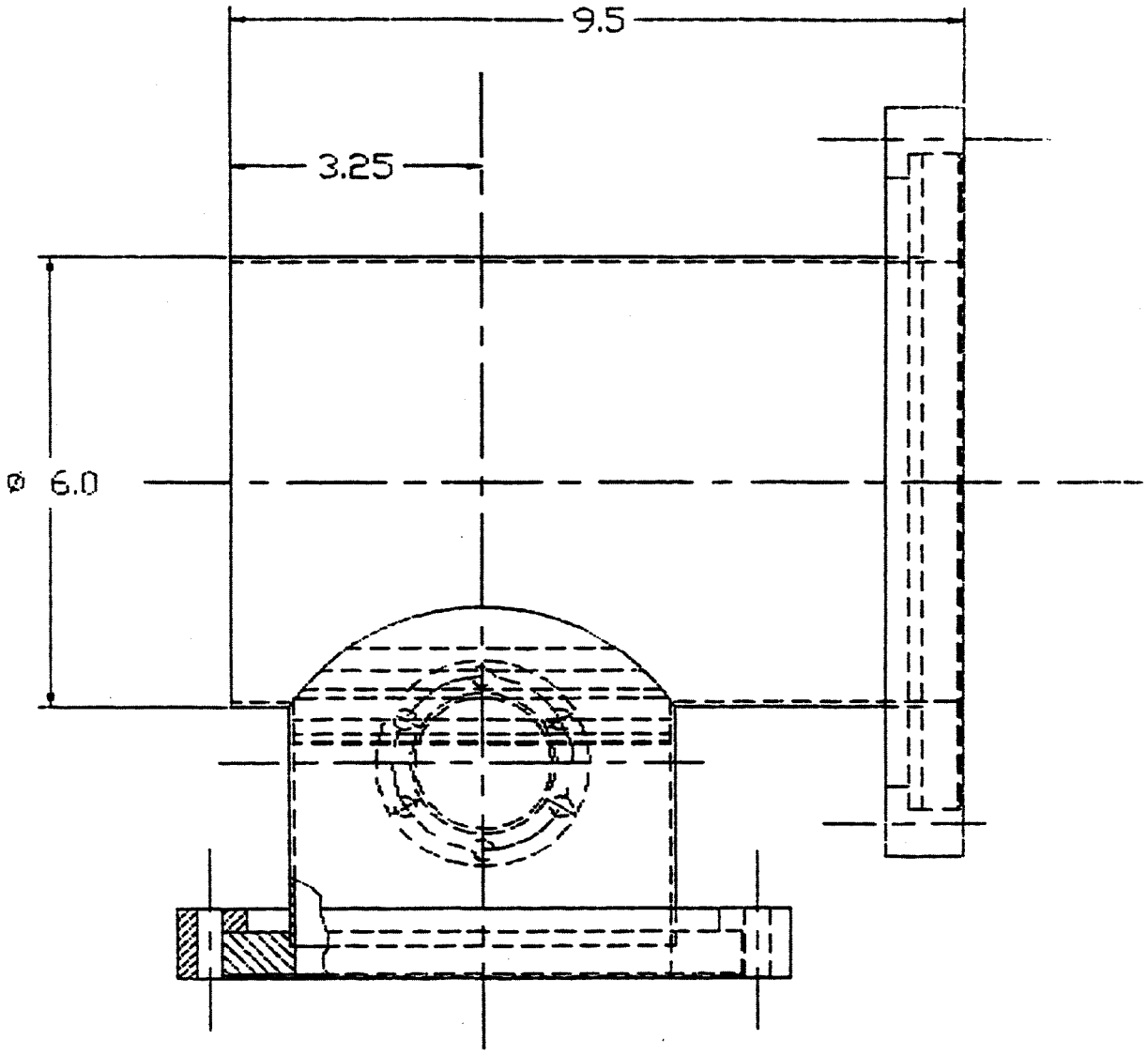

Figure 6-4. The transition piece with pump out connection to UHV station.

S pumping speed at the neck of the pump, $\sim$ 1000 l/s
C linear conductance of the chamber in cm-l/s
1.5×10^5 for quad, 5×10^4 for dipole

Assuming a uniform outgassing rate of $< 5 \times 10^{-13}$ Torr-l/s-cm^2 (except the PUE elements), the average vacuum will be less than 3×10^{-11} Torr

6.3.3. Vacuum Parameters

To achieve outgassing of less than 5×10^{-13} Torr-l/s-cm^2, the selection of material, fabrication, and vacuum processing for every component has to be done with state of the art UHV technology In the absence of fully formulated standards for the construction of any booster component, the procedures developed at NSLS, Isabelle, SLAC and CERN will be adopted, whenever possible. The following serve as guidelines for all components to be installed in the ring vacuum system.

— All the Inconel and stainless steel components after fabrication are to be vacuum fired for at least one hour at 950 C and $< 10^{-5}$ Torr Other material will be vacuum degassed at an appropriate temperature.

— The whole vacuum system is to be baked in situ at 200 C. (All equipment should nevertheless have a "design" temperature of 250 C.)

— Only UHV compatible metal and inorganic material will be allowed inside the vacuum chamber

— Inside welds should be used whenever possible. Outside welds have to be EB welds or full-penetration TIG welds.

— Thorough cleaning shall be performed before and after machining and before welding and assembly

— Every component or setup (including the associated vacuum box) has to meet the following specific outgassing rates:

25 C	operating temperature
5×10^{-13} Torr-l/s-cm^2	5×10^{-12} Torr-l/s-cm^2
each setup 1×10^{-8} Torr-l/s	5×10^{-8} Torr-l/s

— Leak tightness down to $<1 \times 10^{-10}$ std cc/s.

6.4. UHV Pump Body and Vacuum Pumps

The UHV pumping system consists of the titanium sublimation pumps and the small ion pumps. They are installed in the UHV pump bodies located at the down stream end of each half-cell (between the dipole magnet and the correction coil). For ease of cleaning, vacuum firing and installation, they will be flanged to the half-cell vacuum chambers. The schematic of the UHV pump station is shown in Fig. 6-5.

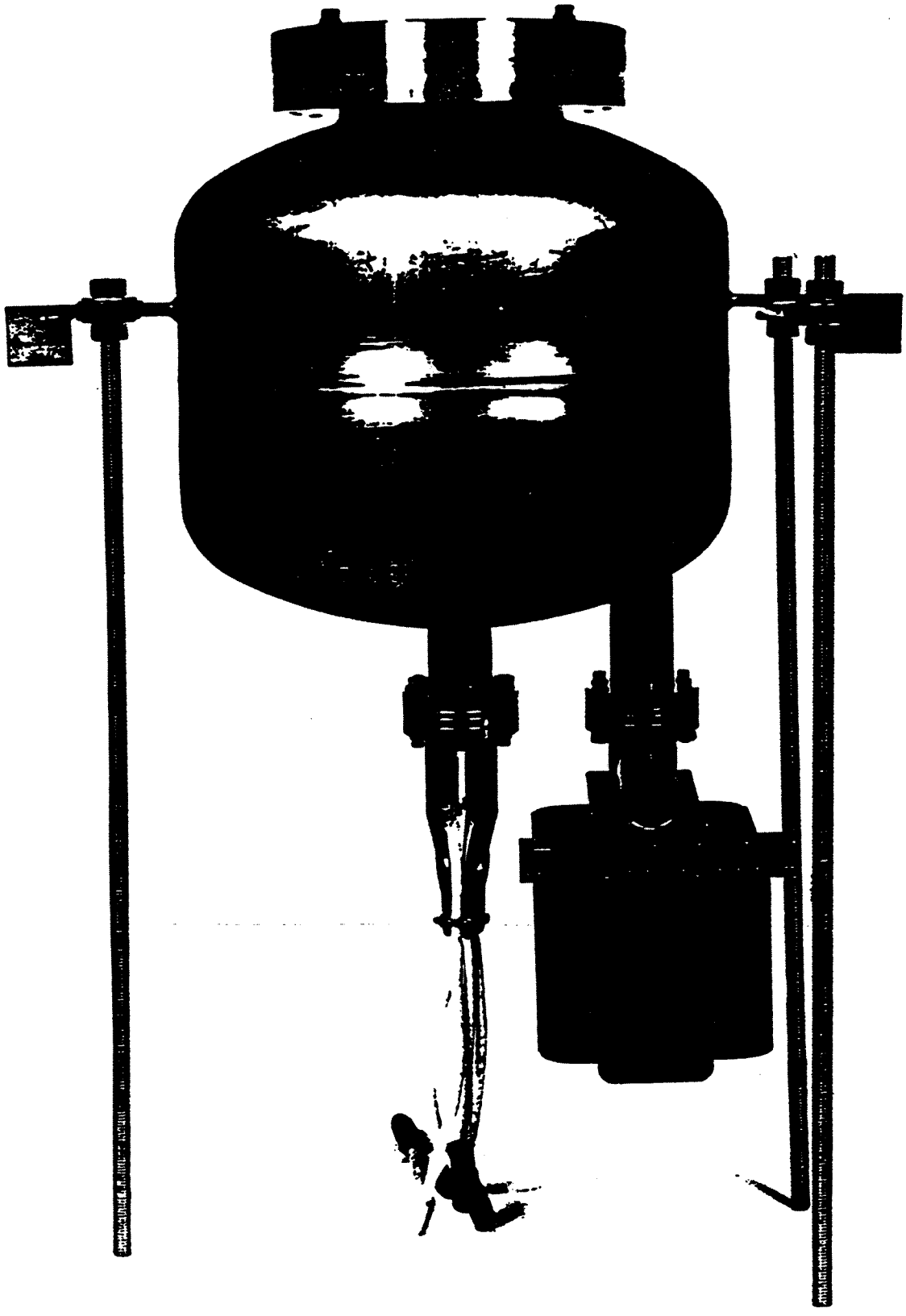

Figure 6-5. UHV pump station.

Each pump body has about 3000 cm^2 inner area which serves as the pumping surface for sublimed titanium. The available speeds at the neck of the pump body are about 1000 l/s for both hydrogen and carbon monoxide. The 20 l/s diode ion pump will pump inert gases such as methane and argon.

To accommodate roughing, two 1.5-inch right-angle valves will be installed at the pump bodies for each vacuum sector. Portable turbopump stations will be used to rough down the vacuum sectors from atmosphere and during in situ bakeout. These stations will be interlocked to protect the vacuum sector and the turbo-pump itself from various failure modes.

To reduce the impact of the high outgassing of special beam components such as bump coils, kickers and septums, additional pumping in the form of NEG cartridges or large ion pumps will be installed at these locations.

6.5. Injection and Extraction Lines

To differentiate the 10^{-11} Torr ring vacuum from the 10^{-7} Torr Linac and AGS vacuums, vacuums of 10^{-9} and 10^{-10} Torr are required for both injection lines and for the extraction line.

The heavy ion injection line is similar to the existing HITL vacuum system. It will be baked to $>$ 100 C and pumped with NEG strips and small ion pumps. Due to the radiation level in the AGS and HEBT tunnels, vacuum monitoring (i.e. GP303 chassis) and control will be located remotely

For the proton injection line, differential pumping with NEG strips or large ion pumps will be necessary to isolate the ring vacuum from the 10^{-6}, 10^{-7} Torr Linac. The vacuum system will also be baked to $>$ 100 C. To prevent catastrophic vacuum failure from HEBT, BLIP, and REF areas, a fast valve of less than 20 ms closing time will be installed at Linac end of this line.

The vacuum system for the extraction to the AGS ring will be similar to that of the injection lines. Special pumping is also required under the stripper foil.

6.6. Vacuum Instrumentation and Control

All the ring vacuum equipment with the exception of titanium sublimation pumps will be monitored and controlled at the chassis and through computers. Due to the presence of the radiation in the tunnel, all the chassis will be located at the Linac House or Building 914. Four device controllers and two stations will communicate with the vacuum equipment and the main frame computers. The general layout of the vacuum equipment and control is shown in Fig. 6-6. Specifications for this equipment are given below·

A. Ion pump power supply· 200 mA short circuit current, 5 kV, local and remote control; Process control relay contacts for interlock; computer control and read back for pump on-off, current (down to 100 nA), voltage and status/interface.

— the new AGS power supply is suitable
— two to three ring ion pumps may be controlled through one power supply

B. Titanium sublimation pump (TSP): 50 A motor driven autotransformer into individual 10 A transformers, switchable by sector to buck boost transformers located in the tunnel at the TSP; current is read through current sensor in the primary leg of the transformer; the TSP will be operated manually whenever the need arises, i.e. 10 minutes every two weeks.

C. Vacuum gauge controller· commercially available gauge controllers will power, monitor and control the gauge tubes from atmosphere to 1×10^{-11} Torr In each sector, one Convectron gauge will interlock all the ion gauges.

D Sector valve control: interlocked by ion gauges and/or ion pumps; open-close manually and due to interlock; computer monitoring only

E. Roughing and Bakeout: monitored and interlocked via portable vacuum gauges and bakeout controllers with optional computer monitoring or control.

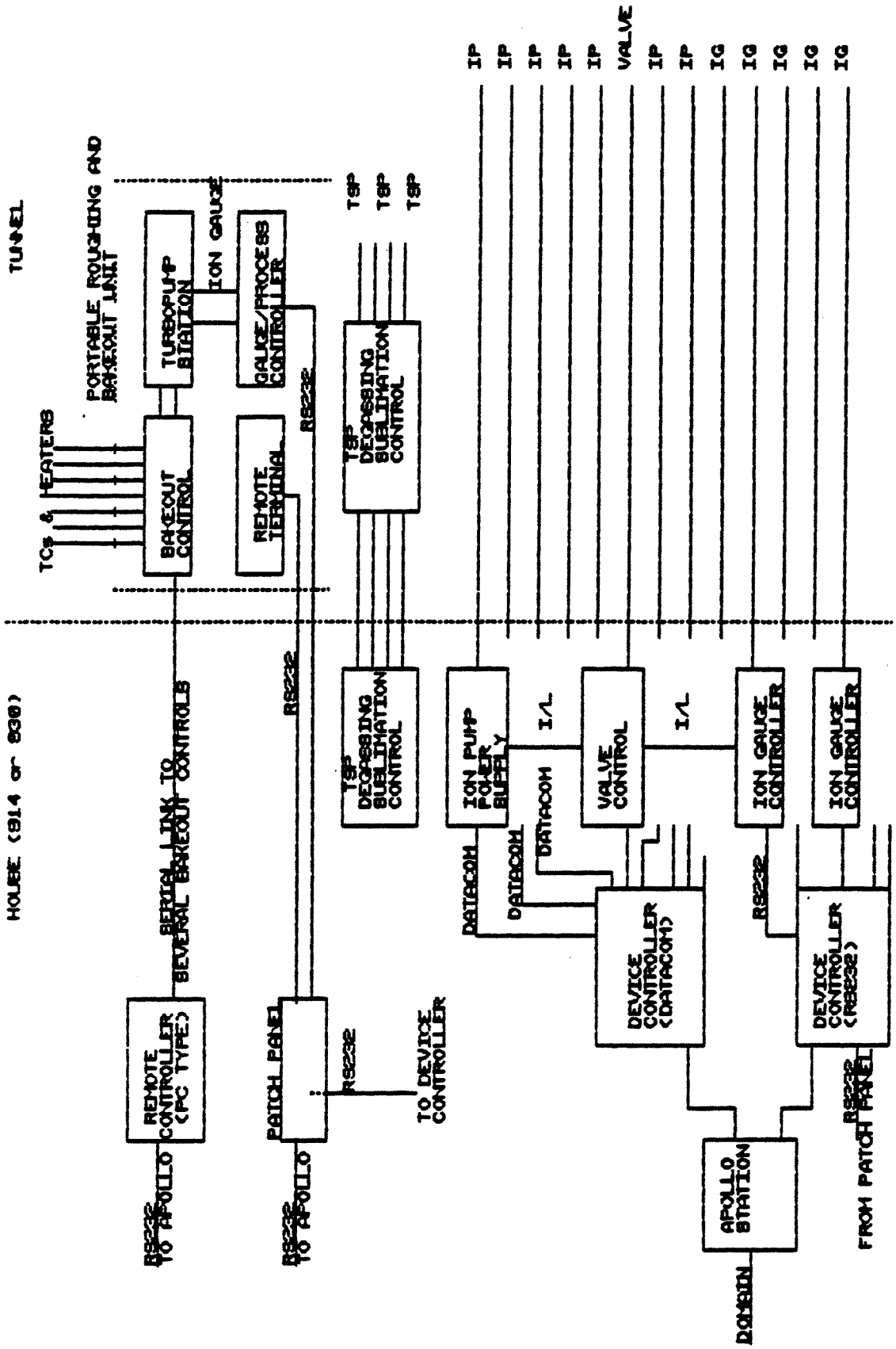

Figure 6 6 Vacuum control and interlock scheme

6.7 Summary of Vacuum Equipment

	Ring	LTB†	TTB†	BTA†
Ion Pump 20 l/s	40	4	10	4
200 l/s	8	7		4
Power Supply	30	11	10	8
Titanium Pump	50			
NEG Strip		20 m	250 m	30 m
Cartridge (500 l/s)				2
Turbopump Portable	4	1	2	1
Fixed		1		1
Ion Gauge 10^{-4} — 10^{-11}	45	4	10	4
Convectron Gauge > 10^{-3}	7	3	10	2
RGA Head	7			
Sector Valve	7	4	10	3
Fast Valve		1		
Isolation Valve	14	2	10	4

†The equipment on the three transfer lines will vary with the layout of the magnets and the beam diagnostic instruments.

CHAPTER 7 RF SYSTEM

7.1. Introduction

The requirement of the AGS Booster to accelerate heavy ions injected from the Tandem Van de Graaff, as well as protons from the AGS Linac, establishes the basic Booster RF parameters.

The AGS Booster will utilize synchronous bunch-to-bunch transfer to the AGS. It will cycle four times for each AGS acceleration cycle and the RF will operate at the third harmonic of the revolution frequency, filling each of the twelve AGS buckets during proton operation. The Booster will cycle once for each AGS cycle during heavy ion operation. The RF frequency has been chosen to be three times the revolution frequency and three of the twelve AGS buckets will be filled during each AGS heavy ion acceleration cycle.

For gold the injection revolution frequency is 71 kHz, but the design allows for even heavier ions with revolution frequencies as low as 59.5 kHz or, for the third harmonic, an accelerating frequency of 178.5 kHz. The highest frequency in the Booster will occur at 1.5 GeV proton ejection: 4.114 MHz.

The RF system performance requirements are summarized in Table 7-1.

The RF system will be designed to accelerate 0.75×10^{13} protons per bunch to insure an adequate safety factor. The expected operating intensity is 0.5×10^{13} protons per bunch as shown in the table.

7.2. RF System Design

7.2.1. System Configuration

To cover the frequency variation from 178.5 kHz to 4.114 MHz, with different voltage ranges, different beam loading criteria, and different output impedance specifications, more than one type of accelerating system is needed. For protons, the AGS Linac output energy, nominally 200 MeV, sets an injection frequency into the Booster of 2.523 MHz. The proton system, designated Band III must, therefore, operate over the range of 2.523 MHz to 4.114 MHz. (For design purposes, Band III will operate from 2.4 MHz to 4.2 MHz.) The lower frequency range, 178.5 kHz to 2.5 MHz, will be used only for heavy ions. Any heavy ion requirement over 2.5 MHz will be provided by the proton system.

The accelerating cavities are ferrite loaded and the resonant frequency is changed by a dc bias variation of the permeability of the ferrite. In the proton system the variation in frequency is 1.75:1 representing a permeability charge of a factor of 3.06:1. This variation is relatively small. In the heavy ion range, however, the total frequency variation is nearly 14:1, a permeability variation of 196:1. The dc bias to accomplish this change in a single system is too great. The heavy ion system is, therefore comprised of two systems. Band I covers the range from 178 kHz to 675 kHz. Band II covers the range from

TABLE 7-1 RF System requirements.

	p	p↑	S^{+14}	Au^{+33}
RF Amplitude				
injection	45 kV	7.35 kV	0.67 kV	1.77 kV
ejection	53 kV	40 kV ?	< 17 kV	< 17 kV
at max. accel.	90 kV	40 kV	≤ 17 kV	≤ 17 kV
Harmonic Number	3	3	3	3
RF Frequency				
injection	2.5 MHz	2.5 MHz	0.446 MHz	0.213 MHz
ejection	4.11 MHz	4.11 MHz	3.89 MHz	3.06 MHz
Phase Space Area/A	1.5 eV-s	0.3 eV-s	0.071 eV-s	0.071 eV-s
Intensity (per bunch)	0.5×10^{13}	3×10^{11}	5×10^{9}	1.1×10^{9}
Total Gap Impedance ($f_{rf} = 4.1$ MHz)	< 24 kΩ	—	—	—
Acceleration Time	62 ms	≥ 66.5 ms	≤ 0.7 s	≤ 0.7 s
Max. Beam Power Delivered to Beam	140 kW	—	< 0.5 kW	< 0.5 kW
Maximum B	9.5 T/s	9.5 T/s	< 3.5 T/s	< 3.5 T/s
B_{inj}	1.5 T/s	0.0 T/s	0.0 T/s	0.0 T/s

600 kHz to 2.5 MHz.

In addition to the frequency range, the next important criterion for the RF design is the voltage requirement for beam acceleration. For the heavy ions this has been established as 17 kV peak RF voltage. With protons the requirement is 90 kV peak RF voltage.

7.2.2. Cavity Design

The design of the acceleration cavities is determined by the ferrite materials available. The primary problem is the maximum heat loss in the ferrite which can be accommodated. For a conservative design the heat loss (which is acceptable with water cooling), averaged over a machine cycle, is about 250 mW/cc in the ferrite. With a duty cycle of 50% a heat loss of 500 mW/cc may be used but the RF amplifier must, of course, be capable of supplying the highest power load *not* the average.

The greater the amount of ferrite which can be installed in a cavity, the lower the RF flux density and, therefore, the lower the power loss. Since, in ferrites, the loss increases as the square (or higher power) of the flux density it is important to utilize the available cavity straight section length to hold as many ferrite rings as possible. The constraints are: the inner radius of the ferrite rings, determined by the vacuum chamber size and necessary clearance to the chamber, and the outer diameter determined by the capability of the ferrite manufacture to make large rings. The outer diameter has a practical maximum of about 50 cm. The number of ferrite rings which can be used is limited by the axial length requirement for cooling plates, cavity end plates, bellows, flanges, accelerating gaps, voltage clearances, and lead clearances. All of these reduce the available ferrite space.

The basic relationship between the voltage on the cavity and the RF flux density (which determines the losses) is $V = n\phi$ where ϕ is the time derivative of the flux density and n is the number of RF turns in the winding. Since the cavities have a single turn, $\phi = BA$ (B = flux density, A = area), and, for sinusoidal excitation, $\phi = \omega\phi$ ($\omega = 2\pi f$) and thus $V = \omega VA$ The relationship between B and losses depends upon the availability of ferrites, each of which must be measured individually

Ferrites are nonmetallic oxides which exhibit ferromagnetism. Their resistivity at radio frequencies is many orders of magnitude higher than that of magnetic metals. This allows them to be used at frequencies well above those for metals. The methods of manufacturing ferrites, however, are much more critical than for metals and requires exact mixtures of oxides, long sintering cycles with very accurate control of time and temperature, and finally, grinding the ceramic-like material to its proper dimensions.

The only way to determine the characteristics of the finished material are measurements under the same operating conditions of frequency, flux density and dc bias. After surveying the fabricators who have the capability of making large ferrite pieces (there are no more than five available), and measuring both small and large sample rings, we have established the maximum flux densities commensurate with the losses within our cooling design.

With the design criterion of 17 kV peak RF voltage in the heavy ion cavities we can satisfy the parameter with a single RF cavity for Band I and a single cavity for Band II. The 90 kV peak RF voltage cavity for protons would require too high a flux density in a single cavity and Band III, for protons, will utilize two cavities with a peak voltage of 45 kV per cavity A further reason for using two cavities for the proton system is the problem of voltage breakdown at a total voltage of 90 kV

Except for the gap tuning capacitors it is planned that the heavy ion cavities for Bands I and II will be identical in terms of construction, type of ferrite and number and size of ferrite rings.

As the cavities are tuned by dc biasing of the ferrite each cavity will be a "cavity station" consisting of two separate cavities connected with the bias arrangement such that the RF and dc fluxes are parallel in one cavity and anti-parallel in the other (see Figures 7-1 and 7-2). This automatically provides a cancellation of the coupling of the RF energy into the dc circuits. Bypass capacitors and a decoupling inductor are used to take care of imbalances in the characteristics between the two cavities in a cavity station.

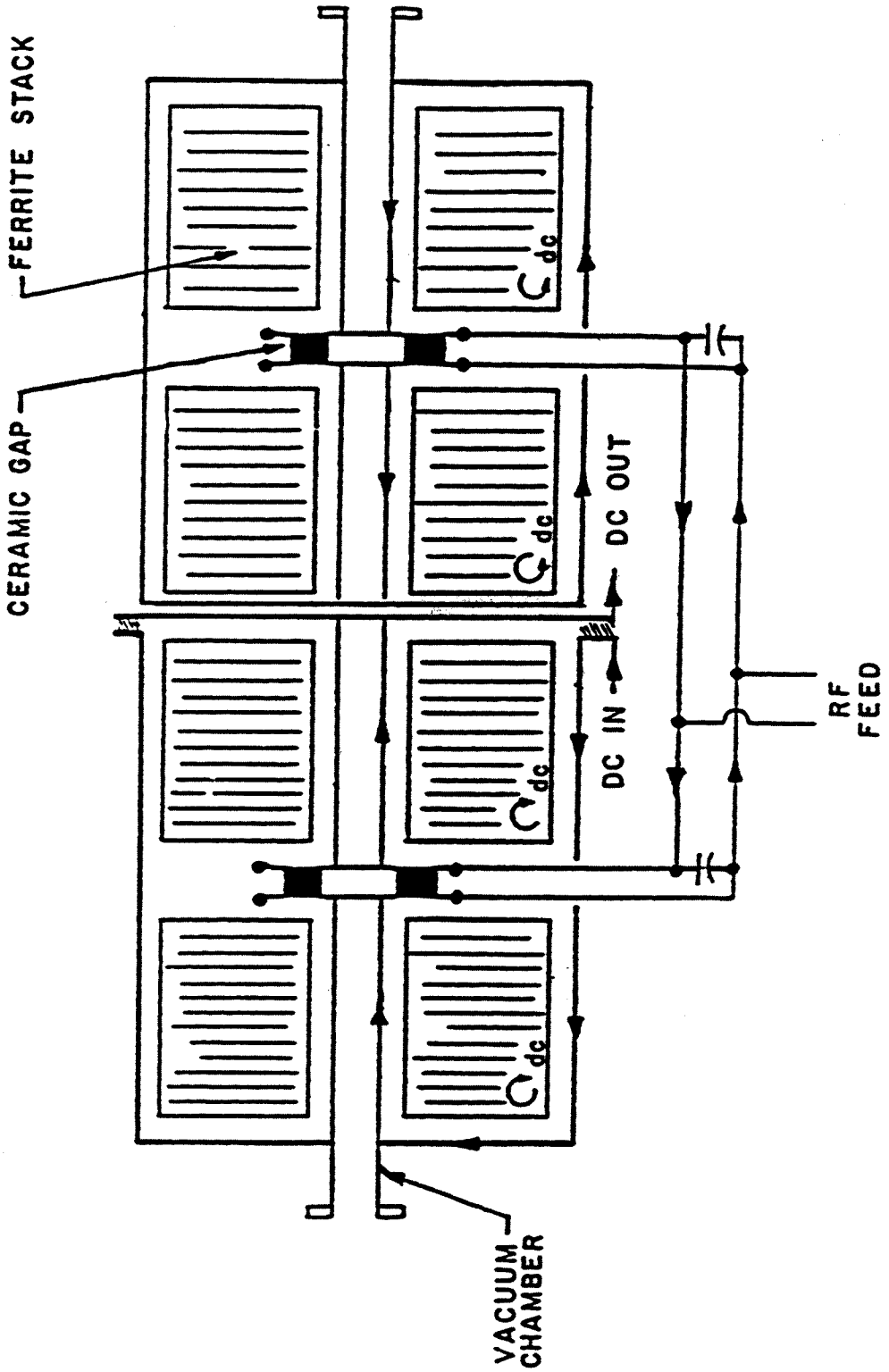

Figure 7 1 Schematic cross section of ferrite cavities to be used for Bands I & II

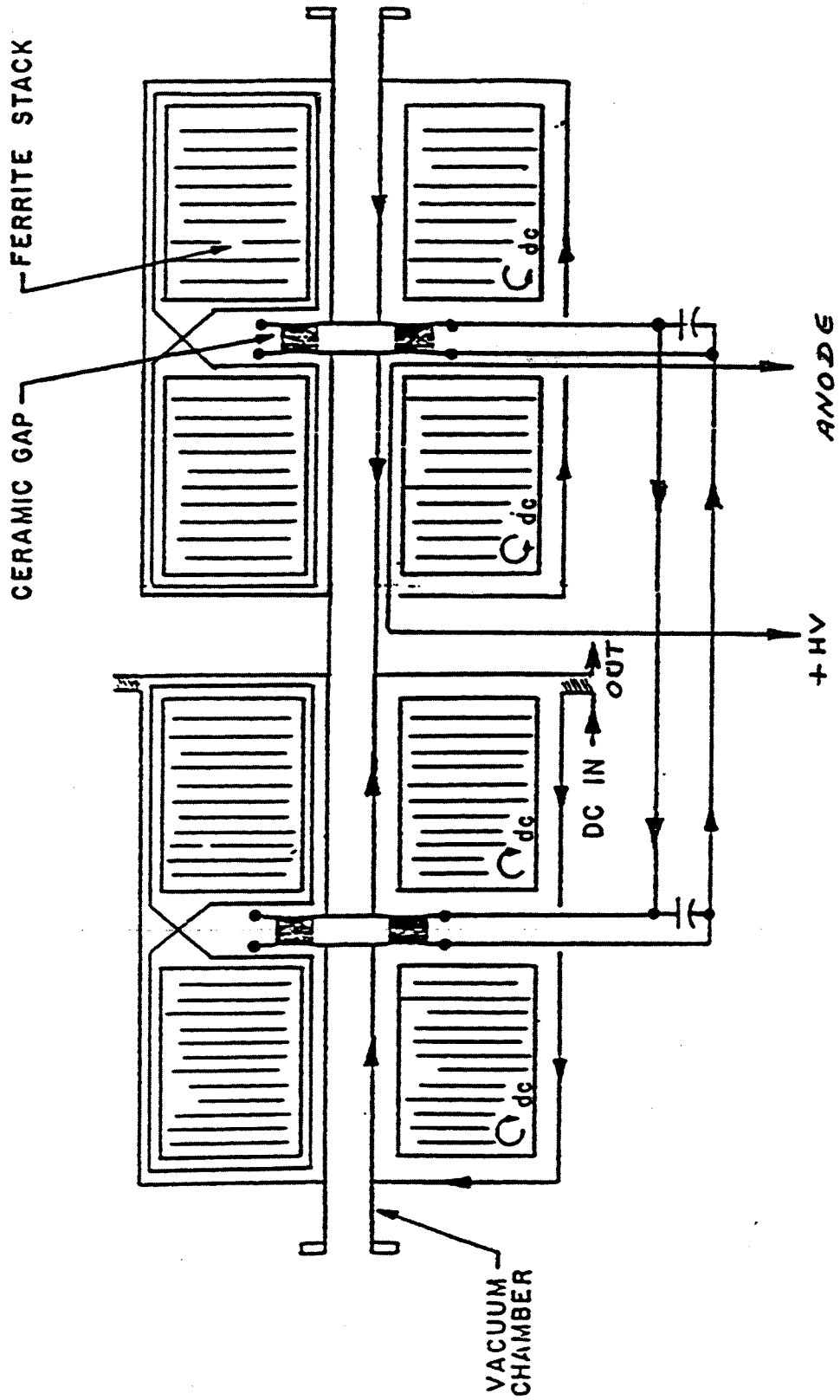

Figure 7-2 Schematic cross section of ferrite cavity for Band III

With two cavities in each station, the two accelerating gaps are in parallel in each station with a peak voltage of half the the required station voltage on each gap. Thus, 8.5 kV/gap in the heavy ion cavities and 22.5 kV/gap in each proton cavity is needed. For the balanced cavities a push-pull drive arrangement is used, and each gap swings one half of the voltage with respect to ground, 4.25 kV to ground for the heavy ion cavities and 11.25 kV to ground for the proton cavities.

7.2.3. Beam Loading

The beam intensities with heavy ions are low enough that beam loading is not significant with respect to the ferrite losses. With the proton system, however, the beam intensity is high enough to have a significant effect on the RF system. This presents itself in several ways. The beam power which the RF system must supply is quite large and the amplifier must be capable of providing this power as well as the ferrite losses. The beam is bunched and it extracts energy from the gap capacitance in a transient fashion. The system must be able to supply the in-phase and quadrature components of beam current and the loaded shunt impedance must be sufficiently small for stable operation.

As an added complication the gap capacitance is determined by the ferrite inductance. By adding more ferrite to reduce losses the inductance is raised which lowers the required tuning capacitance. We cannot, however, go below the capacitance required for stable operation. With the ferrite which is intended for the proton cavities it may be necessary to reduce its initial inductance with a dc pre-bias to lower the permeability and allow the gap tuning capacitance to be increased.

7.2.4. RF Amplifiers

The RF amplifiers will have the final stage(s) located directly at the cavity The low level and RF control system will feed the final stage(s) from a remote location. For the heavy ion cavities the location of the high power stage is a matter of convenience. For the proton system the location of the final stage right at the cavity is absolutely necessary to reduce the impedance which is seen by the beam. Any unnecessary length of connection from the amplifier to the gap raises the output impedance of the system as seen by the proton beam.

The proton system amplifier presently being designed will use a large high power tetrode with a high perveance. This tube requires low drive power Although the system is push-pull only one tube is used. (See Figure 7-2.) One side of the accelerating gap is driven with respect to ground. Inside the cavity a closed "figure 8" loop couples the two halves of the cavity to each other in such a fashion as to provide exact push-pull operation. The single tube has enough power capability to supply the full cavity power as well as the beam power. The tube is operated class AB.

The output tube drives the cavity from the anode. To keep the high dc potential out of the cavity, for personnel safety reasons, there are several options. It is possible to use a high voltage decoupling capacitor from the anode to the gap, but this increases the

output impedance. Another method is to use a positive grounded dc anode supply, but this introduces high voltage decoupling problems in all the low level input and cathode circuits. A third method, which appears to offer the best solution, is to run an insulated loop from the anode around the ferrite and returned at the shorted end of the cavity (see Figure 7-3). This provides the RF excitation with no direct dc connection to the cavity

There is a stability criterion on the total shunt impedance for an RF system feeding a high intensity (beam loaded) machine. This is known as the Robinson resistance. This sets a maximum allowable output impedance of the RF drive system if no feed-back techniques are employed. The design output impedance contemplated for the Booster is well under the Robinson resistance.

The drive stages to the final amplifier will be operated push-pull, with transformers coupling to the grid of the final amplifier tube. double to single ended system.

The low level and control system for the RF will be housed outside the Booster tunnel.

The amplifiers for the heavy ion cavities do not require any special considerations for beam loading or beam stability criteria. The operating voltages are much lower than for the proton cavities. These amplifiers will be used push-pull, with two tubes, directly coupled to the cavities and will also be loop coupled to the ferrite for dc isolation. Again, low level and control systems will be located in the Booster Control Room.

7.2.5. RF Voltage Cycle

The RF voltage cycle in the proton system requires the maximum 90 kV peak near the beginning of the cycle. Above about 3.55 MHz the RF voltage will be decreased gradually to approximately 53 kV From the cavity design standpoint the average power dissipated in the ferrite is reduced significantly and the ferrite cooling requirement is greatly reduced. The repetition rate of cycling is 7.5 Hz with a 50% duty cycle for the RF

For the heavy ion cavities the voltage is nearly constant except at injection with a maximum duty cycle of 50% and a 1 Hz cycling rate.

Relevant proton cycle machine parameters are shown in the figures of Chapter 10.

7.3. RF System Specifications

Table 7-2, RF System Specification, tabulates the design parameters for the high power proton and the heavy ion RF system.

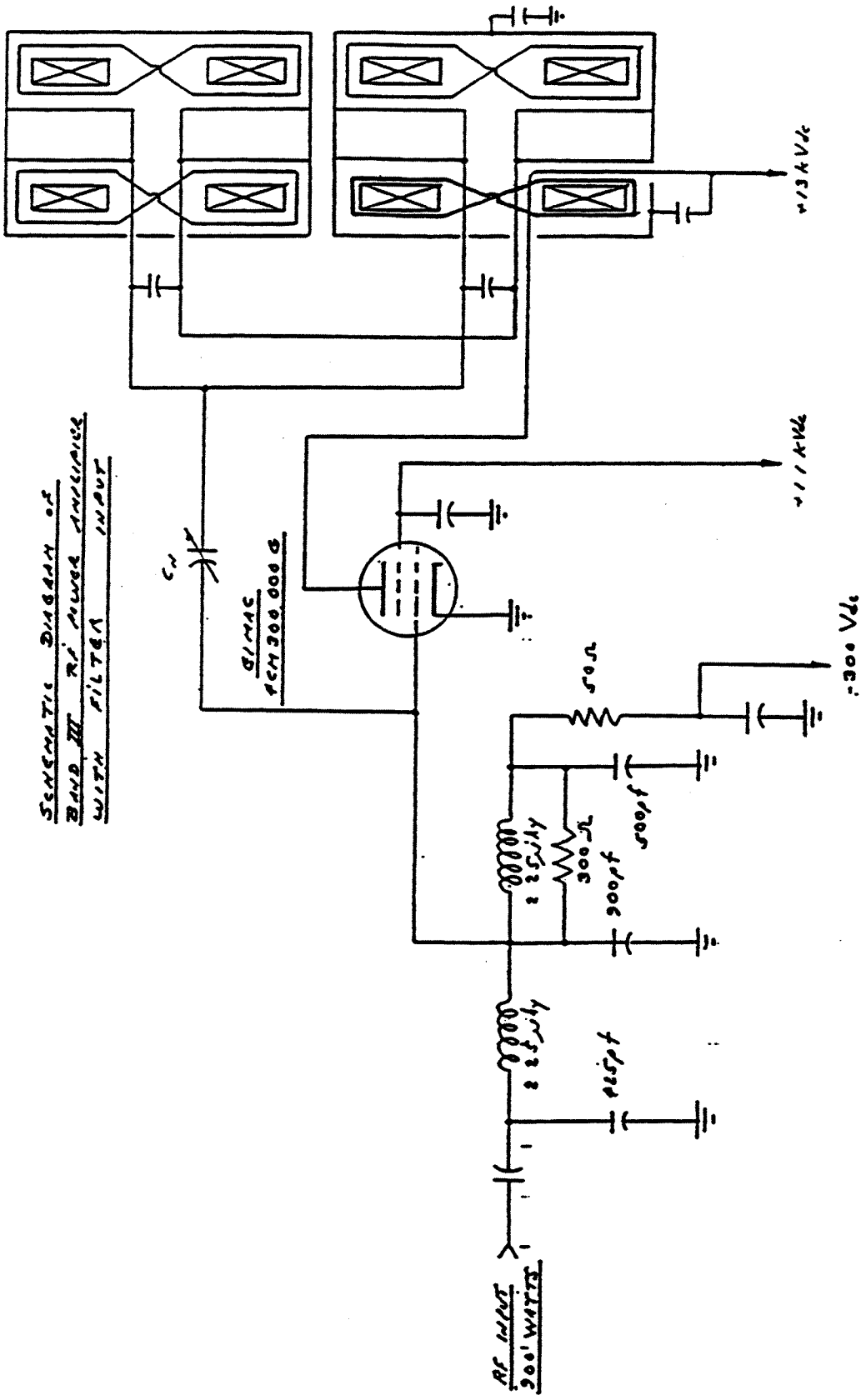

Figure 7 3 Schematic diagram of Band III rf connection

TABLE 7-2 RF System specification.

	Band I	Band II	Band III
Frequency Range (MHz)	0.1785-0.675	0.600-2.5	2.4-4.2
Number of Cavities	1	1	2
Number of Gaps	2 (1 station)	2 (1 station)	4 (2 stations)
Max. Tot. Accel. Volt.	17 (8.5 kV/gap)	17 (8.5 kV/gap)	90 kV (22.5 kV/gap)
Avg. Beam Power	< 250 W	300 W	70 kW/station
Number Ferrite Rings/Station	68	68	56
Size of Ferrites(cm)	50 × 23 × 2.5	50 × 23 × 2.5	50 × 25 × 2.68
Max. Ferrite Power	100 kW	100 kW	64 kW
Avg. Power Density in Ferrite	— (10% duty cycle)	— (30% duty cycle)	100 mW/cc (50% duty cycle)
Min. Capacitance/Gap	—	—	375 pf
Max. dc Bias Current	250 A	250 A	1000 A
Amplifier Type	Push-Pull,Gnd Cathode	Push-Pull,Gnd Cathode	Single-Ended,Gnd Cathode
Output Impedance	—	—	3 kΩ/station
Avail. Peak Power	<200 kW	<200 kW	200 kW/station

7 4. Control Loops

Each RF system will have an AGC loop and a cavity tuning loop. The H.I. systems will require a phase tracking loop since the location of the accelerating cavities cannot be located at an interval of ± 180 electrical degrees.

7.5. Low Level RF System

The low level RF (LLRF) system for the Booster has to fulfill several diverse requirements as the beam species and intensities span the spectrum from low intensity heavy-ions to maximum intensity protons. Special requirements will also be imposed when the Booster serves as an accumulator of polarized protons and when synchronized transfer to the AGS of accelerated beam takes place. A conceptual design is proposed that is very flexible, as to the type of closed-loop control that can be used, and has the potential to have very high sensitivity in the control signals to weak beams.

The basic scheme is to combine a digital frequency program, which provides the possibility of open-loop operation, with analog correction loops, which enter via a voltage controlled oscillator (VCO). Beam RF signals are heterodyned up to a fixed frequency where all processing takes place.

Circuit Description

The essential feature of the system is an up-conversion of the beam and cavity RF signals to a fixed intermediate frequency The phase of the beam with respect to the cavity voltage is measured with a phase detector operating at the intermediate frequency after a narrow band filter which extracts only the fundamental component. The narrow band filter takes out any dependence on the particular bunch shape. A digitally controlled synthesizer, driven off a Gauss Clock accumulator , provides the basic frequency program by outputing a frequency equal to the machine RF frequency plus the intermediate frequency The synthesizer output is mixed with the VCO, whose center frequency is the intermediate frequency If the control input to the VCO is kept at zero then the frequency of the RF system (signal sent to the cavities) is given completely by the synthesizer On the other hand, the control of the VCO can be used to vary the machine frequency in order to implement proportional control loops.

Figure 7-4 is a functional block diagram of the circuit. An intermediate frequency of 10 MHz was chosen as an illustrative example , in practice the choice of frequency would be dictated by commercially available components such narrow band filters and amplifiers. The synthesizer is then programmed to run between 10.2 and 14.1 MHz. The first mixer makes the sum and difference frequencies with the VCO, and a low-pass filter selects the difference frequency only This signal must be level adjusted and closed-loop stabilized then sent to the cavity power amplifier chain. The level program would be derived form the Gauss Clock or a real-time clock, or some combination of both.

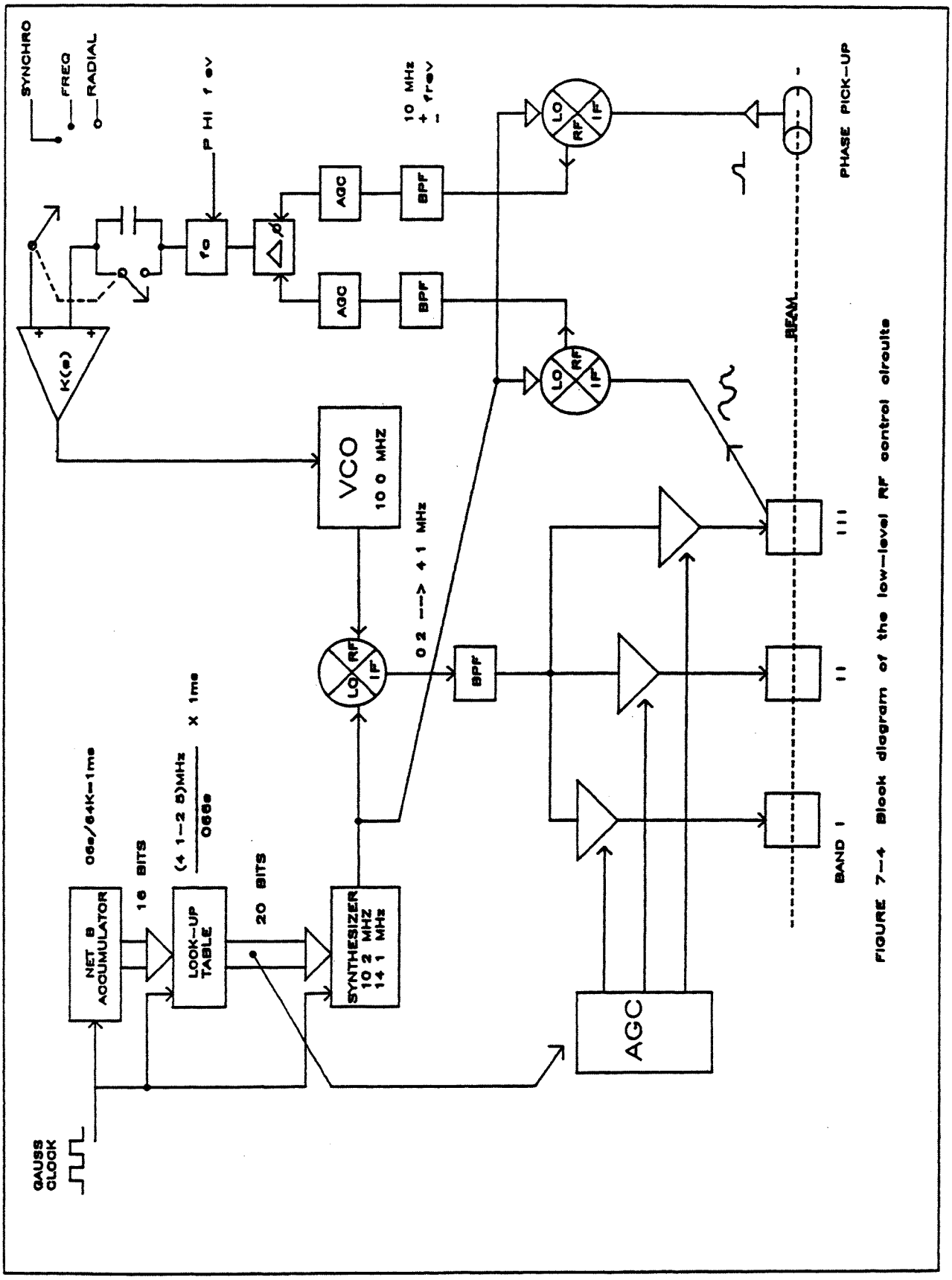

FIGURE 7-4 Block diagram of the low-level RF control circuits

CHAPTER 8. INSTRUMENTATION

8.1. Beam Instrumentation

The instrumentation for the Booster will be described in the following sections.

8.1.1. Booster Ring

8.1.1.1. Pick-Up Electrodes (48 units)

Beam position within the Ring will be monitored by an array of Pick-Up Electrodes (PUEs) at the 48 β_{max} locations (between the quads and sextupoles). The design will provide precision geometry and location, with the wide bandwidth needed for the large frequency swing, at low shunt impedance. The measurement parameters to be provided are:

Absolute accuracy	$\pm$ 0.5 mm
Precision	$\pm$ 0.1 mm
Range	$\pm$ 30 mm
Intensity (charges/pulse)	1×10^{10} to 1.5×10^{13}
Frequency range (protons)	2.5 — 4.5 MHz
(heavy ions)	0.2 — 4.5 MHz
Detector impedance	$< 5\ \Omega$
System bandwidth	0.05 — 30 MHz
Design S/N at min. beam	20 dB

Other design features include:

— At least 6 orbit measurements per cycle
— Capability to measure first turn
— Built-in calibration through the PUEs
— Pulse-to-Pulse gain switching
— Average orbit measurement (100 turns)
— All electrodes read on same cycle
— Built-in calibration through electrodes
— Detectors bakeable to 200 C
— Designed for 3×10^{-11} Torr vacuum
— No mechanical adjustments

A drawing of the prototype detector is shown in Fig. 8-1.

The electronics will be located within three meters of the detector to allow the low frequency response to be compensated. Complete ground isolation will be provided by optical coupling of all signals to the electronics. A block diagram of the circuitry is shown in Fig. 8-2.

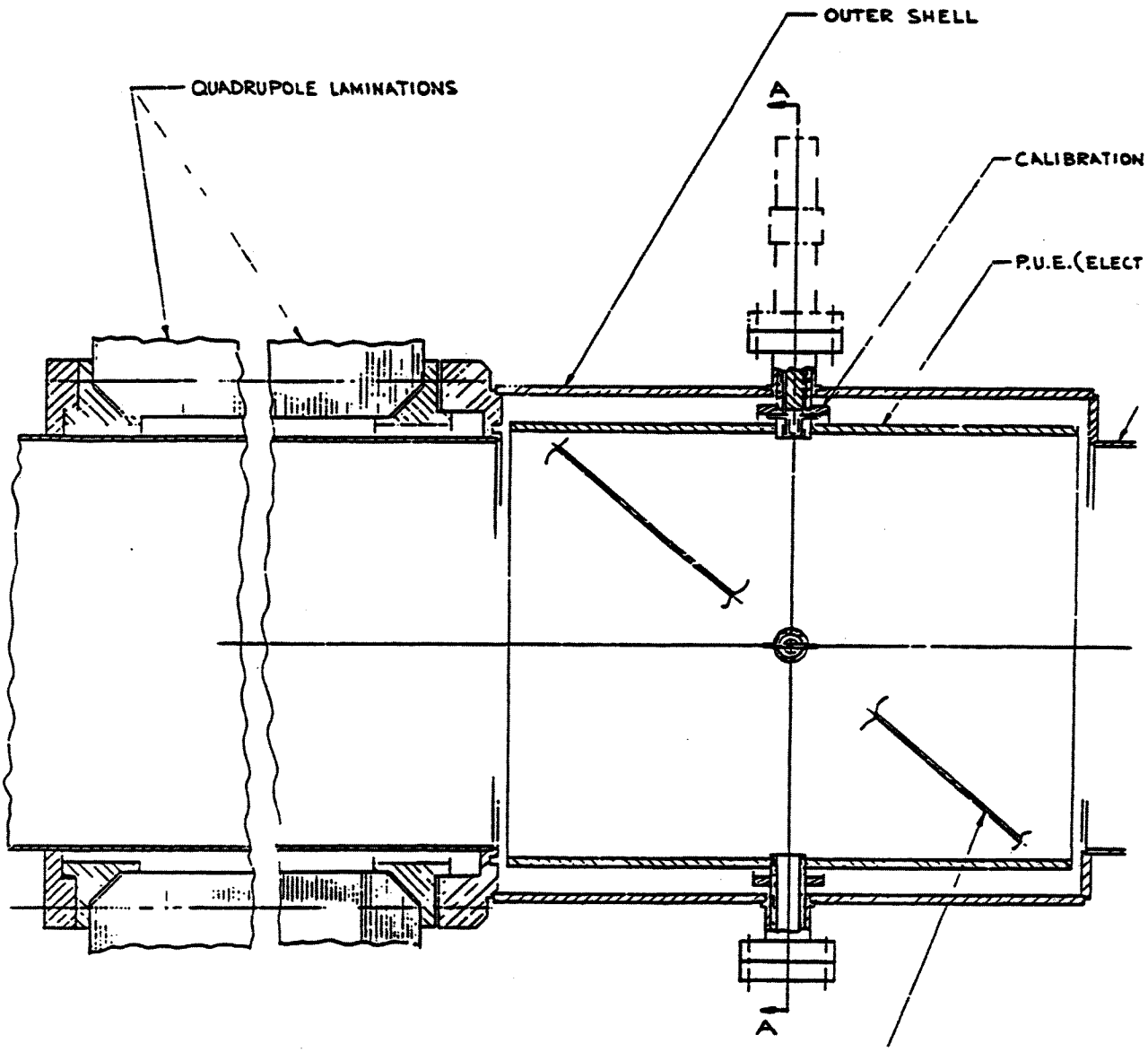

Figure 8-1. Prototype pick-up electrode.

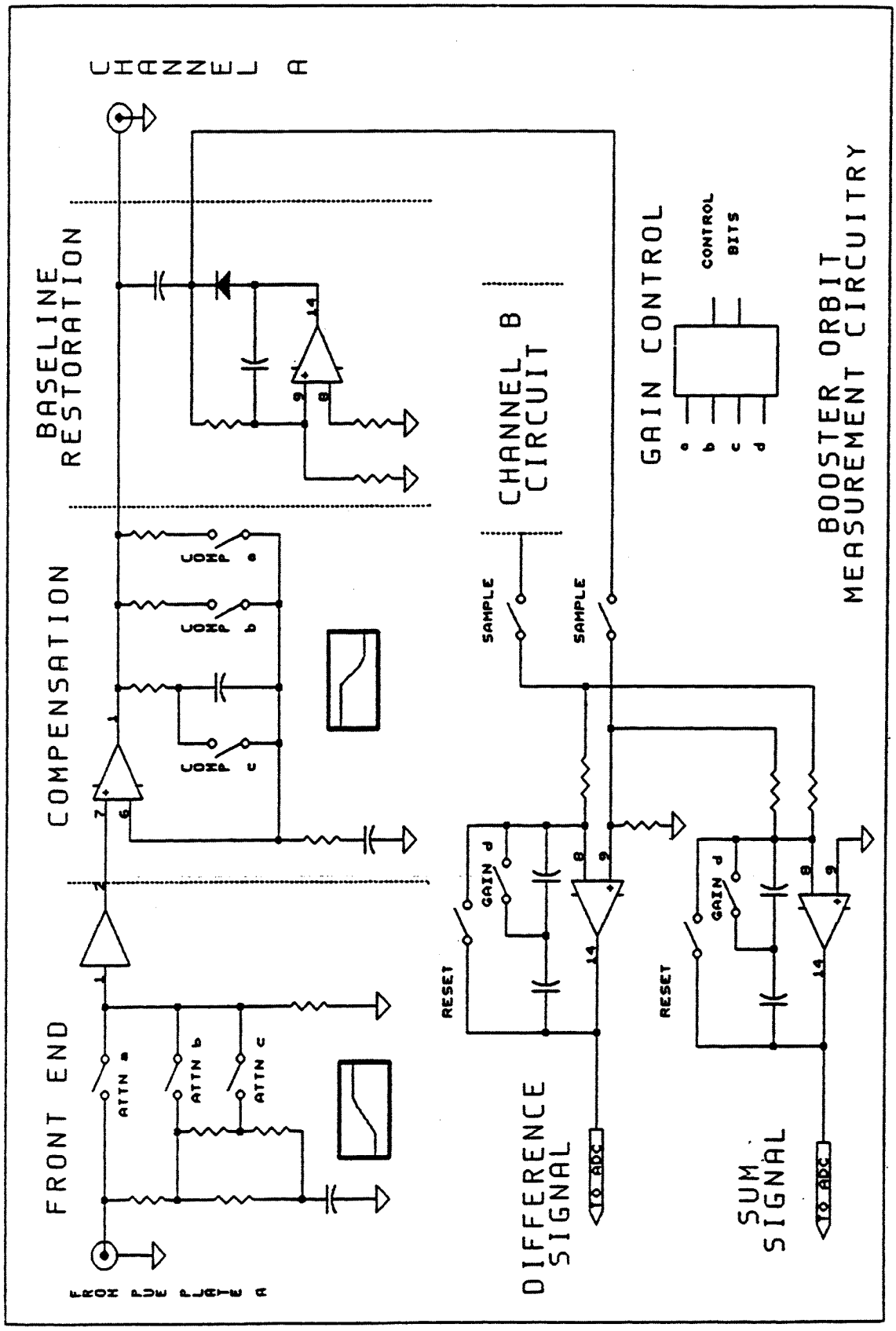

Figure 8 2 Block diagram of PUE electronics

Those functions required wideband bunch observation or dedicated signals, such as the tune meter, damper control, and RF phase and radius control, will receive signals from these same PUEs. The compensated bunch signals will be bridged after the buffer amplifier and transmitted from the tunnel via wideband fiber-optic analog transmission systems.

8.1.1.2. Wall Current Monitor

High frequency bunch density distribution information will be provided by a wall current monitor This unit, which observes the beam image current through a resistance bridging a gap in the beam pipe, will be similar to one in the AGS. Bunch timing may also be obtained from this unit. Bandwidth of the unit will range from a low frequency break at about 1 MHz to a high frequency limit of about 1 GHz. An analog fiber-optic transmission system may also be required for this signal for isolation. If so the high frequency breakpoint will be limited to about 100 MHz.

8.1.1.3. Beam Current Transformers (1 unit)

The intensity of the circulating beam will be measured by means of a beam transformer Because of the very wide intensity range and bandwidth requirements, more than one transformer will be used in this system. The fast rise-time required for injection studies ($< 1\ \mu s$) will be provided by a conventional magnetic-core type transformer However, its low frequency response is insufficient to monitor the polarized beam for the period of twenty injected pulses, so a dc-current transformer (DCCT) will be required also. The units will be designed to cover an intensity range of from 10^{10} to 10^{14} with at least 1% resolution at the low end and 0.1% at the high end. The transformers will meet the standard bakeout and vacuum requirements of other main ring components.

8.1.1.4. Profile Monitors (1 horiz., 1 vert.)

The transverse density distribution of the beam (profile) will be measured by collecting ionized residual gas molecules. Since the Booster vacuum is so high, micro-channel plates (MCP) must be used to enhance the signal to the multichannel collectors. Careful control of the plate gain and ion collection voltages will be required to increase the MCP lifetime with high intensity beams.

8.1.1.5. Tune Meter (1 per plane)

The tune of the Booster will be measured in a simple but elegant way The orbit perturbation of a kicked beam observed by a PUE will be digitized and analyzed using an FFT Triggering the digitization by the RF results in intentional aliasing, causing the spectrum to overlay itself. This produces an enhanced and isolated line at the fractional tune. This technique, developed by FNAL, was successfully used to measure the

tune of the low intensity polarized beam at the AGS.

Several designs for the kicker power supply are being studied, including an adaptation of the design used at CERN. The magnet will be a scaled down version of the other kickers in the Booster and for injection into the AGS.

Signals will be taken from the analog bunch outputs of one of the standard PUEs. It will be processed using a fast integrator and digitizer, gated by the RF The data will be analyzed by hardware/software in a processor on the LAN. To allow multiple tune measurements per Booster cycle, commercial boards with FFT processing times of 10 ms or less are being investigated. The controlled chromaticity of the Booster should allow sufficient ringing for a measurement to be within $\pm$ 0.001 tune units.

8.1.1.6. Damping System

Damping of coherent, transverse-coupled bunch instabilities will be accomplished by applying feedback of signals obtained from position-sensitive pickup electrodes to traveling-wave deflection electrodes after approximately a one turn time delay (see section 2.7 4).

The deflection electrodes will consist of four strip line electrodes of 0.5 m in length and 60 of arc each in width located in the C6 straight section near the pump-out port. The C7 horizontal and the C8 vertical position electrode outputs will be used in the feedback loop.

8.1.1.7 Radiation Monitors (32 locations)

The primary use of the radiation monitors is to detect the location of beam loss as an aid in set-up. An array of 32 extended ion chambers will monitor the radiation from the high intensity proton beam. This system will be similar to that in use at the AGS for many years.

A second system, 100 to 1000 times more sensitive, will be used to monitor the low intensity beams. It will also be sufficiently sensitive to provide a remote readout of the background activation for continuous Health Physics monitoring. The detector for this application has not been selected but will be the same as will be used in the AGS upgrade now in progress.

The signals from the detectors will go to integrators which will provide dose readings for selectable time periods to present at least ten readings per Booster pulse. The design will be similar to the one being developed for the AGS.

8.1.2. Injection Lines

8.1.2.1. Protons

8.1.2.1.1. Current Transformers (2 locations)

There will be two high intensity (100 μA to 100 mA) transformers to monitor the H^- beam and two low intensity (100 nA to 100 μA) for the polarized H^- beam. These will be the same as presently used in the HEBT line. Both are of the conventional tape-wound core, single coil type, with the low intensity unit being acoustically isolated and magnetically shielded. The risetime of the high intensity transformer will be less than 100 ns through the amplifier

8.1.2.1.2. Position Monitors (7 units)

Position monitors will be located at seven places in the line. These will be of the stripline coupler type tuned to the 201 MHz Linac frequency, similar to those developed at CERN. The sensitivity will be sufficient to observe a beam of less than 1 μA. The monitors will be located at the steering dipole locations, two per plane at the start and end of the line.

8.1.2.1.3. Profile Monitors (2 units)

Profile monitors will be located at two points in the line. These will be of the multiwire secondary emission type (HARPs) as used in the HITL line but designed for six-inch diameter pipe. The arrays will have 32 wires per plane at a pitch of about 1 mm. The units will be inserted and retracted pneumatically under computer control.

Gated electronics will allow time dependent profile data to be taken. Real time readout at the Booster cycle rate will be available through the analog multiplexer, independent of digitization requests. The ability to change gain between high and low intensity will be available on a pulse-to-pulse basis. The downstream profile monitor will be placed in a location suited to making a measurement of the emittance prior to injection into the Booster

8.1.2.1.4. Radiation Monitors (8 locations)

An array of radiation monitors will be installed along the beam line. These will be the same extended ion chambers used in the Booster Ring and the existing HEBT line. The eight detectors of the high intensity system will interface with the present Linac FBI circuit to inhibit the beam in case of high radiation. A second high sensitivity system of eight detectors will be installed to help tune the polarized beam losses. These will be the same as used in the Booster Ring.

8.1.2.2. Heavy Ions

8.1.2.2.1. Profile Monitors (7 units)

The profile monitors in the Heavy Ion Line will be the same as used in the HITL line and in the Proton Injection line. There will be seven units installed at bend or matching points. The electronics sensitivity differs from the Proton line since a very low intensity (1 - 100 nA) dc beam must also be measured.

8.1.2.2.2. Current Transformers (3 units)

There will be three low intensity beam transformers installed of the type used in the Proton Injection and HITL lines.

8.1.2.2.3. Faraday Cups (7 units)

Since the Tandem Van de Graaff will provide a dc trace beam of from 1 to 100 nA for tuning the line, the beam current will be measured using the same Faraday Cups and electronics used in the existing HITL line. These will share the same flange as the HARP profile monitors, but will have a separate pneumatic drive.

8.1.3. Ejection Line

8.1.3.1. Bumper Magnet Monitors -- Main Ring

8.1.3.2. Charge State Monitor at Stripper (1 unit)

A spectrometer magnet and multichannel pick-up will be used to monitor the charge state distribution. The detector will be the same HARP as used elsewhere in the beam lines.

8.1.3.3. Profile Monitors (5 units)

HARP profile monitors will be installed at five locations in the Ejection line. These will be in locations where beam matching is critical (e.g. stripper, injection) and in an array from which on-line emittance information can be extracted from the profiles without changing the transport settings and with only slight beam loss. The Charge State Monitor (sec. 8.1.3.2) also uses one of these devices.

8.1.3.4. Current Transformers (3 locations)

The high intensity and low intensity beam current transformers will be located at three locations in the Ejection line. Mechanically these will be similar to the units in the Injection line but with a six-inch clear diameter The electronics will also be different since the beam will be ejected in three bunches which will be too fast for the amplifiers.

Instead integrators will be used, making the output voltages related to total charge, which is more meaningful for the AGS injection.

8.1.3.5. Position Monitors (4 units)

Two horizontal and two vertical position monitors will be located in the downstream section of the line. These will be used to adjust adjacent steering dipoles to bring the beam on line with the AGS injection. The Booster Ring PUEs will be used as the detectors with electronics designed for the single-pass nature of the extracted beam.

8.1.3.6. Radiation Monitors (8 locations)

An array of eight high intensity and eight high sensitivity loss monitors will be installed along the Ejection line. These will be used to tune the extraction process to minimize beam loss, and provide background radiation surveys when the beam is off. The same detectors used in the other Booster radiation monitor systems will be used for this line.

CHAPTER 9. BOOSTER CONTROL SYSTEM

Introduction

The Booster Control System will be an extension of the new AGS Distributed Control System (AGSDCS). This system has been gradually replacing older controls for the AGS and has been applied to the control of heavy ion injection and acceleration and certain polarized proton controls. As with these previous projects, the control system will be improved and expanded in areas appropriate to the demands of this major new accelerator project.

9.1. Control System Central Facilities

9.1.1. Timing

The Booster timing system will function as part of an overall timing system designed to synchronize and trigger the multiple accelerators which form the AGS complex. This will be achieved by means of a new timing system introduced for the purpose and, to some extent, the Booster will serve as a guinea pig for the operation of this system. The global approach will be to treat the Booster as one among several accelerators in the AGS complex which interact to fill the need of a combined physics program, but which also may have physics or studies needs of their own.

Since the Booster will be the first application of this new system, the operation of the overall system is outlined here. When several accelerators are to act cooperatively it becomes necessary to decide how closely to couple these machines and to what extent one intends to support the CERN concept of "pulse to pulse modulation" For the AGS complex, a master timer or "supercycle" generator (SCG) will link our array of accelerators with the intent to have some number of flexible cycle options, such as is done at the PS/SPS, but not to support a general any cycle/any number of accelerators interaction. The SCG will be synchronized to the power line to help with the second order power line dependent effects we have already observed between the AGS and the LINAC. The rather coarse resolution of 1/60 second selected for the SCG is considered adequate for our needs, since dwell or "waste" periods will be used to achieve repetitive, synchronous super-cycles.

Each accelerator in the complex will be supported by a dedicated timing generator assigned to the TVDG, LINAC , BOOSTER, AGS and, eventually, RHIC respectively Cycling of each of these generators will be initiated by a signal from the SCG defining the type of cycle which is to occur. The dedicated generator produces the sequence of timing signals required by that accelerator for a particular cycle eg. a Booster cycle which accelerates protons and extracts them for injection into the AGS. These timing signals are defined to be "absolute" in the sense that they occur a prescribed number of clock ticks after the cycle start. All general purpose timing signals for the cycle will be produced in this way from real-time or gauss clocks. Where cascaded event timing is required, for example when a trigger is required some time after the occurrence of a gauss clock event, the absolute timing technique must be superseded. A limited capacity for

such events will be provided in each Timing Generator

Local timing is required in some circumstances where very high resolution or very close coupling with local hardware is necessary Standard modules with the necessary features will be provided for these applications.

As outlined above, the AGS complex timing system will consist of a hierarchy of timing generators constructed from a generic hardware module set. The specific generators associated with the Booster will be the SUPER CYCLE GENERATOR (SCG) which will serve to synchronize the various accelerators within the AGS complex to each other, and the BOOSTER TIMING GENERATOR (BTG) which will be dedicated to Booster requirements. The BTG consists of three parts, the Timing Clock Generator (TCG), Gauss Clock Generator (GCG), and the RF & BEAM signal Timing Generator (RFTG).

The heart of the SCG, TCG & GCG is something called a Booster Event Encoder and Transmitter; it along with a Signal distribution subsystem form our pulse distribution scheme.

These units turn computer generated codes and/or pulse generated signals into encoded timing streams. There are 256 input channels to an event encoder and thus there are 256 unique events. Each input channel is assigned an 8 bit code. When an event input is triggered, its 8 bit code is generated, encoded onto a 10 MHz clock train and transmitted in a serial format on a single trunk. Typical resolution of event timers is 1.5 μs. The 256 input channels to the event encoder are ordered and thus it is possible for a higher priority event to bump (delay) a lower priority event.

At receiving locations the trunk is tapped and the signal fed to a Booster Event Receiver and Decoder. This block will receive the 10 MHz encoded clock from a Booster event encoder and transmitter; it will decode the 8 bit event code transmitted and will provide a pulse on a specified output channel corresponding to the event code received. The module will detect the start bit to synchronize with incoming data and will also check parity on the incoming transmission as a means of transmission error detection. A parity failure will result in the transmission being ignored by the module. An independent device will report alarms for such failures.

A fiber-optic trunk will be used to transmit the 10 MHz event encoded clock over long distances between the centrally located encoder and transmitter and remote devices in need of timing. Taps on the the trunk will feed event decoders and will also extract the 10 MHz for local use.

9.1.1.1. The Supercycle Generator

The supercycle generator provides global synchronization between the accelerators. The SCG produces among other pulses a number of Booster arming or prepulse signals and a Booster start of cycle signal. All outputs are derived from multiples of the 60 Hz power line period and the SCG itself is synched to a specific power line phase. The nominal rep rate of the SCG is adjustable from 1 to 1.6×10^6 times 1/60 sec or from 16.7 ms to 72 hours. During this super cycle up to 256 action codes can be repeated with a resolution of 1/60 sec as often as necessary At any event time, up to 5 codes can be

generated separated in time by <2 μs. The number of events which may be specified is a readily expanded 2048.

SuperCycle Generator	
Parameter	Value
Count Range	2^{24}
Frequency	60 Hz
No. Events	2048
Codes/Event	5
Devices Required	1

9.1.1.2. The Booster Timing Generator

The Booster Timing Generator produces real-time clocks with a nominal 1 μs resolution. Its operation is similar to that of the SuperCycle Generator but it uses faster input triggers and a 1 MHz clock. Among the signals available from the BTG are the following clock trains: 10 MHz derived from a 10 MHz master clock and synchronized with TCG outputs (this train may be used for local generation of any needed real time clock); a 10 KHz encoded train; a 1 KHz encoded train.

To meet the predictability needs of Booster timing, the BTG is restricted to a single code from the 256 Booster codes at each event time. Because the transmission time for a single code is slightly more than 1 μs, each event occupies two adjacent time slots so that events must be spaced at 2 μs intervals but this is of little significance and does not impair the 1 μs settability The absolute timing range of the BTG is 16.8 S and an easily expanded 2K events will be provided.

Booster Time Generator	
Parameter	Value
Count Range	2^{24}
Frequency	1 MHz
No. Events	2048
Codes/Event	1
Devices Required	1

9.1.1.3. The Booster Gauss Clock Generator

The Gauss Clock Generator produces magnetic field based events with a nominal resolution of one field clock tick, typically 0.1 gauss. It is similar to the SCG and BTG but has up/down input clock trains so that digital summation produces a resultant proportional to the instantaneous magnetic field value. This will allow triggering of accelerator functions at particular magnetic field values as distinct from particular clock times. The magnetic field range is 1.6 MG at this resolution, an artifact of the 24 bit counters used to meet other requirements. A single code is produced at each event.

Booster Gauss Clock Generator	
Parameter	Value
Count Range	2^{24}
Frequency (up or down)	1 MHz
No. Events	2048
Codes/Event	1
Devices Required	1

9.1.1.4. The RF and BEAM Timing Generator

The RF and Beam timing generator produces RF and PUE Clocks and Signals armed by the other generators and clocked by RF zero crossing, phase comparators or beam revolutions. Encoding techniques will not be used here.

9.1.1.4.1. Cascading Timing

Output signals from any of the generators may be used to arm or fire any other generator section via a hardware patch. Since such patching corresponds to the physical configuration of the accelerator, changes will be infrequent and significant. Although software patching would offer flexibility and ease of monitoring, the centralized nature of the Booster's timing makes hardware patching relatively painless and grants the peace of mind offered by a physical connection.

9.1.1.4.2. Local Timing

As discussed in the above, some equipment requires local timing for logical or practical reasons. In most cases, the local timing will be initiated by a trigger from an event receiver Real-time, Gauss Clock or RF counts can then be the source for "autodet" type timers. A multi-channel timing module will be provided. The general purpose timer will support clock rates to 5 MHz and a 16-bit range. Higher resolution applications will be supported by commercial devices or locally designed equipment to be developed.

Local Timing Generators	
Parameter	Value
Frequency	5 MHz
Channels	20
Range	16 bit
Devices Required	10

9.1.1.5. Signal Distribution

The output of the SCG will be fed to each of the dedicated timing generators via suitable cables carrying the encoded pulse train. Event decoders at the receive end produce signals which synchronize and clock generators such as the BTG. Signals are carried from the BTG by co-axial lines dedicated to the TCG and GCG serial trains and by

individual lines carrying the RFTG unencoded pulses. Stations and Device Controllers requiring timing signals will be equipped with event receivers and decoders for the serial trains and buffers for the dedicated lines.

9.1.1.6. Event/Line Monitor

At least one Line Monitor will be installed on each of the TCG and GCG devices. The purpose of these devices is to identify and record each of the events transmitted and to verify correct encoding and reception for each event. They will serve as general diagnostic and monitoring devices for the timing system. Several possibilities for operating mode, such as "learn mode", "absolute mode" etc. have been considered. A selection will be made based on development experience of likely failure modes. At a minimum, the devices will record for each event the identity of the time or gauss event, errors in the reception and the time of reception.

Event/Line Monitor	
Parameter	Value
Count Range	2^{24}
Frequency	10 MHz
No. Events	2048
Codes/Event	1
Devices Required	2

9.1.1.7 Event Receiver/Decoder

Event Receiver/Decoders will be required at each timing generator, each station and most device controllers. The receiver will demodulate the signal to recover the clock and data. The decoder will recognize up to 8 encoded events and produce external signals synchronized to those events. Separate receiver/decoders will be required for time and gauss clock lines. A suitably compact design can be produced by use of a custom integrated circuit developed by FNAL.

Event Receiver/Decoders	
Parameter	Value
Modulation	Base-band
Clock	10MHz
Data bits	8 + parity
Events Recognized	8
Devices Required	30

9.1.1.8. Computer Interface

To provide computer control of the various event generators they interface to the computer network as one or more DEVICE CONTROLLERS. An application program will permit operators to set up supercycles and Booster cycles with help in defining suitable sequences and protection from invalid configurations. An analysis capability to compute duty cycles, power dissipation and unused time within the cycle will be provided. Some monitoring to detect faults or missing signals will be performed. Simulation of some signals, notably the gauss clock, will be necessary to allow testing of accelerator equipment when the Booster is not operating. Automatic switching to the backup clock is desirable with generation of an alarm to alert the operator LINE MONITORS installed at the remote ends of the distribution network will verify that the intended codes are transmitted appropriately and report discrepancies.

Device Controllers	
Controller	Devices
Super Cycle	SCG
Booster Cycle	BTG
Injection/Extraction	RF&B TG

9.1.1.9. Linac, Booster and AGS Synchronization

As an example of use of the timing system we will describe the sequence of events to synchronize the Linac Booster and AGS for proton injection into the AGS. The Linac may be supplying beam to other users under control of the SCG. The Linac is provided with a train of timing pulses by the SCG, one for each linac cycle, typically every eight power line cycles, i.e. every 7.5 Hz. Similarly, the Booster gets a Pre-Pulse (BPP) from the SCG at 7.5 Hz. When the SCG is adjusted to support both the LINAC and the BOOSTER its coded stream of event pulses will contain BPP pulses in addition to prepulses for BLIP and REF The Linac Timing Generator will schedule the Linac equipment and Booster injection will be triggered by a Booster Gauss Clock event. Meanwhile, the AGS will have received a code to begin it to front porch before the Booster reaches full energy Booster extraction will be triggered from another Booster Gauss Clock event while slower extraction equipment is fired by time codes. Fast extraction kickers will be timed from RF signals to cause extraction, transfer and AGS injection. The Linac and Booster will cycle 3 more times at the 7.5 Hz rate. After this, the AGS Timing Generator will schedule the AGS acceleration cycle and the Linac reverts to BLIP and REF operation. If the AGS period is not a multiple of 8/60ths second, a few 1/60th-second slots will be wasted to bring the Linac and AGS back into synchronism for the next AGS cycle. Similarly, some Booster time may be wasted if, between AGS injection cycles, other Booster cycles are required which do not exactly fit the AGS cycle.

Extension of this scenario to include RHIC injection is straightforward. Stored beam time in RHIC would be asynchronous and operator intervention would initiate a

new injection cycle.

9.1.2. Analog Signal Distribution

A general purpose computer controlled analog multiplexer system is required to switch analog signals to oscilloscopes in the consoles. Most of this requirement will be satisfied with a fiber-optic based digital switching system with a nominal effective bandwidth of 100kHz per channel. The system will support the distribution of approximately 500 non-instrumentation analog signals from five origination areas to all the accessible Booster equipment areas.

In addition to the digital system, a reed-relay based sub-system will distribute up to 16 signals, two at a time, over pairs of co-axial cables from each of five buildings to the main control room of the AGS. The nominal bandwidth of these signals will be 350 kHz.

Five co-axial cables will be installed between each of buildings 914 and 930 and the AGS MCR to support the transmission of high-bandwidth signals requiring dedicated cables.

All the above facilities will be available to support Booster instrumentation. Needs beyond the capabilities described are not part of the central system and must be provided by the those responsible for the application.

9.1.2.1. Analog Multiplexer Devices

9.1.2.1.1. 16-Bit Data

Data from 16-bit resolution devices will be transmitted over a digital time-multiplexed data path as streamed data. Each data channel will require less than 4μS for transmission for a cumulative data rate of 250 kilo-samples per second per signal path.

9.1.2.1.2. 12-Bit Data

Data from 12-bit resolution devices will be transmitted over a digital time-multiplexed data path as streamed data. Each data channel will require less than 1.6μS for transmission for a cumulative data rate of 625 kilo-samples per second per signal path.

9.1.2.1.3. Analog Data

The analog multiplexing device will be the CYTEC LX128 dry reed relay multiplexer developed for use in the HITL. This modular device will be configured as a 16×2 multiplexer in this application. The basic switch permits bandwidth to 10 MHz. To isolate the switches from cable charge and to provide gain and bandwidth control, the signals will be buffered by line receivers before the switch.

The following tables illustrate the multiplexers to be installed:

Analog Multiplexers (Digitized Type)			
Location	Number of signals	Number of multiplexers	Bandwidth
Bldg. 911A	32	2	50 kHz
Bldg. 914	128	8	5 kHz
Bldg. 930A	256	16	5 kHz

Analog Multiplexers (Relay Type)			
Location	Number of signals	Number of multiplexers	Bandwidth
Bldg 911A	16	1	100+ kHz
Bldg 914	16	1	100+ kHz
Bldg 930A	16	1	100+ kHz
Bldg 930A	16	1	100+ kHz
Bldg L18	16	1	100+ kHz

Analog Signals (Direct Drive)			
Location	Number of signals	Number of multiplexers	Bandwidth
Bldg 911A	receive 10	Use existing AGS	5 MHz
Bldg 914	send 5		5 MHz
Bldg 930A	0		
Bldg 930A	send 5		5 MHz
Bldg L18	0		

9.1.2.2. Device Controllers

Each multiplexer will be operated via a suitably interfaced device controller The multiplexer control function will share the device controller assigned to access security in buildings 911A, 914 and 930A. (The devices in 930 will be supported from 930A) An additional device controller will be required in building L18. The hardware and coding of these device controllers will follow the design developed for the HITL project.

9.1.2.3. Line Receivers

As mentioned above, line receivers are required between signal cables and the multiplexer switches. A design developed for HITL has proved satisfactory and will be used in the Booster The specifications are given in the following table:

Line Receivers	
Parameter	Value
Input	Differential
Bandwidth	0-350 KHz
CMRR	-60 dB
Gain	0.95 - 2.5 adjustable

9.1.2.4. Multiplexer Signal Distribution

The locations of the various multiplexers are specified above. Most signals are carried in digitized form via a part of the fiber-optic control system trunk. Two fibers with a bandwidth of 25 MHz each are assigned to each building providing a throughput of 500 kilo-samples per second to 1.25 Mega-samples per second, depending on resolution. Any signal can be delivered to any of the five areas.

Each relay multiplexer provides two differential outputs which are cabled back to the Main Control Room. Central multiplexers in the MCR allow selection of any four signals for oscilloscope viewing.

9.1.3. Consoles

Plans for the redesigned AGS Main Control Room call for four consoles in the extended control room. These consoles will be anonymous in that any area of the accelerator complex can be addressed from any console. For reasons of convenience and habit it becomes conventional to conduct certain operations at specific consoles and it is expected that one console will normally be assigned to the Booster With the coming of age of the general purpose workstation, the principal interactive tool for communication with the accelerator will be the APOLLO workstation with its multi-windowed screen, mouse, keyboard, etc. Use of the APOLLO is appropriate to discretionary activities in operations and studies of the accelerator will utilize its facilities. The more complex and interactive operator-invoked monitoring functions will also be performed at the APOLLO station. General purpose display and interaction techniques are being developed and will be tailored to the Booster by suitable file and data-base entries. In addition to these discretionary activities, other routine operations are necessary to indicate the state of the various accelerator sub-systems, to switch analog signals to the display oscilloscopes and to alarm when parameters stray beyond allowed ranges. A second APOLLO processor will be assigned to support these functions and suitable display screens will be standardly allocated.

In addition to the MCR facilities, there will be a standard console in the Linac control room which will be available for Booster control and, during installation and commissioning, there will be single-processor mini-consoles located in buildings 930A and 914.

For field testing of accelerator equipment, any Apollo Workstation can serve as a console in that it can be a source of commands to devices and it can accept messages from stations. All the AGSDCS operation programs will run from any Apollo Workstation so that a Workstation presents a familiar interface. The Workstation is easy to move and can be placed close to equipment being tested.

9.1.3.1. Workstation

The principal operator access to the accelerator will be via a workstation. The main console workstation will be a color APOLLO equipped with a keyboard, mouse, trackball, etc. A graphical and menu driven interface will provide the operator with access to accelerator data and allow the initiation of various modes of Booster operation. Standardized procedures in programming and display will be developed so that functions present a familiar "look and feel" with common commands between disparate operations. Most requests to examine some feature of the operation will result in graphical output, avoiding screenfuls of hard to evaluate numerical data. Specific numeric parameters may be displayed on request or by default where the precision requires digital values but "management by exception" techniques should make it rare for the operator to review tables of numeric data. Similarly, numeric data entries will be by random access to the variables carefully avoiding redundant data entries.

9.1.3.2. Auxiliary Displays

A number of auxiliary displays will be provided to show the status of systems independently of the activity on the main workstation. These displays, which may be alphanumeric or graphical, will usually be assigned to major subsystems such as injection, main magnets, radio frequency and extraction. Interaction with these displays will be via labelable switches and a pointing device, probably a track ball. The use of these displays is more standardized and hence less flexible than the workstation display They therefore supplement and complement the workstation operations rather than duplicating them.

9.1.3.3. Alarm Screen

A dedicated alphanumeric screen at each main console displays a subset of the alarms reported by the surveillance programs.

9.1.3.4. Spreadsheet Control

An alphanumeric screen with switches and a pointing facility will provide for low level control actions on individual device parameters. Use of this mode should be confined to systems for which custom code has not been generated and for diagnostic and debug activities.

9.1.4. Network Hardware

The Apollo HOST computers, embedded in consoles or elsewhere, will be interconnected via Apollo's "Domain token ring" This ring will be a logical extension of the existing AGS and TVDG console ring. Fiber optic cables will be employed to provide ground isolation between widely separated computers. The network interface units (cards) will be standard Apollo products.

The STATION computers will also be interconnected via another token ring. In fact, since the stations are also Apollo processors, it will be possible to combine HOST and STATION functions in the same physical computer Again the network interface units and software drivers will be the manufacturer's standard products.

The HOST ring and the STATION network will be interconnected at two points so that a single point failure cannot break data flow

9.1.4.1. Process Highways

STATIONS will interconnect to DEVICE CONTROLLERS via the IEEE 488 bus as the process highway This choice is made so that existing AGS Device Controller designs may be used for the Booster project with minimum rework. If applications which cannot be supported over IEEE 488 are encountered, ETHERNET interfaces (IEEE 802.3) represent a viable alternate.

Many DEVICE CONTROLLERs will interconnect to accelerator devices via an AGS developed specialized serial process bus called DATACON. This bus will serve to operate most equipment since it offers long distance transmission, transformer isolation and a 1 Mbit/s data rate. There are some applications for which performance requirements exceed the capability of DATACON links. For the PUE system, where excellent RF isolation is desired, an optically coupled version of DATACON will be developed. This link will incidentally offer a higher data rate and a broadcast address capability It may find other applications as device hardware is developed. It appears inevitable that the ubiquitous RS-232C will be used for some commercial device interfaces.

9.1.5. Booster Safety and Security

9.1.5.1. System Scope and Implementation

- The interlock system shall consist of 24V d.c. control relays, 4DPDT, powered by a 24V D C. power supply with battery backup.
- The system shall interlock and monitor the following:
  1 Tunnel lights
  2 Gates
  3 Magnetic power supplies
  4 Crash buttons
  5 Beam stops
  6 Loss radiation monitors
  7 Chipmunk radiation monitors— personnel

8 Vacuum valves (interlock only)
9 Rate-of-temperature-rise detectors
10 Linac status

- Relays shall be housed in the 2 ea 72″ high racks located in in building 930A.
- All interlocks shall have a backup to provide redundancy
- Lights in the tunnel shall be dimmed when the booster is in operation.
- The phone system shall be distributed throughout the booster with direct connection to the main control room.
- The security system shall rely on relays and switches hardwired together to form an integral system. The computer shall serve a monitor only function.
- The safety and security controller shall monitor relay contacts and, through the Domain network, deliver status information to the Booster control console.

9.1.5.2. Equipment Distribution

- All safety and security equipment shall be located in the building 930A. Safety and security monitors shall be mounted in the control room. 2 ea 72″ high racks will be located in the LINAC house.

9.1.5.3. System Cable Distribution

- All cables in the tunnel shall be fabricated from a low smoke, radiation resistant composition (FREP-CPE) or equivalent cable.
- No Teflon sheathed wire or cable shall be used in the booster tunnel.
- The relays shall be mounted in 72″ racks in the LINAC house. A mounting plate will be provided for this purpose.
- Cables from the tunnel will terminate in a terminal box mounted in building 930A. Cables will run from this box to the appropriate part of the AGS interlock system.
- Outputs from the relay rack to the main control room shall terminate in a terminal box mounted on the LINAC house wall. Cables will run from this box to the main control room.
- Cables from the tunnel devices will terminate in 4 wall boxes mounted inside the tunnels. Two will be mounted inside the Booster One will be mounted in the HITL transfer line. One will be mounted so as to service the LINAC injection line and the AGS injection line.

9.1.5.4. Device Controllers

The computer control system will interact with the safety and security system in a monitoring sense only with status information displayed in the main control room and available to operator consoles via the Domain network. The DEVICE CONTROLLER will interface to the security system through opto-isolators connected to dry reed

contacts located in the LINAC house relay racks. A scanning algorithm in the DEVICE CONTROLLER will report changes of state to the STATION via an IEEE 488 link, thus making the data available through the DOMAIN LAN to consoles.

9.2. Booster Control Software

9.2.1. User Interface

9.2.1.1. Introduction

The design of the user interface for the Booster project must take into consideration the different classes of people who will use the system. There are three such classes: technicians and engineers, accelerator operators, and accelerator physicists.

Technicians and engineers are the people who test and commission the subsystems which comprise the Booster Their view of the control system is more focused than the others, and single device control with status readbacks and monitoring is of primary interest. With this type of control, elementary on line testing is easy and the transition from the lab to the field and then to an integrated part of the machine is, in theory, a smooth operation.

Accelerator operators are concerned with running the machines. Hence, their view is a more global one. Operator programs should allow easy startups, ease of operation, and the reporting of post-mortem information for the use of experts later(1). These guidelines ensure optimum run time of the machine with easy fault diagnosis.

The accelerator physicist's view of the machine is performance oriented. High level control programs enable the physicist to fine tune the machine without being concerned with low level device controlling. It should also be easy for the physicist to archive and restore parameters reliably, and plot interesting data and produce hard copy easily The tuning of a machine should not be constrained by the capabilities of the software.

By keeping these views in mind, a core of tools for booster control can be designed and implemented which will satisfy a wide range of users and provide a solid foundation on which to build future developments.

9.2.1.2. Menus

Menu tools provide a uniform medium for control programs to interact with all classes of users at a workstation. The menu package must be well documented and made available to all programmers to ensure that programs present a consistent and familiar "look and feel" Commands and options must be standardized over applications so that users encounter a minimum of difficulty in working with new or unfamiliar programs.

Some types of menu tools available are:

- general menu tools — a means of listing items from which the user will choose.

- pop-up menus — for such things as confirming sensitive items or text input.
- valuators — standard tools for numerical input, for example, pictorial representation with the minimum and maximum allowable values of a controlled variable at either end of a scrollbar, and the current value based on the position of the cursor within that scrollbar

9.2.1.3. Spreadsheet Programs

A spreadsheet style program for controlling simple logical devices and parameters is provided for single device control and monitoring.

Device lists are provided in a logical tree structure for those who are not machine proficient. However, an alternate means of selecting device lists is provided for the more familiar user who has a better idea of what he/she wishes to view or test. This form of random access avoids tediously repetitive tree scanning when accessing machine areas.

Two versions of the spreadsheet are available to users:

- control room version —
  This version runs in the control room on a dedicated screen to free the workstation for other programs. Input to this program is via trackball and input panel.
- local version —
  This is a portable version of the spreadsheet which runs on any remote node. The main use for this would be to be able to run the spreadsheet locally at the device controllers. This enables the user interested in debugging hardware to test that hardware locally as viewed through the software. This is much nearer to operation than the lab testing stage in that the devices are viewed on line through the network and eliminates inconsistencies between design and operation before exposure to the user

  Input to this program is via cursor control through the keyboard and the mouse selecting device.

The spreadsheet program operates at the elementary device level appropriate to the interests of engineers and technicians debugging or maintaining hardware. With the development of higher level interactive graphical control, the relevance of the spreadsheet to the control room will decrease. However it will always serve an essential purpose in verifying the accuracy of more complex procedures.

9.2.1.4. Graphics

Graphics provide a visually appealing and more intuitive view of accelerator systems than conventional spreadsheet programs. There are commercial graphics packages available which can be used as a basis for providing tools to both novice and expert users in the accelerator controls environment. A package will be acquired to support the common graphic applications such as bar charts, x-y plots, histograms, etc.

9.2.1.4.1. Controls-oriented graphics

Graphics provide a means of viewing complex process control systems in a more meaningful manner than looking at a list of devices. For instance, in the case of COMFORT (Control of Machine Functions OR Transport Systems)(3), a graphic interface displays the current trajectory of the beam with beam elements listed below As elements are selected and changed, a plot can be overlayed to show the predicted corrected trajectory or the differences between actual and corrected trajectories. Orbit correction programs can make use of similar facilities and, indeed, injection displays can usefully graft transport displays onto orbit data. Another application is a system in use at Fermilab where a graphics monitor displays a live schematic of an accelerator system providing static symbols showing components and dynamic symbols displaying real time data(2). Although the first application interacts with a "geographical" view of accelerator components and the latter with a "schematic" of the controlled system, there appears to be no reason why the applications cannot be accomplished with common software. The common need is for a graphics description language coupled to real accelerator parameters via the machine data base. This has already been accomplished in the system of reference(2) and others.

The design of these control-displays requires care and inspiration with much input from accelerator physicists who will make the most demanding use of their features. Reference(2) mentions the use of artists in the design of comprehensible displays and also cautions that the graphic displays can place much greater demands on data acquisition procedures than spreadsheets. It may be concluded that the graphic displays must be integrated into an overall system strategy consistent with all system limitations.

(1) F Beck and M. Gormley, "Computer Control of Large Accelerators", Design Concepts and Methods, Fermilab-Conf-84/43, May 1984

(2) Glenn Mayer, Stephen Beck, Ralph Pasquinelli, "Control of Stochastic Cooling & RF Systems Using Interactive Graphics", Fermi National Accelerator Laboratory, Particle Accelerator Conference, Wash, D C., 1987

(3) M. Lee, S. Clearwater, E. Theil, V Jacobsen, and V Paxson, "Modern Approaches to Accelerator Simulation and On-line Control", Stanford Linear Accelerator, Los Alamos National Laboratory, and the Lawrence Berkeley Laboratory, Particle Accelerator Conference, Wash, D C., 1987

9.2.2. Booster Alarms

9.2.2.1. Overview

Faults are reported by exception in the AGSDCS for both hardware and software alarms. The AGSDCS alarm system is currently being extended in a manner which will satisfy the needs of the Booster An alarm will be generated whenever the malfunction of an alarmable system component is detected. Alarmable system components include devices, device controllers, stations, hosts, network components, and server programs. Conditions in a system component that can generate an alarm are maintained in that components static database. A shared memory copy of this database exists in stations

and hosts. Operators will be given the abilitv to dvnamically alter this shared memory copy, to mask out alarmable conditions, enable others, etc. Alarms will be categorized and color coded by severity level. A method will exist to query the system for outstanding alarms.

9.2.2.2. Alarmable System Components

Alarmable system components will be organized in a hierarchical manner At the highest level, one must ensure that the Alarm Receiver Server and the host on which it runs have not themselves faulted. Fault recovery is also reported.

Watchdog programs which execute in stations and hosts will have the responsibility for generating alarms. All alarms will be sent to the Alarm Receiver Server

- The Watch Task in the station detects and sends alarms whenever a device or device controller has faulted.
- A Network Monitor Program running in one of the hosts will poll the network and generate an alarm whenever a station, host, or network component does not respond.
- A Node Master Program running in a server node will generate an alarm whenever a server program faults.
- Watchdog programs will report faults determined by comparing computed beam performance parameters to prescribed limits.

When a primary system component alarms, secondary system components also alarm, and so on. It is planned that this cascading effect will be remedied by adding some intelligence about component dependencies into the Watchdog programs and/or the Alarm Receiver Server

9.2.2.3. Static Database Alarm Data

Alarmable conditions for system components are maintained in the offline database. From this offline database, a live database is generated and distributed among stations and hosts using a "need to know" principle, i.e. stations need only know about the devices they will be monitoring and controlling, the Node Master Program need only know about the server programs it is watching, etc.

9.2.2.4. Dynamic Database Alarm Data

Operations staff will be able to alter the dynamic database pertaining to alarms. For example, the watch mask for a status field in a device can be toggled off, the tolerance for a setpoint can be altered, etc. To allow this operation to be rapid, these parameters have been made "live" data. A log of transactions will allow the static data base to be updated appropriately

9.2.2.5. The Alarm Display

Alarms will appear on a dedicated display at each console. They will be color coded by severity with those which require the more immediate attention appearing at the top of the list. Operators will be able to interact via a menu to list deferred alarms, erase alarms, undefer alarms, etc.

9.2.2.6. Alarm Logging

All alarms will be logged with a time stamp so that records of faults may be retrieved for analysis.

9.2.2.7 Queries

Due to the inherent difficulties of obtaining information in a distributed system, some mechanism will exist to query the stations and server programs, to obtain a "current" snapshot of those system components which are in a state of alarm.

9.2.3. Archiving of Booster Devices

9.2.3.1. Overview

Archiving is a methodology for saving the setpoints and commands of controllable devices with the intent of restoring those values to the devices at a later time. As implemented in the AGSDCS, controllable devices include simple devices which have but one setpoint and complex devices like function generators with many setpoints. What is actually archived is a collection of device lists. The accelerator can be modeled as a tree structure with the major subsystems represented as branches of this tree. The lowest branches of this tree, the leaves, will contain the device lists. In this model, the device lists appear as static entities. The management of these lists allows the organization of the accelerator into sub-systems for archival purposes.

9.2.3.2. Header Information

Every Archive will contain header information such as the date, species, etc. Some of this information will be read from a configuration file which will be kept up to date. Operators will also be prompted to enter pertinent comments about the contents and reason for the archive.

9.2.3.3. Synchronous and Asynchronous Archives

At some frequency (e.g. every eight hours), a program will awaken and archive those components of the accelerator required for restorations. This will insure that the restorable state of the machine is preserved within some minimum window of time. This special archive will be called the "CURRENT ARCHIVE" The previous one or two CURRENT ARCHIVES will also be saved. Archives will also be created by operator

request. These archives will be known as "NAMED ARCHIVES" They will be named and created by the operator utilizing the tree model.

9.2.3.4. Restoring Archives

The state of some portion of the accelerator can be restored from an archive created at the same or any higher level of the tree structure. When archives created at a particular branch of the accelerator tree model are restored at any lower branch, all devices in device lists in leaves below the branch will be restored.

9.2.3.5. Performance and Reliability

A reliable combination of hardware and software is required to implement an effective archival system. However, some procedure for handling the existence of unresponsive or errored devices will be included to avoid major omissions due to relatively minor problems. The reliable communication links in the Booster control architecture will all but eliminate communications as a source of errors. The use of powerful APOLLO processors with large virtual memory buffers (16 Megabytes) and the ability to cache reports in both large real memory (1-2 Megabytes) and ample disk space will allow extensive restore operations to be carried out at high speed.

9.2.4. Accelerator Programs

9.2.4.1. Accelerator Modeling

We consider first the Booster-Controls interaction requirements in terms of the three areas the beam passes through: (a) injection, (b) acceleration and (c) extraction and matching to the AGS.

Injection from either the LINAC or the transfer line is fairly conventional.

Standard accelerator programs, which in BNL usage include SYNCH, MAD, etc., are required for machine studies. A standard lattice input needs to be part of any data base so that all modeling programs compute the same machine; the ability to transfer results between such programs is also a requirement. During operation, since the basic machine lattice remains unchanged, a set of outputs (for a "bare" machine) from these programs should be available for use in any "perturbation" treatment. The basic requirements here are to adjust the machine tunes (horizontal and vertical), or rather to maintain their required separation while avoiding the customary resonances.

To begin with, this modeling-operations interaction should not be a "closed loop" procedure; instead, these programs will make available the region of operating parameters to be tried. As experience with the machine, and its matching to the AGS, proceeds, some degree of loop-closing will be developed.

Extraction and matching to the AGS follows the programs used by CERN for the ISR. These are "old" and understood (early 1970's). Fermilab may also be involved in developments of this sort and have newer programs available as they have ring-to-ring

requirements too. The CERN program can do a three point fit: i.e., using three pulses with slightly different values for the steering magnets, a "correct solution" can be found.

In so far as possible, settings that cause the the beam to exceed aperture limitations according to low-order calculations should be flagged. (Very sophisticated calculations are not necessary for this purpose: that aperture is exceeded or is about to be exceeded is what is significant — how closely one can scrape by is secondary)

9.2.4.2. Computation Capability Requirements

A processor for floating point calculations with power of the order of 10 MIPS is needed. This power need not reside in a single unit, but may be distributed among two or three units (since some low degree of parallelism is possible for MAD-like calculations). Apollo processors may serve this purpose. More powerful processors will not be available on the Domain network but will be accessible via an ETHERNET link to the system.

9.2.4.3. Advanced Control Concepts

9.2.4.3.1. Accelerator Programs

The degree of sophistication with which accelerator design programs such as MAD are integrated into the Booster operation will certainly increase with time. Usage can range from an essentially "off-line" approach in which results are compared with measured accelerator conditions to a fully integrated one in which modeling programs are used in closed loops around accelerator systems. To provide a suitable environment for these developments, attention to certain areas of the system architecture should include:

- Access to adequate computational power Response time is a critical factor in implementing systems. It is of little use to accurately diagnose and automatically correct accelerator operation if the reaction time is longer than would be required to find the problem manually A compute engine of 10 MIPS capability has been proposed for the Domain network. Options include increasing this figure and use of site-wide communications to access central site facilities.
- Data Base capabilities. Integration of modeling with the real-time operation will be facilitated by sharing of common data base elements between modeling and control programs.
- Graphics Facilities. It is important that modeling programs allow use of the APOLLO graphics for output no matter where the computation occurs.

9.2.5. Programs for Maintenance and Test

A system as complex as the Booster has of necessity many powerful and complicated electrical and electronic systems. Moreover, these systems are frequently so interconnected that a maintenance person cannot readily determine just which component is the cause of a particular problem or symptom. We intend to develop a library of test programs which can be invoked to analyze and isolate problems and which can be used to

certify the operation of a particular component or subsystem.

In addition to such dedicated programs, all control programs contain some elements of error testing and reporting and can therefore be used as test programs by those responsible for the maintenance of equipment. This has the advantage of testing the equipment under actual rather than simulated operating conditions but is less likely to be specific in pin-pointing the origin of some malfunction. To fully exploit the diagnostic capability of control programs, proper details of error conditions which occur during operation must be saved in a form suited to subsequent repair This is the responsibility of the ALARM program and will be accommodated by it. A suitable reporting and summary procedure must also be implemented for purposes of notification and record keeping.

9.2.5.1. Special Programs

The most elementary form of special "program" consists of spreadsheet device tables organized to assist hardware evaluation. These will be maintained on a branch of the spreadsheet tree optimized for maintenance. Some dedicated programs with facilities not required in normal operation will be useful for evaluation of the major accelerator systems. Test capability implies the existence of some redundancy in the system to provide a cross-check. In this respect, complex systems are more effective than simple ones. Specialized evaluation programs will be provided for at least the main magnet, RF and instrumentation systems.

9.2.6. Accelerator Database

9.2.6.1. Introduction

Because the Booster control system will require significant support from accelerator modeling programs embedded within the control functions, the Booster database must support a sophisticated view of all aspects of the accelerator, including control data and physics data. In addition to those data required to permit effective control of the accelerator, there are many cases where database techniques are convenient for general purpose information storage and retrieval. For this reason, a general purpose commercial database is preferred to ad hoc data structures if the required real-time performance can be achieved. A commercial product called INTERBASE has been acquired to satisfy those requirements. There are three types of data which are addressed in the Booster databases:

1) Static slow-access data
2) Static fast-access control data
3) Dynamic "state of the machine" data

9.2.6.2. The Static Slow-Access Data

There is a great deal of data in the accelerator database which is not used directly for control and need be accessed only in "operator time" Items like the name of the person responsible for the repair of equipment, the location of the equipment and the phone number of the phone close to the device are in the database but do not require a fast access time. Also there are functional relationships among the devices in the accelerator which are useful to high level control programs. Rather than have private data for applications programs, a superior approach is to store the data in a common database even though there may be only one program which uses the data. The data is then available to other potential users and the structure tends to encourage the use of standardized data procedures. Typical use of the database by application programs would be to acquire initialization data at set up time when it is first run. Fast access to this data is not required for these one-time activities so that the standard database queries can be used. Thus, the INTERBASE system will be used directly for this type of activity A menu driven interface will be used for data entry and system calls for retrieval in this context.

Since the Interbase database is flexible and convenient it will be easy to add new fields to existing records and new types of records to the database. This will encourage the storage of all types of functional information about accelerator devices in the database. Report generators and menu driven applications can then be invoked for utility purposes in a general and user-friendly fashion.

In order to have the data in the "off line" database accessible to programs we will have a network wide database server program which can be used by applications to retrieve data (slowly) from the database. We expect access times on the order of 0.2 seconds to access the database. This is fast enough for retrieving data which has a low rate of use.

9.2.6.3. The Static Fast-Access Control Data

A subset of the static data is needed for control of devices. This data includes addressing information for devices, conversion functions, set point limits, and other information needed to send commands to devices. To make this data available at the requisite speed for control system operation, the data is extracted from the slow database (Interbase database) and put into a fixed-format dedicated file called the Device Definition File (DDF) located on a server It is important that the contents of this file are restricted to data which must be accessed rapidly because the size is critical to performance of the access method.

9.2.6.4. The Dynamic Database Structure

The Booster control system will make use of the dynamic database structure in use by the AGSDCS. In this structure the "state of the machine" data is truly distributed. Simple logical devices have their database in the stations while complex logical devices have their data in the device controllers. Queries of the database are made via host to

station requests, with the station examining its own memory or that of the device controller and returning to the host the requested information. This distributed database has proven very satisfactory in operation.

However, the Booster controls will use Apollo workstations to perform the station function. Thus, stations no longer need to store device information in their limited physical RAM, but rather may make use of virtual memory The use of this capability must be evaluated considering issues of speed, reliability, fault and power fail recovery etc. The system capability can be improved with the use of the Apollo and its network utilities should be exploited to the maximum possible degree. Since the weakest aspect of the distributed system is its long response time from console to hardware it will be necessary to examine the use of Domain strategy to improve on previous performance.

9.3. System Engineering

9.3.1. Booster Controls System Architecture

9.3.1.1. Introduction

The Booster controls will be a part of the AGSDCS and Booster control shares a common architecture with the AGSDCS. Not only is the same functionality assigned to the distributed components of the system but the components are expected to be software compatible with the existing system. While some components of the system might change, the functionality of the three levels, console, station, device controller is fixed as are the fundamental data structures of the simple logical device and the complex logical device. The most significant change is at the STATION level where the MULTIBUS systems of the AGSDCS will be replaced by commercial APOLLO workstations, but this change is technical rather than architectural. The architecture is illustrated in Figure 9-1.

9.3.1.2. Stations

As described above, the STATIONS of the Booster control system will be APOLLO workstations. These purchased items offer cost and performance advantages over the custom designs previously used. They will be connected to the Console layer by the manufacturer's DOMAIN token LAN. The operating system in the STATION will be the manufacturer's standard so that CONSOLES and STATIONS will share a common development environment. Code will be written in a high-level language (C) and STATIONS will use the same data structures as CONSOLES. The hardware and software environment will permit expanding the function of the STATIONS wherever this is deemed appropriate.

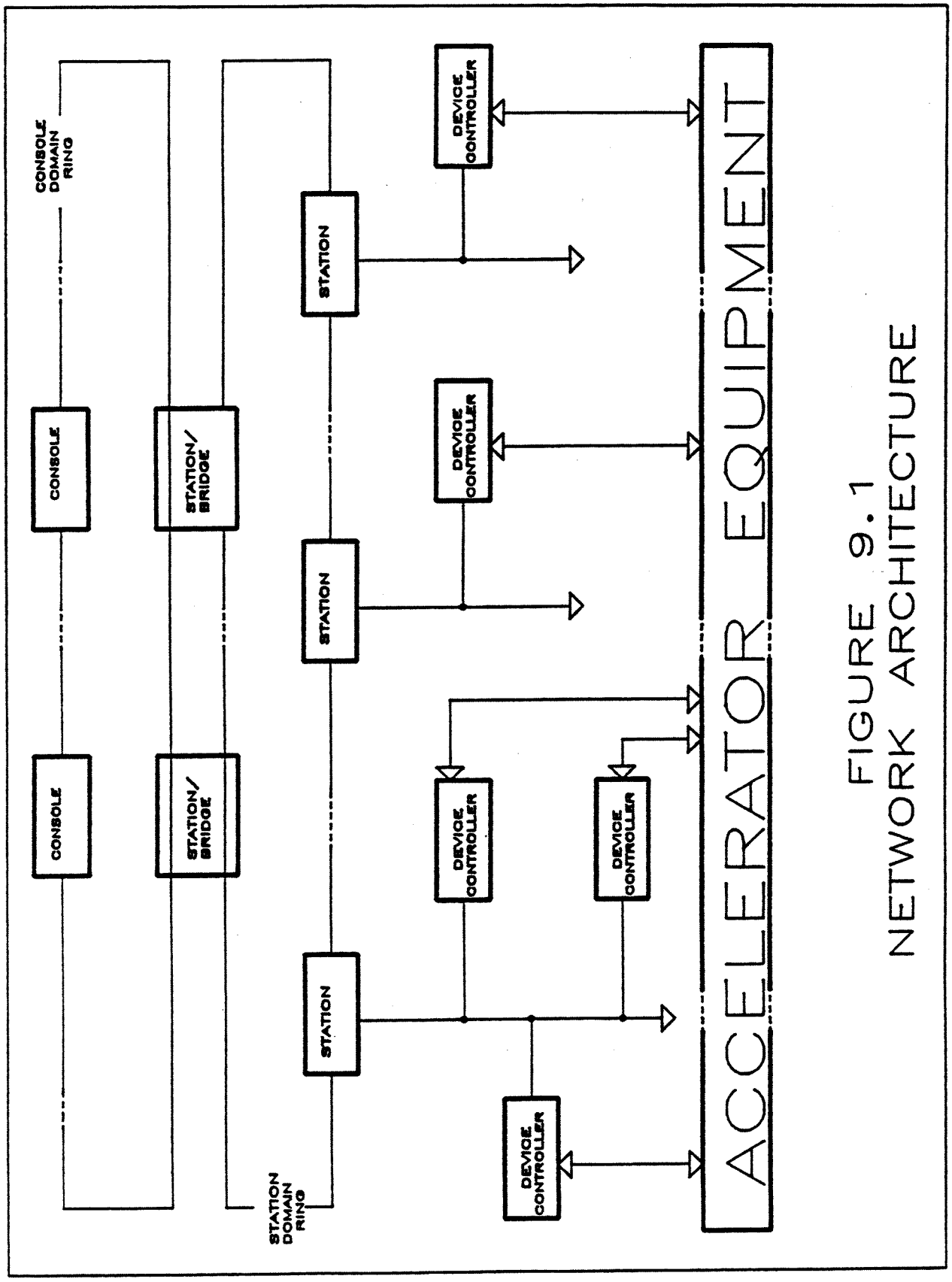

FIGURE 9.1
NETWORK ARCHITECTURE

9.3.1.3. Device Controllers

DEVICE CONTROLLERS will be custom designed MULTIBUS 1 systems as used in the AGSDCS because this system provides the necessary "real-estate" and back-plane power to support the extensive hardware required to interface to accelerator devices. Systems will use the dual-processor approach developed for the AGSDCDS with one processor for communications and the other dedicated to real time control of devices. The standard interfaces to devices include DATACON II, IEEE 488 and RS-232C. Some devices will be operated directly via hardware installed in the MULTIBUS crate.

Some effort will be devoted to improving the development environment of the DEVICE CONTROLLERS. The flexible real-time requirements suggest that the RMX operating system be retained but support facilities can be improved and the use of PROM code will be reviewed.

The IEEE 488 connection between the device controller and the station is discussed in the section on network hardware.

9.3.2. System Integration

From a design point of view, this area deals with the detailed electronic, electrical, mechanical and programmatic "glue"which interconnects the control system to the accelerator and which ties pieces of control apparatus together.

From a physical point of view, we are talking of optical cables, co-axial cables, wire, terminals, connectors and racks.

We will build five standard rack clusters made up of one 24″ rack and two 19″ rack assemblies. These clusters will house the Station computers and Device Controllers for the bulk of the smaller (in volume) accelerator subsystems (timing, analog signal distribution, access security, vacuum). Additional rack space (7 units) will be provided to support device controllers needed for the Power Supply and Instrumentation subsystems.

Additional racks will be provided to match the physical format of the control room consoles as specified by the interdepartmental Operational Aspects Study Group.

9.3.3. Hardware Documentation

In order to avoid significant rework and delays in project completion caused by redesign and mismatched control and accelerator equipment, adequate hardware documentation prior to construction is mandatory A detailed product specification for each module will be generated. A standard format for these specifications has been created.

9.3.4. Software Documentation

We will implement module specifications and documentation similar to that provided in the hardware area. A program library of standardized programs and a retrieval database will also be implemented. Version control and archive protection will be managed by an Apollo product called DSEE.

A "map" of system data and a "plan" for allocation of system resources will be generated.

9.3.5. Maintenance and Test Procedures

Test equipment will be purchased to support the design and construction phases of accelerator work. This equipment will also be used to maintain machine components both during and after project construction.

9.4. Accelerator Control Hardware (Device Controllers)

9.4.1. Power Supply Controllers

9.4.1.1. Power Supplies

The following power supplies must be interfaced into the system:

1. 1 main dipole
2. 2 tune-shift quadrupole (1 vertical and 1 horizontal)
3. 2 main sextupole
4. 144 correction
5. 10 orbit bumps
6. 6 fast kicker
7. 25 extraction
8. 28 heavy ion (hi) injection
9. 18 proton injection
10. 1 hi extraction (spectrometer)

9.4.1.2. Power Supply Control Types

(1) Set-point driven power supplies which receive a time-invariant value which specifies a supply output (current or voltage). This type applies to items 6-10 above.

(2) Function-generator driven which receive a time-dependent set of values which specify output profiles (flattop, front porch, rectify, invert etc.). This type applies to items 1-5 above.

9.4.1.3. Device Controllers

(1) There will be 24 device controllers.

(2) Each controller can control up to 8 function generator or 16 set point driven power supplies.

(3) The interface between the device controller and the function generator type power supplies is totally digital so that the A/DC's and the D/AC's are on the power supply side of the interface.

(4) For control purposes, each supply will be connected to its device controller by a DATACON serial link. All control commands and status reporting will pass via this link. For high speed monitoring of the analog signals within supplies, a unidirectional "streaming" link will convey multiplexed device data to the controller and elsewhere. The results of A/D conversions within a supply are digitally multiplexed onto the data stream with labels indicating the identity of the signal source.

(5) All of the lines will be transformer coupled or optically isolated at the power supply This will isolate dc grounds and prevent ground differentials from causing problems.

(6) All of the ejection power supplies and associated device controllers (3 units) will be located in building 914 with the remaining supplies and controllers (21 units) in building 930.

(7) While each controller can control a maximum of 8 or 16 supplies the actual breakdown will be influenced by proximity, environment and the number of reference values per magnet type. Thus, for example, the main dipole/quadrupole and the 2 main sextupole supplies might be controlled by separate controllers.

(8) The main dipole/quadrupole, tune-shift quadrupole, and sextupole power supplies will require 16 bit accuracy for reference values. The correction supplies and set point supplies will need 12 or 14 bits of accuracy

9.4.1.4. Power Supply Characteristics

(1) The main dipole/quadrupole power supply feeds the ring dipoles and main quadrupole windings in series. The supply is made up of six modules in series, one of which operates in a current regulated mode with the other five voltage regulated. Thus the system is current regulated with the option of varying five voltage outputs to minimize the stress on the current regulator Each of the voltage controlled supplies has a solid state shorting switch across its output to bypass the supply when its voltage is not required. This will allow control of ripple and power factor at values superior to a permanently connected system.

(2) The vertical and horizontal quadrupole tune-adjust power supplies are composed of single modules. For these supplies, current and voltage reference values are developed by function generators and introduced into the regulator circuitry at appropriate points.

(3) The 2 main sextupole and the up to 144 correction supplies will each be current controlled.

(4) All the remaining power supplies (orbit bumps, fast kickers, injection and extraction) will have a set point current control. One exception is the injection fast kicker which is function generator controlled.

Power Supply Summary					
Number PS	Loc	Number Modules	Reg	PS Type	Number of Controls
1	930	6	I&V	Main Dipole/Quadrupole	6
2	930	2	I&V	Tune-Shift Quadrupole	4
2	930	2	I	Main Sextupole	1
144	930	144	I	Correctors	144
				Orbit Bumps	
4	914	4	I	Ejection Orbit	4
3	930	3	I	HI Injec Orbit Bump	3
3	930	3	I	PP Injec Orbit Bump	3
				Injection	
6	930	6	I	Fast Kicker	6
				Extraction	
1	914	1	I	Ext Kicker	1
1	914	1	I	Ext Septum	1
2	914	2	I	Ext Dipole	2
15	914	15	I	Ext Quad	15
3	914	3	I	Ext Vert Steering	3
3	914	3	I	Ext Horz Steering	3
				HI Injection	
13	930	13	I	Quadrupole	13
3	930	3	I	Dipole	3
11	930	11	I	Steering	11
1	930	1	I	Electrostatic Septum	1
				Proton Inj	
13	930	13	I	Quadrupole	13
1	930	1	I	Dipole	1
4	930	4	I	Steering	1
				HI Ejection	
1	914	1	I	Spectrometer	1

9.4.1.5. Representations of Analog Functions

(1) Each of the analog functions will be digitally generated and converted to analog within the power supply Each function is represented by digital values defining a series of vectors having initial values, slopes and time durations. The data will

propagate in this compact form through the system to the device controller and thence via DATACON to a buffer memory in the function generator The memory can accommodate eight 256-vector functions with each function double buffered to allow loading new functions while operating existing ones. The eight functions will be uniquely assigned to specific cycles within a super-cycle. Synchronous switching between functions is accomplished via timing inputs and between buffers by means of a pre-loaded pointer mask. The function generators are driven by a time clock with provision for a gauss clock interrupt. Digital system amplitude resolution is 16-bits.

9.4.2. Booster Vacuum System

9.4.2.1. System Design

Since there is general compatibility between the functionality and requirements of the Booster vacuum system and those of AGS and HITL, the control system design employed for the BOOSTER vacuum is based on using the technology developed for the AGS and HITL vacuum systems. Extension is required only in that the Booster vacuum system is bakeable via permanently installed heaters.

Vacuum control falls into two classes. The first class is the Apollo system. It consists of permanently installed equipment located outside the tunnel and controls and monitors ion gauges, ion pumps and sector valves at all times. The second class is a set of 6 or 7 mobile units which are temporarily attached to sub-sections of the vacuum system during down time for roughing down the ring and transport line systems and for bake-out. For this purpose the system is partitioned into approximately 20 sectors which may be valved off from each other The mobile units allow 6 or 7 sectors to be manipulated at one time. This part of the system will be implemented by the vacuum group who will be responsible for its installation and operation. Use of the portable system will require data access to the areas controlled by the central system so that some link to the APOLLO system will be required.

The first class of vacuum control equipment includes interfaces to dual ion pump power supplies, sector valves and to ion and Convectron gauges. With appropriate selection of equipment, interface designs exist for all these devices.

The second class of vacuum control equipment provides controls for turbo molecular pumps, ion and Convectron gauges, bakeout heaters and thermocouple readbacks. A commercial process controller is proposed for this system with a personal computer to provide remote control.. The PC will be connected via an RS-232 link to the Apollo system. A system of twisted-pair cables will be run to facilitate linking the necessary RS-232 ports on a discretionary basis.

Figure 9-2 shows a block diagram of the total system configuration. Apollo stations will be located in buildings 930 and 914 with IEEE-488 links to the device controllers. Two of the device controllers in each building will be connected to vacuum equipment. Ion pump power supplies and sector valves are interfaced via DATACON. Ion and Convectron gauge controllers are interfaced via RS-232 links.

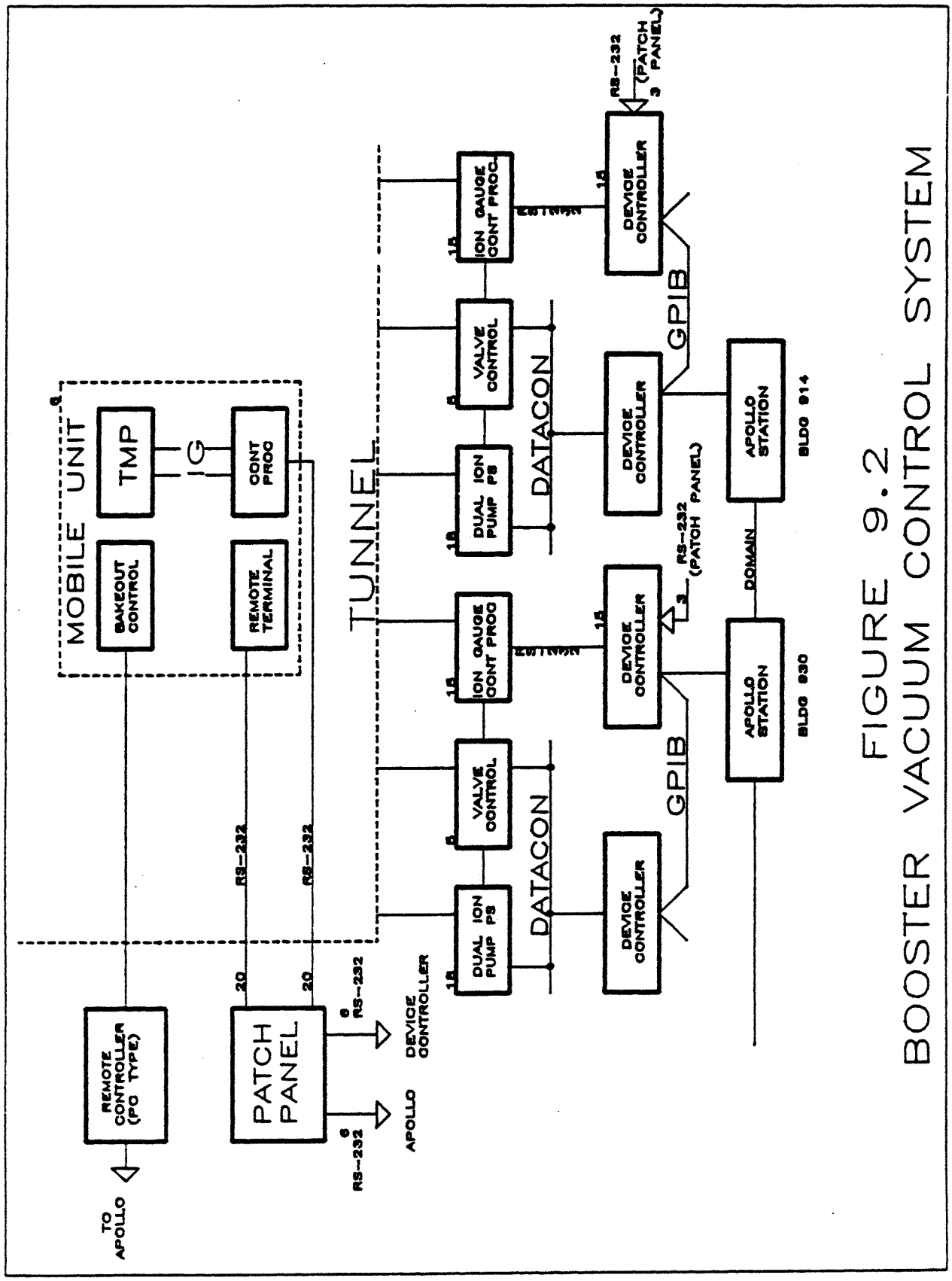
MOBILE UNIT
TMP
IG
BAKEOUT CONTROL
CONT PROC
REMOTE TERMINAL
RS-232
RS-232
20
20
REMOTE CONTROLLER (PC TYPE)
PATCH PANEL
6 RS-232
6 RS-232
TO APOLLO
APOLLO
DEVICE CONTROLLER
TUNNEL
DUAL ION PUMP PS
VALVE CONTROL
ION GAUGE CONT PROC
DATACON
DEVICE CONTROLLER
GPIB
RS-232 (PATCH PANEL)
APOLLO STATION
DOMAIN
BLDG 930
BLDG 914
FIGURE 9.2
BOOSTER VACUUM CONTROL SYSTEM

9.4.2.2. Device Controller

Figure 9-3 shows a block diagram of the device controller for ion pumps and sector valves. All the components are commercial or replicate existing designs so that the design is complete. Figure 9-4 shows the block diagram of the device controller for RS-232 devices. Again the components are available and no new developments are required. The following table lists the components for the four device controllers.

VACUUM DEVICE CONTROLLER COMPONENTS	
Card	Number
186/03 CPU	4
CM-42 IEEE-488	4
DATACON Central	2
DATACON Driver	2
RS-232 16-line Scanners	2

DATACON INTERFACE CARDS	
Card	Number
Dual ion pump power supply	36
Dual sector valve	10

9.4.2.3. Vacuum Device Manual Control

- Convectron Gauge (Injection) — Local pressure readout,PC contacts for CC gauges.
- Bakeout — Heater tapes controlled by Fenwal temperature devices.
- TI Sublimation Pumps — 50A motor driven autotransformer into individual 10A transformers, switchable by sector to buck boost transformers located in the tunnel at the TI pumps. Current is read in the primary leg of the buck boost transformer
- NEG Pump Cartridge — (A) 50A motor driven autotransformer or (B) Individual 20A autotransformers NEG Pump Strip (HITL Injection) SCR controller 3 phase

9.4.2.4. Vacuum Device Computer Control

- Ion Pump P.S. — 200 ma short circuit current, 5KV, local and remote computer control. Process control relay contacts for valve logic.
  - Computer Control— Pump On, Pump Off
  - Computer Read back— Current, Voltage, PS Status
  - DATACON Interface, RS232 or IEEE-488 Interfaces with opto-isolation

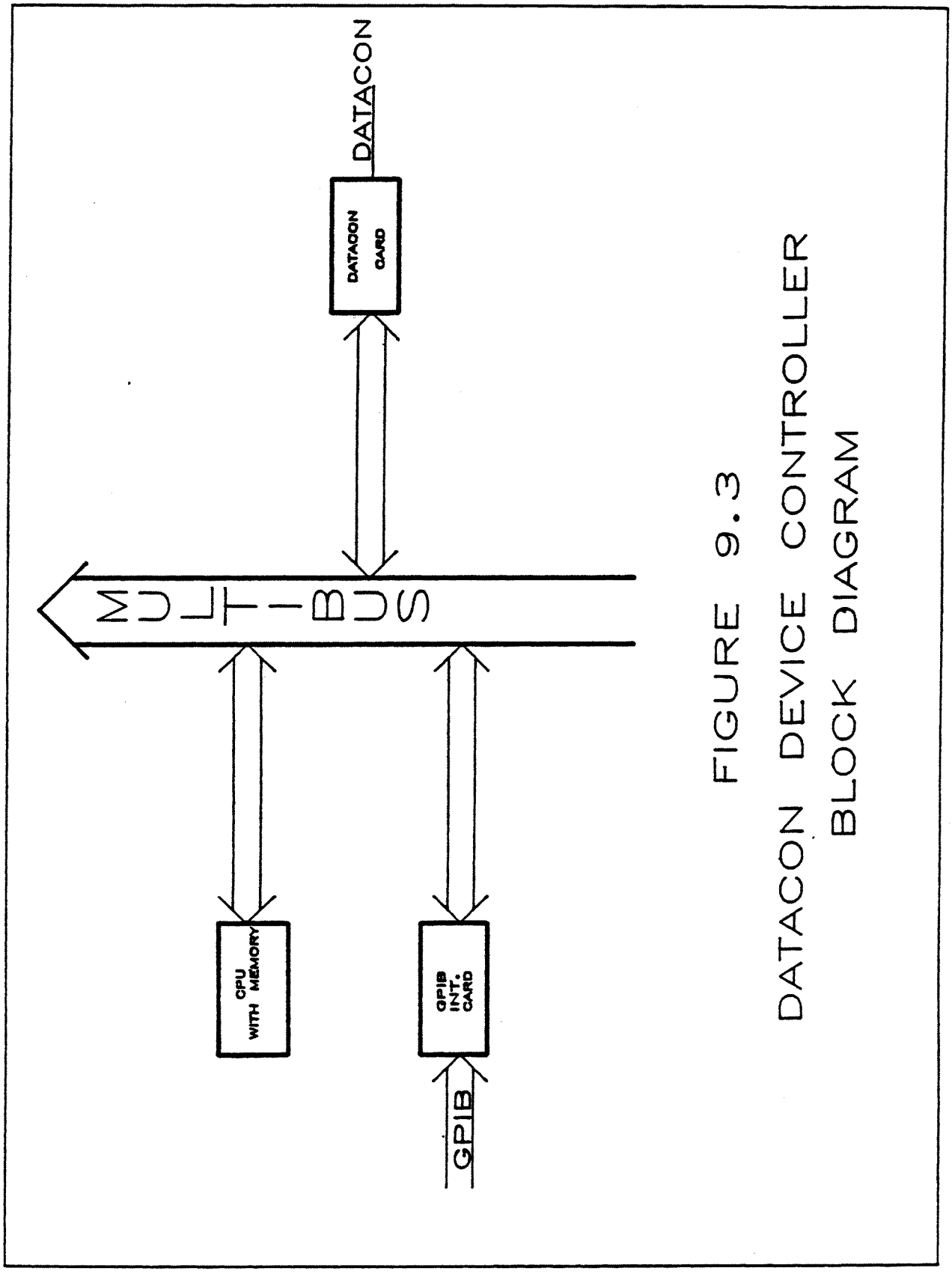

FIGURE 9.3
DATACON DEVICE CONTROLLER
BLOCK DIAGRAM

- Ion Gauge, Convectron Gauge — Local readout of pressure. Other information accessible through the front panel key board. Ion Gauges will automatically be turned on by the Convectron Gauge. Process control relay contacts are available for Valve logic.
  - Computer Control— Gauges On, Gauges Off
  - Computer Readback— Pressures (Torr), Keypad Functions
  - RS232 Interface With Optoisolation
- Valves
  - Computer Control— Open, Close
  - Computer Readback— Open, Close, In-between
  - DATACON Interface
- Cold Cathode Gauge — Local pressure readout, Convectron Gauge interlocked by means of relay contacts. Provides process control relay contacts for Valve interlock.
  - Computer Control— On, Off
  - Computer Readback— Pressure
  - DATACON Interface, RS232 or IEEE-488 Interfaces with Optoisolation
- Portable Turbomolecular Pump — Interface at Sector Valve
  - Computer Readback— Pumps (On, Off)
    — Isolation Valve (Open, Close, In-between)
  - DATACON Interface
- Turbomolecular Pumps (LINAC) — Stationary Pumps (Mechanical and Turbomolecular). Same configuration as AGS.
  - Computer control— Pumps (On, Off)
    — Isolation Valve (Open, Close)
  - Computer Readback— Pumps (On,Off)
    — Isolation Valve (Open, Close, In-between)
  - DATACON Interface

9.4.2.5. Disposition

- All vacuum system controls will reside in 72″ high racks located in the LINAC house. Only buck boost transformers for Titanium Sublimator Pumps will be mounted in the Booster tunnel.
- All cables in the tunnel shall be low smoke, radiation resistant composition (FREP-CPE) or equivalent.
- Terminal boxes with terminal strips shall be mounted on the tunnel wall, in between the pump stations (two pump stations per box). Cables will run from these devices to this box via the cable tray

- Terminal boxes with terminal strips shall be mounted on the LINAC house wall near the vacuum system control racks. Cables will run from these boxes to the equipment racks.
- No Teflon sheathed wire or cable shall be used in the Booster tunnel.
- Device controller disposition— see Figure 9-4.
- Wire used as bakeout extension leads shall be high temperature resistant, 450 degree C with a fiberglass sheath.

9.4.2.6. Computer Control

Vacuum devices will interface the device controller through DATACON and RS-232 links. Device interface cards will be installed in the vacuum devices where necessary to effect DATACON interface. RS232 links will interface Ion Gauges and Convectron Gauges to the Device Controller An RS-232C multiplexer/driver board will be installed in the device controller for interface purposes. Device controllers shall interface to stations via IEEE-488.

9.4.3. Booster RF Controls

The RF system for the Booster envisages three PA/cavity systems — two which cover the heavy ion spectrum sequentially and one for conventional proton operation.. A single Low level system is proposed for all modes of operation.

It is proposed to construct a controller quite similar to the one currently in use for heavy ion operation using the TVDG. The controller would consist of two independent micro-computers: one to construct the necessary frequency and amplitude functions from down loaded commands and a second to control delivery of these functions to the low level system using direct memory access (DMA). The functions and associated control bits can be routed externally to the proper low level channel by a multiplexed switch. The MPX switch is assumed to be an integral part of the low level system. It is assumed that there need not be an operative analog radial control loop, but that an operative phase control loop will be required. Since the response of such a circuit determines potential accelerator beam performance and since the required response varies with the kind of particle accelerated, some additional accelerator physics input is required before engineering can begin. (Under worst case conditions the required response could exceed the capability of our fully digital approach requiring the development of an alternative approach.) Existing designs will have to be modified for such features as negative dB/dt.

There also exists the need for control of the high level stages; we expect to directly apply the design techniques already in use at the AGS for such applications.

By condensing the controls into one multiprocessor device hardware costs are minimized.

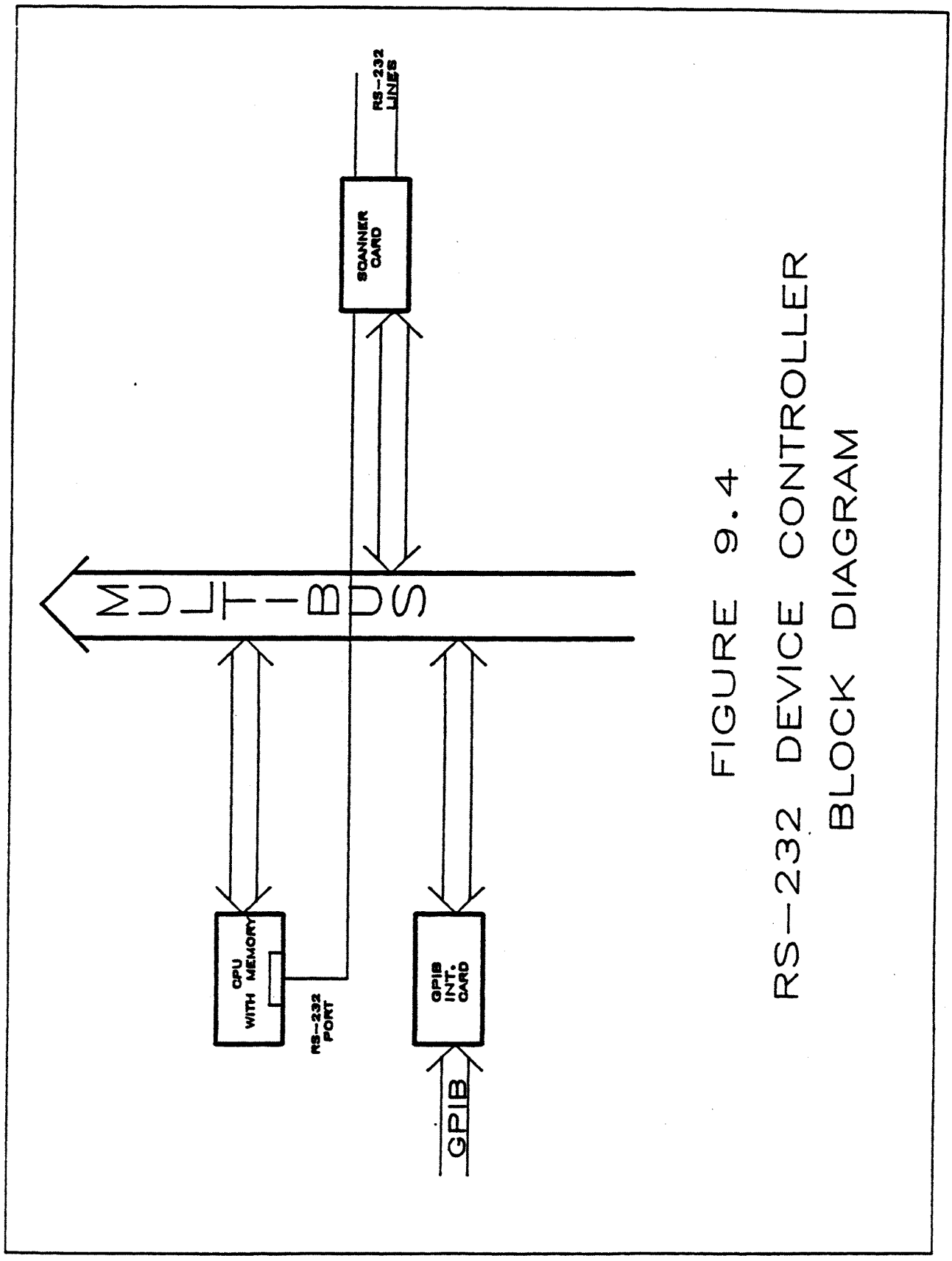

FIGURE 9.4
RS-232 DEVICE CONTROLLER
BLOCK DIAGRAM

9.4.4. Booster Facilities

A Bristol Babcock Telemetrol RDC3350 Controller is the heart of the Facilities Control system. This system will monitor and control the cooling water for the magnets, monitor the HVAC conditions in the magnet power supply enclosures and monitor the dew point in the booster ring. Personal Computer based monitors will be located in the 928 pump room, the Power Room and Room 215 in 911B. This system will operate as a stand alone system with the capability for adding an additional RS-422 drop to the main Booster control room. This would allow a PC to monitor the activities of the Telemetrol RDC3350. It is strongly recommended that one of the following three choices be made to allow the Control Room access to the RDC3350 Controller

Attach a co-processor to an Apollo on the network, this in conjunction with a software package (to be developed) would allow direct access to the RDC3350 Controller

Add process annunciator relays to the RDC3350 Controller This will allow go — no-go information into the data stream.

Add a PC to the Control Room which would access the RS-422 drop mentioned above.

9.4.5. Instrumentation Interfaces

9.4.5.1. Instrumentation Controllers

9.4.5.1.1. General Description

The Booster instrumentation system control will be distributed in units located in buildings 911, 930 and 914. Each controller will be capable of interfacing and controlling at least one third of the Booster instrumentation.

Controllers will be capable of complex reading and digitizing procedures for signals from beam instruments in the Booster ring to provide data to the central control computer Additionally the controller will provide the ability to actuate the insert and retract mechanisms for the various instruments. There will be procedures for inserting mechanisms into the beam before or after the beam pulse. The controller will also provide the ability to set parameters, such as gain, of the instrument electronics

The Instrument controller is intended to provide not only simple (default) status reports and data reports but also to provide data manipulation by the controller and complex data reports, sequenced or multiple actuator control, and interrupts to inform the station when a particular process is finished.

9.4.5.1.2. Hardware Interface

At present, the hardware of the instrumentation interface to Booster diagnostic devices is not defined. A considerable number of device interfaces have been designed for HITL and AGS applications. Similar designs are likely to prove adequate for some Booster applications. In some cases it may be desirable to extend or replace existing

designs because the repetition rate or other parameters of the Booster application demand greater power These applications must be reviewed on an individual basis when details of the instrumentation are defined.

The device hardware interface options which have been implemented to date in HITL and AGS include DATACON, IEEE-488, Digital I/O and Analog Signal connections. Suitable combinations of these interfaces will fulfill most of the needs of the Booster One option which is being subjected to detailed discussion is the use of optical fiber in interfaces to provide superior isolation and noise immunity Decisions on this and other interfacing issues will be made in the immediate future.

CHAPTER 10. ACCELERATOR CYCLES

10.1. Acceleration Cycle for Proton Operation

The following quantities were evaluated for the acceleration portion of the proton cycle of the Booster dipole field strength, rf frequency, rf voltage, dB/dt, height of the moving bucket, bucket length, synchrotron oscillation frequency, kinetic energy of the synchronous particle, synchronous phase angle, and other variables that are required for the calculation of these values. After the first half millisecond, the calculations were done in 0.5 ms steps, but for the first half millisecond of the cycle evaluations were done at 18 time points because some of the parameters are to be rapidly varied over this period. The equations used are those given by S. Ohnuma[1] except as noted below

10.1.1. Assumptions about the Proton Cycle

The acceleration cycle for proton operation is based on Booster Technical Note 49[2] There it was assumed that the area of the moving bucket would be maintained at the constant value of 1.5 eV-s and that the peak rf accelerating voltage would be 90 kV (per turn). Since the harmonic number, h, is 3, and the injection energy is 200 MeV, the initial dB/dt is required to be 1.441 T/s. (A slightly higher value of 1.468 T/s appears in Tech. Note 49, because there the value of γ_{tr} was taken to be equal to ν_h)

The power supplies for the dipole magnets do not allow dB/dt to exceed 9.6 T/s. In the original calculations, after a dB/dt of 9.6 T/s had been reached, the synchronous phase angle was held constant to maintain this value of dB/dt and thus the moving bucket area grew at the end of the cycle. In the calculations below, the moving bucket area *and* dB/dt are held constant by decreasing the rf voltage while simultaneously allowing the synchronous phase angle to increase. It is necessary to decrease the rf voltage anyway in order to reduce power dissipation in the ferrite of the rf cavities, but it is undesirable to allow dB/dt to fall at the end of the cycle since it is necessary to bring the protons up to their ejection energy of 1.5 GeV in about half the time for the complete cycle, 133.3 ms.

The initial portion of the cycle is also modified. The rf voltage is set at 45 kV for a period of 0.2 ms and then increased smoothly to 90 kV over the next 0.3 ms. Because of this modification, the initial moving bucket area is only 0.97 eV-s. Even though dB/dt can now be chosen independently, the moving bucket area is only a weak function of ϕ_s for these small values. When ϕ_s is varied from 5.3 to 0.0 to give dB/dt's varying from 1.5 T/s to 0 T/s, the moving bucket area only goes from 0.97 eV-s to 1.180 eV-s for an accelerating voltage of 45 kV

---

[1]S. Ohnuma, *The Beam and the Bucket — A Handbook for the Analysis of Longitudinal Motion*, TM-1381, Fermilab, January 22, 1986.

[2]J. G. Cottingham, *Proton Cycle for the Booster*, BST/TN #49, (July 1986).

The area of the moving bucket, A_{bk}, is obtained by multiplying the stationary bucket area, A_o, by the moving bucket factor, $\alpha(\phi_s)$, where

$$A_o = \frac{8C}{\pi ch}\left[\frac{Q_b V E_s}{2\pi h\,|\eta|}\right]^{0.5}$$

where:

$$\eta = \frac{1}{\gamma_t{}^2} - \frac{1}{\gamma^2}$$

$$\gamma = (1 - v^2/c^2)^{-0.5}$$

and

C	= machine circumference 201.78 meters	c	= speed of light
		Q_b	= charge state in the booster
V	= peak rf voltage	E_s	= total energy (in eV) of the synchronous particle
h	= harmonic number	γ_t	= transition γ (4.88)

The moving bucket area is calculated from

$$A_{bk} = \alpha(\phi_s)\, A_o$$

$$\alpha(\phi_s) = \frac{\sqrt{2}}{8}\int_{\phi_1}^{\phi_2}\sqrt{f(\phi,\phi_s)}\,d\phi$$

$$f(\phi,\phi_s) = \cos\phi + \cos\phi_s + (\phi + \phi_s - \pi)\sin\phi_s$$

and $f(\phi,\phi_s) = 0$ at ϕ_1 and ϕ_2. ($\phi_2 = \pi - \phi_s$, the unstable fixed point on the separatrix.) The value of ϕ_1 is found numerically and then the integration is performed using a 60-point Gauss-Legendre quadrature formula.

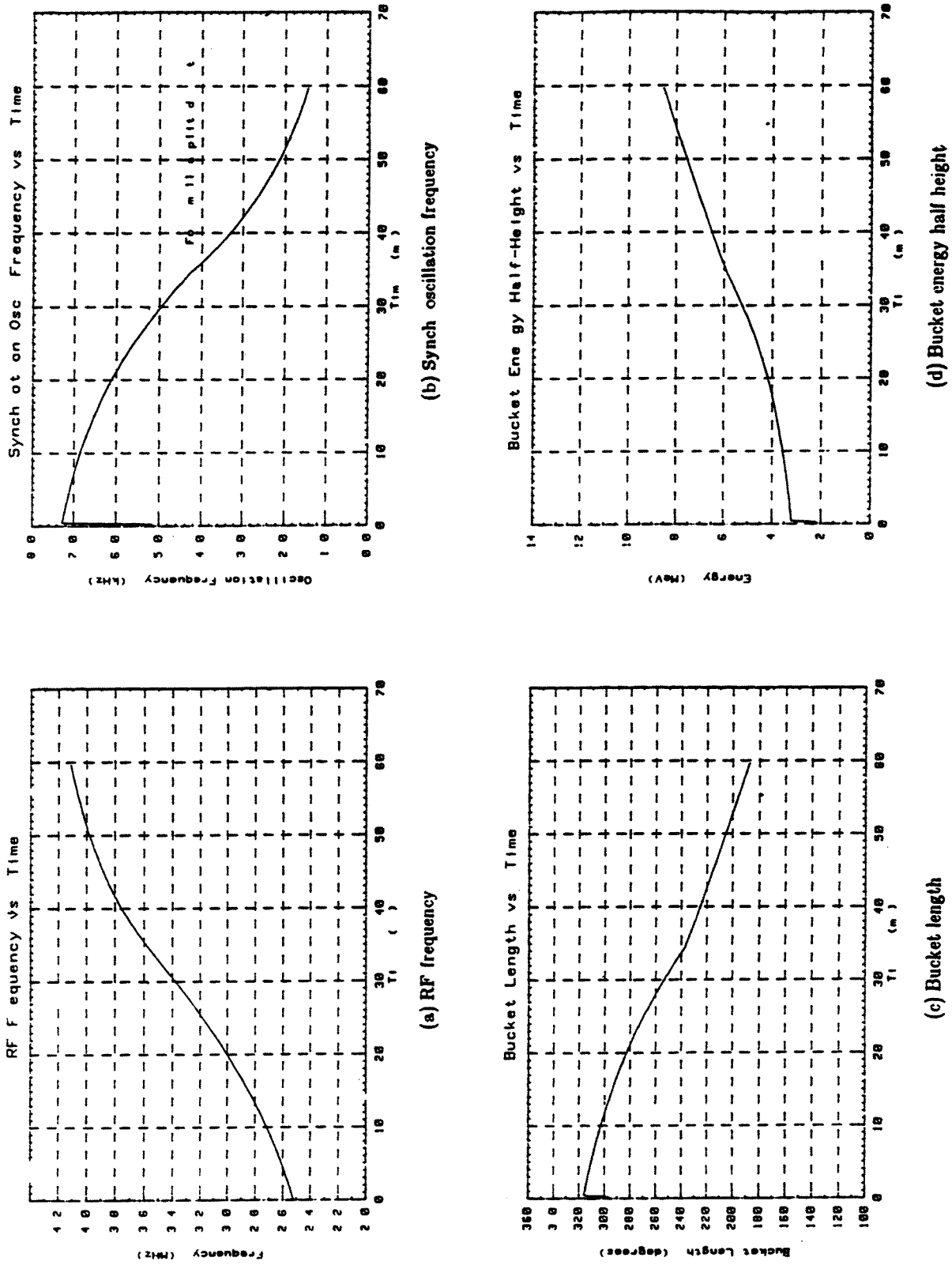

(a) RF frequency (b) Synch oscillation frequency (c) Bucket length (d) Bucket energy half height

Figure 10-1 Graphs of proton cycle parameters

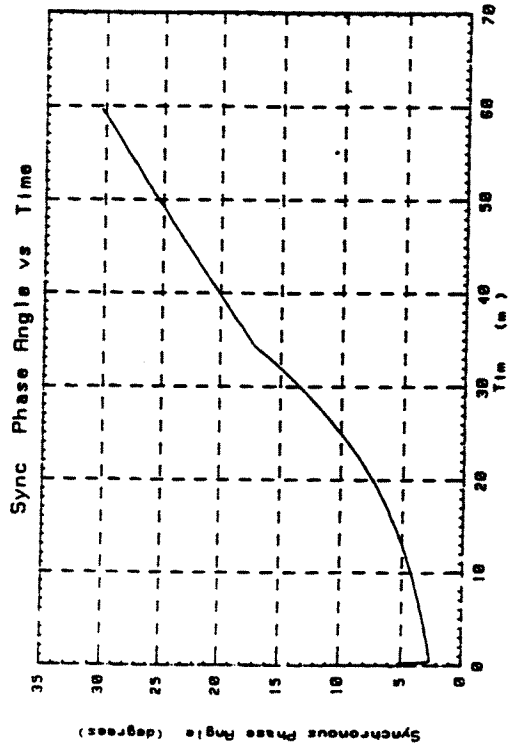

(f) Synch phase angle

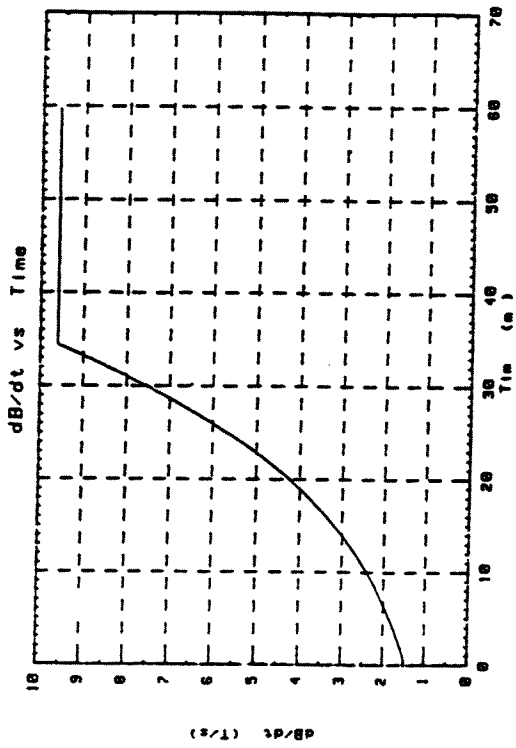

(h) $\dot{B}$

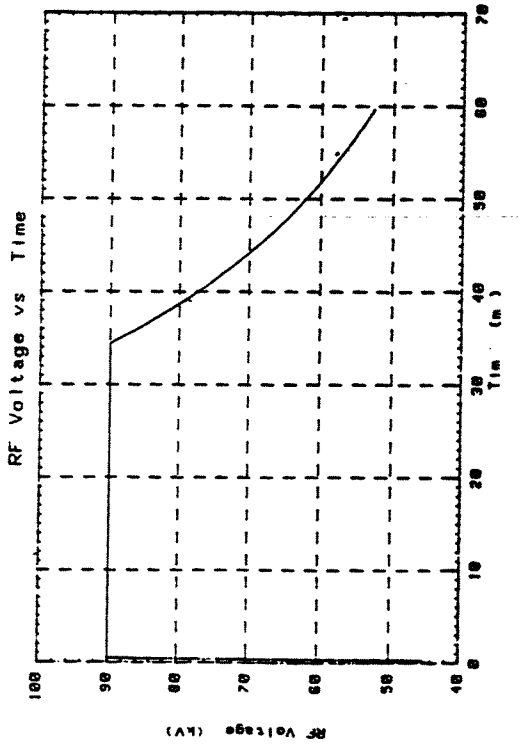

(e) RF voltage

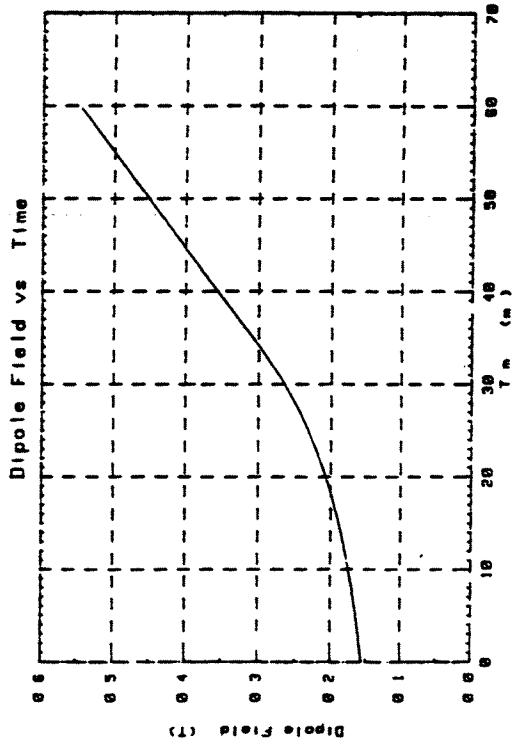

(g) Dipole field

Figure 10-1 Graphs of proton cycle parameters (cont)

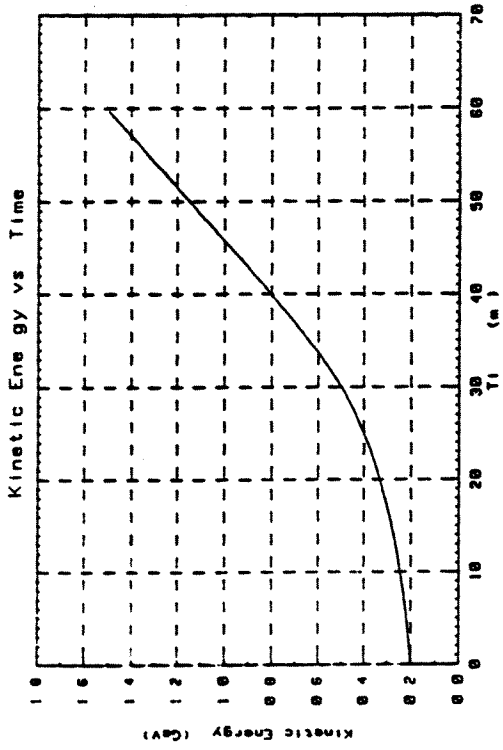

(j) Kinetic energy

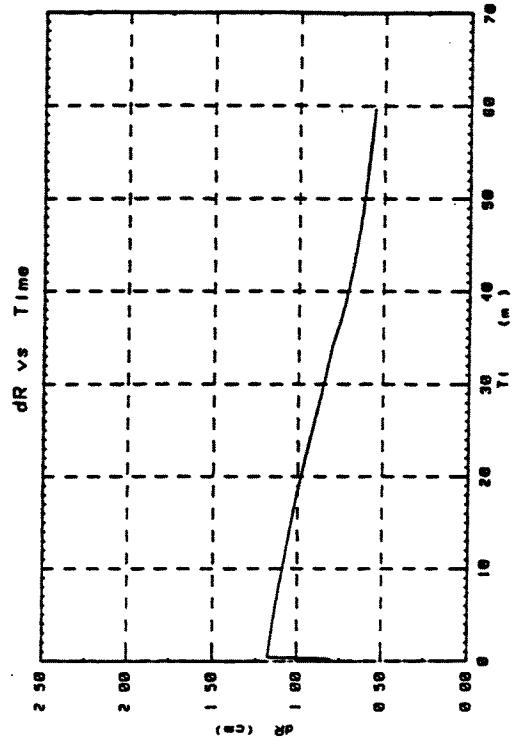

(l) *dR*

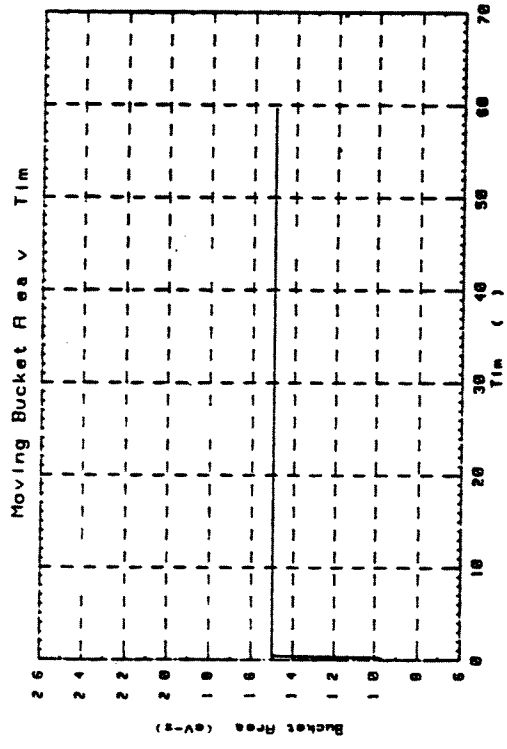

(j) Moving bucket area

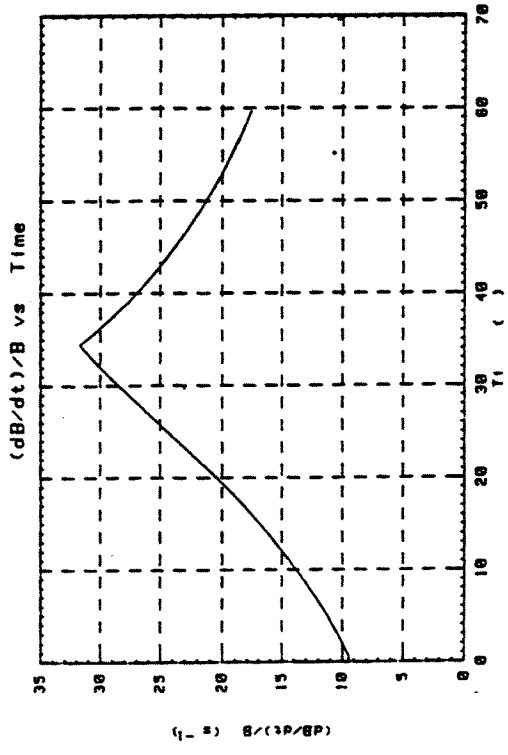

(k) $\dot{B}/B$

Figure 10-1 Graphs of proton cycle parameters (cont)

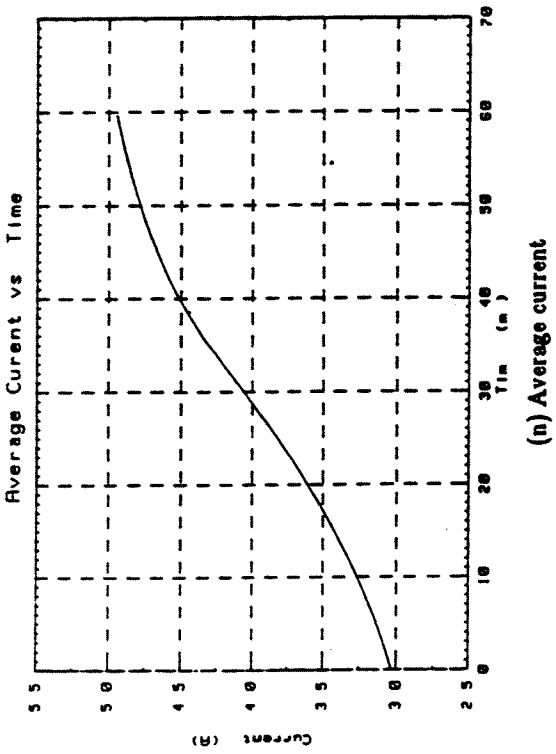

(n) Average current

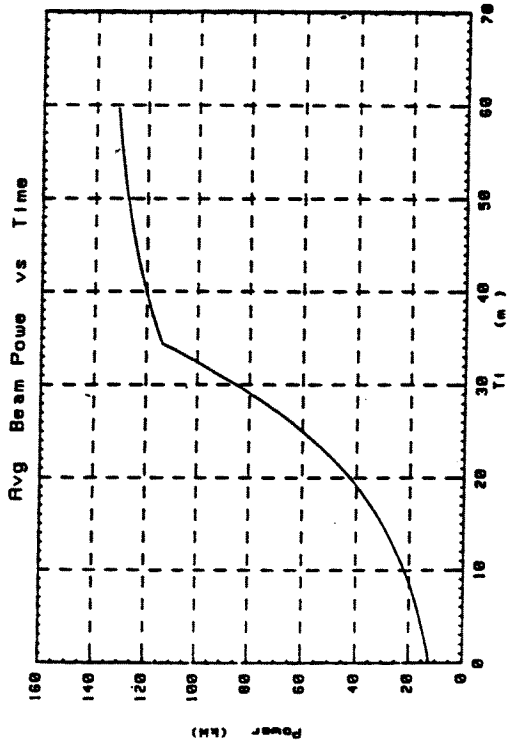

(p) Avg beam power

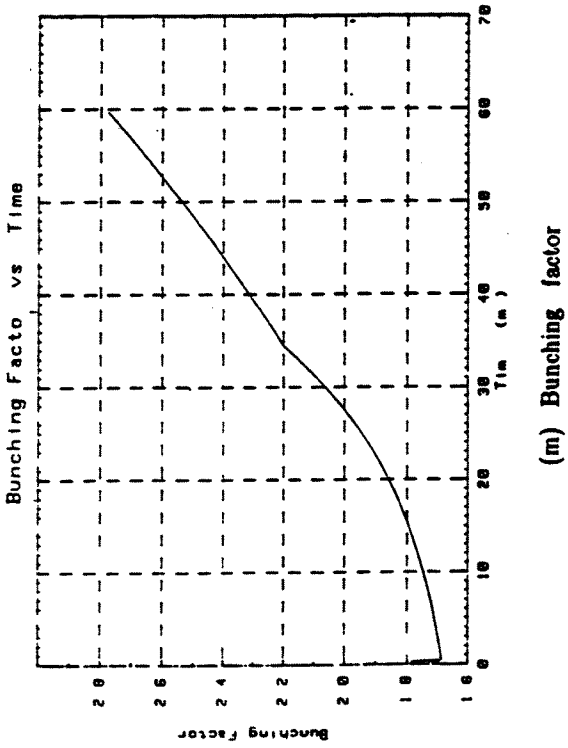

(m) Bunching factor

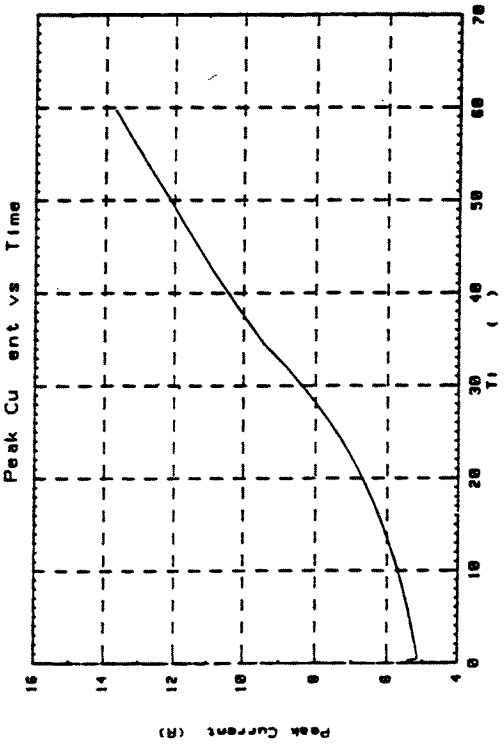

(o) Peak current

Figure 10 1 Graphs of proton cycle parameters (cont)

10.1.2. Other Cycle Parameters

The graph labeled "Bunching Factor" is actually a graph of the ratio of the peak charge density to the average charge density in the bucket, where it is assumed that the entire phase area bounded by the separatrix is uniformly filled with particles.

$$\bar{b} = \frac{\pi\sqrt{2\,f\,(\phi,\phi_s)}}{4\,\alpha(\phi_s)}, \qquad \phi = \phi_s$$

The graphs of quantities involving currents and beam power assumes that the number of particles per bunch is 7.5×10^{12} for design purposes only This value is 50% larger than the nominal value of 5.0×10^{12} particles per bunch.

10.1.3. Time Available for Proton Acceleration

The total time available in the proton cycle is 133.3 ms. Part of this time (> 22 ms) must be available for filter recovery, regulator recovery, and the portion of the current invert ramp below the injection current level. So only about 111 ms is available for ramping up and back down. The present cycle takes 59.8 ms to reach the ejection energy of 1.5 GeV

The details of the cycle at injection are still being studied. The peak rf voltage at injection may not, in fact, correspond to 45 kV per turn. Also, the ramping of the voltage up to 90 kV will probably not follow the curve used here, where it goes smoothly from 45 kV to 90 kV over a time interval of 0.3 ms beginning at 0.2 ms into the cycle.

There is also interest in cycles starting with dB/dt equal to zero. Such cycles can be easily calculated, but an ejection energy of 1.5 GeV can not be reached within 60 ms while maintaining a moving bucket area of 1.5 eV-s without exceeding the 90 kV limit on the peak rf accelerating voltage per turn. (The voltage is required to exceed 90 kV only during the early part of the cycle however) Alternatively, a cycle with a zero initial dB/dt can be obtained within the 90 kV restriction by allowing the time to reach the ejection energy to extend to 66.5 ms.

10.2. Acceleration Cycle for Heavy Ion Operation

It is assumed that constant bucket area acceleration will also be used for each heavy ion species. If the goal is to keep the maximum ΔR the same for all species, then the bucket area per nucleon should have the same value for all ions *if the ions are fully stripped* and *if the ions are traveling at high velocity.* As $\beta \rightarrow 1$, the bucket height, y, goes as

$$y \propto \sqrt{E_{io} Q}$$

and

$$\frac{y}{A} \propto \left(\frac{E_{io}}{A} \frac{Q}{A} \right)^{0.5}$$

where E_{io} is the rest mass energy of the ion, Q the integer charge state, and A the atomic mass number (the number of nucleons). Even though A is an integer and is not equal to the atomic mass, M, of the ion, the value of E_{io}/A is nearly constant, going from 0.939302 GeV for the negative hydrogen ion to 0.930182 GeV for $^{56}Fe^{26+}$ Q/A has a larger variation, but is still between 0.4 and 0.5 for fully stripped ions (excluding protons). However, the ions are fully stripped only after leaving the Booster The table below shows the relative value of $\Delta p/p$ for various ions.

As in the section above, a third harmonic system (h=3) is used for the acceleration system, but the frequency range is assumed to be covered by two or more different cavities, each operating over a limited frequency range.

Capture

Since the heavy ions from the Tandem Van de Graaff have virtually no energy spread, and so-called adiabatic capture takes too long (>100 ms), it is proposed that heavy ions be captured with an r.f. voltage which gives a reasonable synchrotron period of 2.5 ms. The corresponding bunch size is 0.05 eV-s/nucleon/bucket at 0° phase angle. The r.f. voltage should be at this value for about one-fourth of the synchrotron period (0.7 ms). Then the r.f. voltage should be increased to twice the capture voltage which gives a bucket with a size equal to $\sqrt{2}$ times the bunch size. Table 10-2 gives the bunching voltage and corresponding momentum spread for representative ion species.

TABLE 10-1 Q, β, γ, kinetic energy and $\Delta p/p$. Values of $\Delta p/p$ are relative to the value for protons in each instance.

	Booster		AGS	RHIC	
	Inj	Ejec	Inj	Inj	Ejec
Q					
proton	1	1	1	1	1
carbon	6	6	6	6	6
sulfur	14	14	16	16	16
copper	21	21	29	29	29
iodine	29	29	53	53	53
gold	33	33	79	79	79
β					
proton	0.5662	0.9230	0.9230	0.9995	1.0000
carbon	0.1262	0.8714	0.8714	0.9979	1.0000
sulfur	0.1000	0.8715	0.8715	0.9979	1.0000
copper	0.0782	0.8533	0.8533	0.9976	1.0000
iodine	0.0595	0.7902	0.7902	0.9971	1.0000
gold	0.0478	0.6868	0.6868	0.9968	1.0000
γ					
proton	1.21	2.60	2.60	31.37	268.19
carbon	1.01	2.04	2.04	15.60	135.12
sulfur	1.01	2.04	2.04	15.62	135.24
copper	1.00	1.92	1.92	14.33	124.52
iodine	1.00	1.63	13.04	13.04	112.87
gold	1.00	1.38	1.38	12.49	108.40
E/A, (GeV)					
proton	0.200	1.500	1.500	28.5	250.7
carbon	0.008	0.967	0.967	13.6	124.9
sulfur	0.005	0.967	0.967	13.6	124.9
copper	0.003	0.854	0.854	12.4	114.9
iodine	0.002	0.588	0.588	11.2	104.1
gold	0.001	0.350	0.350	10.7	100.0
relative $\Delta p/p$					
proton	1.0	1.0	1.0	1.0	1.0
carbon	0.180	0.064	1.361	2.029	2.000
sulfur	0.325	0.064	1.361	2.029	2.000
copper	0.416	0.070	1.478	2.213	2.173
iodine	0.547	0.088	1.875	2.433	2.396
gold	0.682	0.121	2.558	2.538	2.493

TABLE 10-2 Ion Properties

Ion	E_{inj} (MeV/nucleon)	Q	B_{inj} (kG)	f_{inj} (MHz)	V_{bunch} (kV)	$\Delta p/p$ (%)
carbon	7.5	6	0.576	0.562	0.288	0.15
sulfur	4.7	14	0.519	0.448	0.332	0.19
copper	2.9	21	0.531	0.349	0.445	0.24
iodine	1.65	29	0.590	0.265	0.642	0.31
gold	1.0	33	0.645	0.213	0.877	0.40

A_{bunch} 0.05 eV-s/nucleon/bunch

A_{bucket} 0.071 eV-s/nucleon/bucket, $V = 2\ V_{bunch}$

Acceleration, lighter ions

The acceleration program for the lighter ions is calculated in the following manner First, it is assumed that the initial dB/dt is to be zero and that the maximum dB/dt required for any ion will be less than 2.55 T/s. The initial injection field is calculated from the injection energy, and the ejection field is calculated based on the requirement that all ions are to be accelerated to any energy in the Booster such that, after stripping, they will have the same magnetic rigidity as 2.5 GeV protons (11.0336 T-m), *unless* this would require the dipole field at ejection to exceed the field required for 350 MeV/nucleon gold ions. (This means that if Z/Q_B for a particular ion is greater than 1.588 then the dipole magnetic field at ejection will be the same as for gold ions, 1.274 T The magnetic rigidity of 11.0336 T-m is the design specification for the Booster ejection line.)

An acceleration period of 0.5 seconds is assumed. In order to have a smooth form for variation of dB/dt, a tanh function was adopted. The only other decision to be made is the rate at which dB/dt should rise from near its initial value of zero to near its final maximum value. In the graphs below, this change was assumed to take place over a period of about 25 ms, but it has been found[3] that allowing the dB/dt increase to take place over a much longer period, about 150 ms, can easily be accommodated in the cycle without exceeding the maximum peak rf voltage of 17 kV and with only a modest increase in dB/dt. (The maximum dB/dt must increase from 2.55 T/s to about 2.75 T/s, and the initial slope of dB/dt is somewhat greater)

[3]Mark Rhoades-Brown, private communication.

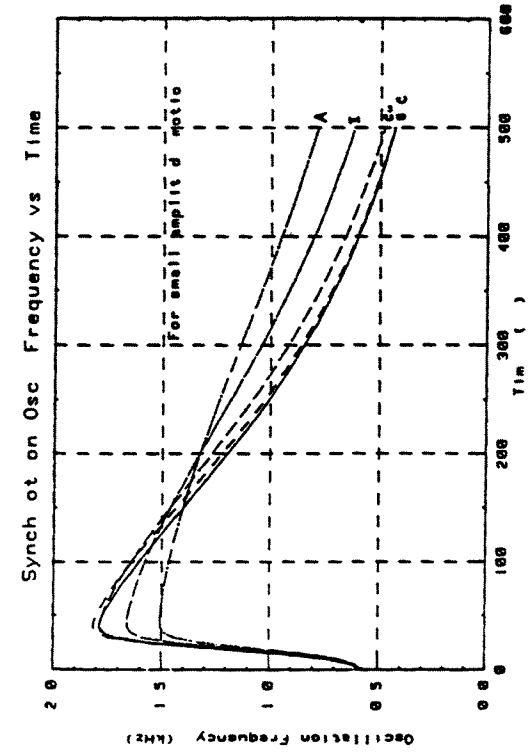

(b) Synch oscillation frequency

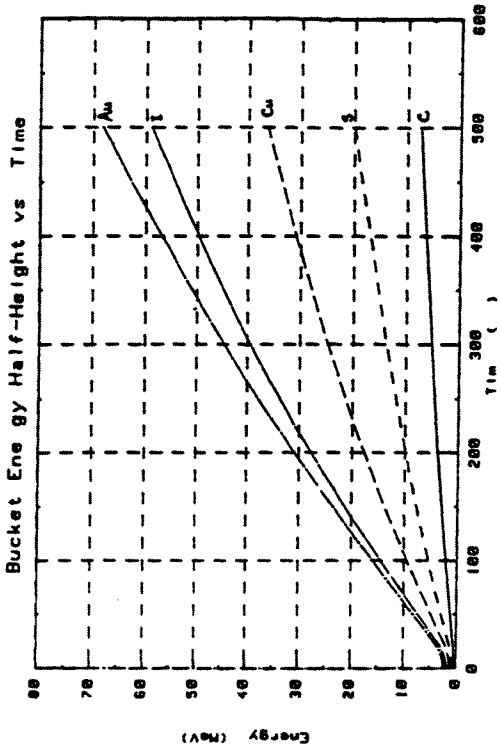

(d) Bucket energy half height

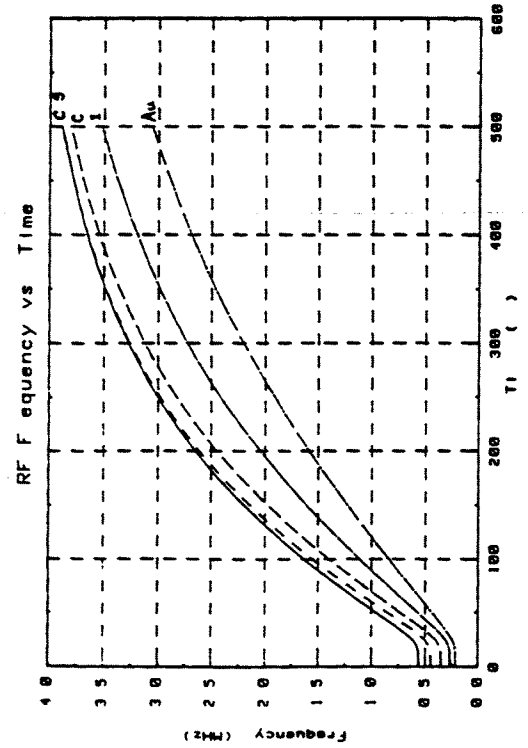

(a) RF frequency

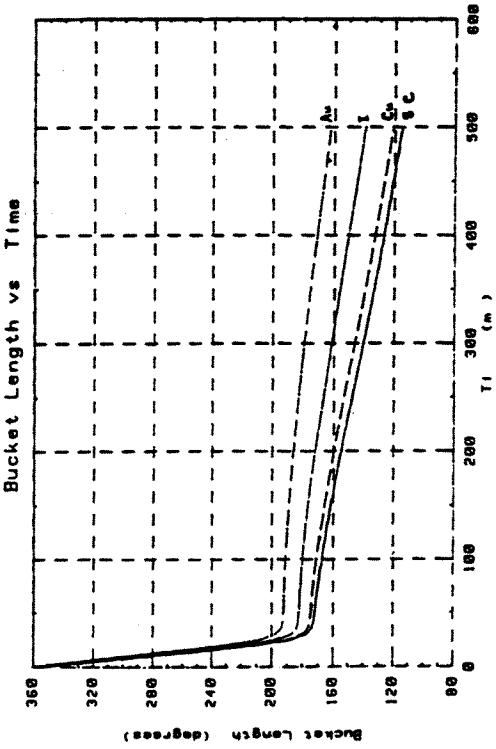

(c) Bucket length

Figure 10-2 Graphs of ion cycle parameters, lighter ions

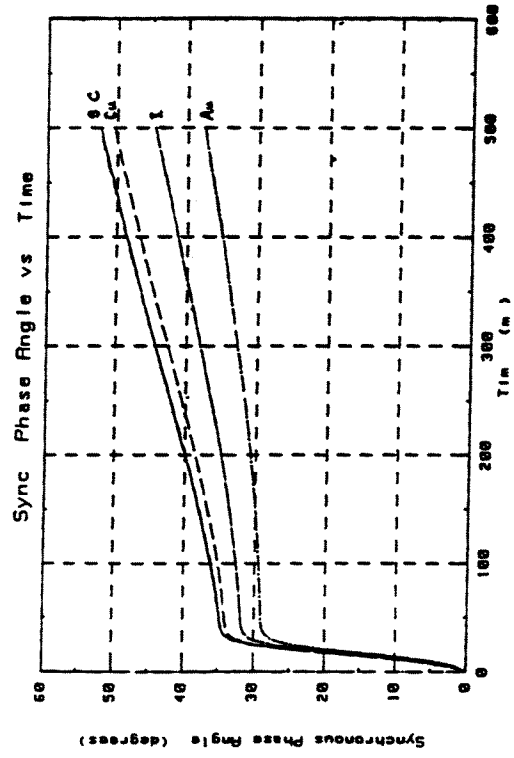

(f) Synch phase angle

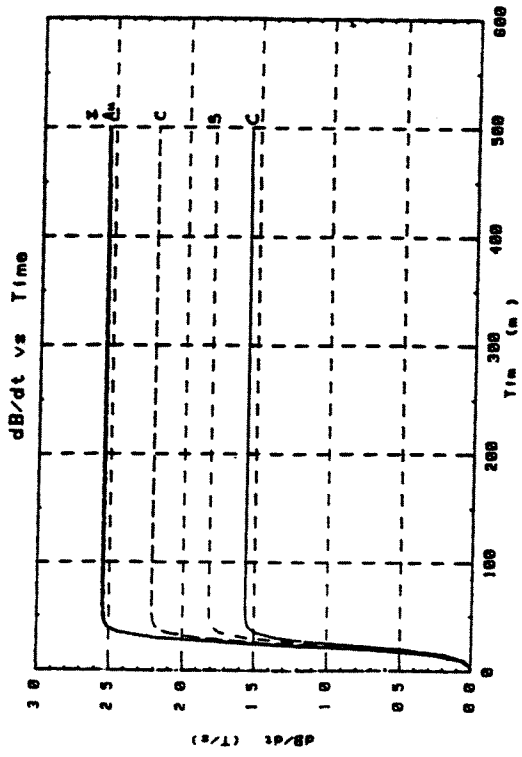

(h) $\dot{B}$

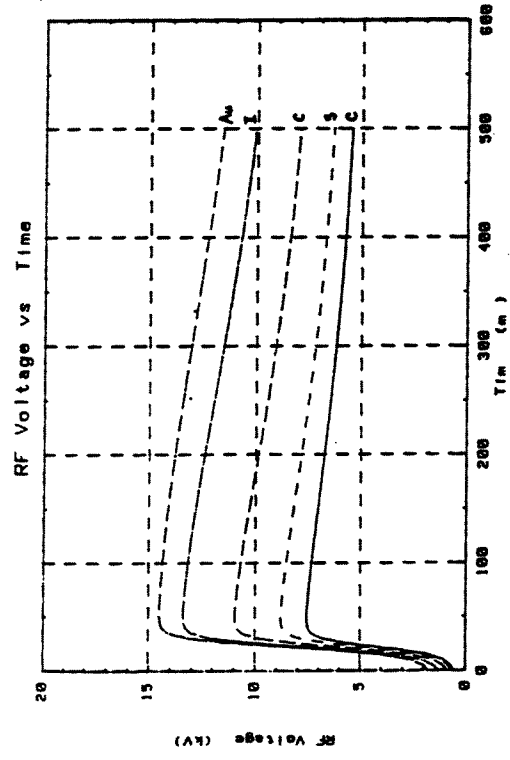

(e) RF voltage

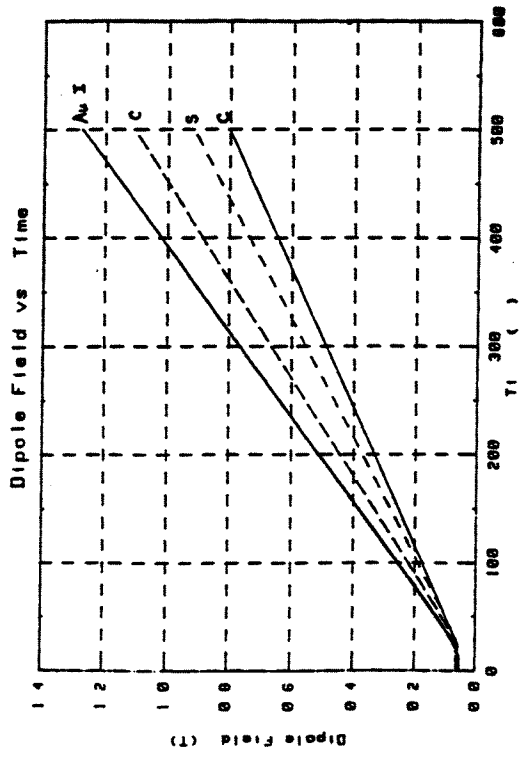

(g) Dipole field

Figure 10-2 Graphs of ion cycle parameters, lighter ions (cont)

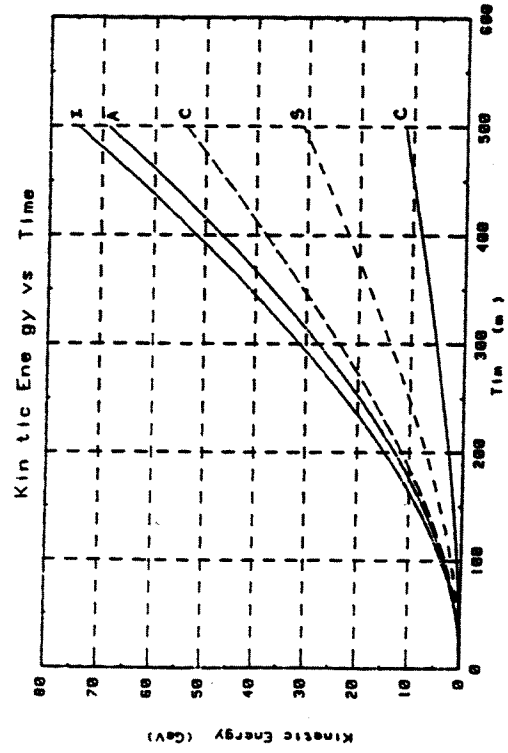

(j) Kinetic energy

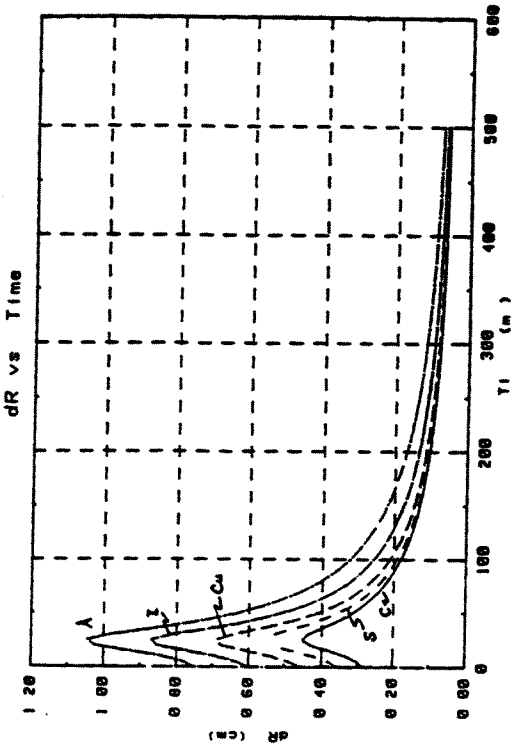

(l) dR

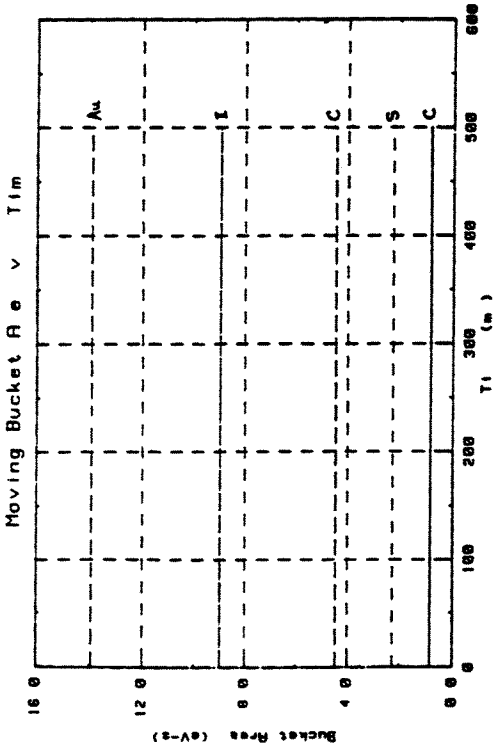

(i) Moving bucket area

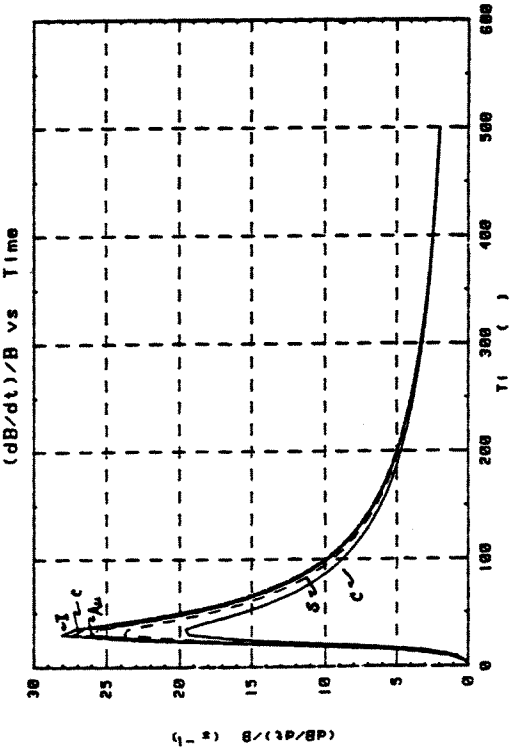

(k) $\dot{B}/B$

Figure 10-2 Graphs of ion cycle parameters, lighter ions (cont)

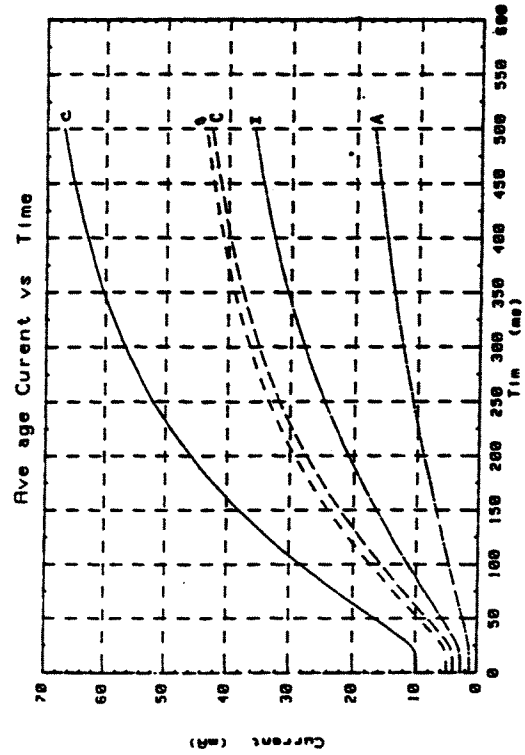

(n) Average current

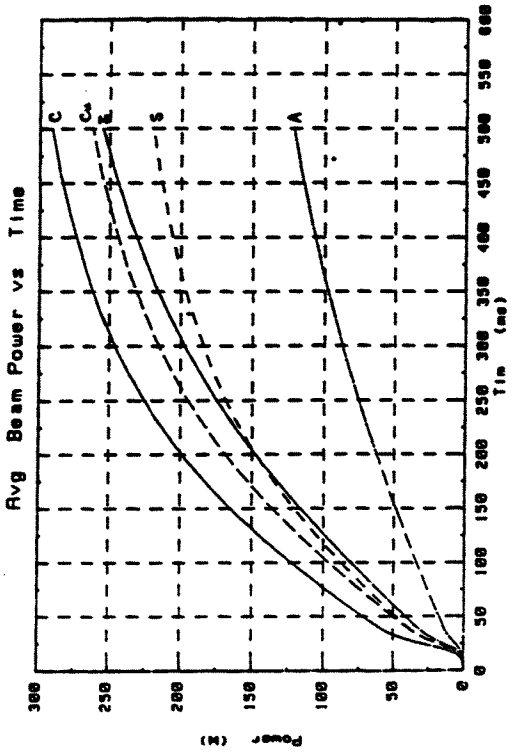

(p) Avg beam power

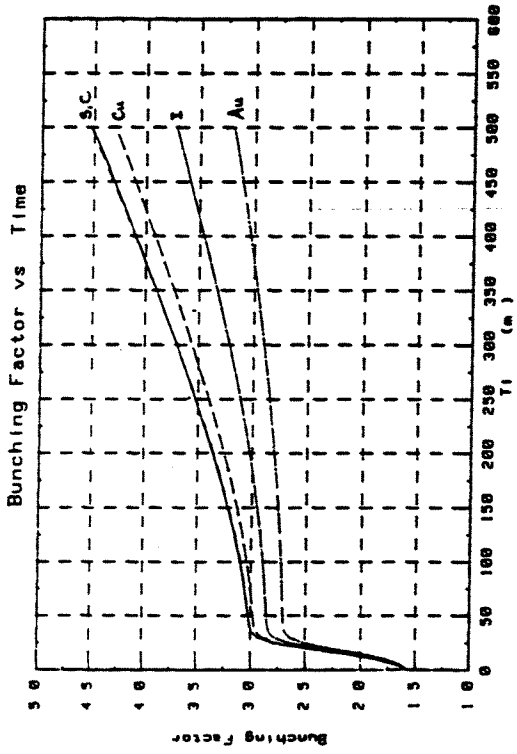

(m) Bunching factor

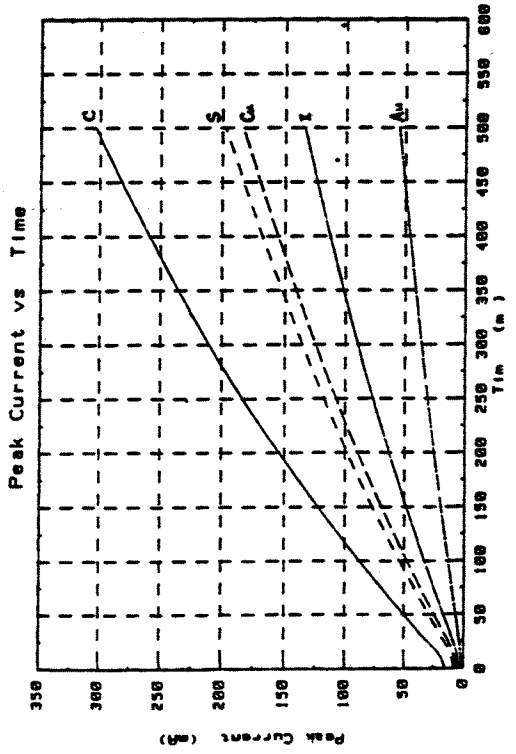

(o) Peak current

Figure 10-2 Graphs of ion cycle parameters, lighter ions (cont)

Acceleration, heavier ions

The acceleration program for gold ions was calculated as in the section above. Then it was discovered that the heavier ions presented a particular difficulty These ions enter the Booster with a relatively small velocity and therefore spend more time being accelerated by the low frequency rf cavity The ferrite in this cavity shows an instability for cavity voltages greater than about 8 kV It is thus necessary to alter the cycle so that dB/dt, after an initial rise, is held constant at a value that allows the 0.07 eV-s/nucleon bucket area to be maintained with an rf voltage that is less than 8 kV until the ion has been accelerated to a velocity that allows the next cavity to take over the acceleration. (This transfer can take place at an rf frequency of 600 kHz.)

Once the cycle has been modified to satisfy this criterion, the ions can no longer be accelerated to their ejection energies within 500 ms unless dB/dt is allowed to rise to levels much higher than 2.55 T/s. However, if a maximum value for dB/dt of 3.2 T/s is adopted, then an acceleration cycle of just over 600 ms is possible. This cycle is shown in the following graphs.

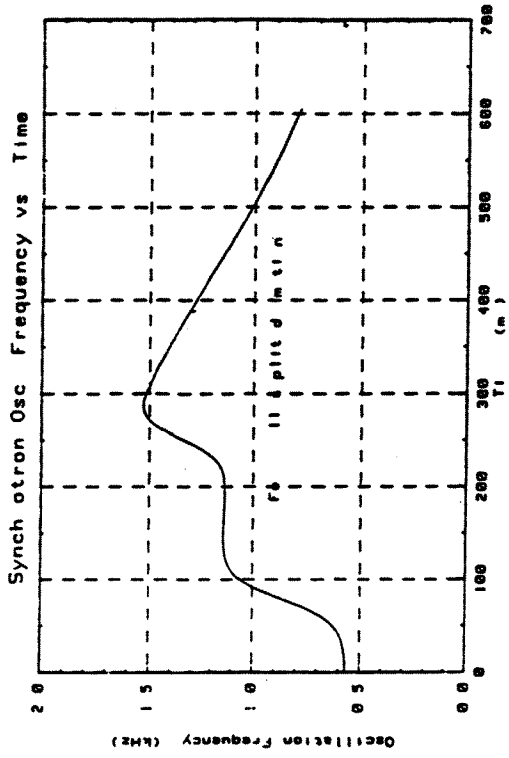

(b) Synchronous oscillation frequency

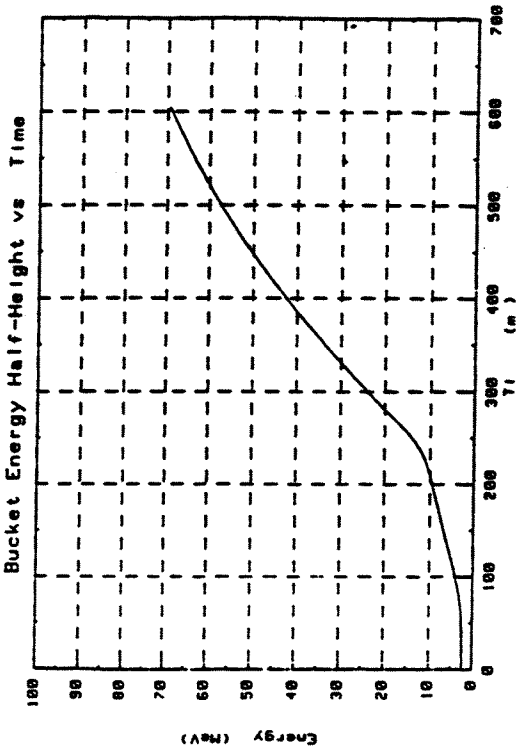

(d) Bucket energy half height

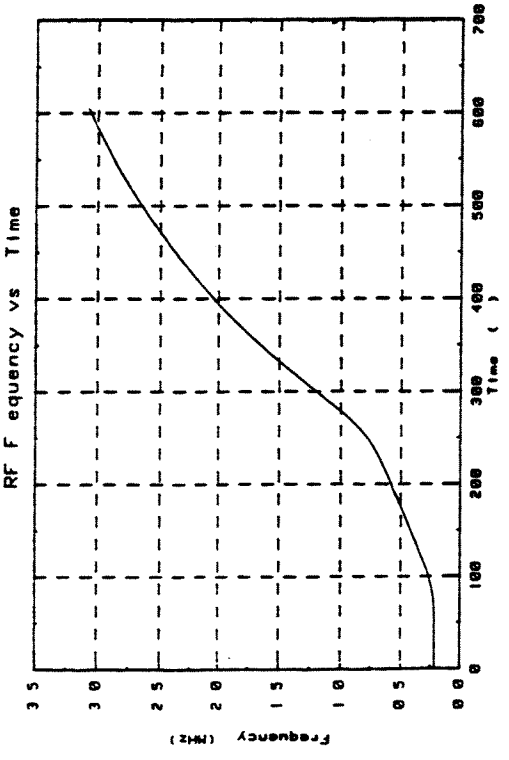

(a) RF frequency

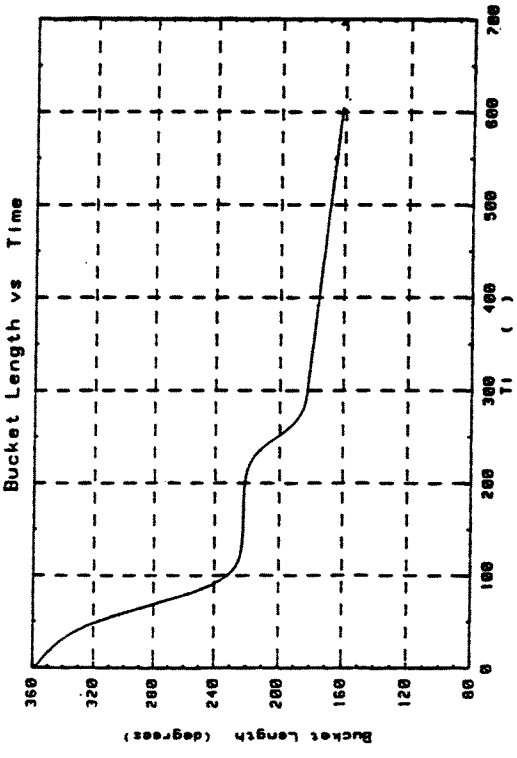

(c) Bucket length

Figure 10-3 Graphs of heavy ion cycle parameters, $^{197}Au^{+33}$

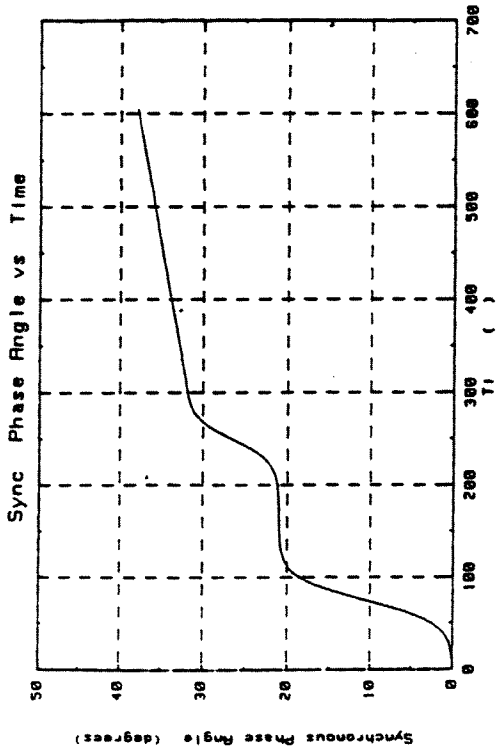

(f) Synchronous phase angle

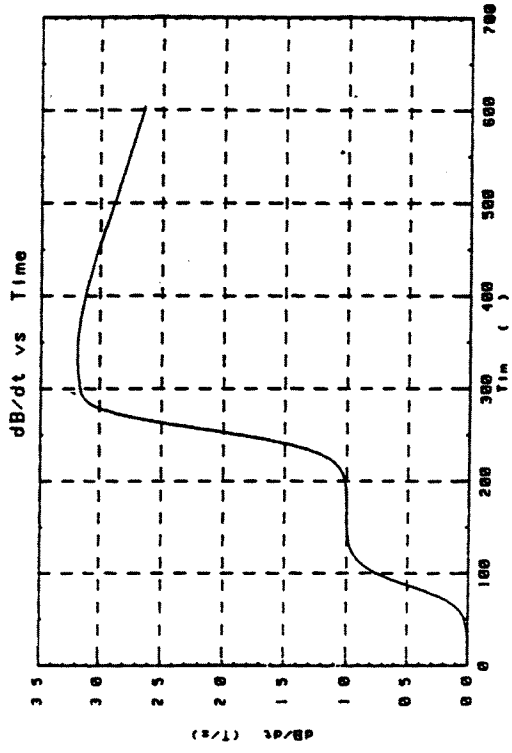

(h) $\dot{B}$

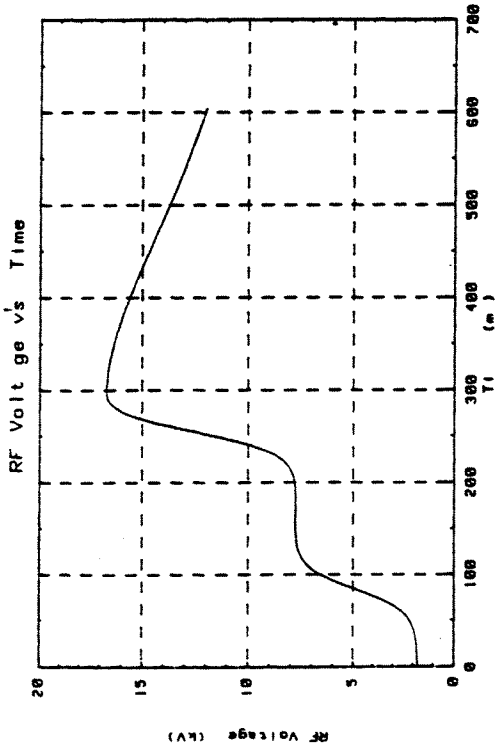

(e) RF voltage

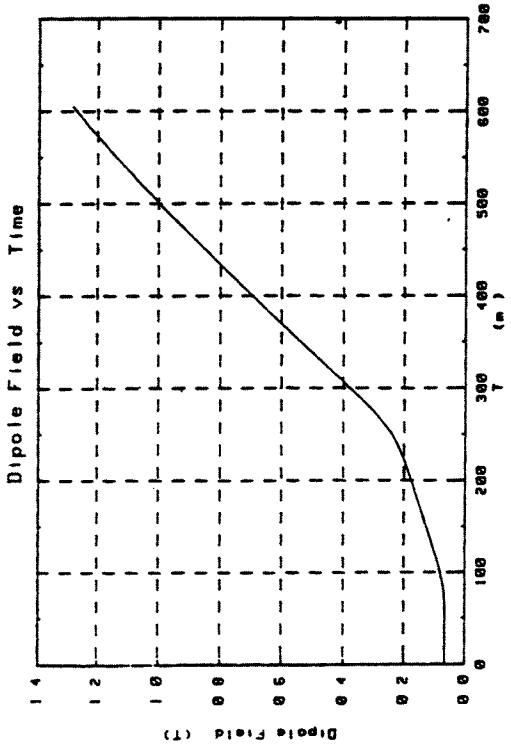

(g) Dipole field

Figure 10-3 Graphs of heavy ion cycle parameters, $^{197}Au^{+33}$ (cont.)

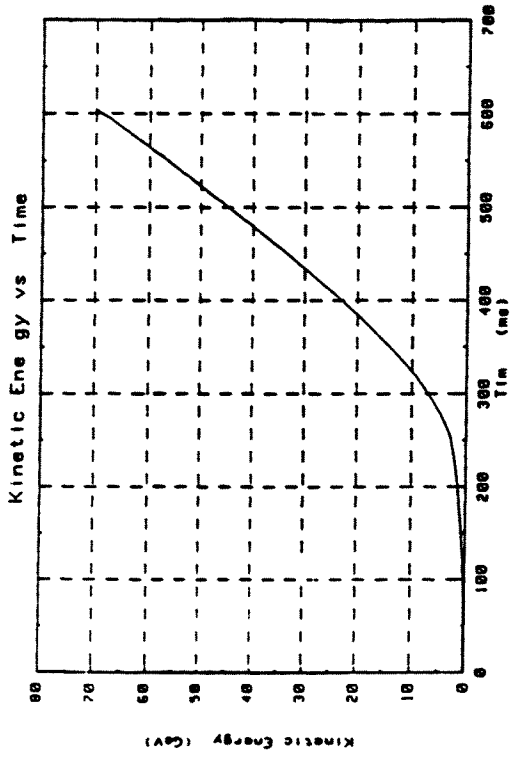

(j) Kinetic energy

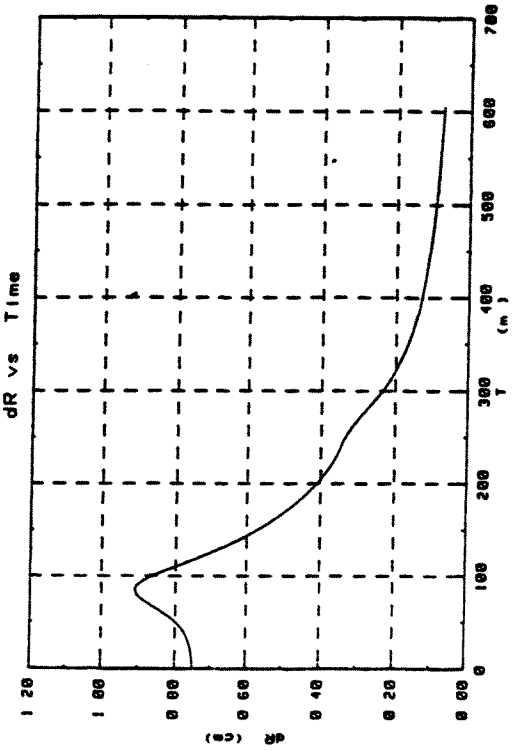

(l) *dR*

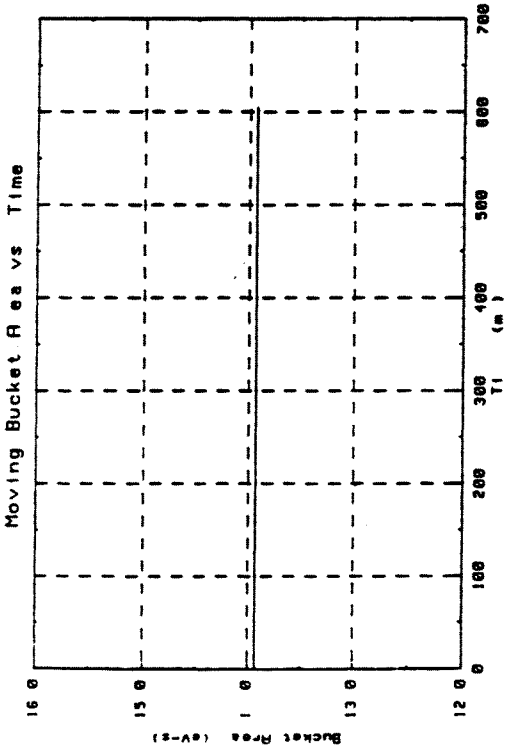

(j) Moving bucket area

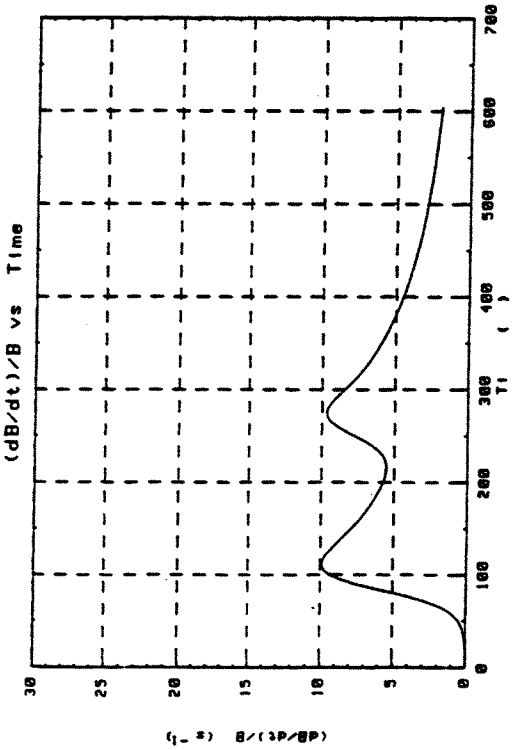

(k) $\dot{B}/B$

Figure 10-3 Graphs of heavy ion cycle parameters, $^{197}Au^{+33}$ (cont)

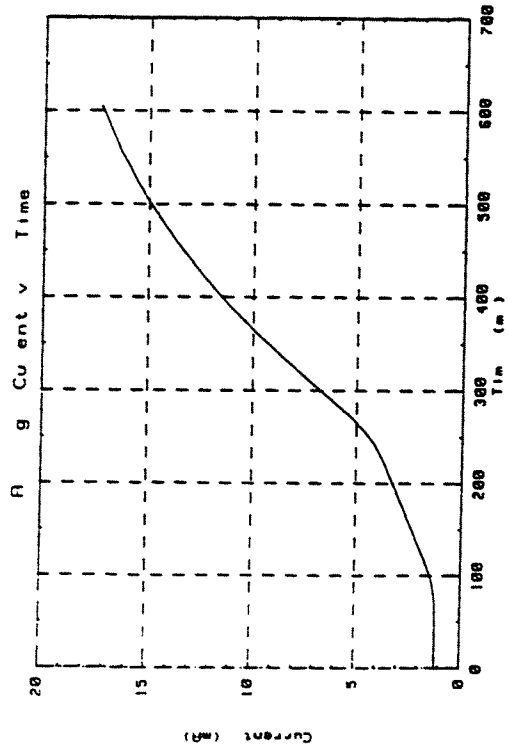

(n) Average current

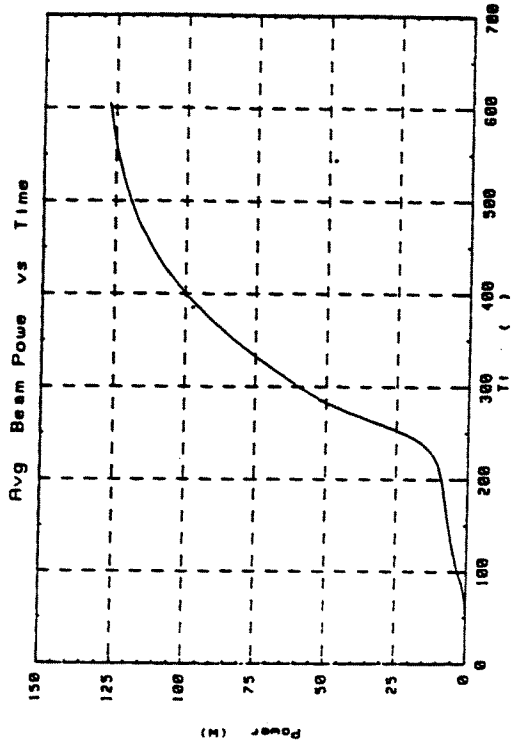

(p) Average beam power

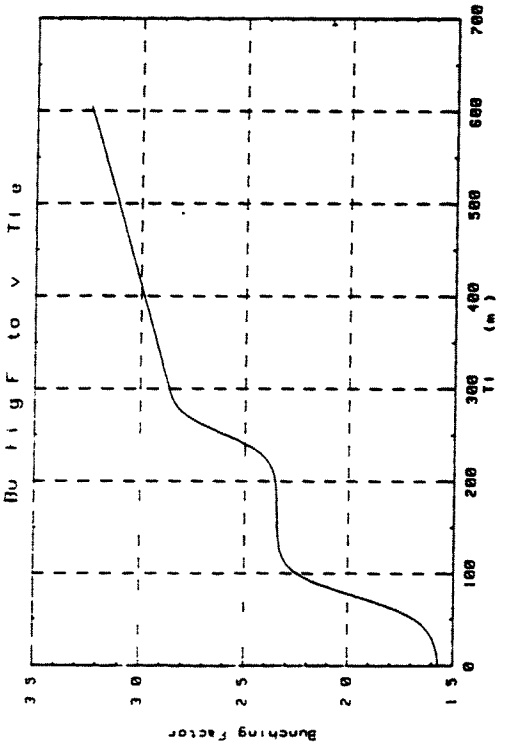

(m) Bunching factor

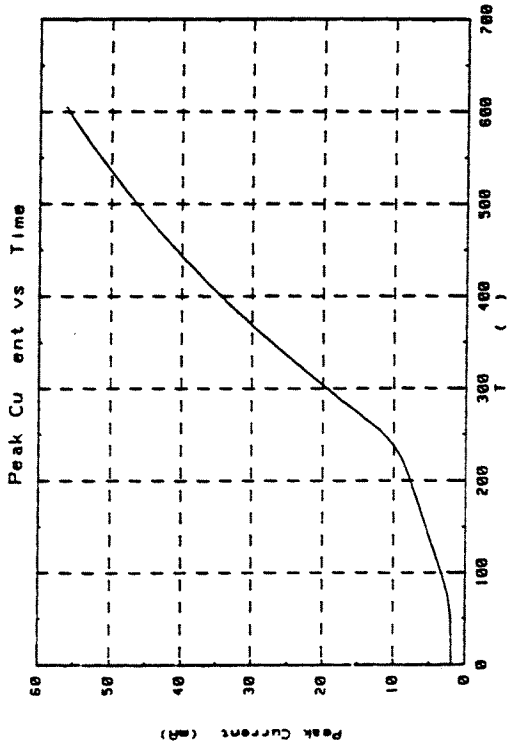

(o) Peak current

Figure 10 3 Graphs of heavy ion cycle parameters, $^{197}Au^{+33}$ (cont)

CHAPTER 11. BOOSTER OPERATION FOR RHIC

11.1. Heavy Ion Particle Intensities in the Collider

As discussed in the 1986 RHIC conceptual design manual[1], the Booster plays a crucial role in the overall performance of the collider In particular, without the Booster, it was decided that it would not be practical to accelerate ions heavier than ^{32}S in the AGS. This was because the vacuum of the AGS (10^{-7} torr) strongly suggested that only fully-stripped heavy ions may be accelerated. Experimental studies[2] on stripping electrons from heavy atoms tell us that for the top Booster kinetic energy of 350 MeV/nucleon, (^{197}Au in a 33^+ charge state), approximately 50% of the heavy ions will be fully stripped on passing through the stripping foil between the Booster and the AGS.

In this chapter we focus on the role played by the Booster in providing a sufficient number of fully stripped ^{197}Au ions to the collider The following discussions illustrate the operation mode of the Booster for RHIC injection and do not necessarily fall solely within the scope of the Booster project. The design specifications for RHIC call for 1.1×10^9 ions/bunch of ^{197}Au. Taking into account the measured stripping foil characteristics[2] at Booster top energy for this species, this corresponds to 2.2×10^9 ions/bunch in the Booster

11.2. h=3 Mode in the Booster

The most recent design performance of RHIC[1] is based on an h=1 radio frequency mode (rf) for the Booster This mode was selected in order to achieve the desired number of heavy ions per bunch for Au, given the expected source currents at the Tandem[1] and the constraint of only accelerating fully stripped ions in the AGS.

In contrast to this original strategy, recent theoretical work[3] has shown quite convincingly that it would be possible to accelerate in the AGS very heavy ions, such as Au, with two electrons in a filled K-shell. This result implies that it should be possible to accelerate Au in an h=3 mode within the Booster and still satisfy RHIC particle intensity requirements. This result also means that it is not necessary to accelerate charge 33^+ Au ions to 350 MeV/nucleon in order to attain the fully stripped charge state on passing from the Booster to the AGS. Only (65-70) MeV/nucleon in the Booster would be required to attain the stripping to the K-shell for Au on passing from the Booster to the AGS. This lower energy for Au allows the stripping foil between the Tandem and Booster (foil S_F in Chapter 4) to be removed, resulting in approximately a factor of four increase in the total particle intensity of Au ions (charge 14^+) entering the Booster from the Tandem.

In Table 11-1 the expected number of Au ions per bunch (h=3) are shown assuming a 200 μA source current and 110 μs pulse at the Tandem. These values at the Tandem have already been achieved. To calculate the Booster harmonic number, the lowest rf frequency was taken to be 215 kHz. In addition to Au, the other heavy ion species of interest are also tabulated. The numbers shown assume a Tandem transmission

TABLE 11-1 Number of Particles/Bunch in the Booster (h=3) for RHIC operation.†

Species	^{12}C	^{32}S	^{63}Cu	^{127}I	^{197}Au
Stripping Foil Efficiency at Foil S_T	39%	30%	27%	20%	12%
Charge at Foil S_T	5	9	11	13	14
Velocity on Entering Booster (β)	0.1261	0.0999	0.0781	0.0595	0.0478
Booster Synchronous Frequency at Injection	187 kHz	148 kHz	116 kHz	88 kHz	71 kHz
Booster Harmonic Number	2	2	2	3	3
Number of Particles per Bunch in Booster	7.76×10^9	7.54×10^9	8.70×10^9	5.64×10^9	4.12×10^9
Booster Space Charge Limit per Bunch	3.3×10^{10}	2.44×10^{10}	1.8×10^{10}	1.0×10^{10}	1.0×10^{10}
Maximum Kinetic Energy at Booster (MeV/nucleon)	1350.8	755.4	345.2	131.4	65.58
RF Frequency at Top Energy	2.71 MHz	2.48 MHz	2.03 MHz	2.15 MHz	1.5 MHz

†Assuming a Tandem source current of 200 μA and a pulse length of 110 μs.

efficiency of 75% and a stacking efficiency of 100% for a eight turn injection into the Booster[4]. Of particular interest is the space charge limit[4] of the Booster for heavy ions. It would seem that the source current can be increased by approximately a factor of two before this limit is reached. A tune shift of 0.3 was assumed for these calculations.

11.3. h=1 Mode in the Booster

It is generally recognized that it is more challenging to build the h=1 rf system than the h=3 system. For instance, at injection for ^{197}Au, the rf frequency would be 71 kHz for the h=1 mode. However, bunching the beam from the Tandem in an h=1 mode would allow a factor of nine increase in the RHIC luminosity

11.3.1. RF System and Acceleration Cycle for Heavy Ions

In Figures 11-1 and 11-2 the voltage and phase requirements of the h=1 rf acceleration are shown, assuming the same B and $\dot{B}$ cycle for heavy ions as in Chapter 10. Comparing the h=1 with h=3 cycles, it can be seen that a maximum voltage of 14 kV would be adequate for the h=1 cycle. The h=3 cycle is designed for a maximum voltage of 17 kV As in Chapter 10, this heavy ion cycle was calculated assuming a constant bucket area of 0.21 eV-s/nucleon.

11.4. Possible Alternatives to the Pure h=1 Mode

The technical challenge of developing an h=1 cavity for the Booster has prompted several investigations of intermediate solutions. These would be useful for increasing particle luminosity within RHIC at a later date. These include: 1) The use of an intermediate Linac, situated between the Tandem and Booster to match the injection frequencies of the h=1 and h=3 modes. 2) Debunching the h=3 mode at top energy into an effective h=1 mode. At top energy (350 MeV/nucleon for charge 33^+ ^{197}Au) the rf frequency for h=1 is 1.02 MHz. 3) Stacking each of the three bunches in an h=3 mode of the Booster into a single bunch in the AGS betatron phase space. This is very analogous to the multiturn injection scheme, currently proposed for heavy ions in the Booster

Of these three alternatives, the first one has been rigorously investigated[5]. The minimum voltage required for an intermediate Linac is,

$$V_L = \frac{(h^2-1)\beta_T{}^2 m_o c^2 A}{2Qe}$$

where Q is the charge state on entering the Linac, β_T is the velocity of the heavy ion from the Tandem and $m_o c^2 A$ the nuclear rest mass. For ^{197}Au, V_L is calculated to be 50.78 MV[5]. This is a substantial machine when measured by any standard and, as a result, strongly implies that the intermediate Linac is not a practical device for the matching proposed here.

The other two suggestions are currently under investigation. Here the study is focussing on particle intensity losses during the debunching or stacking process. At the present time, it seems debunching in the Booster from h=3 to h=1 at top energy is the most practical scheme[6].

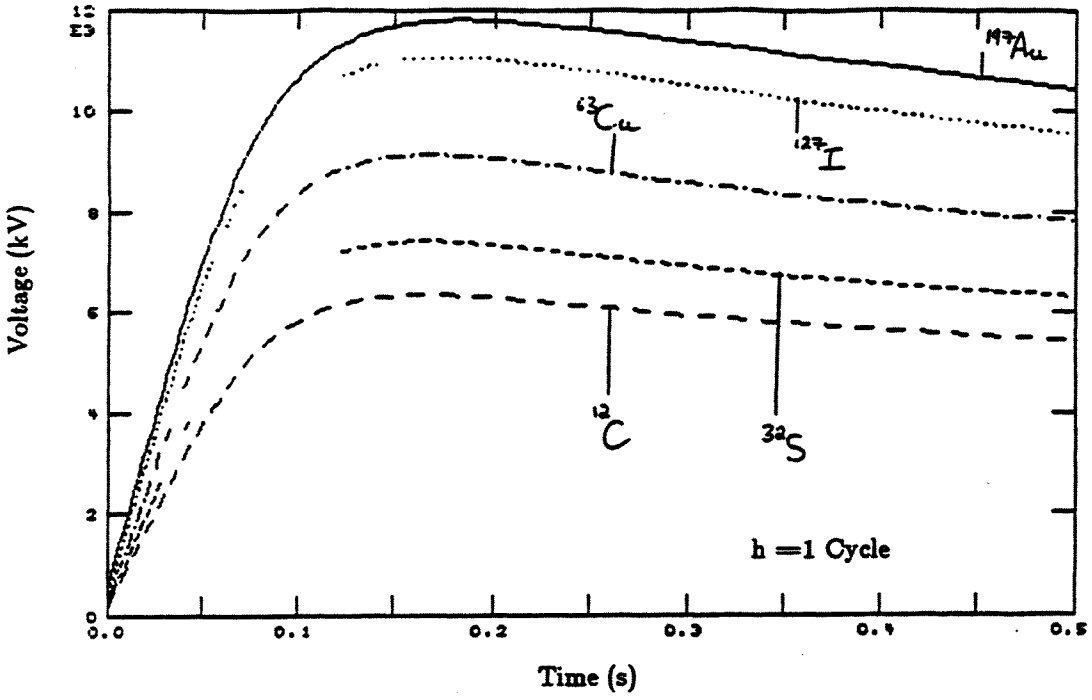

Figure 11-1. Voltage program for h=1 heavy ion acceleration.

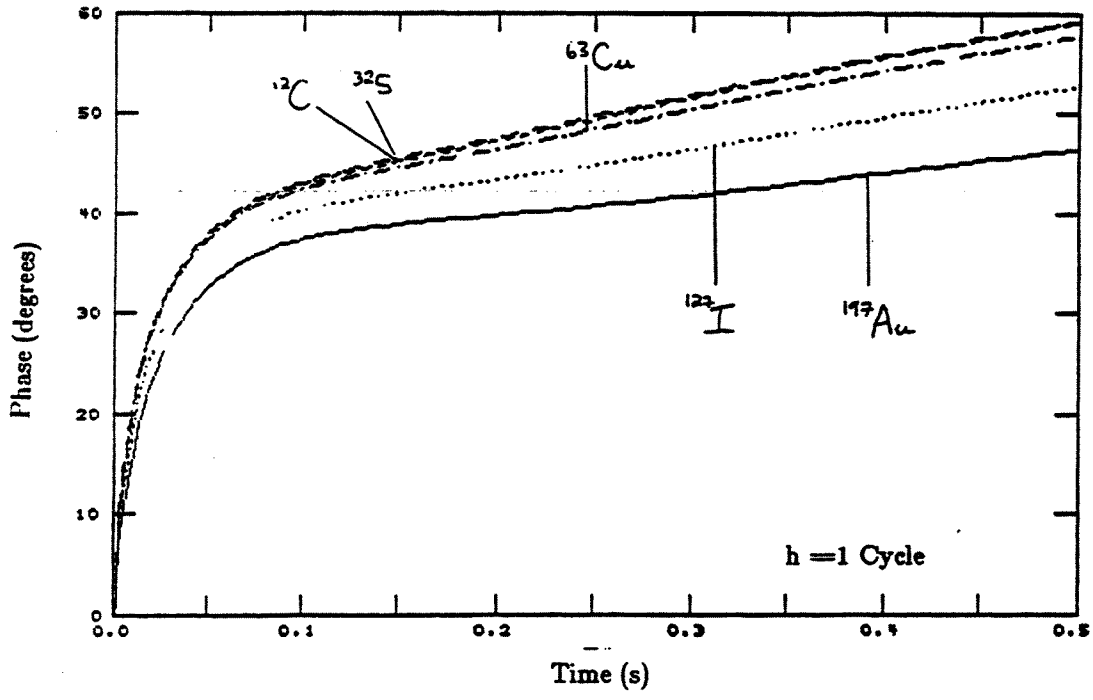

Figure 11-2. Phase program for h=1 heavy ion acceleration.

References

[1] *Conceptual Design of the Relativistic Heavy Ion Collider RHIC.* BNL **51932**, May 1986.

[2] P Thieberger, H. Wegner et. al. IEEE, Vol. **NS-32** (1985), p. 1767

[3] M. J. Rhoades-Brown, "An Alternative Injection Scheme for Heavy Ions into RHIC " RHIC Tech. Note No. **44.**

[4] M. J. Rhoades-Brown and A. G. Ruggiero. "Source Current into the AGS. An Analysis of the RHIC Front-End Injection System." RHIC Tech. Note No. **32.**

[5] M.J. Rhoades-Brown. "The Role of an Intermediate Linac in Matching h=1 to h=3 Heavy-Ion Injection Cycle of the Booster " RHIC Technical Note No. **33.**

[6] J. Wei and J. Claus, private communication.

APPENDIX A. BOOSTER LATTICE RUN AND PLOT

Table A 1 List of Booster parameters at Qx=4 820 Qy=4 830: zero chromaticity and no eddy current sextupoles

Num	Name	L(m)	Bend(rad)	(1/m2)*	bx(m)	Xp(m)	dQx	by(m)	dQy	S(m)
1	QD	0 251875		0 57541623	3 789	0 5462	0 611	13 157	0 603	0 2519
2	S30	0 300000			4 183	0 5664	0 623	12 641	0 607	0 5519
3	BEND	0 400000	0 17463293		9 47	0 9184	0 685	5 413	0 655	2 9519
4	S70	0 400000			11 655	1 0790	0 698	4 247	0 678	3 0519
5	SF	0 000000		0 1821779	11 655	1 0790	0 698	4 247	0 678	3 0519
6	S30	0 300000			12 700	1 1478	0 699	3 853	0 696	3 9519
7	QF	0 251875		-0 55821116	13 158	1 1850	0 103	3 703	0 101	4 2037
8	QF	0 251875		-0 55821116	12 706	1 1804	0 106	3 853	0 111	4 4556
9	S30	0 300000			11 665	1 1498	0 110	4 247	0 123	4 7556
10	BEND	0 400000	0 17463293		5 206	1 0982	0 159	9 087	0 184	7 1556
11	S70	0 400000			4 107	1 1394	0 183	12 641	0 194	7 8556
12	SD	0 000000		0 2949544	4 107	1 1394	0 183	12 641	0 194	7 8556
13	S30	0 300000			3 720	1 1671	0 195	13 157	0 198	8 1556
14	QD	0 251875		0 57541623	3 675	1 1932	0 206	13 644	0 201	8 4075
15	QD	0 251875		0 57541623	3 731	1 2729	0 217	13 157	0 204	8 6594
16	S340	0 700000			12 179	2 0562	0 301	4 247	0 279	12 0594
17	SF	0 300000		0 1821779	12 179	2 0562	0 301	4 247	0 279	12 0594
18	S30	0 300000			13 336	2 7782	0 305	3 853	0 291	12 3594
19	QF	0 251875		0 55821116	13 866	2 8311	0 308	3 703	0 302	12 6113
20	QF	0 251875		-0 55821116	13 435	2 7839	0 311	3 853	0 313	12 8631
21	S30	0 300000			12 389	2 0686	0 315	4 247	0 324	13 1631
22	BEND	0 400000	0 17463293		5 820	1 9186	0 360	9 087	0 385	15 5631
23	S70	0 400000			4 574	1 7515	0 382	12 641	0 396	16 2631
24	SD	0 000000		0 2949544	4 574	1 7515	0 382	12 641	0 396	16 2631
25	S30	0 300000			4 144	1 6799	0 393	13 157	0 400	16 5631
26	QD	0 251875		0 57541623	3 976	1 0501	0 403	13 644	0 402	16 8150
27	QD	0 251875		0 57541623	4 135	1 6808	0 413	13 157	0 406	17 0669
28	S30	0 300000			4 553	1 7535	0 424	12 641	0 409	17 3669
29	BEND	0 400000	0 17463293		9 894	2 5147	0 481	5 413	0 457	19 7669
30	S70	0 700000			12 083	2 7879	0 492	4 247	0 481	20 4669
31	SF	0 000000		0 1821779	12 083	2 7879	0 492	4 247	0 481	20 4669
32	S30	0 300000			13 115	2 9050	0 495	3 853	0 492	20 7669
33	QF	0 251875		0 55821116	13 546	2 9514	0 498	3 703	0 503	21 0188
34	QF	0 251875		0 55821116	13 038	2 8937	0 501	3 853	0 514	21 2706
35	S340	0 700000			4 153	1 4154	0 578	12 641	0 597	24 0706
36	SD	0 000000		0 2949544	4 153	1 4154	0 578	12 641	0 597	24 0706
37	S30	0 300000			3 767	1 2850	0 590	13 157	0 601	24 9706
38	QD	0 251875		0 57541623	3 624	1 1983	0 601	13 644	0 604	25 2225
39	QD	0 251875		0 57541623	3 785	1 1556	0 612	13 157	0 607	25 4744
40	S30	0 300000			4 195	1 1306	0 624	12 641	0 611	25 7744
41	BEND	0 400000	0 17463293		9 644	1 1100	0 685	5 413	0 659	28 1744
42	S70	0 400000			11 923	1 1706	0 695	4 247	0 682	28 8744
43	SF	0 000000		-0 1821779	11 923	1 1708	0 695	4 247	0 682	28 8744
44	S30	0 300000			13 001	1 1934	0 699	3 853	0 694	29 1744
45	QF	0 251875		0 55821116	13 477	1 1912	0 702	3 703	0 704	29 4263
46	QF	0 251875		0 55821116	13 018	1 1470	0 705	3 853	0 715	29 6781
47	S30	0 300000			11 959	1 0697	0 709	4 247	0 727	29 9781
48	BEND	0 400000	0 17463293		5 405	0 6472	0 767	9 087	0 788	32 3781
49	S70	0 700000			4 284	0 5817	0 781	12 641	0 798	33 0781
50	SD	0 000000		0 2949544	4 284	0 5817	0 781	12 641	0 798	33 0781
51	S30	0 300000			3 798	0 5536	0 792	13 157	0 802	33 3781
52	QD	0 251875		0 57541623	3 642	0 5466	0 803	13 644	0 805	33 6300

* B /Brho for quadrupoles and B len/Brho for sextupoles With eddy current sextupoles, SF=-0 03981742 SD=0 49651388

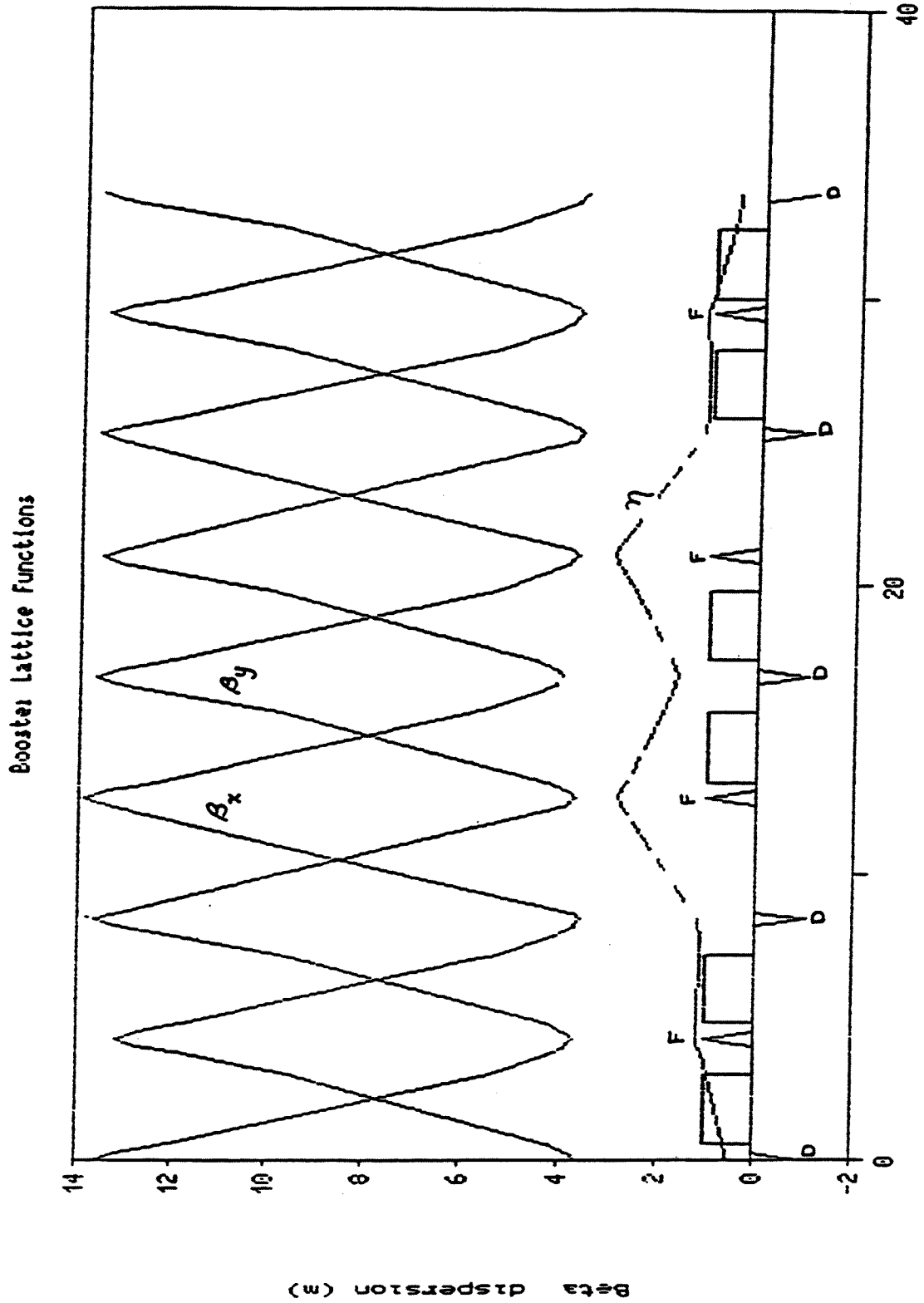

Figure A-1 Amplitude and dispersion functions for the Booster lattice

APPENDIX B. LTB OPTICAL RUN AND PLOT

COMPONENTS IN THE PROTON INJECTION LINE

ELEMENT #	Name	Length (m)	<--APEX Position--> Xbst(m)	Ybst(m)	Next Drift (m)	<--APEX Position--> Eags( )	Nags( )	<--APEX Position--> Esite(ft)	Nsite(ft)
1	PIK1	0 32512	-46 0014	-23 8598	4 500	-662 200	14520 000	98366 267	102360 000
2	PIQF1	0 3	-41 9376	-26 4383	1 000	-502 207	14418 480	98379 602	102351 539
3	PIQD1	0 3	-40 8400	-27 1349	1 000	-458 994	14391 056	98383 203	102349 258
4	PIQF2	0 3	-39 7424	-27 8315	1 000	-415 781	14363 630	98386 805	102346 969
5	PIQD2	0 3	-38 6448	-28 5281	1 000	-372 568	14336 205	98390 406	102344 688
6	PIQF3	0 3	-37 5472	-29 2247	1 200	-329 355	14308 780	98394 008	102342 398
7	PIDL	1 3	-35 8441	-30 3055	0 300	-262 307	14266 230	98399 591	102338 853
8	PIDL	1 3	-34 2106	-30 3300	0 300	-197 994	14265 265	98404 951	102338 772
9	PIQF4	0 3	-33 2500	-29 7601	0 300	-160 174	14287 702	98408 102	102340 641
10	PIDL	1 3	-32 2894	-29 1902	0 300	-122 358	14310 139	98411 254	102342 512
11	PIQF5	0 3	-31 7689	-28 2020	3 723	-101 863	14349 047	98412 961	102345 758
12	PIDL	1 3	-29 6531	-24 1853	2 300	-18 566	14507 183	98419 903	102358 932
13	PIQF6	0 3	-29 8577	-21 0750	1 000	-26 619	14629 636	98419 234	102369 133
14	PIQD3	0 3	-29 9430	-19 7778	2 000	-29 979	14680 707	98418 953	102373 391
15	PIQF7	0 3	-30 0940	-17 4828	1 000	-35 923	14771 063	98418 461	102380 922
16	PIQD4	0 3	-30 1793	-16 1856	2 000	-39 283	14822 134	98418 180	102385 180
17	PIQF8	0 3	-30 3303	-13 8905	1 800	-45 227	14912 489	98417 688	102392 711
18	PIQD5	0 3	-30 4682	-11 7951	1 039	-50 654	14994 988	98417 234	102399 586
19	MDC5beg		-30 5987	-9 8103		-55 794	15073 126	98416 805	102406 094
19	MDC5end		-30 8095	-8 1526	1 000	-64 094	15138 391	98416 109	102411 531
20	MQFC5	0 5	-31 0423	-6 9245		-73 258	15186 743	98415 352	102415 563

OPTICS FOR THE HIGH INTENSITY PROTON

ELEMENT #	Name	Field (T)	Gradient (T/m)	BETA_x (m)	BETA_y (m)	DISPERSION (m)
1	PIK1			3 768	9 294	0 005
2	PIQF1	-	1 4288	14 154	3 549	-0 620
3	PIQD1		-1 6000	5 951	14 741	0 465
4	PIQF2		0 6000	6 648	13 345	0 571
5	PIQD2		1 1630	5 439	17 481	-0 568
6	PIQF3		1 6000	9 772	9 235	-0 789
7	PIDL	0 91	-	3 006	15 537	-0 478
8	PIDL	0 91		1 401	11 754	-1 093
9	PIQF4		1 3245	2 168	5 570	-1 983
10	PIDL	0 91		2 703	4 880	-2 247
11	PIQF5		1 0132	3 802	3 168	-2 917
12	PIDL	0 91		6 444	12 223	-2 182
13	PIQF6		1 0450	15 049	8 828	-3 417
14	PIQD3		1 2039	9 069	15 031	-2 629
15	PIQF7		0 9462	15 010	6 809	-3 225
16	PIQD4	-	0 6651	9 606	8 217	-2 468
17	PIQF8		1 4150	9 594	5 597	-2 118
18	PIQD5		1 6000	0 760	17 031	0 003
19	MDC5beg			5 788	4 676	2 047
19	MDC5end			9 730	3 141	2 645
20	MQFC5	-	0 5546	13 256	3 306	2 951

OPTICS FOR THE POLARIZED PROTON

ELEMENT #	Name	Field (T)	Gradient (T/m)	BETA_x (m)	BETA_y (m)	DISPERSION (m)
1	PIK1			3 768	9 294	-0 005
2	PIQF1	-	1 2455	14 213	3 535	0 622
3	PIQD1	-	-1 5000	7 297	13 770	0 509
4	PIQF2		0 6000	9 773	13 021	0 664
5	PIQD2	-	1 0938	9 042	17 819	0 691
6	PIQF3	-	1 5000	16 529	10 573	0 976
7	PIDL	0 91		5 614	19 354	0 686
8	PIDL	0 91		1 519	15 294	1 249
9	PIQF4	-	1 2221	1 191	7 521	2 131
10	PIDL	0 91	-	2 040	6 276	2 390
11	PIQF5	-	1 5000	4 267	3 604	3 041
12	PIDL	0 91	-	5 988	3 773	-3 002
13	PIQF6	-	1 0019	13 650	10 245	0 029
14	PIQD3	-	-1 0938	8 392	16 324	0 120
15	PIQF7	-	1 0407	11 706	9 467	0 355
16	PIQD4	-	-1 0029	6 335	13 883	0 355
17	PIQF8	-	1 0022	7 370	6 881	0 579
18	PIQD5	-	-1 0009	2 618	11 162	0 440
19	MDC5beg			4 787	5 212	0 555
19	MDC5end			3 941	7 178	0 280
20	MQFC5	-	0 5546	4 049	9 787	0 005

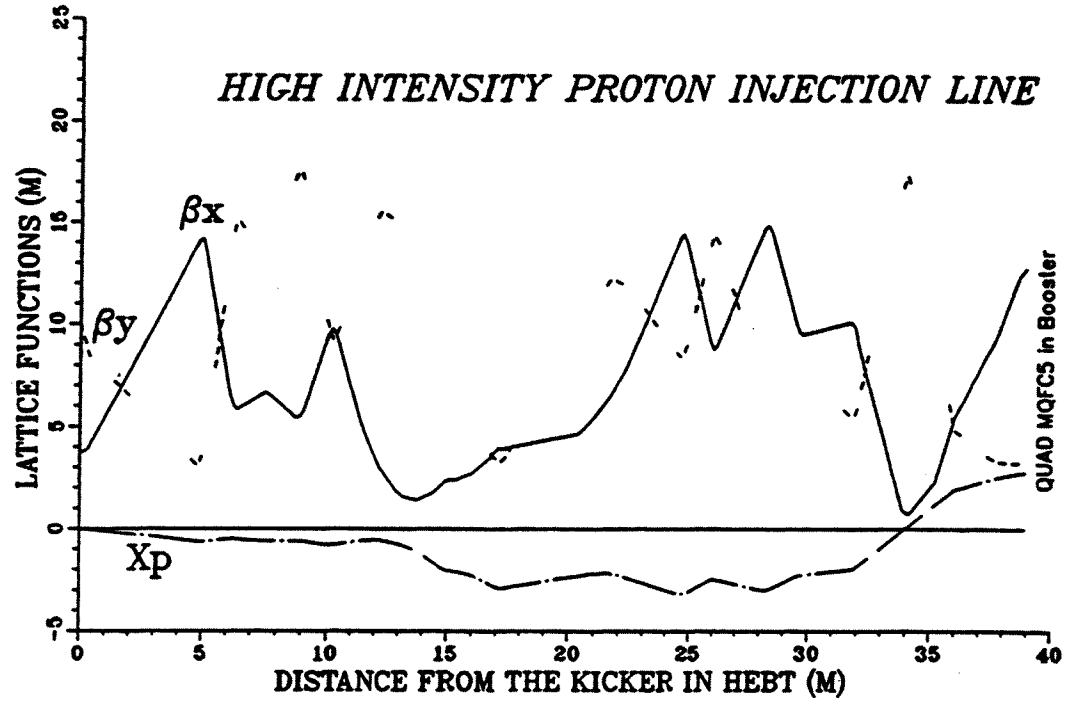
HIGH INTENSITY PROTON INJECTION LINE
LATTICE FUNCTIONS (M)
βx
βy
Xp
QUAD MQFC5 in Booster
DISTANCE FROM THE KICKER IN HEBT (M)

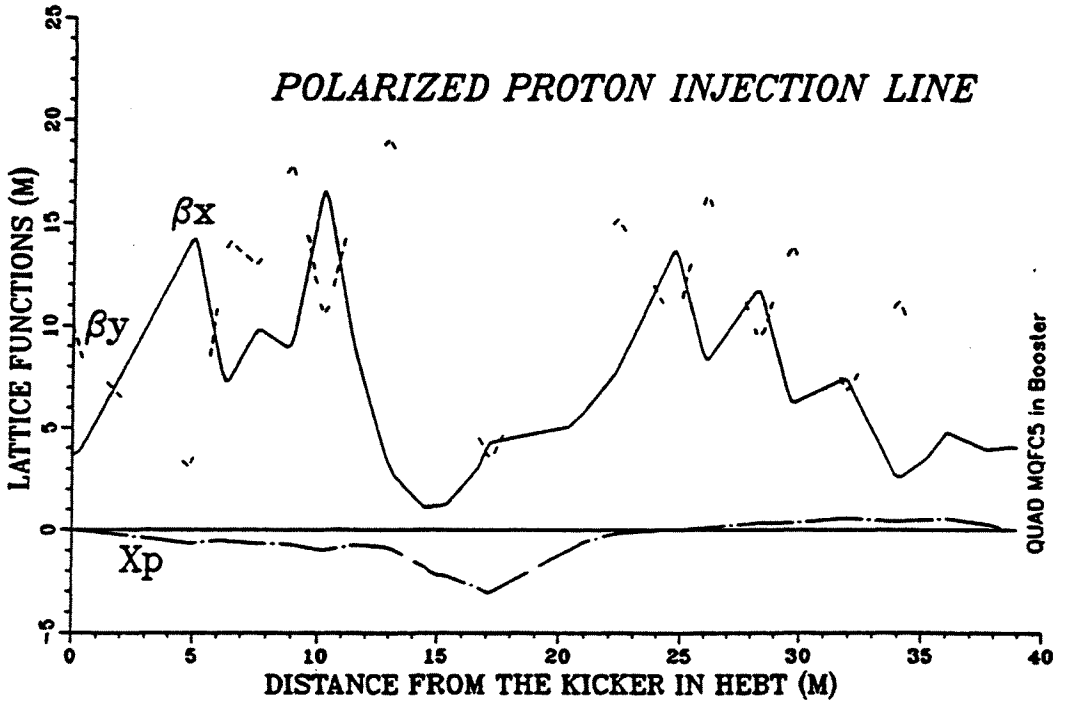
POLARIZED PROTON INJECTION LINE
LATTICE FUNCTIONS (M)
βx
βy
Xp
QUAD MQFC5 in Booster
DISTANCE FROM THE KICKER IN HEBT (M)

APPENDIX C. HTB OPTICAL RUN AND PLOT

NEW HEAVY ION TRANSFER LINE IS BEING DESIGNED

APPENDIX D. BTA OPTICAL RUN AND PLOT

TABLE D-1 Beam optics for BTA line.

Position	s	Q_x	β	α	x	D	Q_y	β_y	α_y
	0.0000	0.000000	3.6345	0.008826	0.530508	-0.014597	0.000000	13.6616	0.000000
Q_d	0.2519	0.010887	3.7818	-0.600621	0.536511	0.062411	0.002970	13.1741	1.912226
S30	0.5519	0.022915	4.1745	-0.708567	0.555235	0.062411	0.006759	12.0585	1.806186
Bend	1.7519	0.060301	6.3516	-1.101036	0.680247	0.145810	0.025974	8.2327	1.382024
Bend	2.9519	0.085044	9.4327	-1.460050	0.904735	0.228100	0.054708	5.4248	0.957862
S30	3.2519	0.089879	10.3386	-1.559653	0.973165	0.228100	0.063991	4.8819	0.851822
S30	3.5519	0.094296	11.3043	-1.659256	1.041595	0.228100	0.074297	4.4026	0.745781
S_f	3.6519	0.095684	11.6395	-1.692457	1.064405	0.228100	0.077974	4.2570	0.710435
S30	3.9519	0.099614	12.6848	-1.792059	1.132834	0.228100	0.089759	3.8626	0.604394
Q_f	4.2037	0.102700	13.1428	-0.004624	1.169927	0.065559	0.100417	3.7121	0.000000
Q_f	4.4556	0.105786	12.6894	1.783459	1.165665	-0.099300	0.111074	3.8626	-0.604394
S30	4.7556	0.109714	11.6489	1.684619	1.135875	-0.099300	0.122859	4.2570	-0.710435
KiB1	5.9556	0.129510	8.0111	1.339221	1.064871	-0.018965	0.159572	6.4710	-1.134596
KiB1	7.1556	0.159083	5.2533	0.953132	1.090416	0.061513	0.183768	9.7031	-1.558758
S30	7.4556	0.168683	4.7141	0.844145	1.108870	0.061513	0.188461	10.6701	-1.664799
S30	7.7556	0.179371	4.2403	0.735158	1.127324	0.061513	0.192735	11.7008	-1.770839
S_d	7.8556	0.183190	4.0969	0.698829	1.133476	0.061513	0.194075	12.0585	-1.806186
S30	8.1556	0.195448	3.7103	0.589842	1.151930	0.061513	0.197863	13.1741	-1.912226
Q_d	8.4075	0.206545	3.5662	-0.010695	1.188585	0.230432	0.200833	13.6616	0.000000
Q_d	8.6594	0.217625	3.7213	-0.612812	1.268717	0.407780	0.203803	13.1741	1.912226
S30	8.9594	0.229827	4.1223	-0.723703	1.391051	0.407780	0.207592	12.0585	1.806186
S25	9.2094	0.239063	4.5072	-0.816112	1.492995	0.407780	0.211019	11.1775	1.717819
S120	10.4094	0.273333	6.9982	-1.259675	1.982331	0.407780	0.231850	7.5638	1.293657
S30	10.7094	0.279803	7.7873	-1.370566	2.104665	0.407780	0.238500	6.8194	1.187617
S35	11.0594	0.286537	8.7919	-1.499938	2.247388	0.407780	0.247190	6.0313	1.063903
KiK	12.0594	0.301953	12.1614	-1.869574	2.653207	0.403859	0.278807	4.2570	0.710435
S30	12.3594	0.305705	13.3165	-1.980465	2.774365	0.403859	0.290593	3.8626	0.604394
Q_f	12.6113	0.308640	13.8473	-0.102264	2.826454	0.008524	0.301250	3.7121	0.000000
Q_f	12.8631	0.311564	13.4171	1.790268	2.778634	-0.387112	0.311907	3.8626	-0.604394
S30	13.1631	0.315270	12.3711	1.696245	2.662500	-0.387112	0.323693	4.2570	-0.710435
KiB2	14.3631	0.333722	8.6770	1.374400	2.240751	-0.315358	0.360406	6.4710	-1.134596
KiB2	15.5631	0.360721	5.8074	1.010794	1.906601	-0.241205	0.384601	9.7031	-1.558758
S30	15.8631	0.369387	5.2323	0.906357	1.834239	-0.241205	0.389294	10.6701	-1.664799
S30	16.1631	0.379001	4.7198	0.801920	1.761878	-0.241205	0.393568	11.7008	-1.770839
S_d	16.2631	0.382431	4.5629	0.767108	1.737757	-0.241205	0.394908	12.0585	-1.806186
S30	16.5631	0.393433	4.1340	0.662671	1.665396	-0.241205	0.398696	13.1741	-1.912226
Q_d	16.8150	0.403399	3.9669	0.008580	1.634731	-0.003029	0.401667	13.6616	0.000000
Q_d	17.0669	0.413376	4.1251	-0.644244	1.663861	0.235036	0.404637	13.1741	1.912226
S30	17.3669	0.424414	4.5425	-0.747153	1.734371	0.235036	0.408425	12.0585	1.806186
Bend	18.5669	0.459045	6.7848	-1.116673	2.061783	0.310304	0.427640	8.2327	1.382024
Bend	19.7669	0.482432	9.8754	-1.452263	2.478157	0.383211	0.456375	5.4248	0.957862
S30	20.0669	0.487061	10.7751	-1.546712	2.593120	0.383211	0.465658	4.8819	0.851822
S30	20.3669	0.491308	11.7315	-1.641161	2.708084	0.383211	0.475964	4.4026	0.745781
S40	20.7669	0.496446	13.0948	-1.767093	2.861368	0.383211	0.491426	3.8626	0.604394
Q_f	21.0188	0.499440	13.5250	0.079164	2.906749	-0.023932	0.502083	3.7121	0.000000
Q_f	21.2706	0.502444	13.0169	1.914327	2.849383	-0.430230	0.512741	3.8626	-0.604394
S30	21.5706	0.506280	11.9005	1.806821	2.720314	-0.430230	0.524526	4.2570	-0.710435
Spt1	22.5706	0.521997	8.6452	1.448467	2.253153	-0.504094	0.556143	6.0313	-1.063903
SLSP	22.6706	0.523869	8.3591	1.412631	2.202743	-0.504094	0.558736	6.2477	1.099250

Position	*s*	Q_x	β	α	*z*	*D*	Q_y	β_y	α_y
Spt2	24.0706	0.558241	5.1061	0.910936	1.448754	-0.573033	0.587049	10.0184	-1.594105
SSTQ	24.9706	0.591181	3.7567	0.588417	0.933025	-0.573033	0.599530	13.1741	-1.912226
SQH	25.2225	0.602272	3.4830	0.498156	0.788692	-0.573033	0.602465	14.1598	2.001256
SQH	25.4744	0.614189	3.2548	0.407896	0.644359	-0.573033	0.605199	15.1903	2.090286
S30	25.7744	0.629385	3.0423	0.300390	0.472449	-0.573033	0.608217	16.4763	-2.196326
S60	26.3744	0.662273	2.8109	0.085377	0.128629	-0.573033	0.613581	19.2391	2.408407
EQ_d1	26.8744	0.688602	3.5574	-1.698741	-0.153635	-0.579056	0.617804	16.9993	6.514944
S50	27.3744	0.706583	5.5292	2.244891	-0.443163	-0.579056	0.623592	11.1233	5.237111
ED1	27.8744	0.718529	8.0378	-2.770019	-0.723245	-0.541149	0.632938	6.5251	3.959278
DR1	28.3744	0.726966	11.0775	-3.309536	-0.993820	-0.541149	0.650376	3.2047	2.681444
EQ_f2A	28.8744	0.733707	11.5805	2.388427	-1.132339	-0.001402	0.687151	1.6148	0.757641
EQ_f2B	29.3744	0.742155	7.0539	5.901907	-0.995165	0.538686	0.742937	1.4255	-0.348299
DR2	30.3188	0.832544	0.4370	1.104525	-0.486432	0.538686	0.821528	2.7849	-1.091158
EQ_d3	30.8188	1.107677	0.6368	-1.536687	-0.267511	0.355060	0.847013	3.2482	0.242798
Strip	31.2188	1.156913	2.7107	-3.648088	-0.125487	0.355060	0.867109	3.1061	0.112392
Sben	32.2188	0.181739	15.2854	-8.926592	0.229572	0.355060	0.918418	3.2073	-0.213625
EQ_f4	32.7188	0.186191	18.5162	3.259334	0.356559	0.137563	0.939853	4.8673	-3.495320
S50	33.2188	0.190902	15.4138	2.945467	0.425341	0.137563	0.951861	9.0415	-4.853089
ED2	35.6207	0.236454	4.5782	1.513888	1.070393	0.399895	0.970359	47 4452	10.912580
S40	36.0207	0.252425	3.4821	1.226274	1.230351	0.399895	0.971588	56.5802	11.924985
EQ_d5	36.5207	0.277473	3.1710	-0.553838	1.593534	1.082585	0.972964	54.3729	15.970335
SRT	37.5958	0.321726	4.8383	-0.996880	2.757451	1.082585	0.977563	25.4760	10.907375
ED3	39.9977	0.373126	11.5417	-1.761886	5.587779	1.275649	1.294709	0.2721	-0.560543
S50	40.4977	0.379528	13.3925	-1.939686	6.225603	1.275649	1.411799	2.0402	-2.975679
EQ_f6	40.9977	0.385463	12.5070	3.583707	6.192528	1.405604	1.433348	7.2144	-8.094096
SBSH	42.3977	0.414873	4.6420	2.034162	4.224682	-1.405604	1.445339	47.9485	21.001709
EQ_d7	42.8977	0.434827	3.7100	-0.032725	3.978478	0.402430	1.446791	58.0992	2.242933
SSH	51.3977	0.615005	23.7617	-2.326298	7.399133	0.402430	1.480916	27 4689	1.360625
EQ_f8	51.8977	0.618282	24.1598	1.551594	7.300467	-0.794432	1.483806	28.3424	-3.154420
SXSH	52.8196	0.624734	21.4188	1.421569	6.568069	-0.794432	1.488500	34.4870	-3.510611
ED4	52.9758	0.625907	20.9713	1.443886	6.444344	-0.790017	1.489210	35.5929	-3.570949
SDF1	55.1317	0.645028	15.4293	1.126765	4.741173	-0.790017	1.497129	52.7856	-4.403890
EQ_d9	55.6317	0.650178	16.0705	2.457299	4.610045	0.260559	1.498631	51.1937	7 466437
SDF2	57.6810	0.665583	27.9813	-3.354826	5.144011	0.260559	1.507708	25.2469	5.194797
EQ_f10	58.1810	0.668370	28.0208	3.279075	4.972225	-0.940958	1.511075	23.0107	-0.548382
SDF3	63.8675	0.755153	4.2901	0.894051	-0.378583	-0.940958	1.545181	31.0754	-0.869826
EQ_d11	64.3675	0.775391	3.6808	0.343783	-0.861806	-0.999571	1.547746	30.4808	2.040109
SDF4	68.2771	0.939650	5.6360	-0.843898	-4.769666	-0.999571	1.575121	17.1175	1.378013
EQ_f12	68.7771	0.953251	5.8553	0.422426	-4.983787	0.151442	1.579776	17.7531	-2.698337
SDF5	73.5187	1.094663	6.3744	-0.531883	-4.265697	0.151442	1.604285	53.8300	-4.910116
EQ_d13	74.0187	1.105966	8.2811	-3.513850	-4.588175	-1.461174	1.605788	48.9100	14.135841
SDF6	76.6019	1.129478	37.1889	-7.677215	-8.362559	-1.461174	1.638487	3.2779	3.529691
EQ_f14	77.1019	1.131524	38.4430	5.312731	-8.372813	1.420741	1.684104	1.0095	1.260927
S50	77.6019	1.133747	33.3203	4.932621	-7.662442	1.420741	1.830873	0.3900	-0.021880
ED5	78.8364	1.141018	21.7763	4.354101	-5.924161	1.390587	2.029031	4.3539	-3.189127
S5AG	80.5480	1.159948	9.5559	2.785325	-3.543911	1.390587	2.056517	22.7884	-7.580652
S05	80.6028	1.160876	9.2534	2.735101	-3.467707	1.390587	2.056892	23.6270	-7.721248
EQ_d15	81.1028	1.170257	8.2979	-0.703061	-3.089374	0.146967	2.059959	26.7273	1.924104
S05	81.1576	1.171303	8.3755	-0.712930	-3.081320	0.146967	2.060286	26.5169	1.914462
SL20	83.1642	1.203427	11.9617	-1.074279	2.786415	0.146967	2.074334	19.5422	1.561438
S1F	83.4690	1.207374	12.6333	-1.129168	2.741620	0.146967	2.076878	18.6067	1.507814
SptA	84.6782	1.221087	15.6274	-1.346921	2.526983	0.208038	2.088325	15.2174	1.295078
S02	84.6982	1.221291	15.6814	-1.350523	2.522823	0.208038	2.088534	15.1657	1.291559
SptA	85.9074	1.232388	19.2108	-1.568276	2.234339	0.269109	2.102644	12.2994	1.078823
S1F	86.2122	1.234851	20.1835	-1.623164	2.152315	0.269109	2.106695	11.6581	1.025199
SSS	86.2122	1.234851	20.1835	-1.623164	2.152315	0.269109	2.106695	11.6581	1.025199

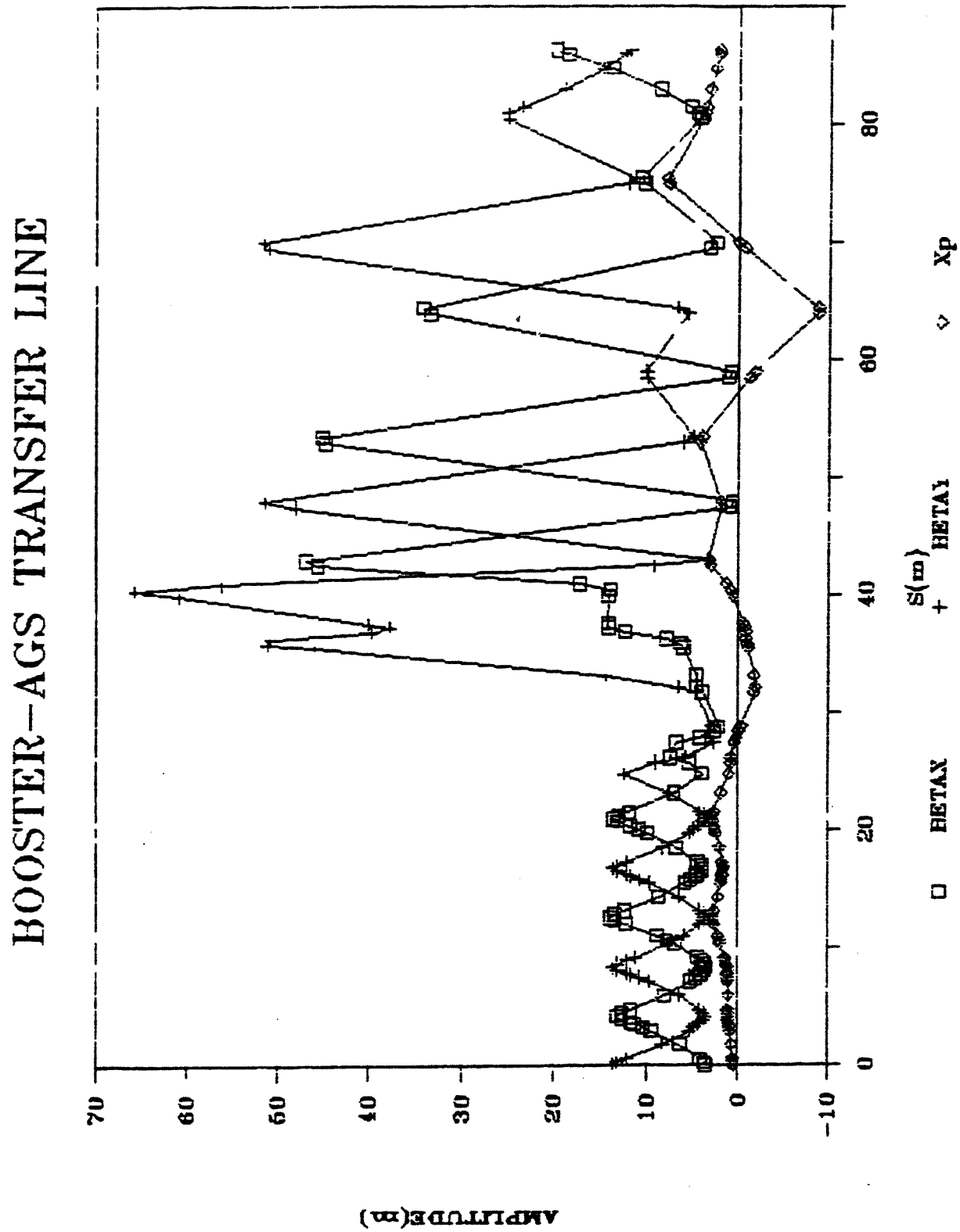
BOOSTER–AGS TRANSFER LINE
AMPLITUDE(m)
S(m)
BETAX
BETAY
Xp
70
60
50
40
30
20
10
0
-10
0
20
40
60
80

APPENDIX E. STRAIGHT SECTIONS

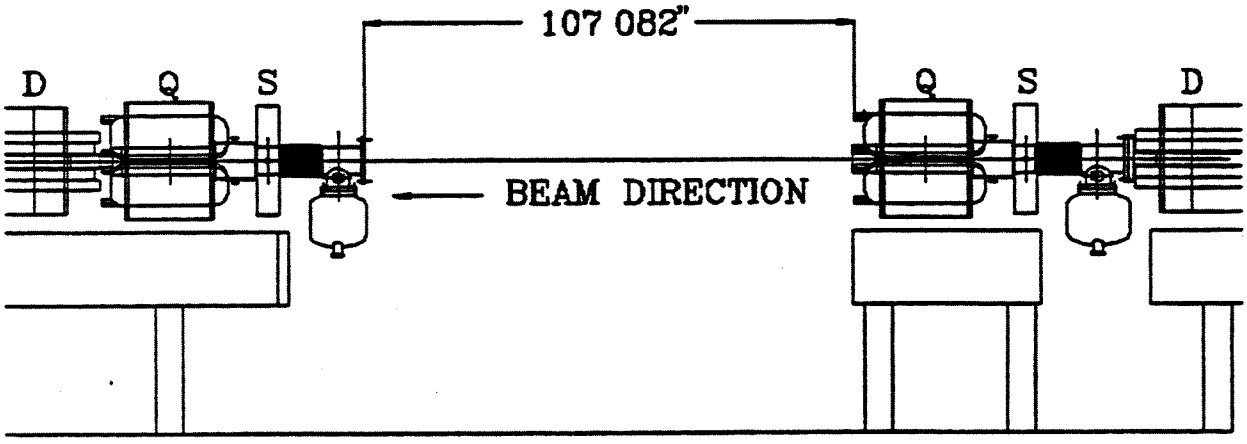

Figure E-1. Free straight section.

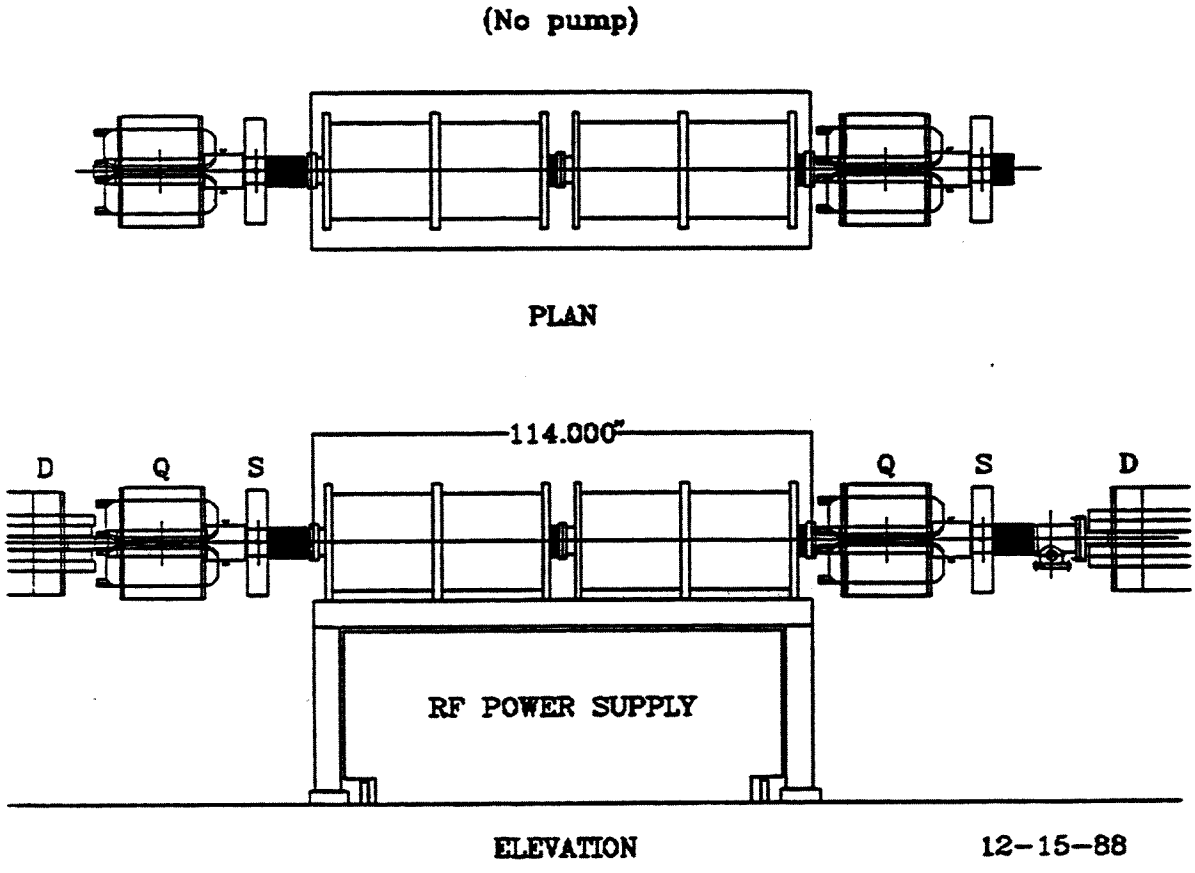

Figure E-2. Booster Cavity Half-Cell A6.

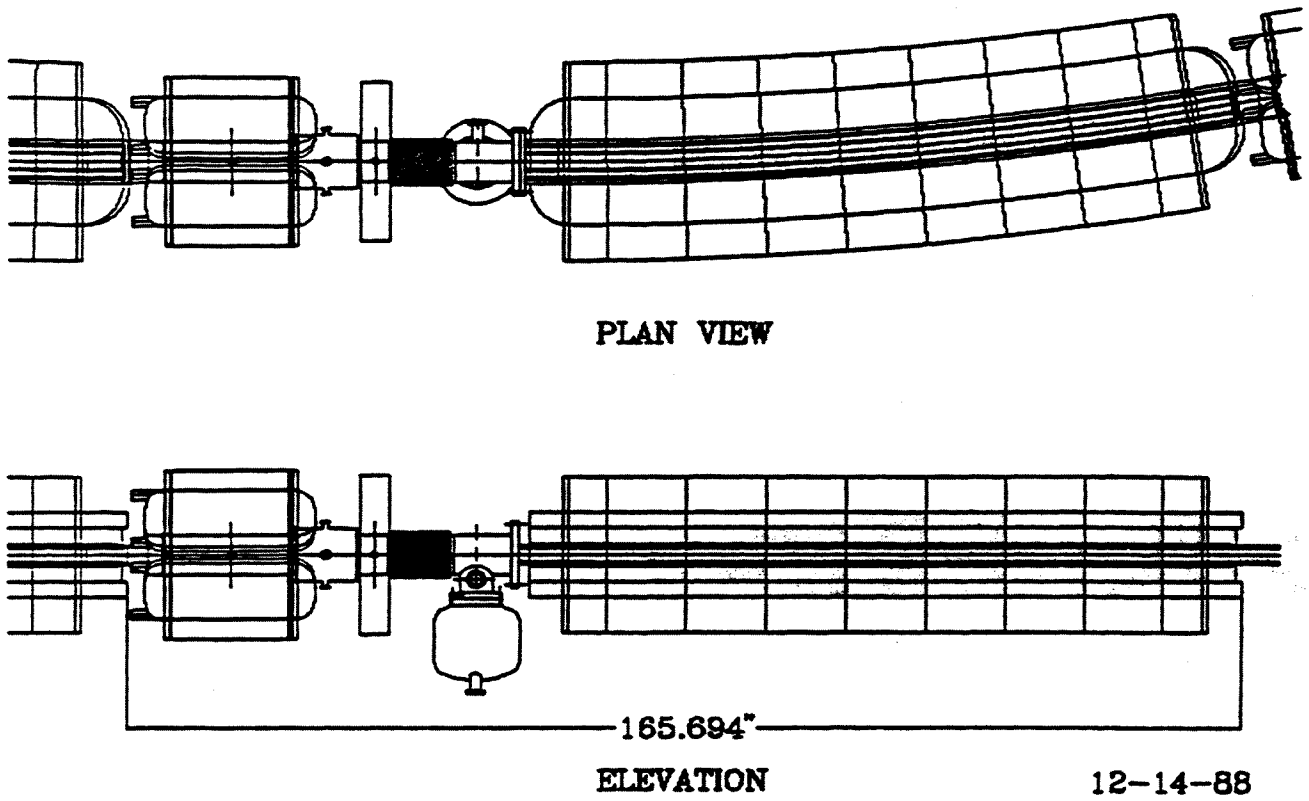

Figure E-3. Booster Dipole Half-Cell A1.

(All dimensions are in inches.)

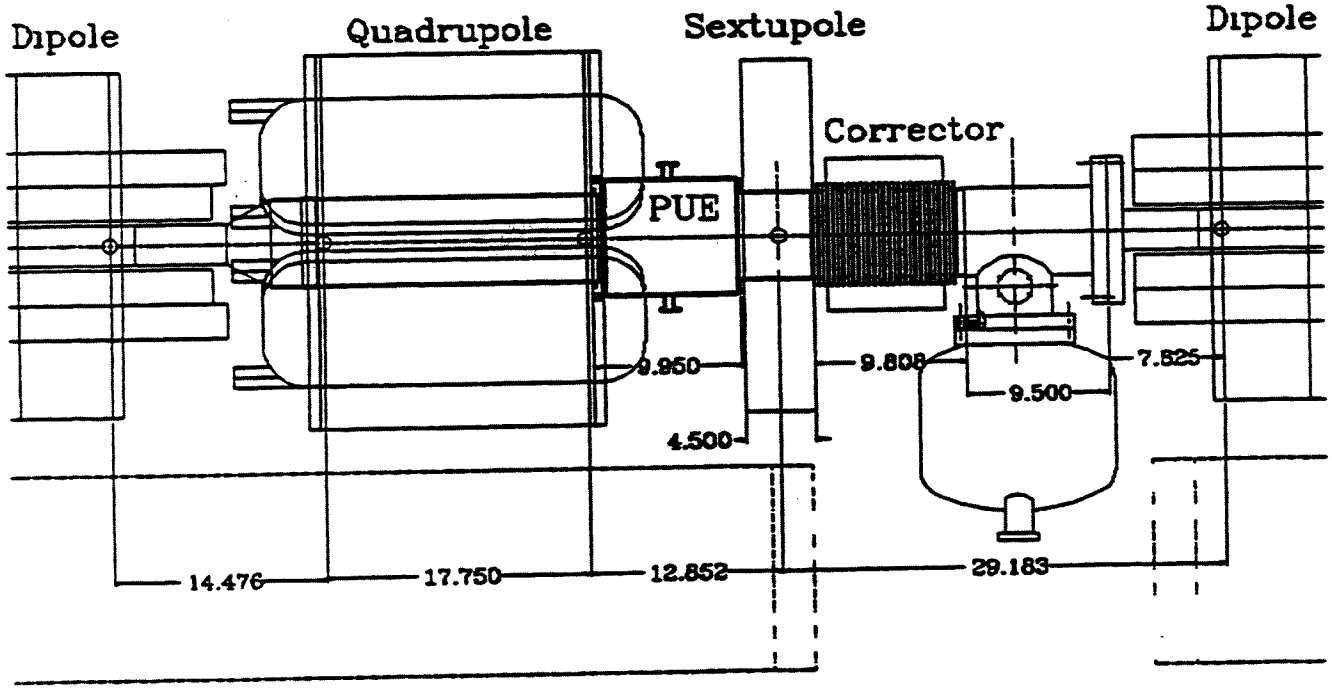

Figure E-4. Booster Correction Package.

APPENDIX F BOOSTER TECHNICAL NOTES

Booster Technical Notes			
Number	Author	Title	Date
1	E. Courant, Z. Parsa	The Booster Lattice	01/15/86
2	Z. Parsa	Booster Parameter List	01/16/86
3	Z. Parsa, F Dell	Booster Coordinates	01/17/86
4	G. Morgan, S. Kahn	Calculation of Eddy Current in the Beam Tube	01/28/86
5	G. Danby, J. Jackson	Booster Dipole Field Computations	01/10/86
6	Z. Parsa	Booster Coordinates	01/28/86
7	R. Gupta, Y Y Lee	The Heavy Ion Injection Line for the AGS Booster	02/06/86
8	G. Morgan	Selection of Magnet Lamination Material and Thickness on the Basis of Eddy Current	02/12/86
9	Y Y Lee	Requirement for the AGS Booster Correction Elements	02/12/86
10	Z. Parsa	Booster Parameter List with 1,2, 4,7 Sextupole Configurations	02/12/86
11	King-Yuen Ng	Single Bunch Instabilities of the RHIC Booster	02/28/86
12	E. Raka	RF Beam Loading in the Booster	02/28/86
13	H. Halama	Notes on Booster Vacuum	02/27/86
14	J. Cottingham	Ejection Septum Concept Design	03/05/86
15	G. F Dell, S. Y Lee, G. Parzen	The Dynamical Aperture of Booster	03/05/86

Booster Technical Notes			
Number	Author	Title	Date
16	R. Gupta, S. Y Lee, Y Y Lee, F Zhao	Transfer Line Between the AGS Booster	03/05/86
17	E. Courant, Z. Parsa	Chromaticity Correction for the AGS Booster with 1,2,4,7 Sextupole Configurations	03/05/86
18	G. F Dell	Aperture Study of the AGS Booster w/ and w/o Eddy Current Multipole	03/10/86
19	S. Y Lee, J. M. Wang	Coherent Instability in the Booster	03/10/86
20	Z. Parsa	Booster Parameter List with 40 kV RF Voltage	03/10/86
21	J. Claus	Eddy Current in Booster Vacuum Chambers	03/14/86
22	Y Y Lee	Aperture Comparison Between the AGS and the Booster	03/18/86
23	J. Kats	Evaluation of the Chromaticity Sextupoles for the AGS Booster	03/20/86
24	G. Parzen	Aperture Limitations Due to Non-Linear Coupling	04/02/86
25	Z. Parsa	Booster Parameter List with Enlarged Q5	04/17/86
26	E. Courant, Z. Parsa	Booster Lattice w/ Enlarged Q5 & 1,2,4,7 Sextupole Configuration	04/21/86
27	Z. Parsa	Booster Coordinates with 1,2,4,7 Sextupoles	04/23/86
28	J. G. Cottingham	Consideration Effecting the Booster Magnet Cycle	04/30/86
29	G. Morgan	Effect of Interface Resistance Between Magnet Laminations	04/30/86

Booster Technical Notes			
Number	Author	Title	Date
30	J. G. Cottingham	Booster Vacuum Chamber Considerations	04/30/86
31	J. G. Cottingham	R. F Bucket Area	05/06/86
32	Z. Parsa, S. Tepikian	Alternate AGS-Booster Lattice	05/07/86
33	S. Y Lee	Alternate Conceptual Lattice for the AGS-RHIC Booster	05/16/86
34	Z. Parsa, S. Tepikian	Analysis of Resonances in the AGS Booster	05/17/86
35	Z. Parsa, S. Tepikian	Resonance Analysis for Standard Booster Lattice with Split Tunes	05/30/86
36	J. Kats	Evaluation of the Booster Resonance Lines	05/28/86
37	G. F Dell	Tracking Results From a Hybrid Booster Lattice at Working Points $(\nu_x, \nu_y) = (4.83, 4.82)$ and (3.83 and 3.82)	05/30/86
38	J. G. Cottingham	Four Kicker Injection Into the Booster	05/30/86
39	G. F Dell	Comparison of On & Off Diagonal Working Points for the AGS Separated Function Booster	06/02/86
40	G. F Dell, S. Y Lee	Split Tune Operation of A Hybrid Booster Lattice $\nu_x = 3.820$, $\nu_y = 4.830$	06/05/86
41	G. Parzen	Space Charge Effect in the AGS Booster for High Intensity Proton Operation	05/22/86
42	Z. Parsa, S. Tepikian	Overview of the Structure Resonances in the AGS-Booster Lattices	06/12/86

Booster Technical Notes			
Number	Author	Title	Date
43	Z. Parsa	Booster Parameter List with 60 kV RF Voltage and Increased Ejection Energies	06/18/86
44	R. Phillips	Report of Lamination Contour Measurements using the Korda 83 with Touch Probe	07/29/86
45	M. Meth	Calculation of Booster Power Requirements Based on a Constant RF Bucket Area	06/12/86
46	J. Claus, S. Y Lee	Combined Function Lattice for the AGS-RHIC Booster	06/23/86
47	Y Y Lee, L. G. Ratner	H^- Injection for the AGS Booster	06/23/86
48	A. G. Ruggiero	Comment on Systematic Resonances	07/02/86
49	J. G. Cottingham	Proton Cycle for the Booster	07/02/86
50	G. Morgan	Temperature Rise in the Vacuum Chamber Due to Eddy Currents	07/08/86
51	Y Y Lee	Estimate of Eddy Current Power	07/09/86
52	Y Y Lee	Heavy Ion Acceleration RF Program	07/10/86
53	Z. Parsa	Booster Parameter List with 90 kV RF Voltage	07/17/86
54	M. Meth	Calculation of Booster Power Requirements & Power Line Flicker for 1.5 GeV Proton Operation	07/17/86
55	Y Y Lee	Expected Heavy Ion Intensity in the Booster	07/19/86
56	J. G. Cottingham	Capture and Acceleration of Heavy Ions	07/17/86

Booster Technical Notes			
Number	Author	Title	Date
57	M. Meth	System Layout & Component Values of Dipole and Quadrupole Power Supplies	07/25/86
58	Z. Parsa, S. Tepikian, E. Courant	Fourth Order Resonances in the AGS-Booster Lattice	08/14/86
59	Z. Parsa, S. Tepikian	Analysis of Alternate Booster Lattice using Non-Linear Coupling Complete with Harmonics	08/18/86
60	Z. Parsa	Booster Parameter List	08/21/86
61	Y Y Lee	The AGS Heavy Ion Operation	09/03/86
62	J. G. Cottingham	The Design of Voltage Control Feedback Loops for Multiphase Rectifier Systems	09/16/86
63	B. McDowell	Structural Tests of Selected Prototype Dipole Magnet Vacuum Chambers	10/22/86
64	M. Puglisi, A. Massarotti	The RF System for the Booster· Conceptual Design	09/26/86
65	J. G. Cottingham, G. H. Morgan W L. Stokes	The Effect of Stamping Burrs on Interlamination Resistance	10/24/86
66	P J. Gollon	Booster Tunnel Shielding Calculation	10/24/86
67	G. Morgan	Magnet Lamination Eddy Currents Re-examined	11/04/86
68	G. H. Morgan	Revised Calculation Lamination Interface Resistance	11/10/86
69	S. Y Lee, X. F Zhao	The Linear Effect of the Space Charge Force	12/16/86

Booster Technical Notes			
Number	Author	Title	Date
70	M. Plotkin	Proton Cavity for the AGS Booster	12/18/86
71	B. McDowell	Eddy Current Heating of Booster Dipole Vacuum Chamber	01/21/87
72	S. Y Lee, S. Tepikian, X. F Zhao	On the Operation Window of the Booster Lattice	01/30/87
73	M. Meth	Spectrum Analysis of the Power Line Flicker Induced by the Electrical Test of the Prototype Booster Dipole	02/06/87
74	Z. Parsa	Quick Reference Guide to the Booster Lattice and RF Parameters	03/06/87
75	G. Parzen	No Coupling Window in the Choice of Chromaticity in the AGS Booster	04/03/87
76	G. F Dell	Consideration of the Cross Sectional Profile of the Booster Vacuum Chamber	04/08/87
77	M. Plotkin	General Design Feasibility Curves for Booster Ferrite Cavities	04/22/87
78	G. Parzen	Space Charge the Need for a Vertical Injection Field Bump	05/05/87
79	R. Thomas	H^- Stripping in the Booster Proton Injection Line	05/07/87
80	Zohreh Parsa	Chromaticity Window Operation of the AGS Booster	06/15/87 06/15/87
81	G. Bunce	Polarized Proton Luminosity in RHIC	06/23/87
82	E. Higgins	Some Issues Concerning Beam Sensing Pick-Ups	07/01/87
83	G. Parzen	The Effect of Sextupole Fields on the Space Charge Limit	07/13/87

Booster Technical Notes			
Number	Author	Title	Date
84	M. Meth, A. Ratti	Push-Pull Operation of the RF Cavity	07/20/87
85	M. Plotkin	Booster Proton Cavity with Voltage Reduction during the Cycle	07/29/87
86	A. J. Stevens	Air Activation in the Booster Tunnel	08/06/87
87	R. Gupta, G. Morgan	Magnetic Forces on the Laminations of the Booster Dipole	08/10/87
88	M. Puglisi	Beam Loading Compensation and Robinson Instability Limit	08/15/87
89	A. J. Stevens	Booster Soil, Component and Water Activation	09/01/87
90	R. Gupta, R. Damm, Y Y Lee, & W T Weng	H^- & Heavy Ion Injection Lines for the Booster	09/17/87
91	Z. Parsa, E. Raka	Acceleration Parameters for the AGS Booster	09/17/87
92	M. Meth, A. Ratti	Specifications & Design of RF Power Amplifier for Proton Cavity	09/21/87 09/21/87
93	R. Casey	Additional Booster Shielding Calculations	10/22/87
94	H. C Hseuh, J. Slavik	Outgassing of Booster Dipole Chamber	10/30/87
95	B. McDowell	Development of a Three Point Roll Bend of Booster Dipole Vacuum Chamber	10/30/87
96	W Stokes	Booster Dipole Block Fabrication	11/06/87
97	R. L. Witkover	Beam Instrumentation for the Booster Transport Lines	11/06/87

Booster Technical Notes

Number	Author	Title	Date
98	A. G. Ruggiero	Longitudinal Stability of Individual Bunches in the AGS Booster	11/13/87
99	Z. Parsa	Booster Survey & Linear Lattice Parameters with Program MAD	11/30/87
100	Z. Parsa	AGS Booster Geometry and Coordinates	11/30/87
101	Z. Parsa	AGS Booster Lattice with Thick Lens Sextupole	12/11/87
102	J. Wei, & S. Y Lee	Simulation of the Multiturn Heavy-Ion Injection in the Booster	12/08/87
103	M. Meth	Stability of Screen & Grid Power Supplies for the RF Power Amplifier for the Proton Cavity	12/30/87
104	A. G. Ruggiero	Review of Space Charge Calculations	01/06/88
105	M. Meth	Response of the Co-Generation Plant to Power Swings of the AGS Booster	01/25/88
106	M. Meth, A. Ratti	Frequency Spectrum Generated by AGS Booster Power Swing Heavy Ion Cycle	01/27/88
107	J. Milutinovic & A. G. Ruggiero	Closed Orbit Analysis for the AGS Booster	02/01/88
108	G. Parzen	Space Charge Effects in the AGS Booster	02/01/88
109	Jian Zhang	Calculation of the Booster Proton Cavity Using the "Superfish" Program	02/02/88
110	T Robinson	Some Design Considerations for Extension of HITL to the Booster	02/08/88

Booster Technical Notes			
Number	Author	Title	Date
111	G. F Dell	Eddy Current Multipoles and Sextupole Configurations	02/23/88
112	J. Milutinovic & A. G. Ruggiero	Effects of Quadrupole Gradient Errors in the AGS Booster	02/23/88
113	M. J. Rhoades-Brown & A. G. Ruggiero	An Alternative Injection Scheme for Heavy Ions Into The Booster	03/02/88
114	E. Higgins and V Stanziani	Booster Pick-Up Electrode Signal Processing	03/21/88
115	J.Wei, S. Y Lee, A. G. Ruggiero	R.F Capture of the AGS Booster	04/08/88
116	H.C. Hseuh	Booster Beam Loss Due to Beam-Residual Gas Charge Exchange	04/20/88
117	A. J. Stevens	Conceptual Design of the Booster Beam Dump	04/21/88
118	F Z. Khiari, A. U. Luccio & W T Weng	ESME at BNL. Status Report & Simulation Study of Proton RF Capture in the BNL Booster	04/25/88
119	G. F Dell	Coordinates of Magnet Survey Markers & Tunnel Survey Monuments for the AGS Booster	04/26/88
120	E. P Coldon, D Shi, & Z. Parsa	Transverse Space-Charge Effects in the AGS Booster During Injection	04/29/88
121	Zohreh Parsa	Coordinates of the Magnets and Survey Monuments for the AGS Booster	05/09/88
122	R. L. Witkover	Proposal for a Beam Profile Monitor for the Booster Ring (with Application to the Upgraded AGS)	05/11/88
123	J. Wei and S. Y Lee	Effect of Injection Energy Spread in Multi-turn Injection on AGS Booster	05/13/88

Booster Technical Notes			
Number	Author	Title	Date
124	E. Beadle	Radiation Effects on a Fiber-Optic Repeater	08/05/88
125	S. Tepikian	Random Sextupole Correction	08/05/88
126	M. Meth	Preliminary Design of RF Power Amplifier for Upgraded AGS	08/10/88
127	G.Parzen	Effect of Resonances on the Space Charge Limit	08/18/88
128	F Khiari, A. Luccio	Effect of a Wall Impedance on the RF Capture of a Chopped Beam in the AGS Booster	08/22/88
129	M. Meth	System Analysis of Electrical Energy Storage Systems	08/29/88
130	J. Zhang	Some Voltage Feedback Loops for the RF System of the AGS Booster	09/14/88
131	A. Luccio	Computer Study of Harmonic Orbit Correction in the AGS Booster	10/03/88
132	S. Tepikian	Skew Quadrupole Corrections	10/10/88
133	W Zhang, J. Bunicci, W Frey, & A. Soukas	Report on the Test and Measurement of the Fast Kicker System	12/22/88
134	F Khiari, A. Luccio, & A. Ratti	Longitudinal Higher-Order Modes of the Booster Proton RF Cavity ...	12/30/88